APPLICATION OF THIN COPPER SULFIDE FILMS IN SOLAR CELLS

PREPARATION AND CHARACTERIZATION OF THIN COPPER SULFIDE FILMS FOR THEIR APPLICATION IN SOLAR CELLS

By

KAMAL RAJKANAN, B.Sc. (Honours), M.Sc

A Thesis

Submitted to the School of Graduate Studies

in Partial Fulfilment of the Requirements

for the Degree

Masters of Science

McMaster University

April 1978.

MASTER OF SCIENCE (1978) MCMASTER UNIVERSITY

(Physics) Hamilton, Ontario.

TITLE : Preparation and Characterization of Thin Copper Sulfide Films for their Application in Solar Cells.

AUTHOR : Kamal Rajkanan, B.Sc.(Honours) (University of Rajasthan)
M.Sc. (Indian Institute of Technology, New Delhi)

SUPERVISOR : Professor J. Shewchun

NUMBER OF PAGES: xii, 172

ABSTRACT

Two methods for preparing semiconductor grade copper sulfide films, to be used in low cost thin film solar cells, have been investigated. The sulfurization method involves the controlled chemical conversion of copper films into the desired copper sulfide phase. The other method of evaporating Cu_2S pellets is more adaptable for an all evaporated thin film solar cell. The copper sulfide films obtained by these methods were characterized using x-rays, cathodoluminescence, electrical and optical methods. The use of optical method in monitoring the stoichiometry of thin copper sulfide films has been illustrated. The photovoltaic properties of thin copper sulfide films obtained by these methods, were also investigated using Cu_2S - Si heterojunctions. The behaviour of these junctions indicates that 900 Å thick copper sulfide film is required for optimum photovoltaic conversion. This result may be of some importance in Cu_2S - CdS solar cells in further reducing their thickness. Cu_2S - Si heterojunctions can also be used to monitor the properties of copper sulfide, as silicon is a well characterized substrate.

ACKNOWLEDGEMENTS

I wish to express my appreciation to my supervisor, Dr. J. Shewchun for his interest in this work. The support and technical help of Mr. L. Goodridge, A. Kazandjian, T. Vanderwel and G. Chapman, at various stages of this work, is gratefully acknowledged. I am deeply indebted to Mr. R. Singh for his generous moral support and stimulating discussions. Special thanks are due to Prof. J.J. Loferski (Brown Univ.), Dr. J.P. Marton (Welwyn Canada Ltd.) and Dr. R. Clarke (Garrett Manufacturing Ltd.) for their encouragement and for providing facilities at their disposal.

The financial support of the Physics Department, during this work, is to be gratefully acknowledged. The greatest and very personal gratitude, however, is due to my parents and family. Without their understanding and constant encouragement, it would have been impossible to undertake this assignment.

TABLE OF CONTENT

LIST OF TABLES

LIST OF FIGURES

CHAPTER 1 - INTRODUCTION

It has been well recognized that the use of single crystals of semiconducting materials in solar cells is a major obstacle in bringing their cost low enough for general terrestrial applications. A great variety of compound semiconductors are now known which can be used to make polycrystalline thin film solar cells using inherently less expensive fabrication processes. Many of these compound semiconductors show only one type of conductivity, either p- or n- type, because of equilibrium density of native defects (vacancies, interstitials etc.) which act as donors or acceptors. This makes it necessary to use two different compound semiconductors to form a p-n heterojunction to get the photovoltaic effect. Also, with polycrystalline semi-conductors, good homojunction diodes should not be expected because of preferential diffusion of carriers along the intercrystalline boundaries.

Copper sulfide - cadmium sulfide thin film cells have been under investigationsfor quite some time. So far these cells have the best conversion efficiencies among all compound semiconductor heterojunctions and are adaptable to cheap fabrication methods. However, their efficiencies are lower than with those achieved in silicon solar cells; also they have problems with instabilities in their output characteristics. Although both Cu_2S and CdS compound semiconductors are suitable for photovoltaic conversion, the above limitations appear to be caused by poor understanding of the junction formation. Historically, these cells were fabricated by the deposition of copper onto the cadmium sulfide substrates and were treated as Schottky barriers. Later it was discovered at the Harshaw Chemical

Company and then by other research groups that the photovoltaic properties are actually due to a heterojunction between Cu_2S and CdS - Cu_2S being formed by the chemical conversion of copper layer. Since then various techniques to make Cu_2S layer on CdS in a controlled manner have been tried. Most important of these techniques are so called "wet" process and the "dry" process. These techniques depend on the chemical reaction at the surface of CdS and are therefore hard to control in terms of junction quality.

Two techniques have been developed in this work - namely the sulfurization of copper films and the vacuum evaporation of Cu_2S. It has been shown that these techniques provide the necessary control over the fabrication of copper sulfide films and the copper sulfide films so formed are responsible for photovoltaic conversion. Cu_2S-Si heterojunctions have been used to monitor the film quality as well as other methods like x-rays, cathodoluminescence, electrical - optical parameters analysis, etc.

This work has been divided in four major parts. In the first part, the development of Cu_2S -CdS solar cells and the physical properties of copper sulfide phases have been reviewed. The reason why chalcocite phase of copper sulfide is more efficient in photovoltaic conversion is also discussed. In the second part, the sulfurization and the vacuum evaporation methods have been discussed. The third part is devoted to the different experimental techniques which have been used to characterize the copper sulfide films prepared by sulfurization and evaporation methods. The use of optical measurements for characterizing the film stochiometry has also been illustrated.

In the last section, the photovoltaic effects in Cu_2S films have been discussed. Cu_2S - Si heterostructures were used for this purpose as the Si provides the advantage of being a well characterized substrate.

Essentially, two methods were investigated in this work to prepare semiconducting copper sulfide thin films. The preparation variables were controlled and optimized by monitoring the physical properties of copper sulfide films. These films were used to investigate the photovoltaic characteristics of Cu_2S - Si heterojunctions. The results obtained by such investigation could be useful in the quality control of Cu_2S - CdS solar cells.

CHAPTER 2

BACKGROUND MATERIAL

2.1 DEVELOPMENT OF $Cu_{2-x}S$ - CdS SOLAR CELLS:

2.1.1 Single crystal Photovoltaic Cells:

Reynolds[1,2] discovered a strong photovoltaic response in CdS - Cu_2S rectifiers in May, 1954. A copper layer was electroplated onto an indium doped, etched CdS crystal. The junction formation was completed by heating for 30 seconds at 350 ^{o}C. An efficiency of 1.5 % was initially achieved.

After Reynolds' discovery, work on the photovoltaic effect was initiated by Aerospace Research Laboratories (ARL) which included outside work at Harshaw Corporation. Hammond and Shirland[3-5] were able to improve the efficincy beyond 5% by 1959. They investigated a number of methods of junction formation: (a) Cu electroplated and oxidized to Cu_2O, (b) deposition of Cu_2O from solvent slurry, (c) Cu evaporation and oxidation, (d) decomposition of copper acetate and oxidation

to Cu_2O and (e) evaporation of solvent slurry of Cu_2S. All the initial cells were of a backwall construction, i.e. the light must penetrate the cadmium sulfide crystal before reaching the junction. Hammond and Shirland constructed the first frontwall cell by etching away the excess Cu_2O material from the barrier, thus enabling the light to pass through the junction before reaching the CdS.

Williams and Bube[6] made Cu - CdS cells with undiffused metal - semiconductor junctions. Bockemuehl[7] diffused copper into photoconductive, dark insulating CdS. This produced two potential barriers, one at the surface and one in the bulk. This structure was unsuitable for photovoltaic effect.

Recent work on single crystal cells by Bube[8 - 10], Miya[11], and Boer[12,13] was carried out primarily to simplify the study of the photovoltaic properties of the copper sulfide-cadmium sulfide system.

2.1.2 Thin Film Photovoltaic Cells:

The first polycrystalline CdS thin film photovoltaic cells were made by Carlson et al[14,15] at Clevite on glass and

copper substrates in a frontwall and backwall configuration. A thin film of Cu_2S was applied to the CdS film. Low temperature baking at 150 to 200°C was necessary to activate the barrier. The efficiency was less than 0.1% due to the high CdS bulk resistance. Attempts were made to reduce the resistance by heavy doping.

Gorski at Harshaw[4,16] tried to reduce the series resistance by means of thicker vacuum deposited CdS films up to 100 μm. He adopted a silver paint grid to reduce the resistance of the Cu_2S layer. The barrier layer was formed by electroplated mossy copper that was air heated at 275°C.

The early cells suffered not only from a high series resistance, they also degraded on storage due to moisture and showed a lack of reproducibility in forming the active layer on the CdS and providing satisfactory electrical contacts. The subsequent development was carried out mainly by Harshaw and Clevite who maintained pilot lines, and initially by RCA as well.

a. Work at RCA:

The most notable achievement of RCA was to pioneer the use of Kapton as a plastic substrate. This started the development of flexible, lightweight CdS solar cell arrays using frontwall illumination. Kapton is stable at higher temperatures and can, therefore, stand the deposition of CdS at an optimum temperature around 200°C.

b. Work at Harshaw:

A frontwall cell on a molybdenum substrate was developed at Harshaw.[17] Molybdenum is a good match for the thermal expansion coefficient of CdS. The cells were laminated between two plastic sheets, Mylar or kapton, to inhibit curling using a nylon (Capran) adhesive. Griffin[18] replaced the top contact of conductive silver paint by an electrofomred fine metal mesh. This improved the cell efficiency by reducing the series resistance. Gold grids gave the best results.[19] A pressure contact was formed between the metal grid and the Cu_2S layer during lamination. Evaporated grids were also tried, but they produced too high a series resistance. A 40-100 Å zinc layer between the molybdenum substrate and the CdS provided a better ohmic contact. The molybdenum substrate was later reduced from 2 to 0.3 mil by chemical milling to reduce the weight of the cell.[19]

In the final work at Harshaw[20] the grid was changed from gold to gold-plated copper to reduce the cost. The grid was thermocompressed into the cell by passing through heated rollers. The nylon lamination was replaced by clear epoxy in order to increase the stability of the cell.

c. Work at Clevite:

Clevite perseveredwith a backwall cell until 1965, using a Pyrex or Kapton substrate, also copper foil. A peripheral indium contact to the CdS caused deterioration of the cell and was replaced by a metal film or mesh, and by evaporated gold strips on kapton. The barrier layer was formed by means of a Cu_2O slurry followed by baking at 250 to 300°C. Formation by electroplating, vacuum evaporation, and thermal decomposition were also tried.[21] The counterelectrode was formed by conducting silver paint or evaporated gold stripes. Water vapor caused the cells to

deteriorate rapidly initially.

In 1965 Clevite[22] switched to frontwall cells with molybdenum or Kapton substrates. The cell instability caused by contact deterioration at the grids was solved by means of conducting adhesive. Improvements in the barrier formation method by going to a CuCl dip resulted in efficiencies between 4 and 6% from a 50 cm^2 cell. This technique is now widely known as "clevite" or "wet" process. A combined frontwall-backwall cell on a polymide substrate showed substantially lower efficiencies and was difficult to reproduce.[22,23]

In the final version of the clevite cell[24] nylon was replaced by clear epoxy resin to eliminate degradation in humid ambients. Copper or silver in contact with the barrier causes degradation to the cell output after high temperature exposure. The silver epoxy grid contact was therefore replaced by a gold pigmented epoxy. The electroformed gold metal mesh was replaced by a gold-plated copper mesh.

d. Other Developments:

In 1958 Cabannes[25] evaporated a layer of copper on top of a CdS film. Initially, there was a very high resistance and no photovoltaic effect. The application of a dc electric field caused a sudden decrease in the resistance and a photovoltaic response with a maximum in the red.

A frontwall-backwall cell was developed by Itek.[26] The barrier layer was formed by copper evaporation followed by air baking for 15 min. at 400°C. Copper evaporation was also employed by Pastel,[27] by Balkanski and Chone,[28] and by Anshon and Karpovich.[29]

A major effort in the CdS thin film solar cell development was made by the S.A.T. Company in France.[30-34] The construction of the cells is basically the same as in the final Clevite version, except that Aclar as well as Kapton is used as cover material. By improvements in the different layers, gridding, and encapsulation the efficiency of the cell has increased from 3% in 1968 to 7% in 1970 at air mass zero.† Similar cells have also been developed by the International Research and Development Company in England[35], by AEG-Telefunken in Germany[36,37] and the University of Delaware.[38]

Mickelsen and Abbott of the Boeing Corporation[39] investigated a dry barrier formation process. Purified cuprous chloride was evaporated from a quartz crucible, followed by a two minute bake at 180°C in air or hydrogen. The efficiency was only 3% at air mass zero. An attempt was made to carry out most of the fabrication steps by vacuum evaporation. The metallization of the Kapton substrate was changed to a NiCr-Cu-Cr layer. A number of materials were tested to encapsulate the cell. Silicone R63-488 gave the best adherence. CuCl evaporation was also attempted by researchers at the University of Delaware.[40] This method has been perfected at Philips laboratories,[41] and is now known as "Philips" or "dry" process. The cells produced routinely had efficiencies in the 4-5% range, although occasional cells of 8% were also obtained.

---

†Air mass zero defines the solar illumination intensity just outside the earth's atmosphere.

2.2 PROPERTIES OF Cu - S COMPOUNDS:

2.2.1 Phases of Cuprous Sulfide:

Transition metal compounds are rarely stochiometric to less than 0.1%. The phase diagrams of several transition metal compounds are complicated and this is indeed true for the Copper-Sulfur system. The phases which are known to be stable at room temperature include Cu_2S (chalcocite), $Cu_{1.96}S$ (djurleite), $Cu_{1.8}S$ (digenite), $Cu_{1.75}S$ (anilite) and CuS (covellite) The value of x in $Cu_{2-x}S$ need not be exactly the same as just given, but there exists a range of x values in which a given member of Cu-S system can exist. For example, at room temperature, chalcocite can have x values between 0.000 to 0.005, djureleite between 0.03 to 0.07, etc.[53,54] The copper-sulfur phase diagram (Fig 1,2) has been reviewed by Cook et al.[42,43] The most important structural properties of the predominant cuprous sulfide phases are shown in Table I. It may be noted that all phases undergo transitions at relatively low temperatures.

X-ray studies of the Cu-S system were carried out by Djurle.[44] At the time of his investigations, only three minerals of the Cu-S system were known: Cu_2S (chalcocite), $Cu_{1.8}S$ (digenite), and CuS (covellite). During the course of his work he identified another compound, $Cu_{1.96}S$ (djurleite). In addition, each of these compounds (with the exception of CuS) exists in several phases, depending upon the temperature. Cu_2S below 110°C has an orthorhombic structure with cell dimensions a = 11.88 Å, b = 27.32 Å and c = 13.49 A. At higher temperatures (110°C - 470°C), it transforms into a hexagonal structure and above 470°C into a face centered cubic structure.

FIGURE 1: Cu - S phase diagram according to Cook. For enlargement near Cu_2S phase, see Figure 2.

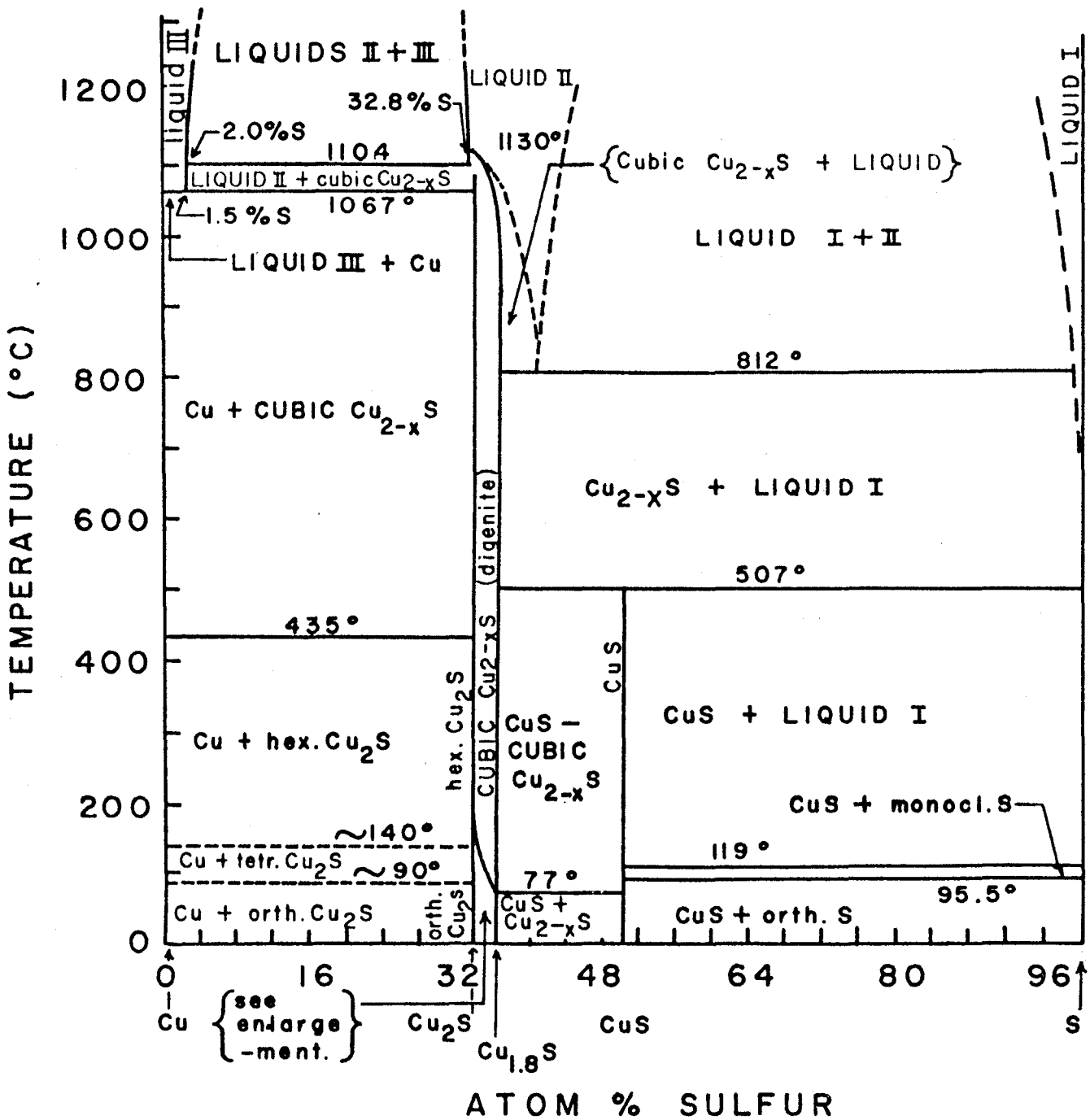
LIQUIDS II+III
LIQUID III
LIQUID II
LIQUID I
32.8% S
2.0% S
1104
1130°
{Cubic Cu2-xS + LIQUID}
LIQUID II + cubic Cu2-xS
1067°
1.5 % S
LIQUID III + Cu
LIQUID I+II
812°
Cu + CUBIC Cu2-xS
Cu2-xS + LIQUID I
507°
435°
CUBIC Cu2-xS (digenite)
hex. Cu2S
CuS
Cu + hex. Cu2S
CuS — CUBIC Cu2-xS
CuS + LIQUID I
CuS + monocl. S
~140°
119°
Cu + tetr. Cu2S
~90°
77°
95.5°
Cu + orth. Cu2S
orth. Cu2S
CuS + Cu2-xS
CuS + orth. S
TEMPERATURE (°C)
0
200
400
600
800
1000
1200
0
16
32
48
64
80
96
Cu
{see enlargement.}
Cu2S
Cu1.8S
CuS
S
ATOM % SULFUR

FIG. 1

FIGURE 2: Enlargement of Cu -S phase diagram from $Cu_{2.00}S$ to $Cu_{1.72}S$.

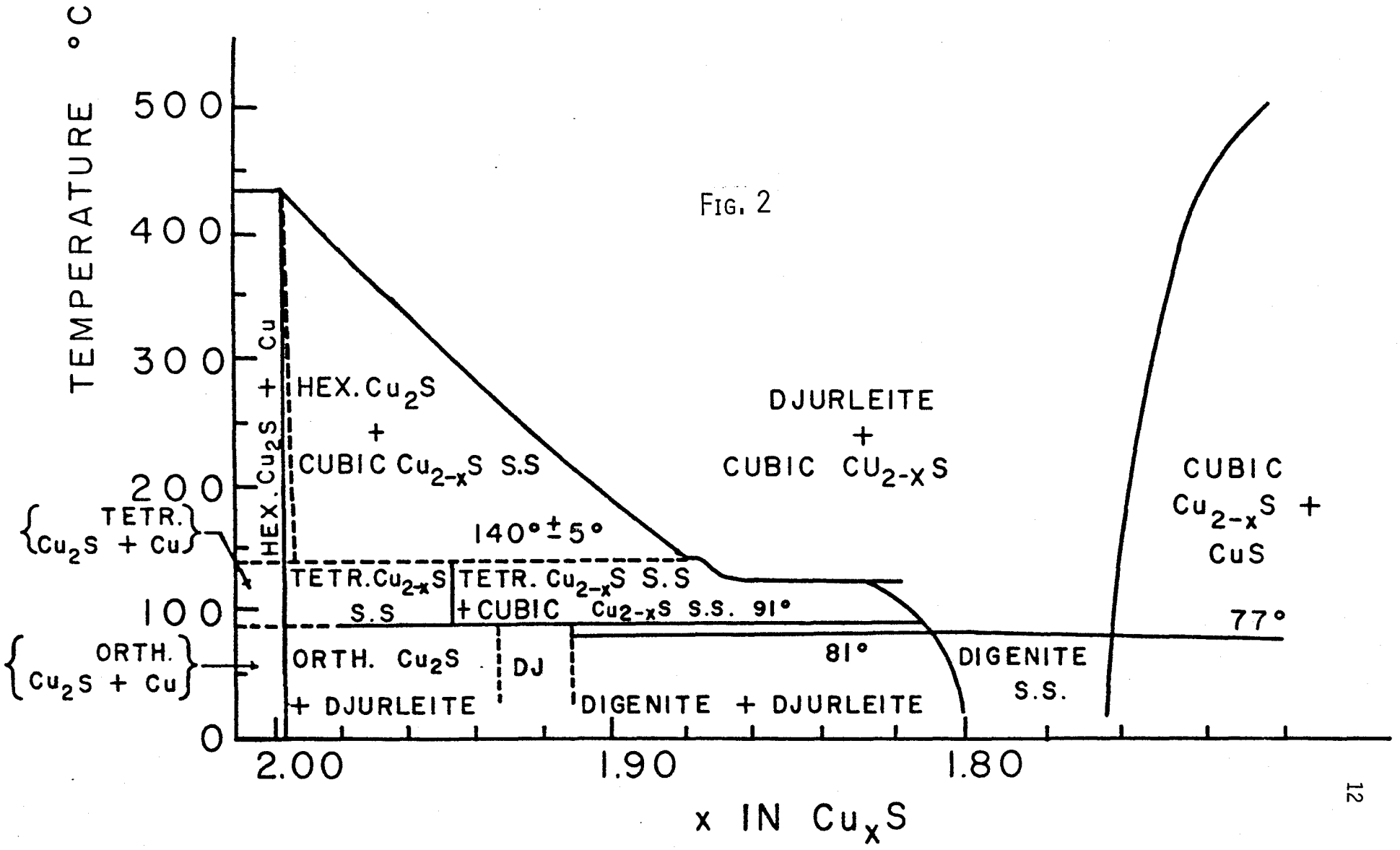
TEMPERATURE °C
500
400
300
200
100
0
HEX. Cu2S + Cu
HEX. Cu2S + CUBIC Cu2-xS S.S
DJURLEITE + CUBIC Cu2-xS
CUBIC Cu2-xS + CuS
{TETR. Cu2S + Cu}
140° ± 5°
TETR. Cu2-xS S.S
TETR. Cu2-xS S.S + CUBIC Cu2-xS S.S. 91°
77°
{ORTH. Cu2S + Cu}
ORTH. Cu2S + DJURLEITE
DJ
81°
DIGENITE + DJURLEITE
DIGENITE S.S.
2.00
1.90
1.80
x IN CuxS

FIG. 2

TABLE I

PREDOMINANT PHASES OF CUPROUS SULFIDE

Phase	Composition	Structure	Lattice Constants a_o (Å)	b_o (Å)	c_o (Å)	Reference	Phase Transition Temp.	High Temp. Structure	Reference
Chalcocite	Cu_2S	orthorhombic	11.8	26.9	13.4	Rahlfs[50]	103.5°C	hexagonal	Djurle[44], Roseboom[45]
		pseudohexagonal	11.90	27.28	13.41	Buerger[51]	110°C		Posnjak[48]
			11.881	27.323	13.491	Djurle[44]	435°C	cubic	Jost[49]
		Cu_2S films grown on CdS	11.848	27.330	13.497	Cook[43]			
			11.88		13.49	Singer[52]			
			11.82	27.0	13.45	Palz[30]			
Djurleite	$Cu_{1.96}S$	orthorhombic	15.71	13.50	26.84	Roseboom[45]	93°C	hexagonal	Roseboom[45]
Digenite	$Cu_{1.8}S$	pseudocubic	5.56			Djurle[44]	~80°C	cubic	Cook[43]

$Cu_{1.96}S$ was found to have a "low symmetric" structure at room temperatures which transforms to a face centered cubic structure above 100°C. $Cu_{1.8}S$ is face centered cubic with a homogeneous range extending from $Cu_{1.82}S$ to $Cu_{1.70}S$. CuS is always hexagonal.

Roseboom[45], one of the first to study the mineral Djurleite, carried out extensive studies of the Cu-S system, studying both synthetic as well as natural phases at temperatures below 500°C. Cook[43] found a new metastable phase of composition $Cu_{1.75}S$. This is not surprising in light of the work of Morimoto et al.[46,47] They found a new mineral with a narrow range of composition near Cu_7S_4 which changed to the metastable digenite phase when ground and polished. Cu_7S_4, called Anilite, is closely associated with digenite and mixed phases were always observed in the dominantly anilite specimens. At room temperature, digenite solid solutions decompose to mixtures of anilite and djurleite.

The defect structure of Cu_xS consists of a highly ordered S sublattice and a disordered Cu lattice with two Cu+ ions associated with each S^{2-} ion.[12,42] Such a structure had been proposed by Rau[53,54] for high temperature $Cu_{2-x}S$. The djurleite phase, $Cu_{1.96}S$, is more stable than Cu_2S but is formed only in the presence of Cu^{2+} ions.[12] Knowledge of the defect structure is quite important, because the electro-optical properties heavily depend on lattice defects.

2.2.2 Optical Properties of Cuprous Sulfide:

The optical properties of cuprous sulfide have been measured by a number of experimenters (see Table II). Figure 3 indicates that Cu_2S possesses an exceptionally high absorptivity in the visible region of the spectrum and a high transmission in the infrared.

Various detailed absorption measurements on cuprous sulfide films of different stoichiometric composition indicate the presence of band edges at 1.2 and 1.8 eV. Bube, Lind, and Dreeben[56] carried out absorption measurements in heavily copper doped CdS. An absorption edge at 1.21 eV, in agreement with Eisenmann's[57] results, indicated the presence of a second phase of Cu_2S distributed throughout the crystal.

There still seems to be disagreement about whether it is a direct or indirect gap semiconductor. The primary evidence about the semiconducting properties of Cu_2S derives from optical absorption measurements on samples that were reputedly Cu_2S. Cusano[58] observed a rise in the absorption at 1.8 eV. Marshall and Mitra[59] confirmed the presence of an indirect bandgap at 1.21 eV. Sorokin[60] measured the photoconductivity and optical absorption of evaporated Cu_2S films; he postulated the existence of a direct bandgap at 1.9 eV. Shiozawa[55] concluded from an analysis of the above data that Cu_2S possesses absorption edges at 1.2 and at 1.8 eV. Finally, Ramoin et al.[61] concluded from absorption measurements on evaporated films that Cu_2S possesses a direct bandgap at 1.7 eV and an indirect bandgap at 1.05 eV. They also observed an impurity absorption band between 1.3 and 2 μm.

Table II indicates some reported values for the bandgaps in $Cu_{1.8}S$ and $Cu_{1.96}S$.

Table II

Optical Properties of Cuprous Sulfide

Reference	Structure	Stoichiometry	Measurements	Band Gap
Eisenmann[57]	evap. film	Cu_xS $1 \leq x \leq 2$	absorption, reflection	
Bube[56]	Cu doped CdS	Cu_2S ppted. 2nd phase	transmittion	1.21
Cusano[58]	CdS film dipped in CuCl	$Cu_{2-x}S$	absorption	
Harshaw[19]	CdS crystal with electropl. Cu_xS layer	Cu_2S	reflectivity, transmission	
Marshall & Mitra[59]	polycrystals	Cu_2S	absorption, reflection	1.21 at 300°K 1.26 at 80°K
Sorokin[60]	evap. film	Cu_2S	absorption photoconductivity	1.84 1.93
Ellis[65]	flash evap. film	$Cu_{1.8}S$	transmission	
Shiozawa[55]	evap. film and CdS crystal dipped in CuCl	$Cu_{2-x}S$	transmission, reflection, refractive index	1.21, 1.83
Kryzhanovskii[66]	evap. film	Cu_2S_{1+x}	reflection	
Selle & Maege[67]	evap. film		absorption, refractive index	1.22 at 300°K 1.25 at 90°K
Egorova[68]	CdS film dipped in CuCl	Cu_2S	transmission	
Nakayama[62]	evap. film	$Cu_{1.8}S$ Cu_2S $Cu_{1.96}S$	transmission & reflection	2.3 1.0 1.5
Ramoin[61]	evap. film	Cu_2S	absorption	1.7, 1.05
Gustavino[69]	evap. film	$Cu_{1.8}S$	transmission, reflection	2.6
Mulder[63, 64]	CdS crystal dipped in CuCl	Cu_2S	transmission	1.2, 2.5
Couve[70]	evap. film	$Cu_{1.9}S$	transmission	1.93-2.00

FIGURE 3: Absorption coefficient of Cu_2S, as reported by various authors. Note the sharp rise at about 1.2 eV.

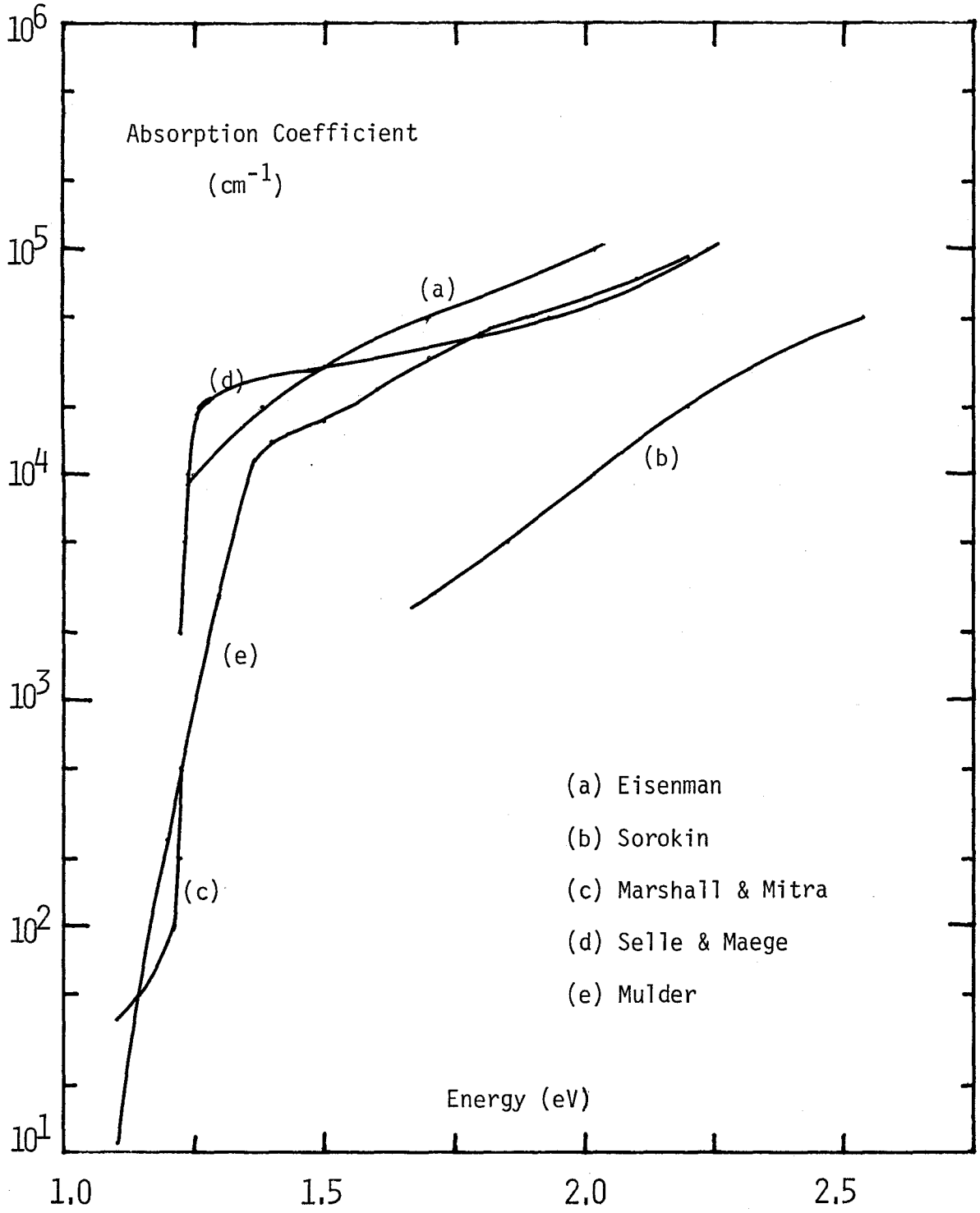
Absorption Coefficient
(cm^{-1})
10^6
10^5
10^4
10^3
10^2
10^1
(a)
(b)
(c)
(d)
(e)
(a) Eisenman
(b) Sorokin
(c) Marshall & Mitra
(d) Selle & Maege
(e) Mulder
Energy (eV)
1.0
1.5
2.0
2.5

FIG. 3

Because it is difficult to control the Cu/S ratio in films, there are substantial differences in the values of material parameters reported in the literature. Thus Eisenman[57] reported that films of what he understood to be Cu_2S had optical absorption constants in the photon energy range 1.2 eV $\leq h\nu \leq$ 2.5 eV which are about an order of magnitude larger than those subsequently reported for "Cu_2S" by Sorokin et al.[60] Marshall and Mitra[59] measured the absorption constant of "Cu_2S" for values of $h\nu$ closer to the absorption edge than either Eisenman or Sorokin did. More recently, Nakayama[62] measured the absorption constant of covellite (CuS) and showed that its values in the 2.0 eV $\leq h\nu \leq$ 2.5 eV range are smaller than the values measured by Sorokin on his "Cu_2S". From these data and more recent measurements of the optical transmission of Cu-S compounds, it is reasonable to assume that the samples used by Sorokin et al. were not Cu_2S as reported but rather a Cu-S compound having a composition intermediate between that of Cu_2S and CuS.

The most comprehensive study of the optical properties of Cu_2S and other members of the Cu-S family is that reported in a series of papers by Mulder[63,64] of the Philips Laboratories, Eindhoven. He prepared tiny crystals of Cu_2S by dipping small CdS crystals into a CuCl solution and allowing the reaction to proceed until the CdS had been completely transformed into Cu_2S. His crystals had dimensions of a few microns on a side and their thickness was between about 0.2 μ to 0.5 μ. He then transformed the Cu_2S crystals into djurleite, digenite and covelite by controlled oxidation. He measured the optical transmission of these tiny crystals with the help of a microspectrophotometer. Mulder measured both the index

of refraction and the absorption constant of these crystals as a function of polarization of the incident light (see Fig. 4-7).

Mulder found that the absorption constant of Cu_2S rises rapidly from an absorption edge around 1.2 eV until it reached a plateau value of about 4×10^4 cm^{-1} and then beginning around 1.8 eV it rises again until its value reaches about 2×10^5 cm^{-1} at 2.5 eV. The onset of absorption in the other Cu-S compounds occurs at somewhat higher values of $h\nu$; they, too, exhibit a kind of absorption plateau followed by a rise to values 10^5 cm^{-1}. The index of refraction values lay in the range $\sim$3.0.

Mulder interpreted his data in terms of an indirect transition followed by a direct transition. For Cu_2S, he calculates a value of about 1.15 eV for light polarized along the a-axis of crystals and 1.4 eV for light polarized parallel to the c-axis. The direct gap turned out to be about 2.5 eV. He found that the value of the "indirect" gap increased as x increases. He proposed an explanation of this behaviour based on an energy band model in which the conduction band has a single minimum at k=0 and the valence band has two maxima: one associated with indirect transitions and therefore located at $k \neq 0$ and the other located at k=0. He attributed his observed increase in the indirect gap to a "Burstein shift" in which the Fermi level moves deeper into the valence band with extremum of $k \neq 0$, which results in transitions to the conduction band occuring from lower lying levels within the valence band. The proposed band model is unusual in that valence bands with extrema at $k \neq 0$ are not encountered in any of the well known semiconductors like Ge, Si, III-V and II-VI materials. Furthermore, it is questionable whether one can classify an absorption process which has a saturation plateau around 10^5 cm^{-1} as an indirect transition. As we shall point out later,

FIGURE 4,5,6 & 7: Optical constants (n and k) of $Cu_{1.995}S$, $Cu_{1.95}S$, $Cu_{1.86}S$ and $Cu_{1.77}S$, respectively. Data taken from Mulder.[63,64] $\perp$ and // signs are for light polarized in perpendicular and parallel direction, respectively.

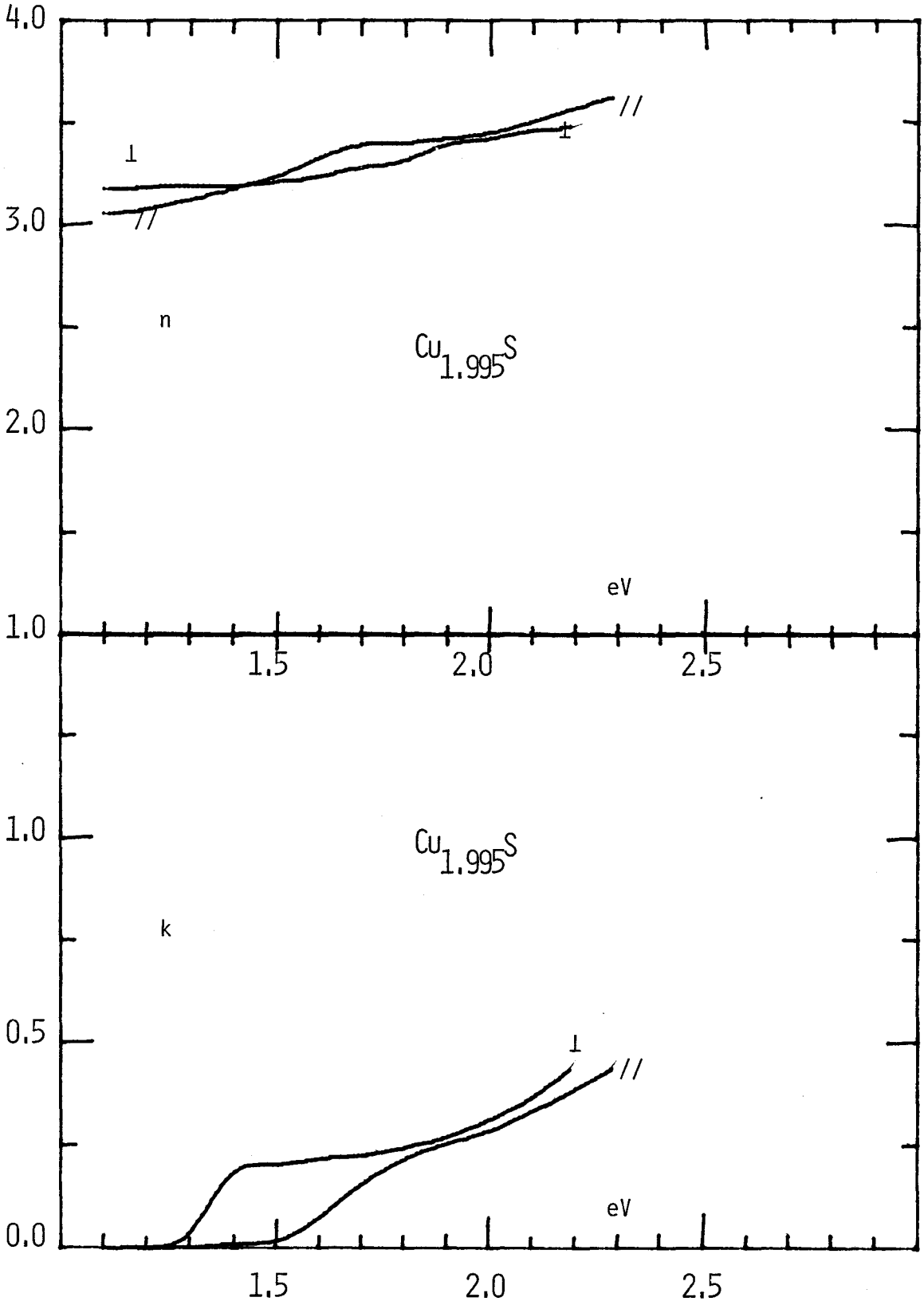

FIG. 4

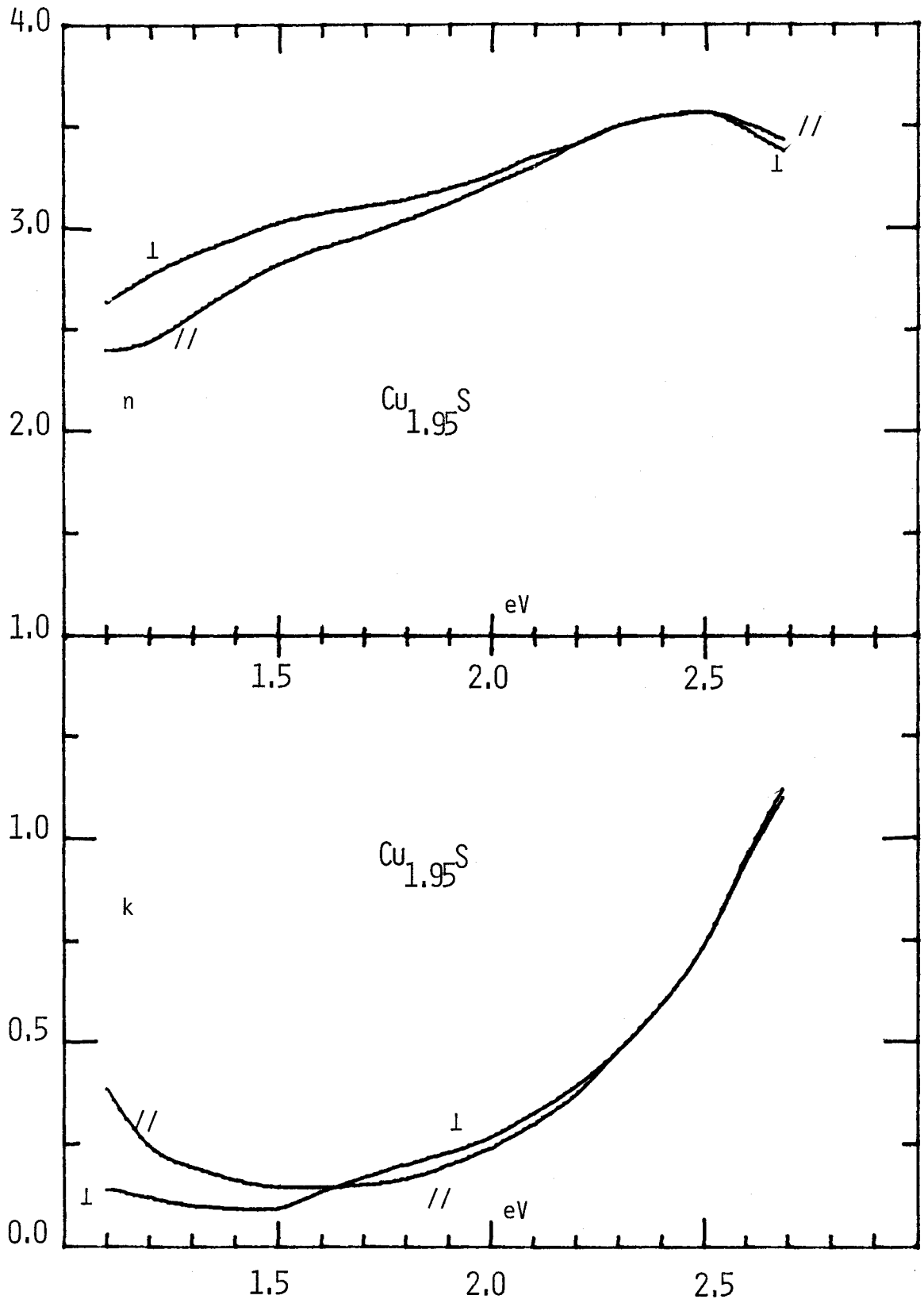

FIG. 5

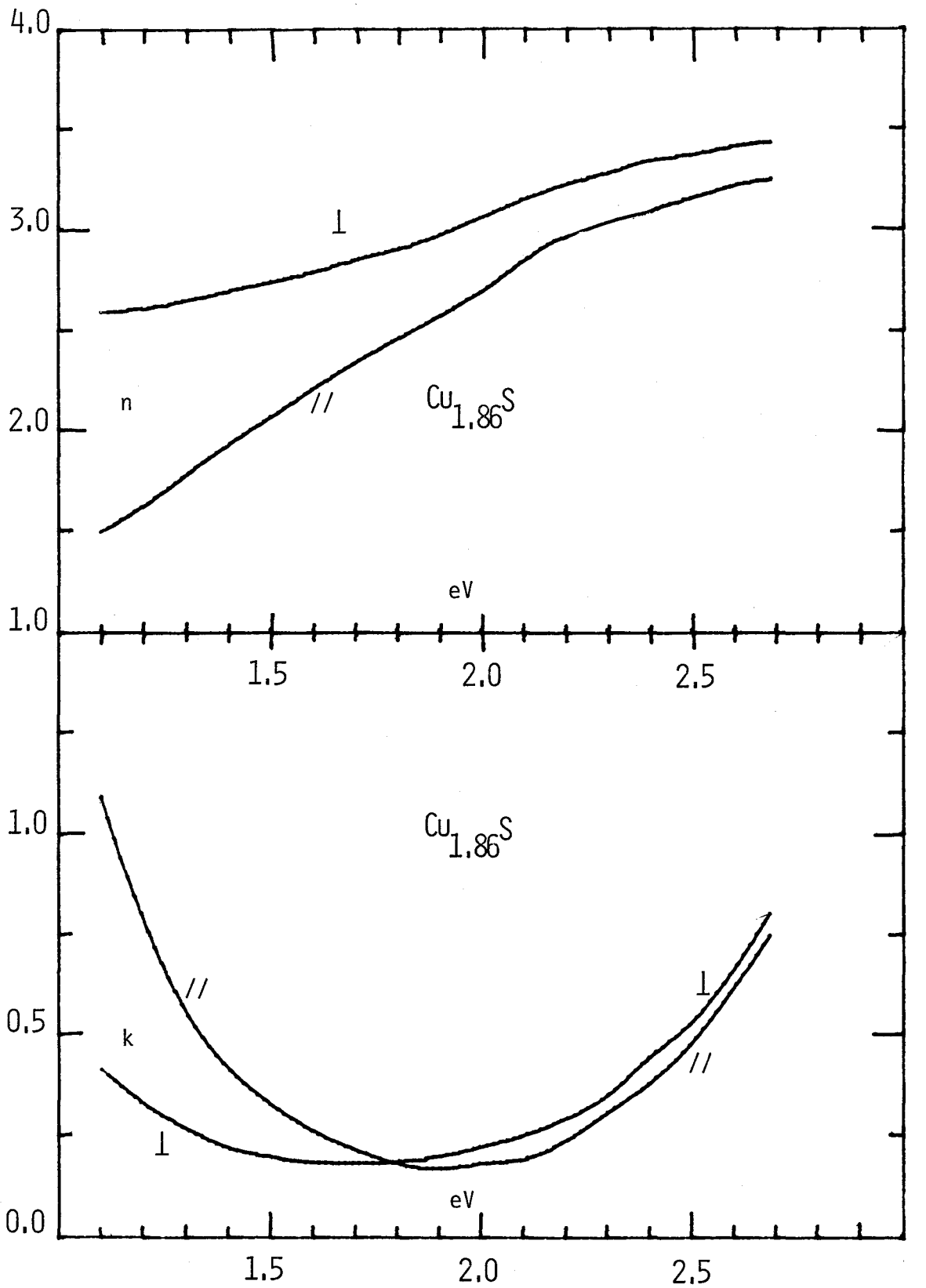

FIG.6

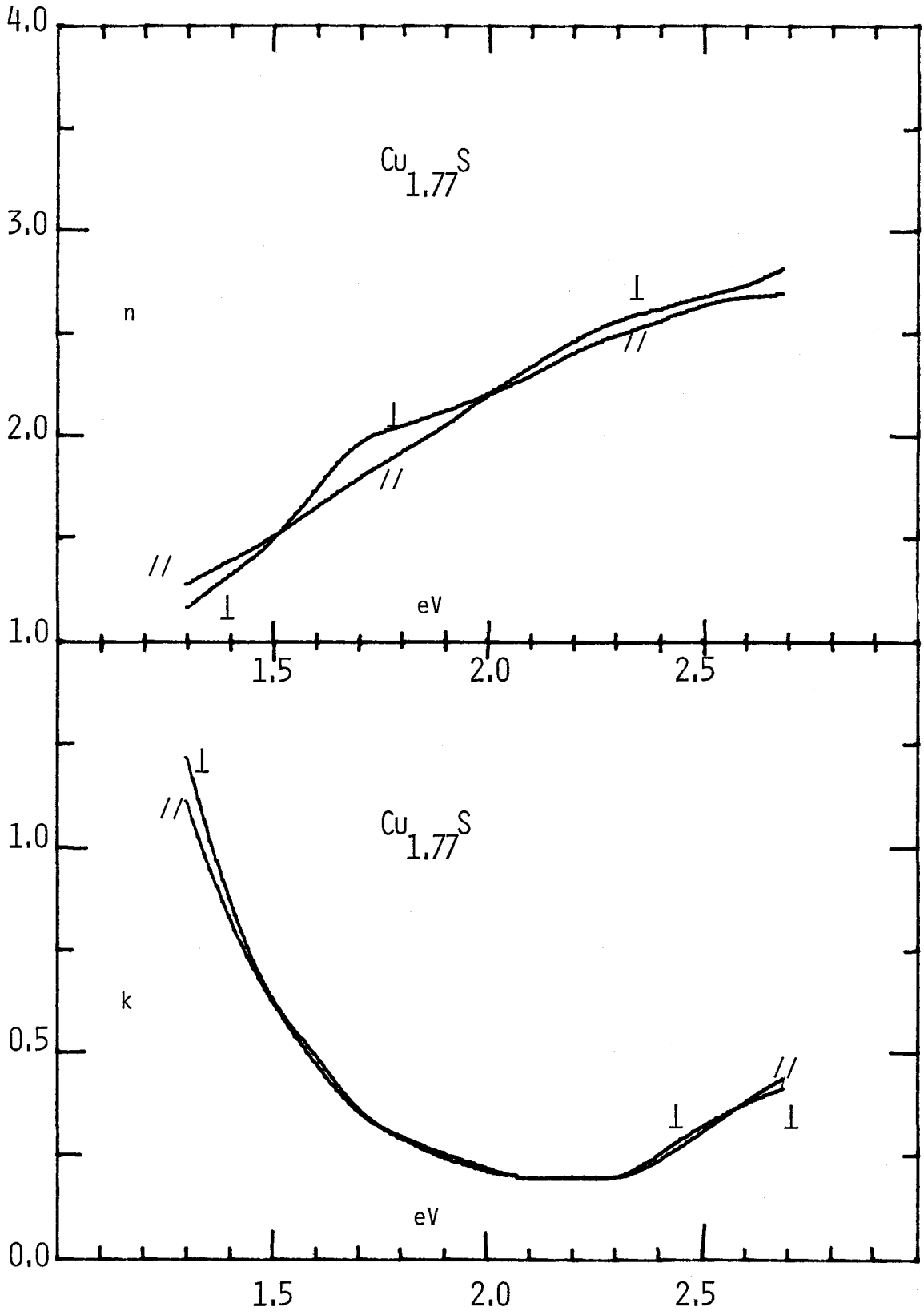

FIG. 7

our studies of cathodoluminescence of Cu_2S suggest that a luminescence peak at about 1.2 eV has a shape like that one would expect for band - to - band transitions in a direct gap semiconductor.

A study of optical absorption in Cu_xS thin films was recently reported by Couve et al.[70] They measured the absorption, resistivity and the value of x in the composition of Cu_xS films produced by evaporation of Cu_2S onto glass substrates. They were unable to obtain good reproducible absorption data for values of $h\nu$ lower than about 1.7 eV. They were able to fit their data for $h\nu > 1.7$ eV in terms of a direct gap transition in which the value of E_g is a function of film resistivity rather than of composition. Their range of x values for Cu_xS lay between 1.89 and 1.95, i.e., their samples had compositions closer to djurleite than to chalcocite. The direct gap value reported by these authors ranged between 1.93 and 2.00 eV.

Summarizing the optical transmission data, it appears to be well established that the absorption data for Cu-S compounds in the range chalcocite through digenite ($Cu_{1.8}S$) can be fitted by the theory of direct transitions for values of $h\nu \gtrsim 1.7$ eV. Absorption constant values greater than 10^5 cm^{-1} have been measured for photon energies in this range. Mulder attributes the transitions beginning in his chalcocite crystals around 1.1 eV to indirect transitions; however this is not a completely satisfying explanation since the absorption constants in this "indirect" region reach a "plateau" at which their values approaches 4×10^4 cm^{-1}. According to Mulder, the magnitude of the "indirect" gap increases as one progresses from chalcocite to djurleite to digenite; he attributes this change to changes in the position of the Fermi level in the material.

According to Couve[70], the value of the "direct" gap observed for higher photon energies also increases as the Fermi level approaches the valence band, i.e. as the resistivity decreases. These results are difficult to understand in terms of the behaviour of better known semiconductors and indicate the need for further studies of the Cu - S system. In this work, however, we have limited ourselves to the preparation techniques of copper sulfide films and their identification, from a solar cell point of view.

2.2.3 Electrical and Thermal Properties of Cuprous Sulfide:

Cuprous sulfide is known to be a p-type semiconductor. Whether a compound is a semiconductor or not, depends among other things on its crystal structure. We would like to understand why cuprous sulfide exists as a p-type semiconductor. In copper-sulfur compounds, sulfur is highly oxidizing agent with oxidation number 2-. In Cu_2S, copper has oxidation number 1+ with a completely filled 3d shell; but it can easily be oxidized to a 2+ state with very little excitation energy supplied by the crystal lattice. Therefore, whenever possible, a sulfur atom will capture two electrons from a single copper atom creating a local CuS molecule, i.e. a copper vacancy in Cu_2S lattice. In this manner, in a cuprous sulfide crystal, it is expected that while the anion sublattice is practically undefected, the cation sublattice will show cation vacancies, giving p-type semiconductor characteristics to the crystal. Actually, because of oxidizing nature of sulfur (tendency to create holes), all members of Cu-S family have p-type semiconductor nature.

Electrical measurements on Cu_xS have resulted in various values for galvanomagnetic parameters depending on the form of the copper sulfide layer. Because it is difficult to control the Cu/S ratio, there are substantial differences in the values of material parameters reported in the literature and they are difficult to understand in term of the behavior of better known compound semiconductors.

Hirahara[71-74] measured the electrical conductivity, the thermal expansion, heat capacity, specific heats, thermal emf, and Hall effect in cuprous sulfide from room temperature to 600°C. Cu_xS produced by heating a "pure" copper block and sulfur powder (of the proportion of

Cu_2S) in a sealed evacuated pyrex tube at 600°C had a mobility of 12 cm^2/v-s and an impurity concentration of 2X $10^{19}/cm^3$ according to Hirahara. Conductivity vs. temperature measurements on these samples showed abrupt changes at 470°C and 110°C. His samples probably had a very high concentration of Cu_2S (they could have been pure Cu_2S) since phase changes in material of this composition occur at these two temperatures. Sulfur rich samples showed a higher Hall constant (up to two orders of magnitude) than the stoichiometric or sulfur deficient samples, which had poor conductivity. The orthorhombic phase between 110° and 470°C exhibits ionic conductivity which was first measured by Tubandt et al.[75] at 220°C.

Eisenmann[57] measured the temperature dependence of the conductivity over a wide temperature range and as a function of the stoichiometry. Cu_2S shows a room temperature resistivity of 100 ohm-cm. There is a decrease by about four orders of magnitude on going from Cu_2S to $Cu_{1.8}S$. In the higher resistivity range evaporated films are strongly affected by exposure to oxygen.

In 1968, Abdullaev and co-workers[76] reported measurements on single crystal Cu_2S. The salient features of their investigations are that the crystals had a mobility of 25 cm^2/v-s and a hole concentration of 7.4 x $10^{19}/cm^3$. Intrinsic and impurity activation energies were found to be 1.8 eV and 0.064 eV, respectively. Anomalies in their measurements occured at temperatures of 125°C and 480°C.

More recently, Couve et. al.[70] described a set of measurements on Cu_xS. They evaporated Cu_2S source material onto polished silica and obtained films of thicknesses between 0.45 and 2.5 microns. The value of

"x" was determined by the method of cathodic reduction (described briefly in their paper) and found to vary between 1.89 and 1.95. The resulting films were of poor quality and their data on Hall measurements and optical transmission measurements did not agree very well with other published data.

The electron diffusion length in Cu_2S layers was measured by Shiozawa,[77] Gill and Bube[78] and Mulder.[79] The last two experimenters utilized light microprobes. Shiozawa and Bube obtained diffusion lengths from less than 0.1 to 0.4 μm. Mulder[79] obtained a diffusion length of 0.7-0.8 μm.

Table III lists the electrical properties of cuprous sulfide. The very high carrier concentrations shown indicate that cuprous sulfide layers are extremely degenerate. This is consistent with the high cation defect density observed in copper sulfide films.

Table III

Electrical Properties

Reference	Resistivity (Ω-cm)	Hall Mobility (cm^2/V.sec)	Carrier conc. (cm^{-3})	Stoichiometry	Activation energy (eV)
Hirahara[71-74]		12	10^{19}-10^{21}	Cu_2S	
Eisenmann[57]	10^{-3}-10^{-2}			$\sim Cu_2S$	
Cusano[58]	10^{-2}-10^{-3}	2	$>10^{20}$	$Cu_{2-x}S$	
Harshaw[80]	10^{-1}-10^{-2}	1-10	10^{18}-10^{19}		
Potter & Schalla[81,82]			10^{20}-10^{21}		
Ellis[65]	6-65			$Cu_{1.8}S$	
Abdullaev[76]		25	$7.4x10^{19}$	Cu_2S	0.064
Selle & Maege[67]	2	7	$4x10^{15}$	Cu_2S	0.43
Nakayama[62]	$4.3x10^{-3}$	0.51	$2.8x10^{21}$	$Cu_{1.8}S$	
	$2.8x10^{-2}$	10^{-2}	$\sim 10^{22}$	$Cu_{1.96}S$	
	$6.7x10^{-2}$	3.6	$2.6x10^{19}$	Cu_2S	
Gustavino[69]	$2\text{-}3x10^{-3}$	1.75	$1.6x10^{21}$	$Cu_{1.8}S$	
Martinuzzi[83]	10^{-1}-10^{-2}	1.5	10^{20}	Cu_2S	0.05,1.8
Bougnot[84]	$5x10^{-2}$			Cu_2S	0.11,1.8
	$2x10^{-3}$	7	$4x10^{20}$	$Cu_{1.94}S$	0.01,.06,.42
	$7x10^{-4}$	5	$1.8x10^{21}$	$Cu_{1.85}S$	

2.3 Phases of Copper Sulfide for Efficient Photovoltaic Conversion:

From the mass change of chemiplated Cu_xS films on CdS and etching in KCN it was concluded by the Harshaw group[20] that the Cu is in the form of digenite, $Cu_{1.8}S$. A similar analysis at Clevite[55] indicated a stoichiometry of $Cu_{2.0025}S$ and suggested the presence of the chalcocite form.

The layer produced by cuprous ion treatment of doped or undoped CdS films was identified by Cusano[58] with the aid of electron diffraction to be Cu_2S, but generally with departure toward excess sulfur, $Cu_{2-x}S$. The digenite modification, $Cu_{1.8}S$, was sometimes observed. Spakowski et al.[85] examined the cuprous sulfide layer on CdS single crystals by means of electron diffraction. Thin layers showed the high temperature hexagonal modification of chalcocite, Cu_2S, whose lattice structure matches that of CdS closely. X-ray examination of thicker films indicated the orthorhomibic room temperature modification of chalcocite. The orthorhombic form was also identified by Potter and Schalla[81,82] on evaporated CdS films and by Singer and Faeth[52] and Shiozawa[55] on single crystal CdS by means of x-ray analysis. In later experiments Cook, Shiozawa, and Augustine[42] observed both chalcocite and djurleite by x-ray diffraction of single crystals that had been dipped in CuCl.

Nakayama[62] carried out x-ray analysis of the cuprous sulfide layer of ceramic cells after barrier formation by means of copper sulfate. Chalcocite, djurleite, and digenite were identified depending on the treatment.

Electron microprobe analysis of the barrier layer in CdS thin film solar cells by van Aerschodt[86] indicated a constant copper concentration in the bulk of thicker $Cu_{2-x}S$ layers. A slightly copper doped region extended into the CdS and a slight Cd doped region exists in the Cu_2S

near the interface. Cl was also found near the interface.

In 1973, Palz et al.[34] reported that the short circuit current was extremely sensitive to the composition of the Cu-S layer. They obtained the highest value of I_{sc} when x = 2.00; this value of x corresponds to the chalcocite phase. They found that I_{sc} (and the efficiency) decreased by an order of magnitude when x decreased from 2.00 to 1.96. They assumed that when x = 1.96, the Cu-S layer was djurleite because this phase is stable at 300°K for the composition range $1.91 \leq x \leq 1.96$. In their experiments they determined the value of x by an electrochemical method[70] which yields only the average value of x in the Cu_xS layer. Such an average value of x can be produced either by a mixture of phases or by a single phase. This technique is also unable to provide information about variation of composition with depth or with position on the surface of the Cu_xS layer. Therefore the electrochemical analysis does not provide unambiguous information about the composition of the film. The one analytical technique which provides such information is analysis of the x-ray diffraction pattern, since chalcocite, djurleite, digenite and other phases in the Cu-S system differ from each other in the structure they assume, a structure which is identified by x-ray diffraction studies. Palz et al.[34] did not report any x-ray diffraction analyses of their samples. This is understandable in view of the thickness of the Cu_xS layers commonly encountered on efficient Cu-Cd-S cells like those studied by Palz et al. This thickness is in the range 0.1 to 0.2 μ; to obtain a good x-ray diffraction pattern the sample thickness should be in excess of about 1 μ. In spite of these reservations about the meaning of the x-values measured

by Palz et al., their conclusions is well founded, i.e., high values of I_{sc} (and efficiency) require x values close to 2.00 which means that the film needs to be chalcocite: $Cu_{2.00}S$. More conclusive proof based on optical properties, was provided by Philips laboratories[41] that chalcocite, Cu_2S is the only $Cu_{2-x}S$ phase yielding high conversion efficiencies when combined with CdS.

CHAPTER 3

PREPARATION OF THIN COPPER SULFIDE FILMS

3.1 Introduction:

From the previous chapter, it is apparent that the major techniques for forming copper sulfide films on cadmium sulfide, are so called "wet" process and "dry" process. These techniques depend on chemical reaction of cuprous chloride with cadmium sulfide and eventually cuprous sulfide grows topotaxially on cadmium sulfide. Because of the lack of complete understanding of chemical reactions between cuprous chloride and cadmium sulphide on the surface of cadmium sulfide, these techniques lack in the reproducibility. Also these techniques require washing after the reaction is complete. Moisture is one of the reasons for the instability of Cu_2S - CdS solar cells. We have devised new techniques for producing semiconductor grade copper sulfide - namely the chemical vapor deposition (CVD) and vacuum evaporation of

copper sulfide. Both techniques have proved very successful and are widely used in semiconductor industry for producing different semiconductors. These techniques also remove the possiblity of moisture degradations.

3.2 Growth Process of Copper sulfide in CVD:

Knowledge of surface reaction potential, thermodynamic constants and fluid-dynamical properties of the reacting species can be utilized to find out the reaction rate and the stoichiometry of the copper sulfide - two very important parameters to watch carefully to get good semiconductor grade copper sulfide reproducibly. A tenative theory has been developed to give an idea of these parameters for a given set up.[87,88]

Because we are using H_2S with H_2 to transport sulfur, therefore the first thing to find out is the gas composition over the substrate. The major parameters affecting this, would be the temperature inside the reaction tube and the input mixture composition. Other parameters are flow velocity and the diffusion coefficients of the composites in the carrier gas and to some extent the geometry of the reaction tube and the substrate boat (because they affect the flow). At present only a simple model is being used in which we first postulate different gross reactions by which the input gas mixture of hydrogen and hydrogen sulfide can dissociate or react by itself

before it passes over the substrate. Then by knowing the equilibrium constants and applying the boundary conditions that the total mixture pressure is 1 atm. (in open flow system) and the ratio of S- atoms and H- atoms should be the same as in the input gas mixture, the actual gas composition at that particular reaction temperature can be found. The following reactions were postulated:

$$
\begin{aligned}
H_2 &\rightleftharpoons 2H & k_1 &= p_H^2/p_{H_2} \\
H_2S &\rightleftharpoons H_2 + S & k_2 &= p_{H_2} \times p_s/p_{H_2S} \\
2S &\rightleftharpoons S_2 & k_3 &= p_{S_2}/p_S^2 \\
3S_2 &\rightleftharpoons S_6 & k_4 &= p_{S_6}/p_{S_2}^3 \\
4S_2 &\rightleftharpoons S_8 & k_5 &= p_{S_8}/p_{S_2}^4 \\
Cu(s) &\rightleftharpoons Cu(v) & k_6 &= p_{Cu}
\end{aligned}
\qquad (3.1)
$$

(k's are equlibrium constants and p_i is the partial pressure of ith species).

And the boundary conditions were:

1) $\Sigma p_i = 1$ atm.

2) $$\frac{p_{H_2S} + p_S + 2p_{S_2} + 6p_{S_6} + 8p_{S_8}}{2p_{H_2} + p_H + 2p_{H_2S}} = \frac{p_{H_2S}\ (input)}{2p_{H_2}\ (input) + 2p_{H_2S}} \qquad (3.2)$$

If more rigorous calculation is desired, then in second boundary condition, diffusion coefficients of the constitutents in the carrier gas, stagnant layer thickness above the substrate etc. would be needed for the fact that besides the above reactions, the diffusion of the constituents through the gas stagnant layer towards the substrate also affects the gas composition right over the substrate. The result of above calculations is

that for our present experimental set up H_2S does not really decomposes at 300°C when the dilution is low up to 0.5% in H_2. But for higher temperature and low input H_2 partial pressures we have to follow above technique to get the gas composition because in these conditions more dissociation of H_2S is expected.

After the gas composition is known, the next problem is to find out how different constitutents react with the Cu film and hence the reaction rate. In deriving the rate equation we have assumed that the whole mechanism is divided into two parts - first is the mass transfer of the reactants through the stagnant layer over the substrate and secondly the surface reaction. We further assumed that the reaction mechanism is governed by the Cu diffusion through copper sulfide lattice and that the overall reaction is of first order. The last two assumptions may not be fully justified but the simplicity of the formulation due to these assumptions make them worth assuming for a tenative theory.

For the reaction -

$$2Cu + H_2S \rightleftharpoons Cu_2S + H_2$$

in H_2 ambient the following result can be readily obtained by considering both forward and reverse reactions:[87,88]

$$R = \frac{h_G(H_2S)}{N(Cu_2S)} \times \left[\frac{C_G(H_2S) - \frac{1}{k} \cdot C_G(H_2)}{1 + \left(\frac{1}{k.h_G(H_2S)} + \frac{1}{k_s} \right) \cdot h_G(H_2S)} \right] \qquad (3.3)$$

where:

R	-	rate of growth of Cu_2S (thickness/time)
h_G	-	mass transfer coefficient (thickness/time)
$N(Cu_2S)$	-	number of Cu_2S molecules/cm^3 = 2.12 x 10^{22} mol/cm^3
k	-	equilibrium constant for above reaction
C_G	-	gas concentration over the substrate (mol/cm^3)
k_s	-	surface reaction rate (thickness/time)

Mass transfer coefficient can be determined as:

1) $h_G = \frac{D_G}{\bar{\delta}}$ (without any temp. grad. over substrate)[89]

2) $h_G = \frac{D_G}{\bar{\delta}} \cdot \frac{\Delta T}{T} \cdot \frac{1}{\ln(T_s/T_g)}$ (with temp. grad. over substrate)[90]

3) $h_G = \frac{D_G}{\bar{\delta}} \cdot \frac{\Delta T}{T} \cdot \alpha \cdot \frac{T_s^{\alpha}}{T_s^{\alpha} - T_g^{\alpha}}$ (with temp. grad. & thermal diffusion)[90]

In the above formulae -

$D_G = D_o \left(\frac{T}{T_o}\right)^2$ where D_o is diffusion constant at T_o = 273°K and T is temperature in °K.

T_g = gas temperature in °K

T_s = substrate temperature in °K

$\Delta T = T_s - T_g$

α = thermal diffusion factor[90]

$\bar{\delta}$ = stagnant layer thickness given by-

$x/\bar{\delta} = 0.023\ R_e^{0.83}\ Sc^{1/3}$ for circular cross section reaction tubes[91]

x = length of substrate

R_e = Reynold number for the gas flow

Sc = Schmidt number for gas flow

Surface reaction rate frequency is given by[92]

$$K_{reac} = \frac{k_B T}{h} \exp\left(\frac{\Delta S}{k_B}\right) \exp\left(-\frac{E_a}{k_B T}\right) \quad (\text{time}^{-1})$$

where:

k_B = Boltzman constant

T - temperature

h = Planck's constant

ΔS = molar entropy change during reaction

E_a = activation energy for surface reaction

Therefore it is reasonable to write the surface reaction rate as:

$$k_s = K_{reac} \cdot \sigma_c$$

where σ_c is the collision diameter for Cu_2S = 2.827 Å.

In this way reaction rate can be determined. Once the amount of the deposited S- atoms is known, the resultant phase and stochiometry can be predicted from the Cook's phase diagram[43] for Cu -S system.

3.3 EXPERIMENTAL SET - UP & RELATED EXPERIMENTS

Chemical vapor deposition of copper sulfide in usual sense is quite difficult because of its low vapor pressure[93] and high rate of polymerisation of dissociated S-vapor. Faktor & Garrett[94] suggest an alternative way to overcome such problems in CVD - e.g. employment of a transport agent which reacts with the substrate to form the desired molecules. There are some reports in the literature on producing $Cu_{2-x}S$ by the sulfurization of copper using H_2S gas or S-vapor[96-103] but none of them do it with the intention of producing semiconductor grade copper sulfide except for one[104].

In our experiments, semiconductor grade, polycrystalline films of copper sulfide can be conveniently prepared by sulfurizing copper films deposited on some suitable substrate by external means (vacuum deposition, electro-plating etc.) and by adjusting the different reaction parameters (sulfur concentration, reaction time etc.) various phases of Cu - S system can be produced.[105] The CVD system has been so developed that the sulfurization can be achieved either using commercially available chemical purity grade H_2S gas (can be further purified using a solid CO_2 trap) or by insitu production of S-vapor/H_2S. Ultra high purity H_2gas from Engelhard Hydrogen Purifier (using Palladium diffusion process) is used as carrier gas/dilutant and laboratory purity N_2 gas as general purge gas. With some modifications this system could also be adapted to organic vapors containing S-molecules to bring about sulfurization.

The system and its controls are shown in figures 8-11 . Mainly it is a horizontal single zone Lindberg furnace of 2070 Watts, converted into two zone furnace with the help of an external heater. Typical temperature profiles of the furnace are shown in figures 12-13. The reaction tube is

FIGURE 8: Schematic of the sulfurization system.

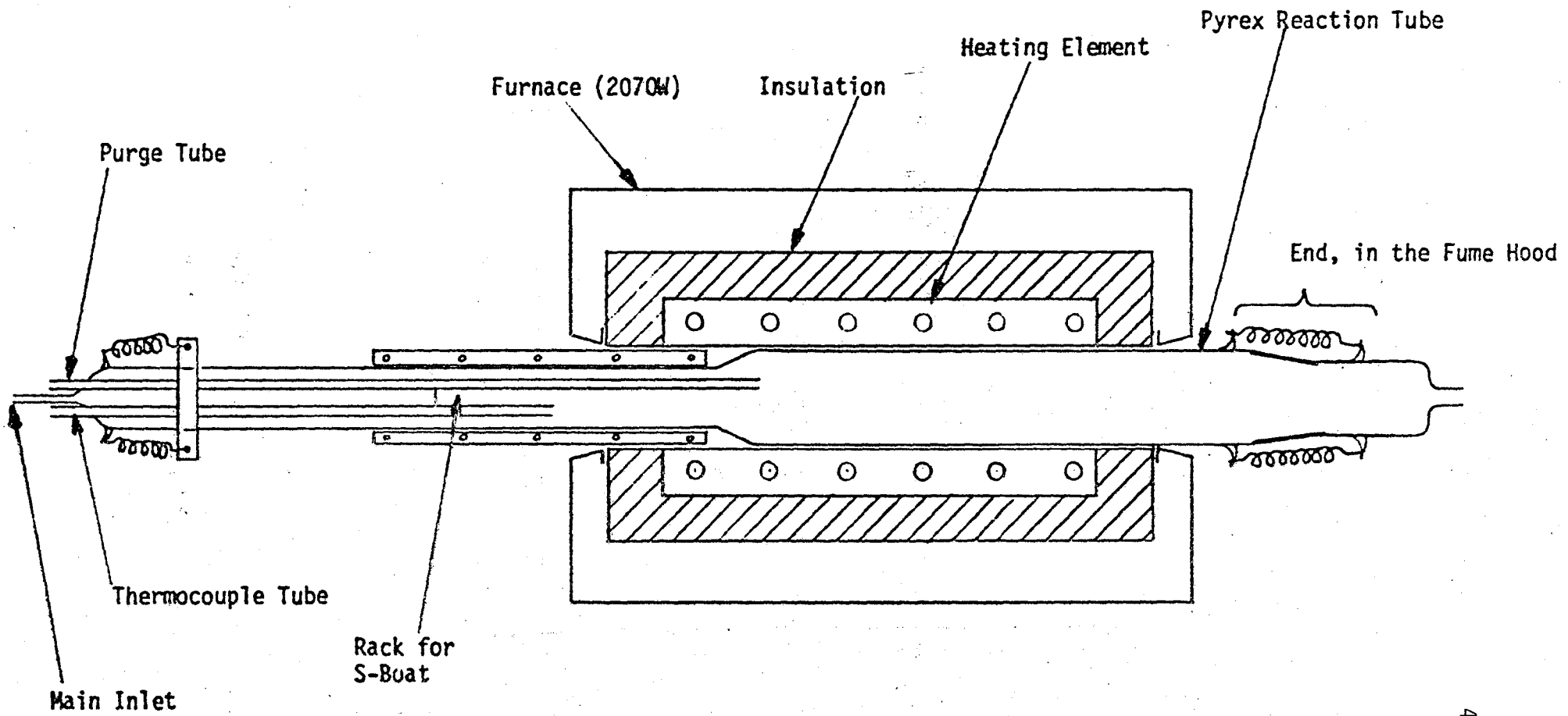
Pyrex Reaction Tube
Heating Element
Furnace (2070W)
Insulation
Purge Tube
End, in the Fume Hood
Thermocouple Tube
Rack for
S-Boat
Main Inlet

FIG. 8

FIGURE 9: Flow diagram for the sulfurization system.

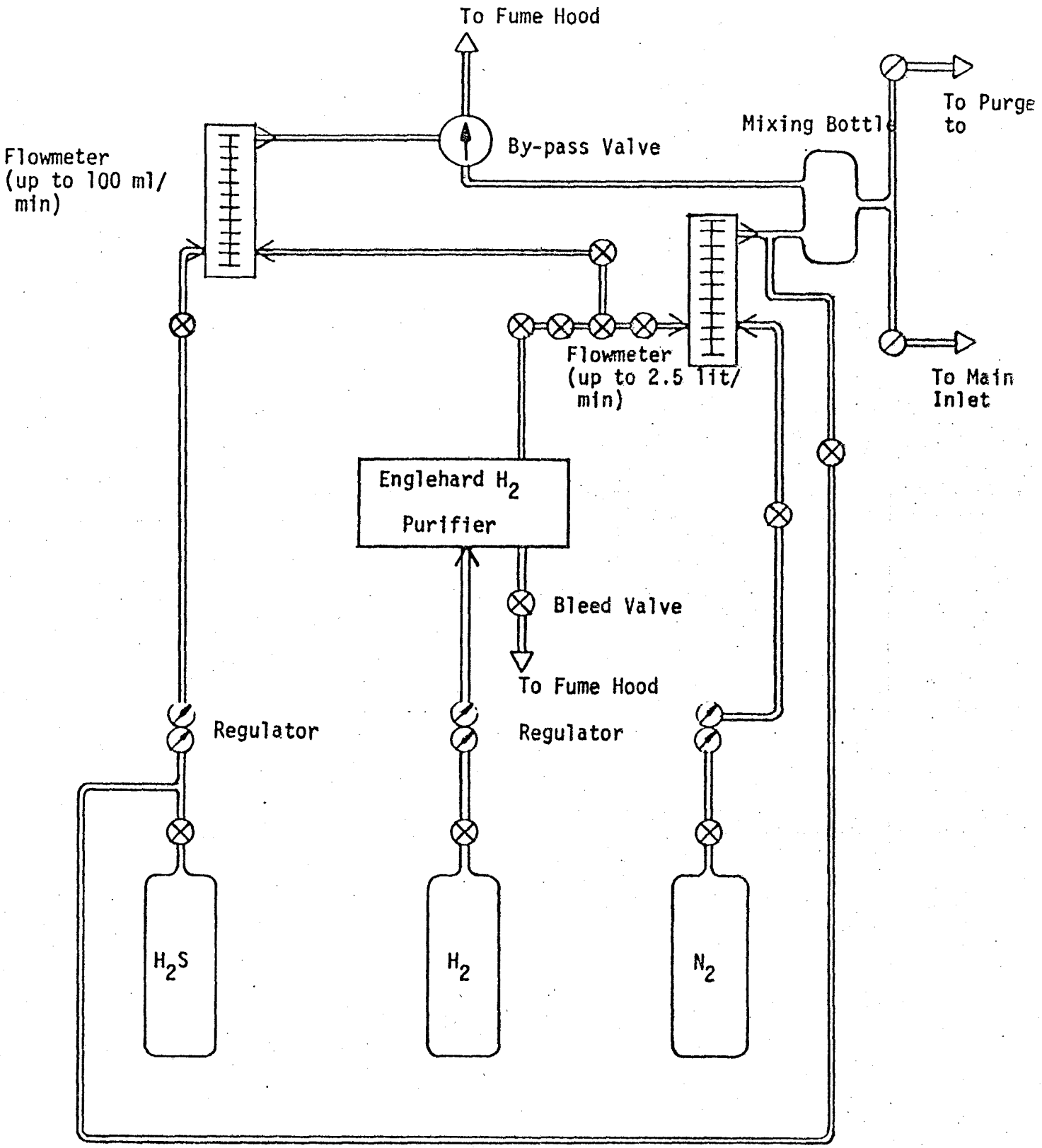
To Fume Hood
By-pass Valve
Mixing Bottle
To Purge to
Flowmeter (up to 100 ml/ min)
Flowmeter (up to 2.5 lit/ min)
To Main Inlet
Englehard H_2 Purifier
Bleed Valve
To Fume Hood
Regulator
Regulator
H_2S
H_2
N_2

FIG. 9

FIGURE 10: Connection scheme of the gas regulators.

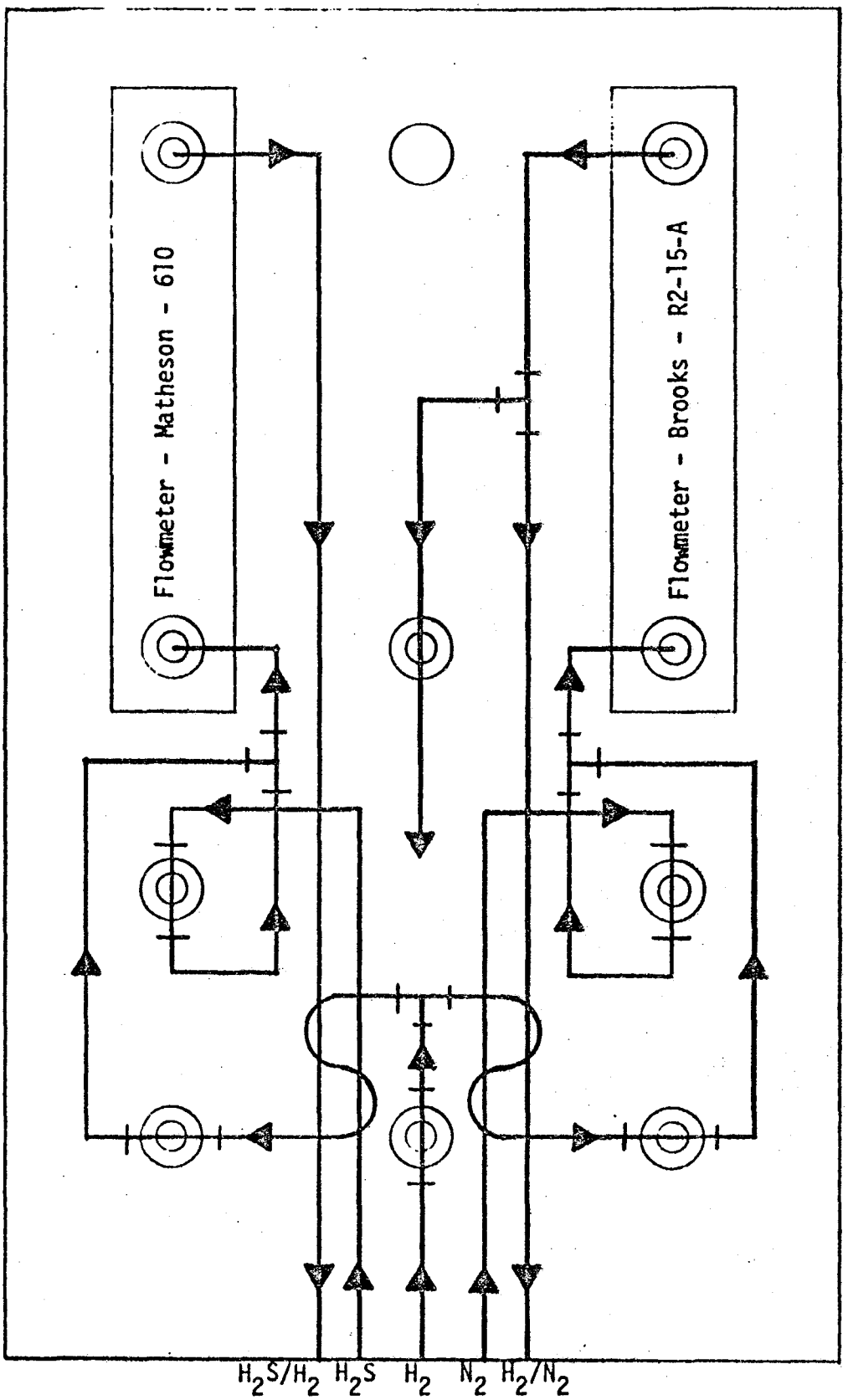
Flowmeter - Matheson - 610
Flowmeter - Brooks - R2-15-A
H_2S/H_2
H_2S
H_2
N_2
H_2/N_2

FIG. 10

FIGURE 11: Connection scheme for the gas mixing bottle.

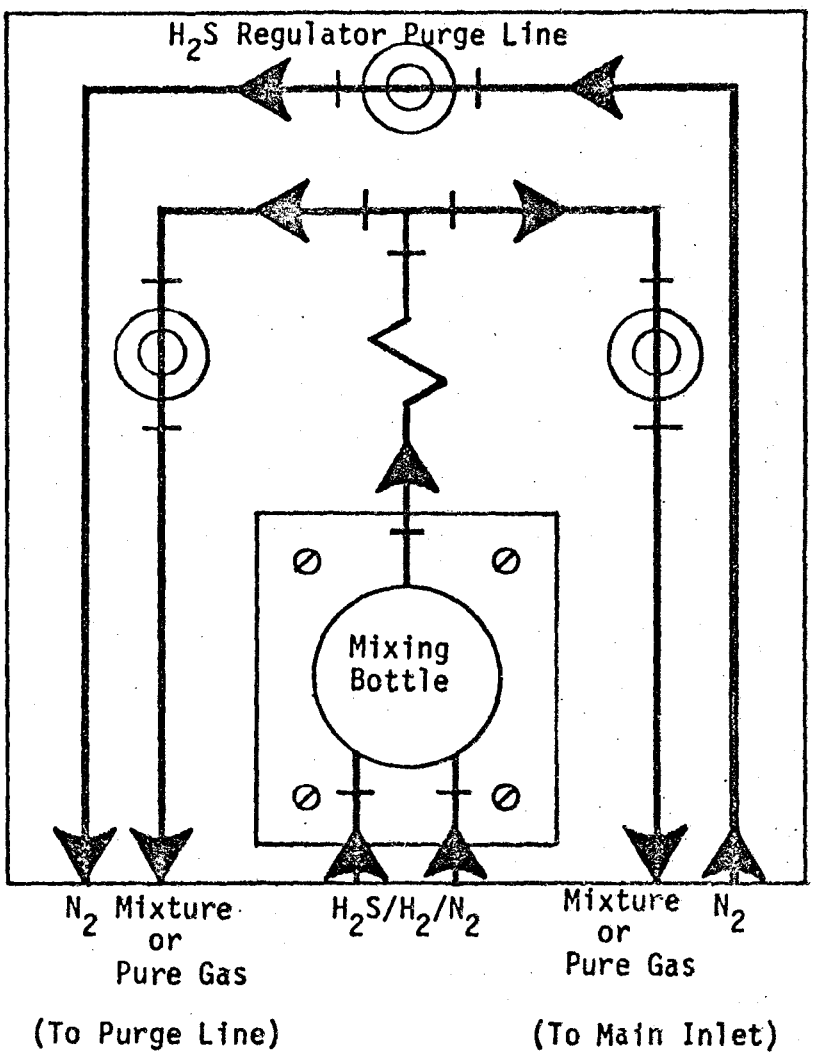
H_2S Regulator Purge Line
Mixing Bottle
N_2
Mixture or Pure Gas
$H_2S/H_2/N_2$
Mixture or Pure Gas
N_2
(To Purge Line)
(To Main Inlet)

FIG. 11

FIGURE 12: Temperature profile of the sulfurization furnace with external heater off.

FIG. 12

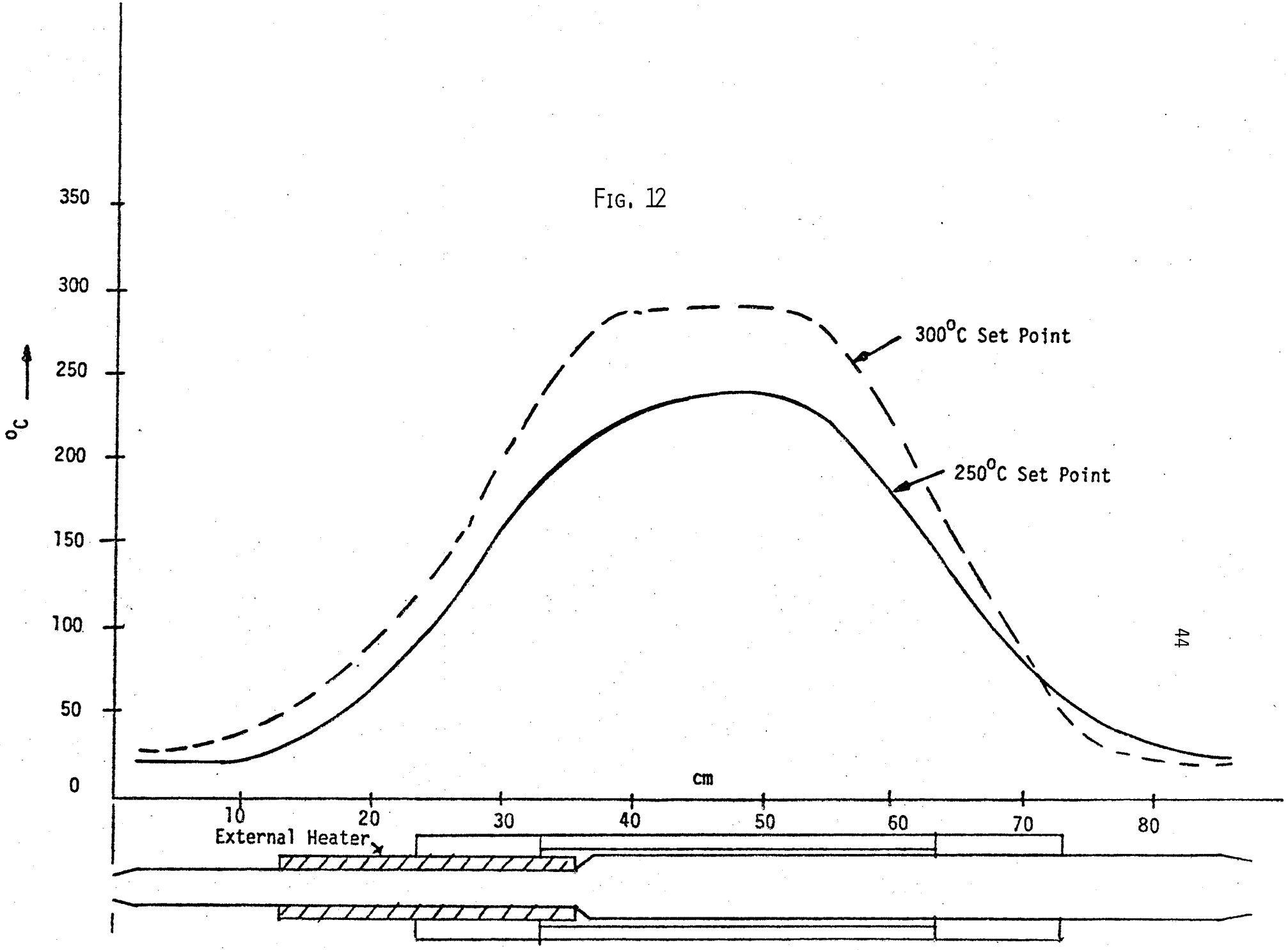
350
300
250
200
150
100
50
0
°C
300°C Set Point
250°C Set Point
cm
10
20
30
40
50
60
70
80
External Heater

FIGURE 13: Temperature profile of the sulfurization furnace with the external heater on.

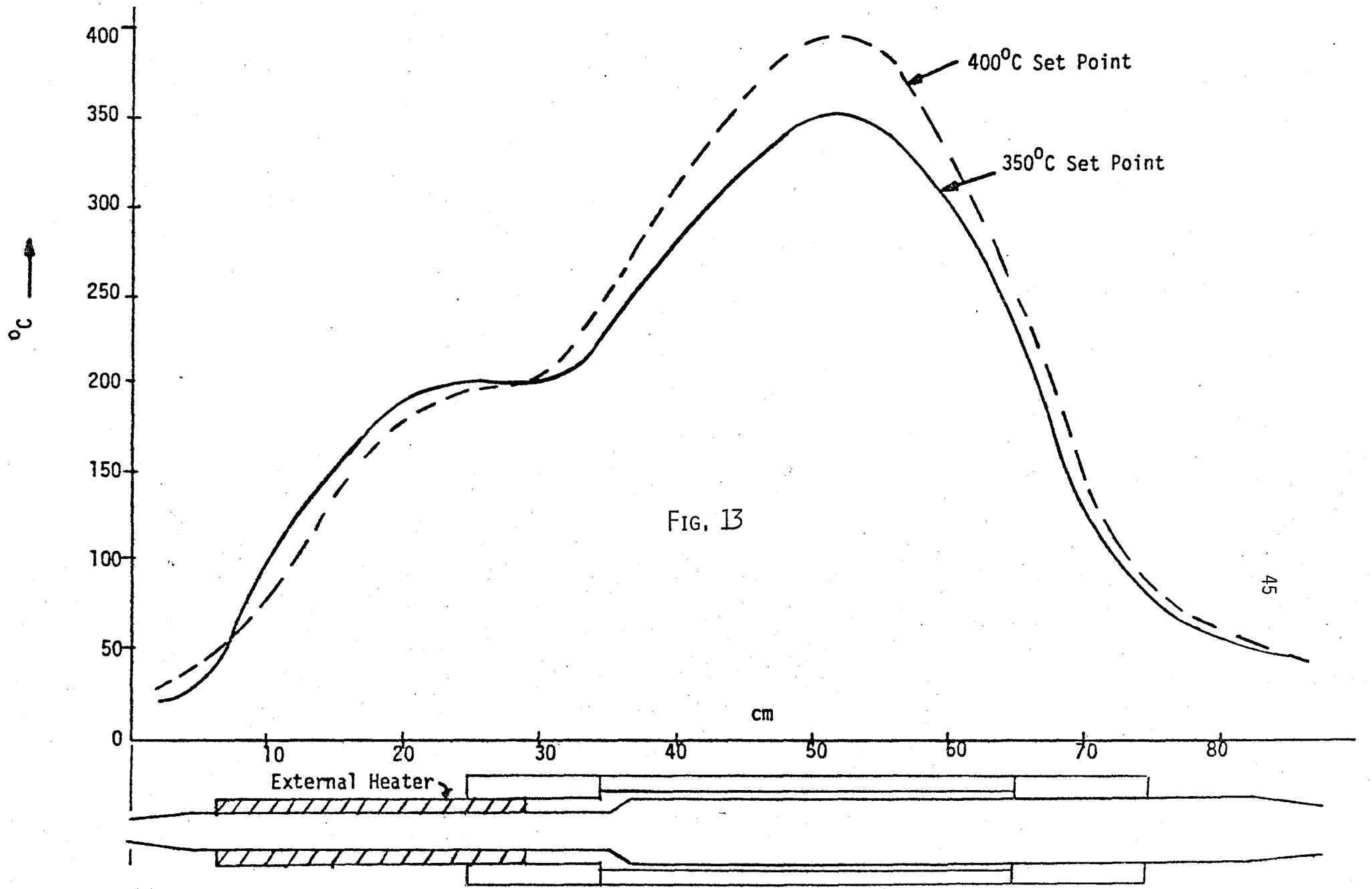
400
350
300
250
200
150
100
50
0
°C
400°C Set Point
350°C Set Point
cm
10
20
30
40
50
60
70
80
External Heater

FIG. 13

made of Pyrex and its exhaust goes into a fume hood. The whole system is also covered with another fume hood to guard against any accidental leak. One part of the reaction tube is engulfed by the external heater and is used to evaporate sulfur when insitu production of S-vapour/H_2S is desired. The S-boat can rest on the rack formed by the thermocouple tube and purge tube connected to the end cap. The purge tube goes beyond S-boat so that during purging, S- vapors are contained with S-source section of the reaction tube. When external H_2S gas is used, the S-boat is not placed inside the reaction tube.

The gas flow rates are controlled by two calibrated rotameter type flowmeters - one of these can handle equivalent flows up to 100 ml/min. (used for H_2S gas) and other up to 2.5 lit/min. (used for H_2 and purge gas) of air at atmospheric pressure. The actual layout of the connections is shown in figures 10,11.All the connections and joints are of 316 stainless steel to avoid any corrosion by H_2S and all of them are regularly leak tested.

Studies have been carried out using external H_2S gas for sulfurization. The present sulfurization procedure adopted after several modifications is as follows:

1) Maintain the temperature of the furnace at the desired temperature (300°C) with precleaned and etched reaction tube containing substrate boat.

2) Before sulfurization keep the tube flushed with bubbling N_2 flowrate ≈10 ml/min.) at all times.

3) Just before sulfurization purge the tube using H_2 for at least 15 min. at a flowrate of 3 lit/min. at 14 psig. This is done because H_2 is much more pure than N_2 and we want to reduce contaminations as much as possible.

4) Open the end cap in the fume hood and place the sample on the substrate boat and push it in the heart of the furnace where the temperature

profile is flat (≈37 cm. from the end cap). Close the end cap and the fume hood.

5) Keep purging H_2 for another 15 min. during which time the sample comes into thermal equilibrium and the Cu surface is reduced by the flowing H_2 so that no oxide layer is left behind.

6) During above period, stabilise the flowrate of H_2S gas (=15 ml/min. at 14 psig.) and keep it bypassing using the bypass valve.

7) Let the sulfurization take place for the desired time (depends on the Cu film thickness for a given H_2S concentration, temperature, flowrates etc.) by switching the H_2S flow so that instead of bypassing it, it mixes with H_2 in the mixing bottle (fig11). At about 300°C and above, the H_2S concentration and flowrates, copper conversion rate has been found to be about 2 Å/sec.

8) As soon as sulfurization is over, again bypass the H_2S and close the H_2S gas bottle. Wait for another 10 min. so that all the H_2S is removed from the reaction tube. Sulfurization time is counted from the instant when H_2S is mixed with H_2 to when it is again bypassed, to compensate time lag due to finite volume to be covered by the gas between the valve and the substrate.

9) Open the fume hood and the end cap inside it to push back the substrate boat to the edge of the reaction tube. Close the end cap and wait for the cooling of the sample (∿ 5 min.).

10) Remove the sample from the reaction tube. Purge the H_2S regulator with H_2 (H_2S, if purged with N_2 dissociate inside the hot reaction tube and therefore white elemental Sulfur gets deposited on the cooler parts of the reaction tube, like end caps.)

11) After purging the regulator, close the purge valve. After some time stop H_2 flow and return to N_2 bubbling thru the reaction tube, round the clock.

After the set up of the sulfurization unit and some initial experiments to get familiarized with the system, it was used on regular basis for producing copper sulfide to characterize the system. Copper foils obtained from several sources (Noranda Mines Ltd., BDH Chemicals - 99.9 - 99.95% pure, and Material Research Corp.) were sulfurized. Before sulfurization some of them were etched in freshly prepared ferric chloride solution/dilute aqua regia, but the results were not satisfactory because these etchants were too fast and therefore produced etch pits to cause nonuniform sufurization. On the other hand foils which were mechanically polished (up to 0.05 μ final polish) and ultrasonically cleaned in organic chemicals gave good and uniform sulfurized films. Sulfurization rate has been monitored by finding out the mass difference for the foil before and after sulfurization for a fixed time.[105] The Cu foils of about 1-2 mils thickness were not completely sulfurized in a single run of 30-60 min. after which the mass increase was noted down. Therefore the following scheme was used to find out the conversion rate:

If the mass increase is Δm then the mass of Cu_2S formed is $m_{Cu_2S} = (M_{Cu_2S}/M_S).\Delta m$, because Δm is due to deposited sulfur molecules only (M is the molecular weight). The above use of M_{Cu_2S} is justified from the Cook's phase diagram of Cu -S system, which says that till the addition of 33% S- atoms, the only phases present will be Cu_2S and Cu, which is the case for incomplete sulfurization of Cu foil. Now the thickness of Cu_2S layer will be $t_{Cu_2S} = (m_{Cu_2S}/\rho_{Cu_2S}.A)$ where ρ_{Cu_2S} is the density of Cu_2S and A is the area of sulfurized film. Therefore the thickness of Cu film which was sulfurized

will be $t_{Cu} = t_{Cu_2S}/1.9311$. The factor of 1.9311 comes because the thickness of Cu_2S, t_{Cu_2S}, after the sulfurization of t_{Cu} thick copper layer will be:

$$t_{Cu_2S} = \frac{M_{Cu_2S} \cdot \rho_{Cu}}{2.M_{Cu} \cdot \rho_{Cu_2S}} \cdot t_{Cu} \qquad (3.4)$$

$$= 1.9311 \; t_{Cu}$$

Therefore if the time for sulfurization is noted, conversion rate can be found out.

After the rate was found, thin 99.99% pure Cu films were vacuum deposited on other precleaned substrates (glass, silicon wafers, aluminum foils, etc.) to bring about complete sulfurization of Cu film in reasonable time and to confirm above rate. To increase the adhesion of Cu on glass substrates, a 30-40 Å Al layer was deposited before Cu evaporation. It was found that for 300°C with 0.5% H_2S in H_2 flowing at 3 lit/min (14 psig) before entering the reaction tube, the conversion rate of sulfurizing Cu into Cu_2S was about 2 Å/sec. This is interesting to note that our tentative theory give about 6 Å/sec for the above conditions. The conversion rate for slow flow rate (1 lit/min) was much faster as also predicted by the theory and was rather hard to monitor.

3.4 EVAPORATION OF CUPROUS SULFIDE:

Vacuum deposition of Cu_2S was first attempted by Clevite. Initially this was done on backwall cells. The Cu_2S was evaporated onto a glass substrate followed by the CdS layer.[14,15] At a much later stage it was attempted to form the junction by vacuum deposition of Cu_2S, followed by immersion in Na_2S. In another variation copper was vacuum deposited followed by immersion in a solution of sulfur in benzene. None of these attempts was successful in making efficient solar cells.

Recently, Couve et.al.[70] have tried to evaporate cuprous sulfide. Composition of their films was around $Cu_{1.9}S$. David et.al.[106] and Ellis[65] employed flash evaporation of cuprous sulfide powder. Copper sulfide has also been deposited using reactive sputtering technique by Hsieh.[107] Of all the possible techniques, we have chosen to evaporate from resistive heated filament as this is the cheapest possible technique to evaporate.

To provide copper sulfide films for different experiments, an NRC 3117 high vacuum evaporator was set-up. High purity Cu_2S pressed bars were evaporated from a Tungsten boat. Although Mo and Ta boats are also used in the industry for resistive filaments, these elements are "wetted" by Cu_2S and therefore are not useful for our purpose. To contain the evaporation stream and to allow a view of the source during the melt and subsequent evaporation sequence, a pyrex glass shroud was designed.[108] A schematic of the system is shown in fig.14 . Various substrates were arranged on a work holder which could be cooled by running water or could be heated by cartridge heating filaments (Chromalax). The source to substrate distance was held constant at 20 cm. The temperature of this work holder

FIGURE 14: Schematic of the evaporation system. An NRC 3117 high vacuum system has been used.

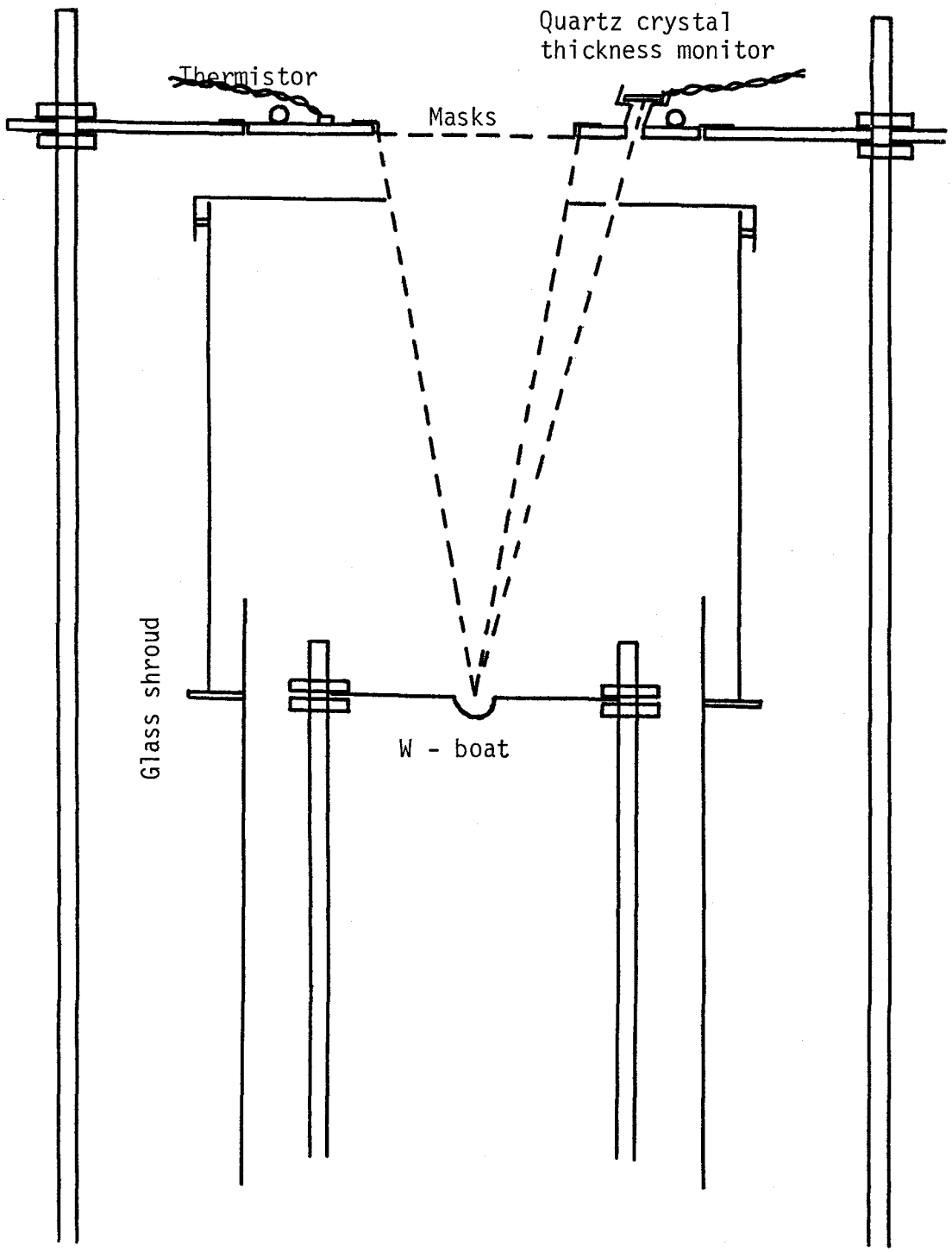
Quartz crystal
thickness monitor
Thermistor
Masks
Glass shroud
W - boat

FIG. 14

was monitored by a thermistor (Fenwell Elect. GN32P422). The thickness of the evaporated films was controlled using a quartz crystal monitor placed near the substrates and the rate of evaporation was controlled using the XTM-200 rate controller (Inficon). The substrate preparation is discussed in Chapter 5.

After mounting the substrates and placing about a 200 mg charge of Cu_2S pressed bar in the 5 mil thick tungsten dimple boat, the bell jar is pumped down. Vacuum of 1 to 2 x 10^{-7} Torr is reached using the cold trap. Substrate temperature is usually maintained at 17°C. The actual evaporation is divided into a number of stages including rise time, soak time, rate adjustment, evaporation and finally the firing of remaining charge from the boat in preparation for the next run. A schematic of the evaporation sequence is shown in Fig. 15.

For solar cells, besides the evaporation of Cu_2S, contact evaporations are also needed. The contacts were evaporated in an Edwards vacuum system at about 10^{-4} - 10^{-5} Torr. For contacts to the Cu_2S, high purity gold (Ventron Corp., Alpha products) was evaporated from a tungsten conical filament boat (GTE Sylvania) and for back-contact to n-Si, first a Cr-layer was deposited from Cr coated W-wire (R.D. Mathis) followed by gold deposition.

FIGURE 15: Schematic of evaporation sequence for copper sulfide pressed bars.

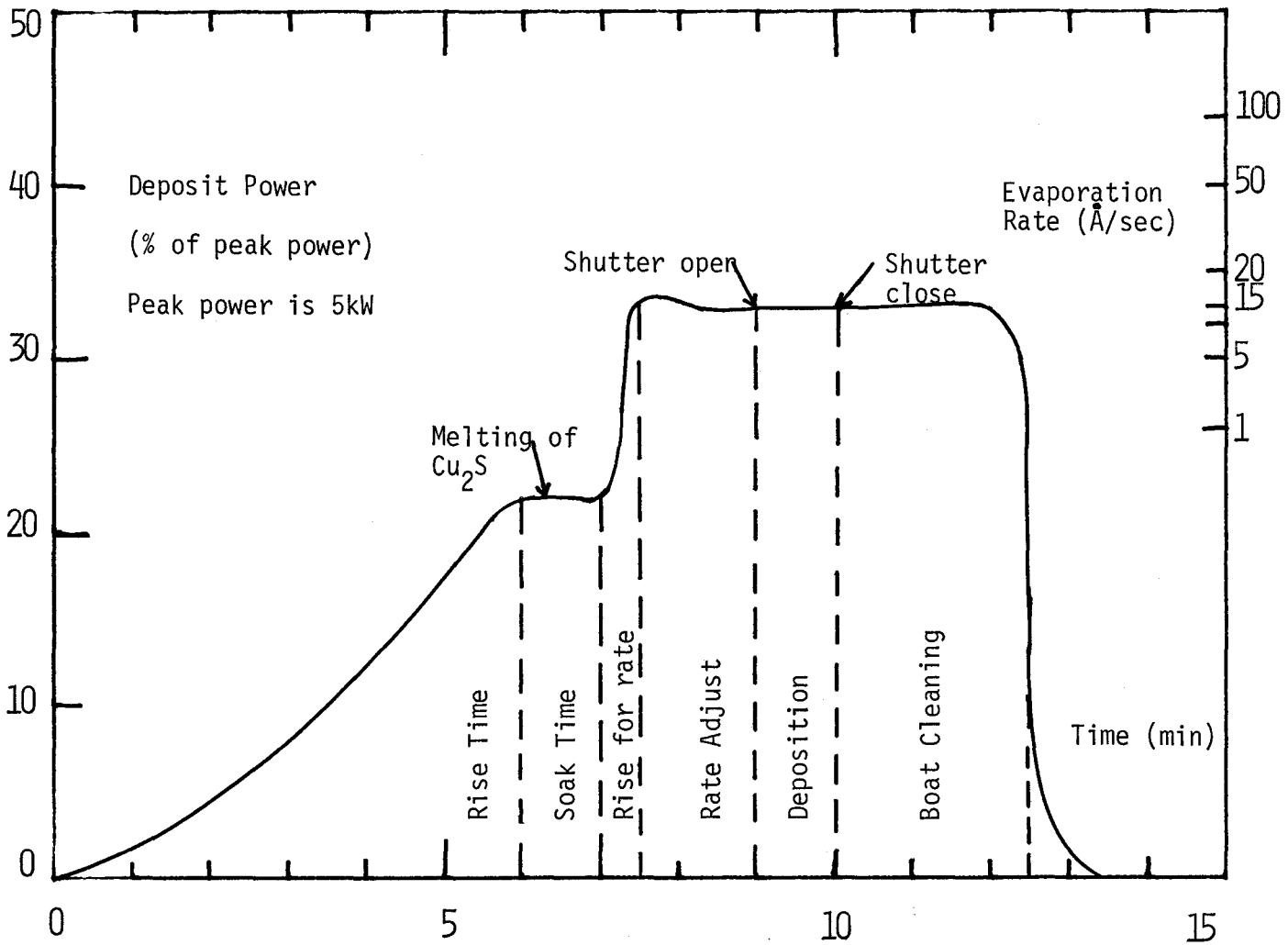
50
40
30
20
10
0
Deposit Power
(% of peak power)
Peak power is 5kW
100
50
20
15
5
1
Evaporation
Rate (Å/sec)
Shutter open
Shutter
close
Melting of
Cu_2S
Rise Time
Soak Time
Rise for rate
Rate Adjust
Deposition
Boat Cleaning
Time (min)
0
5
10
15

FIG. 15

3.5 PREPARATION OF Cu_2S PRESSED BARS

For evaporation purposes, high purity of copper sulfide charge is essential. Commercially availabe cuprous sulfide (Matheson Coleman and Bell, for example) is not pure enough to use for semiconductor purposes. Therefore we established a technique to obtain high purity Cu_2S powder which then could be pressed into bars for evaporation.

Pure cuprous sulfide was synthesized by firing stochiometrically weighed pure copper powder (Grade 1, from Johnson Mathey Chem. Ltd.) and vacuum sublimed sulfur. In principle, it appears to be easy, but there are couple of details to look after. One of the problems is that copper and sulfur are weighed only up to four decimal places using a chemical balance (Mettler, type H15 electronic balance was used). Therefore to obtain right stochiometry, weights of copper and sulfur have to be chosen in such a manner that the fourth decimal of their weights is not significant - a small error in the weights would lead to a different Cu-S compound.

Further, although high purity copper and sulfur were used, it is necessary to reduce the copper powder and sublime the sulfur powder again before the use to remove any remaining traces of impurities. The copper powder was reduced in Ar - H_2 atmosphere at 550°C to remove any oxide film formed during storage. Sulfur is difficult to sublime. As it is evident from its phase diagram[109] in Fig. 16, it sublimes only

FIGURE 16: Phase diagram of sulfur.

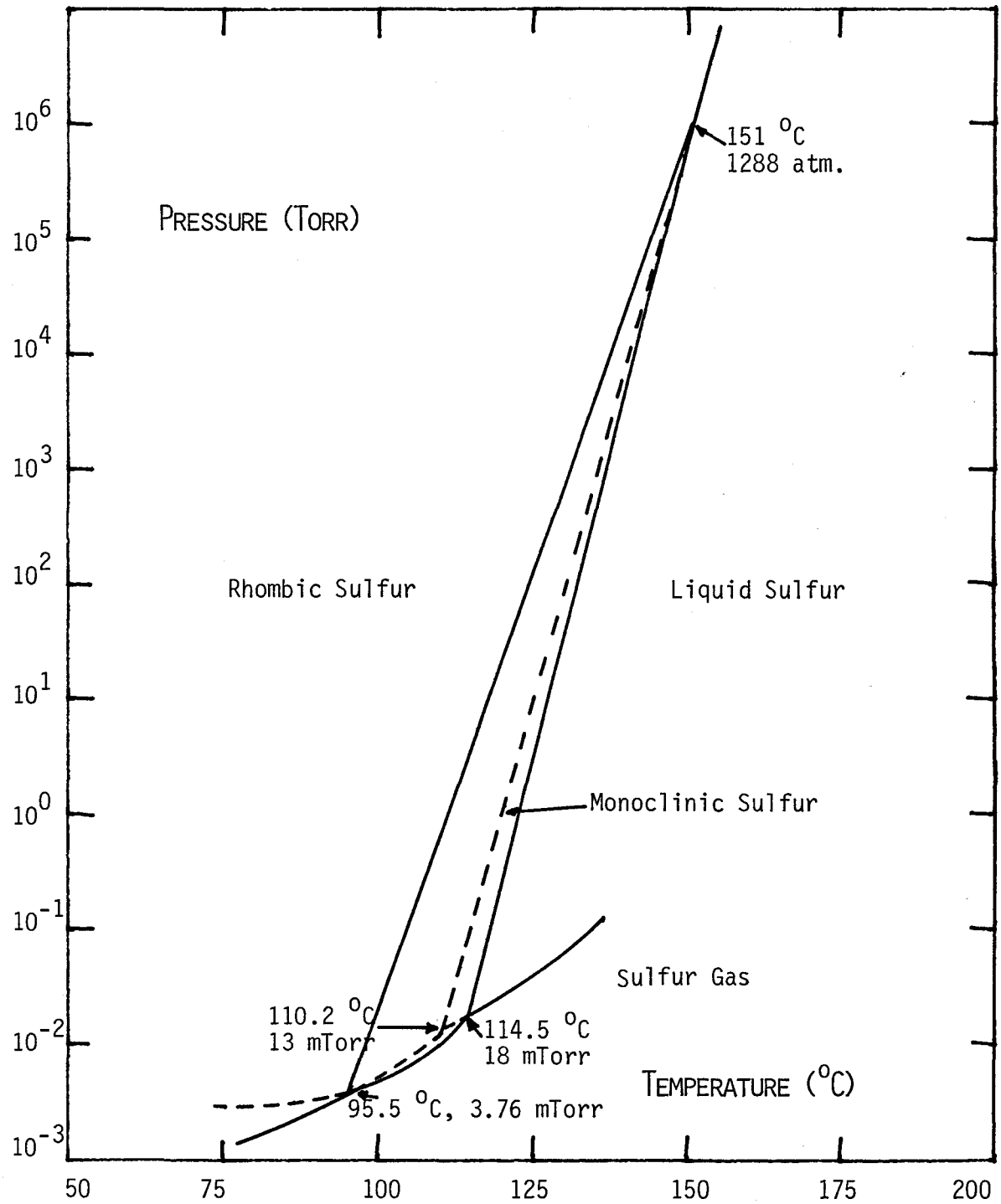
PRESSURE (TORR)
10^6
10^5
10^4
10^3
10^2
10^1
10^0
10^{-1}
10^{-2}
10^{-3}
151 °C
1288 atm.
Rhombic Sulfur
Liquid Sulfur
Monoclinic Sulfur
Sulfur Gas
110.2 °C
13 mTorr
114.5 °C
18 mTorr
95.5 °C, 3.76 mTorr
TEMPERATURE (°C)
50
75
100
125
150
175
200

FIG. 16

below ∿4 mTorr at 96°C. The sublimator was therefore evacuated during the sublimation.

The reaction between copper powder and sulfur powder is highly exothermic. Therefore, they were put in a quartz tube and sealed carefully under vacuum of better than a millitorr. The reaction was carried out at 400°C for about 12 hours. After this, the resultant Cu - S compound was x-rayed, crushed and refired until the final composition as obtained from x-ray, was Cu_2S. Usually it takes only one refiring after initial reaction.

Cuprous sulfide powder, so obtained, was pressed into bar shaped specimens for evaporation purposes. A hydraulic press (Specac) and up to 10 tons of applied pressure were used. High pressures were found necessary to exclude trapped gases from the bars. Such gases caused the bar to "dance" upon heating in the vacuum and base pressure in the bell jar increased rapidly.

CHAPTER 4

CHARACTERIZATION OF COPPER SULFIDE THIN FILMS

4.1 X-RAY DIFFRACTION:

X-ray diffraction provides a well developed and positive method for identifying materials. The x-ray equipment employed for crystallographic analysis of copper sulfide, is a standard Philips powder diffractmeter with automatic scanner. Data is collected on a strip chart recorder and peaks are analysed for their relative angular position, 2Θ. Cu Kα radiation ($\lambda \simeq 1.54$ Å) was used in all experiments.

The x-ray diffraction pattern of Cu_2S (Chalcocite) is distinctly different from that of $Cu_{1.96}S$ (Djurleite) or $Cu_{1.8}S$ (Digenite). Figure 17 shows the calculated x-ray patterns for chalcocite and djurleite, as given by Cook[43]. Figure 18 shows the observed x-ray patterns for the chalcocite and djurleite mineral samples, as obtained by Brown University, U.S.A.[110]. For these samples, only the stronger lines are recorded to avoid confusion with the background noise. Examination of these spectra shows that neither mineral is "pure", but that one of the Cu-S phases dominates.

X-ray data taken on the pressed bars of Cu_2S is shown in Table IV along with many of the spectra reported in the literature[111]

FIGURE 17: Calculated x-ray patterns of chalcocite (Cu_2S) and djurleite ($Cu_{1.93}S$) phases of copper sulfide.

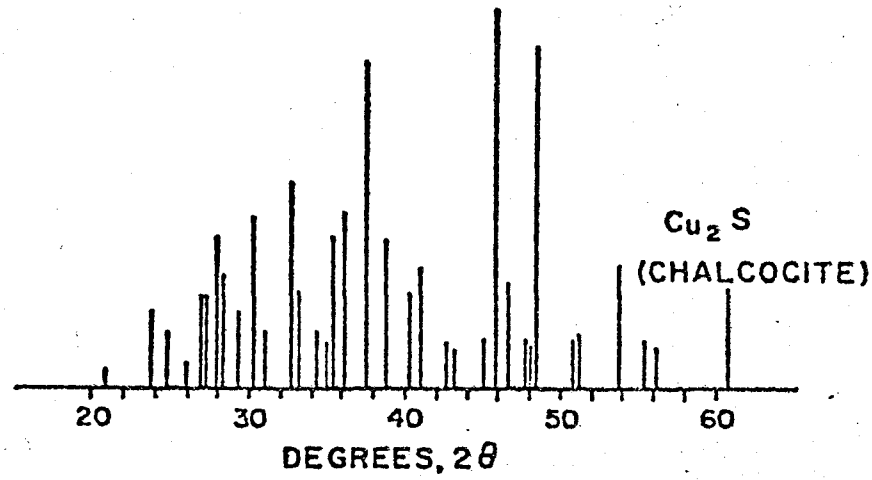
Cu_2S
(CHALCOCITE)
20
30
40
50
60
DEGREES, 2θ

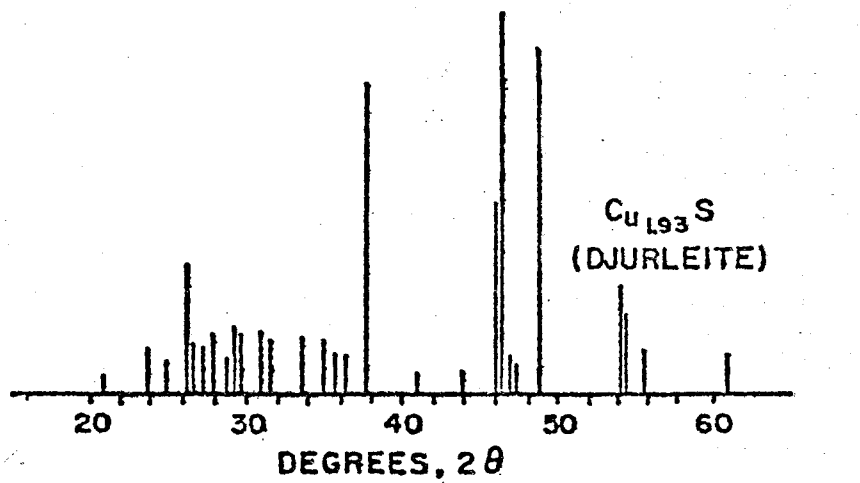
$Cu_{1.93}S$
(DJURLEITE)
20
30
40
50
60
DEGREES, 2θ

FIG. 17

FIGURE 18: Observed x-ray patterns of chalcocite and djurleite minerals obtained by Brown Univ.

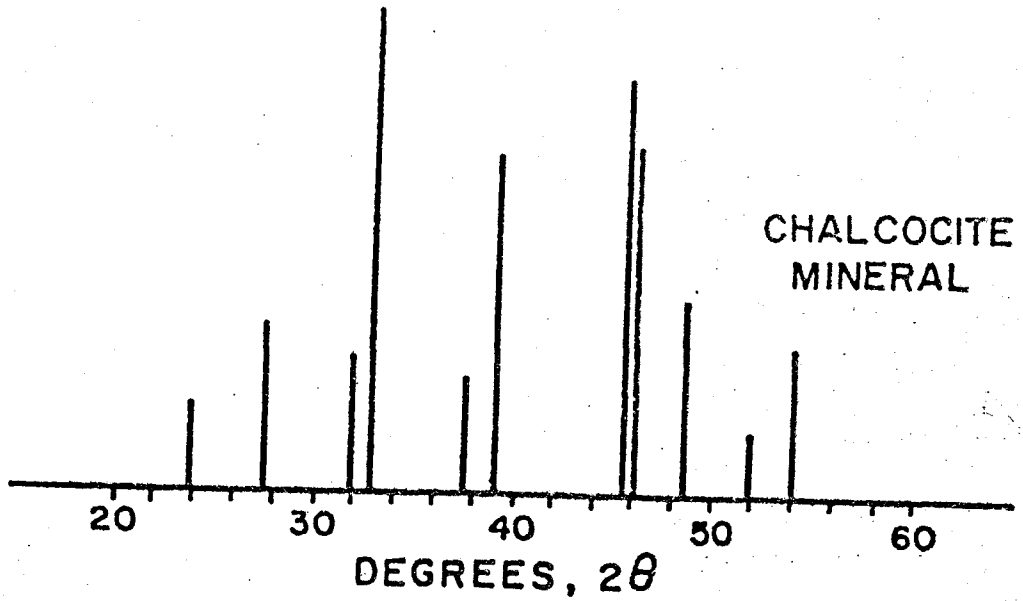
CHALCOCITE
MINERAL
20
30
40
50
60
DEGREES, 2θ

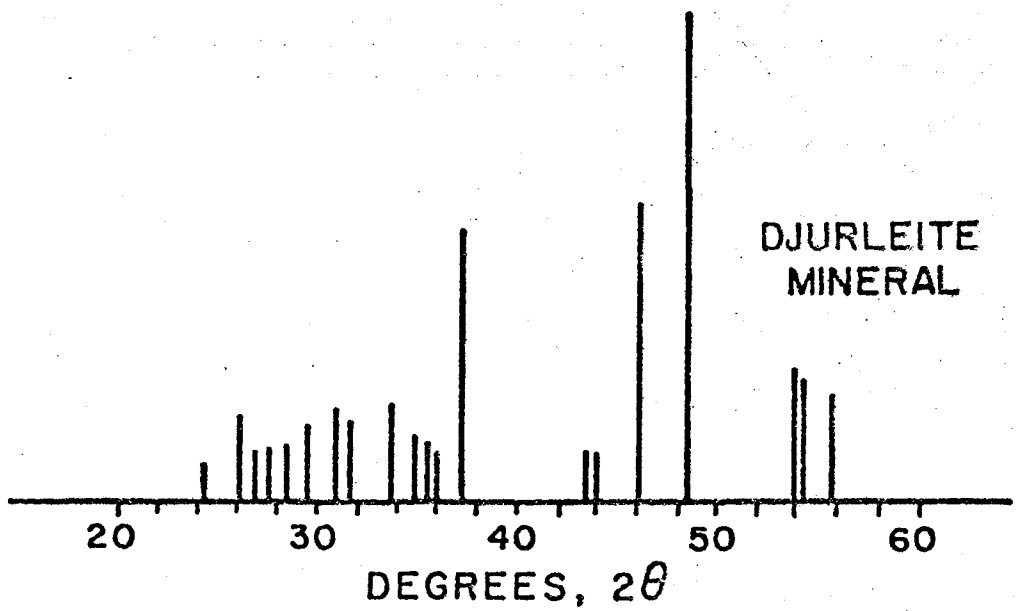
DJURLEITE
MINERAL
20
30
40
50
60
DEGREES, 2θ

FIG. 18

TABLE IV

MAJOR X-RAY PEAK POSITIONS (2θ) OF Cu_2S

Relative Intensities in Parenthesis (>20%)

Cu_2S Pressbar	Cu_2S Chalcocite	Cu_2S Hexagonal	$Cu_{1.93}S$ Djurleite	Cu_xS 1.96>x>1.86	$Cu_{1.8}S$ Digenite
			26.3(35)		
				26.6(55)	
27.3(25)					27.7(35)
28.1(22)					
28.3(28)		29.3(88)	29.3(18)		
				29.7(45)	
30.4(32)	30.3(45)				
				31.2(75)	
					32.2(45)
	32.9(55)				
				34.0(65)	
35.4(27)					
36.3(32)	36.3(45)				
37.4(77)	37.5(85)	37.4(100)			
			37.6(85)		
				37.9(90)	
38.6(23)					
40.8(27)					
44.6(30)	45.8(100)				
46.0(65)		46.0(86)			46.1(100)
			46.3(95)	46.8(100)	
48.4(100)	48.5(90)		48.6(100)		
53.5(20)		53.8(42)			
54.2(15)			54.2(20)		
				54.6(40)	54.6(20)
				56.4(20)	

for various forms of $Cu_{2-x}S$. The x-ray pattern of the pressed bar is also shown in Figure 19.

X-ray analysis of bulk specimens is readily performed. However, the situation is quite different in the case of thin films. A good x-ray pattern requires a certain minimum thickness of the material and this thickness has to be established empirically. In the case of $Cu_{2-x}S$ films, it was found that a film of about 5000 Å was required to make reasonable identification of the x-ray pattern. For thinner films, another method was employed. The film was carefully scraped and a slurry was made using some acetone. Usually this slurry was enough for x-ray identification. Another problem with thin films is that because of preferred orientation effects[112], the intensity ratio is not maintained. The identification is therefore, made by the position of peak lines only.

Figure 20 shows the x-ray spectra of $Cu_{2-x}S$ on Aluminium substrates. About 9000 Å thick evaporated copper films were sulfurized. The spectra show that the conversion was incomplete. These samples are mostly Cu_2S, but contain extra lines denoting some mixture of phases plus free copper. The x-ray spectrum for copper film sulfurized on silicon substrate is shown in Figure 21. Here sulfurization is complete and every line of Cu_2S is present with proper intensity ratio. The spectrum contains only one unidentified line marked by an arrow. In Figure 22, x-ray spectrum

FIGURE 19: X-ray spectrum of a pressed bar of Cu_2S.

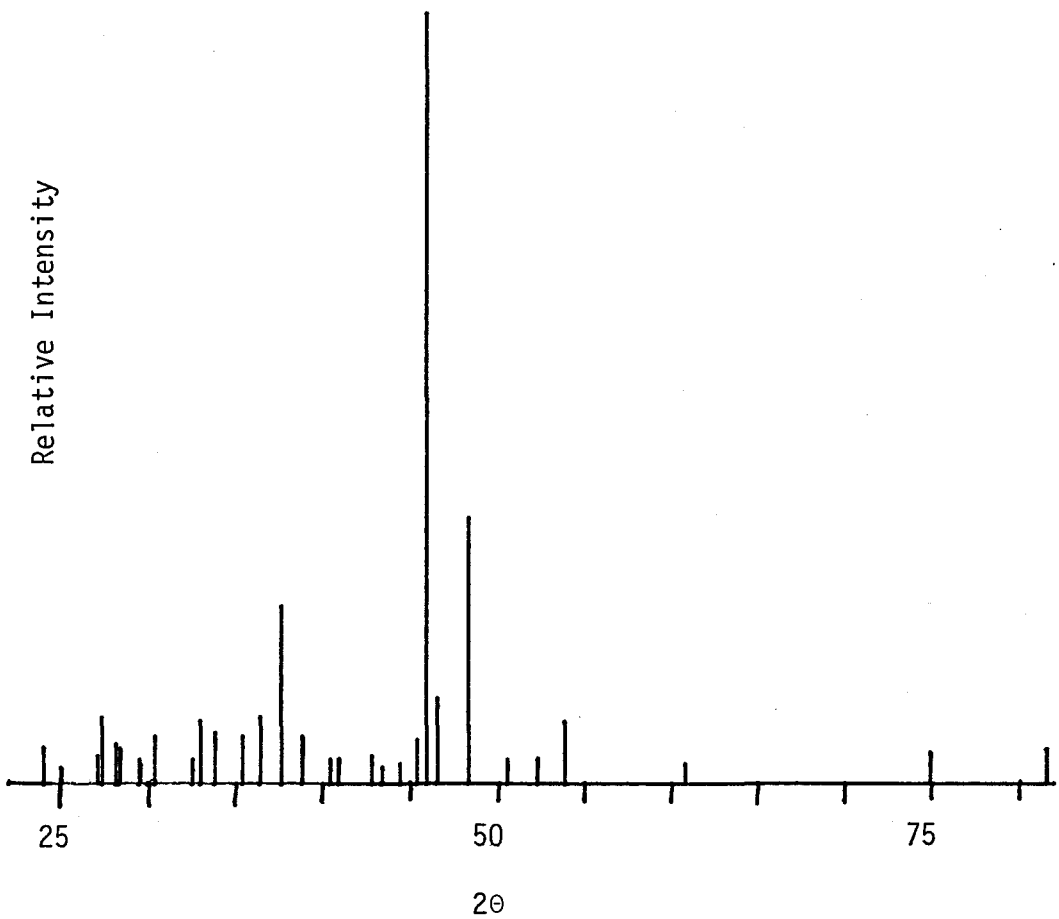

FIG. 19

FIGURE 20: X-ray spectra of sulfurized copper films on aluminium substrates.

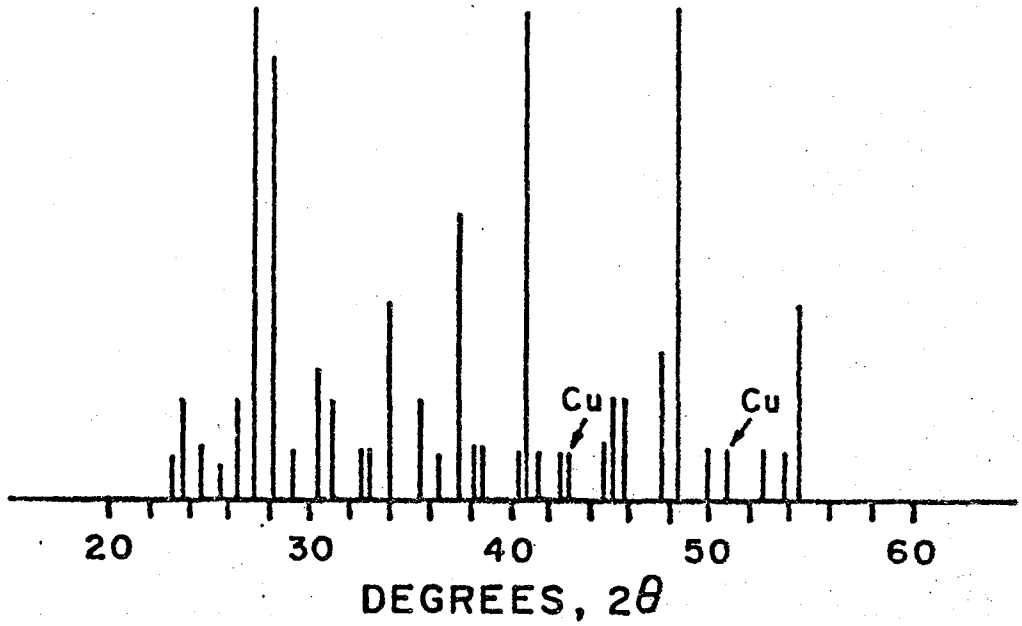

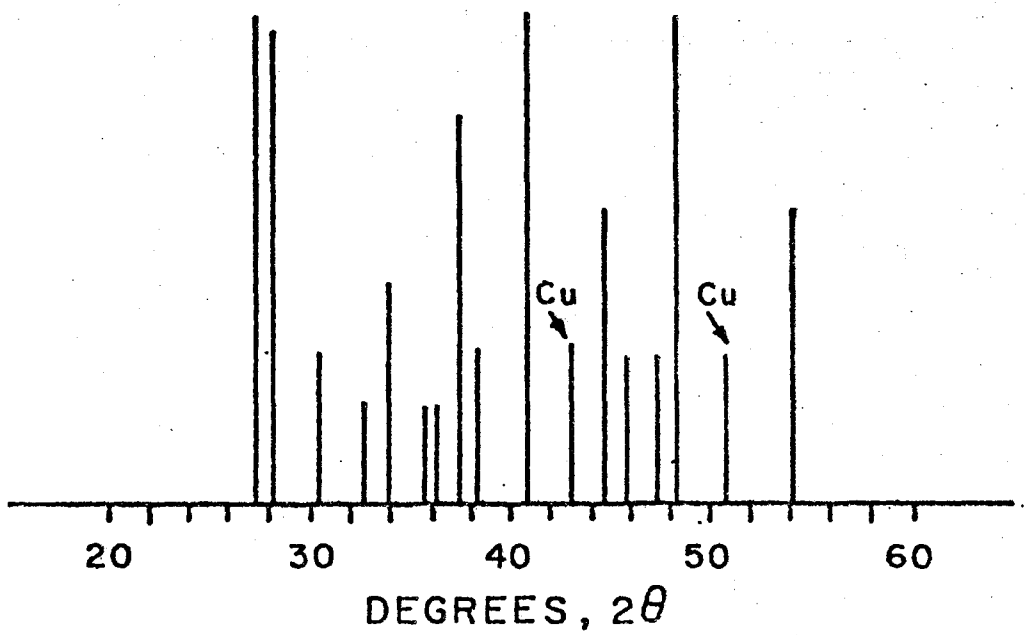

FIG. 20

FIGURE 21: X-ray pattern of sulfurized copper film on silicon substrate.

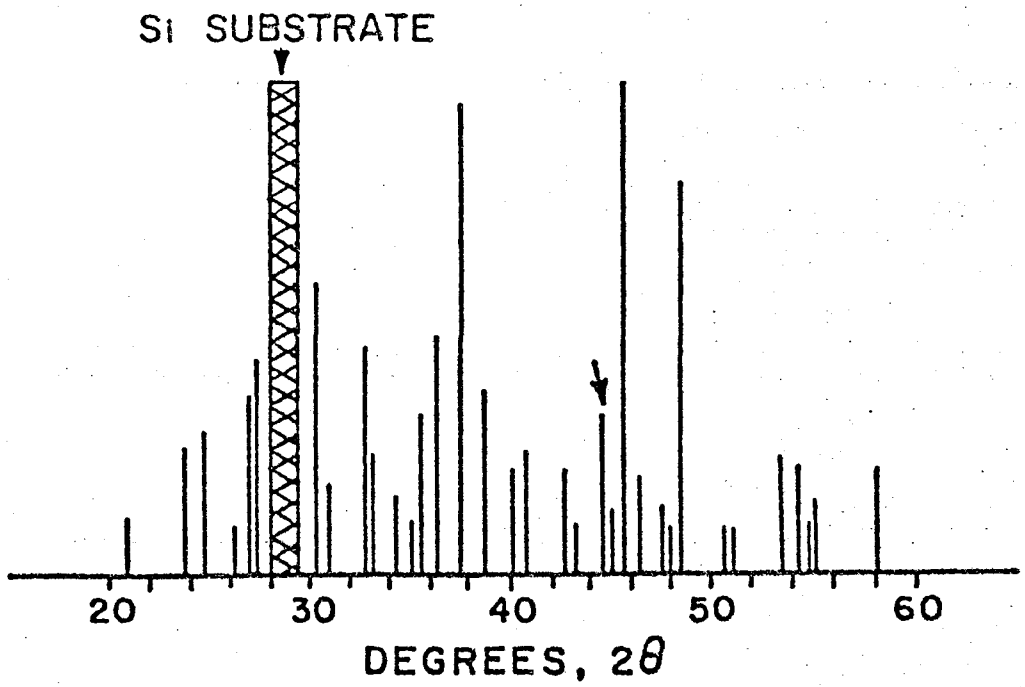

FIG. 21

FIGURE 22: X-ray spectrum of sulfurized copper film on glass slide.

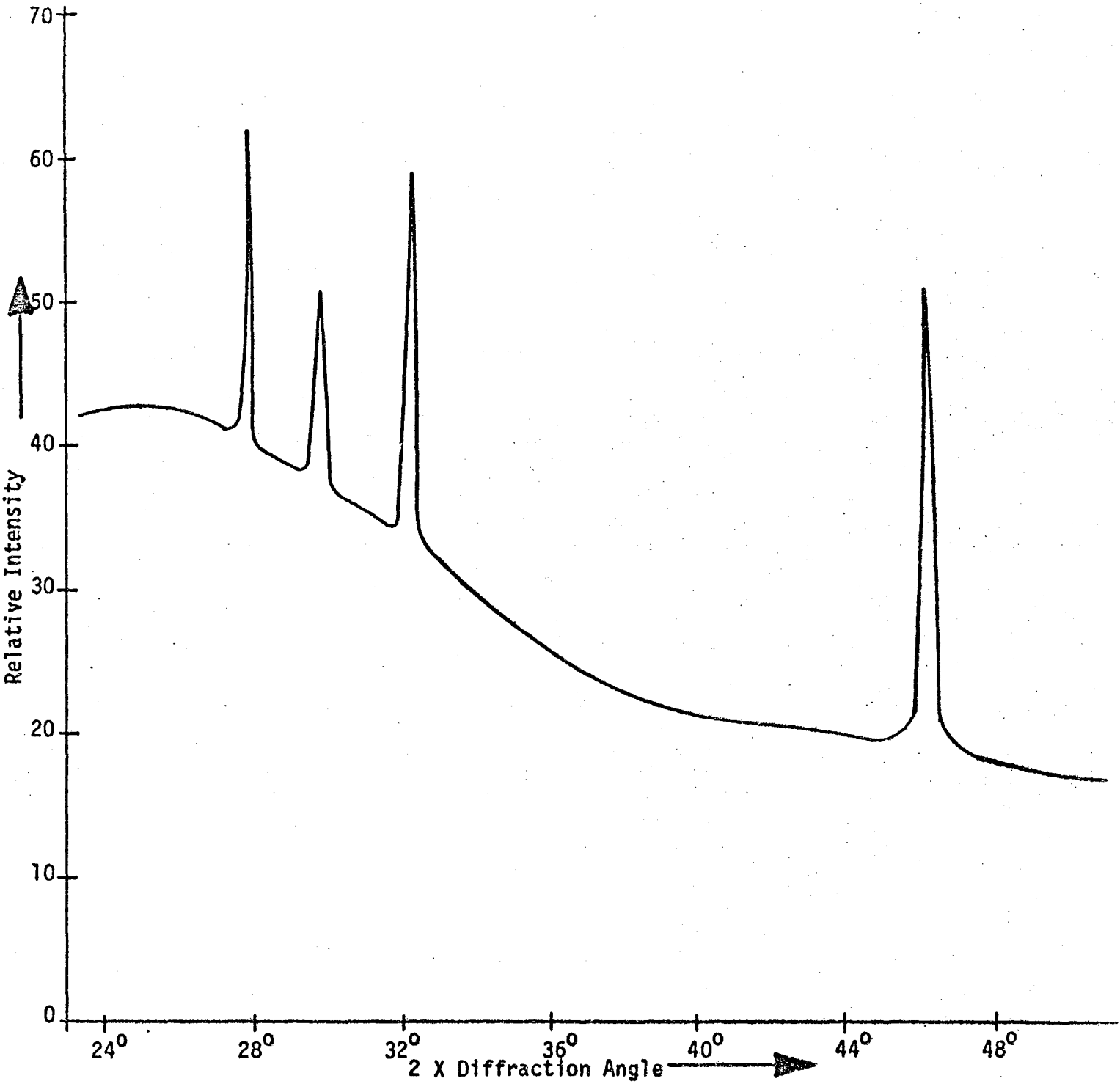
70
60
50
40
30
20
10
0
Relative Intensity
24°
28°
32°
36°
40°
44°
48°
2 X Diffraction Angle

FIG. 22

for 5000 Å thick $Cu_{2-x}S$ prepared by sulfurization at 300°C of a 2500 Å film of copper on a glass slide. The continuous background is contributed by the amorphous nature of glass. X-ray pattern for similarly prepared 3000 Å thick $Cu_{2-x}S$ film is shown in Figure 23. Both specimens appear to have a digenite structure. The different intensity ratio in the two samples is presumably caused by the orientation effects.

Figure 24 shows the x-ray patterns for the evaporated films of copper sulfide. Only the stronger lines are shown. The x-ray spectrum of the starting pressed bar is also included for easy comparison. It can be noticed that most of the starting x-ray lines are present in both samples. The variation in the line intensity can again be attributed to the preferred crystallographic orientations in the thin films.The extra lines in the film x-rays are due to djurleite phase. Therefore,the film composition appears to be between Cu_2S and $Cu_{1.96}S$.This type of behaviour has been observed in almost every evaporated film of copper sulfide. However, reflectance-transmittance measurements indicate that the film composition is closer to Cu_2S than to $Cu_{1.96}S$. (These measurements are to be referred as "optical" measurements, unless otherwise stated.) X-ray pattern of 1μ thick sample was taken directly, but for the sample of 1500Å thickness, a slurry had to be made for x-ray analysis.

FIGURE 23: X-ray spectrum of sulfurized copper film on glass slide.

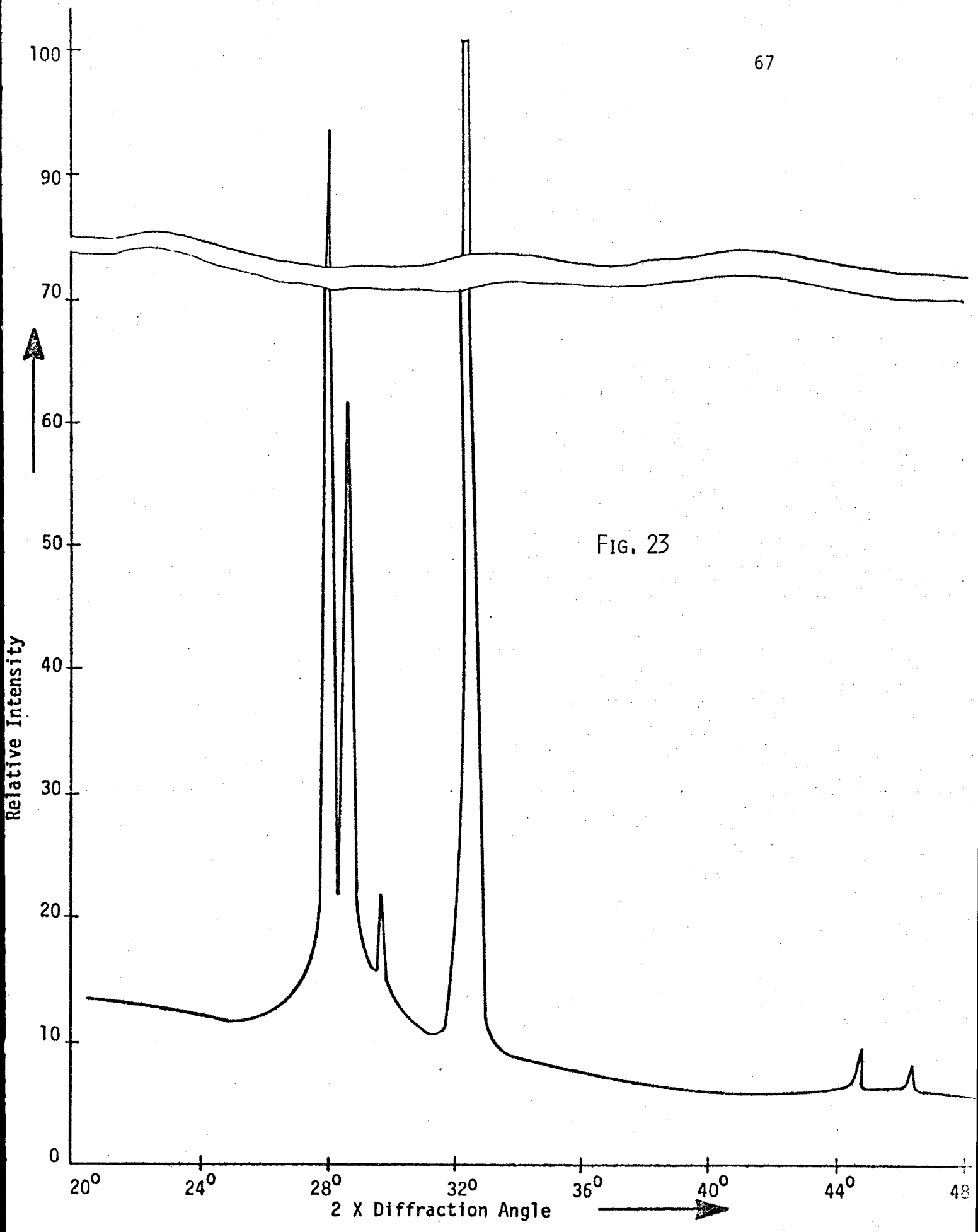
100
90
70
60
50
40
30
20
10
0
Relative Intensity
20°
24°
28°
32°
36°
40°
44°
48
2 X Diffraction Angle

FIG. 23

FIGURE 24: X-ray spectra of evaporated copper sulfide films on glass substrates. The background due to glass substrate has been substracted. The x-ray pattern of the starting pressed bar is also shown.

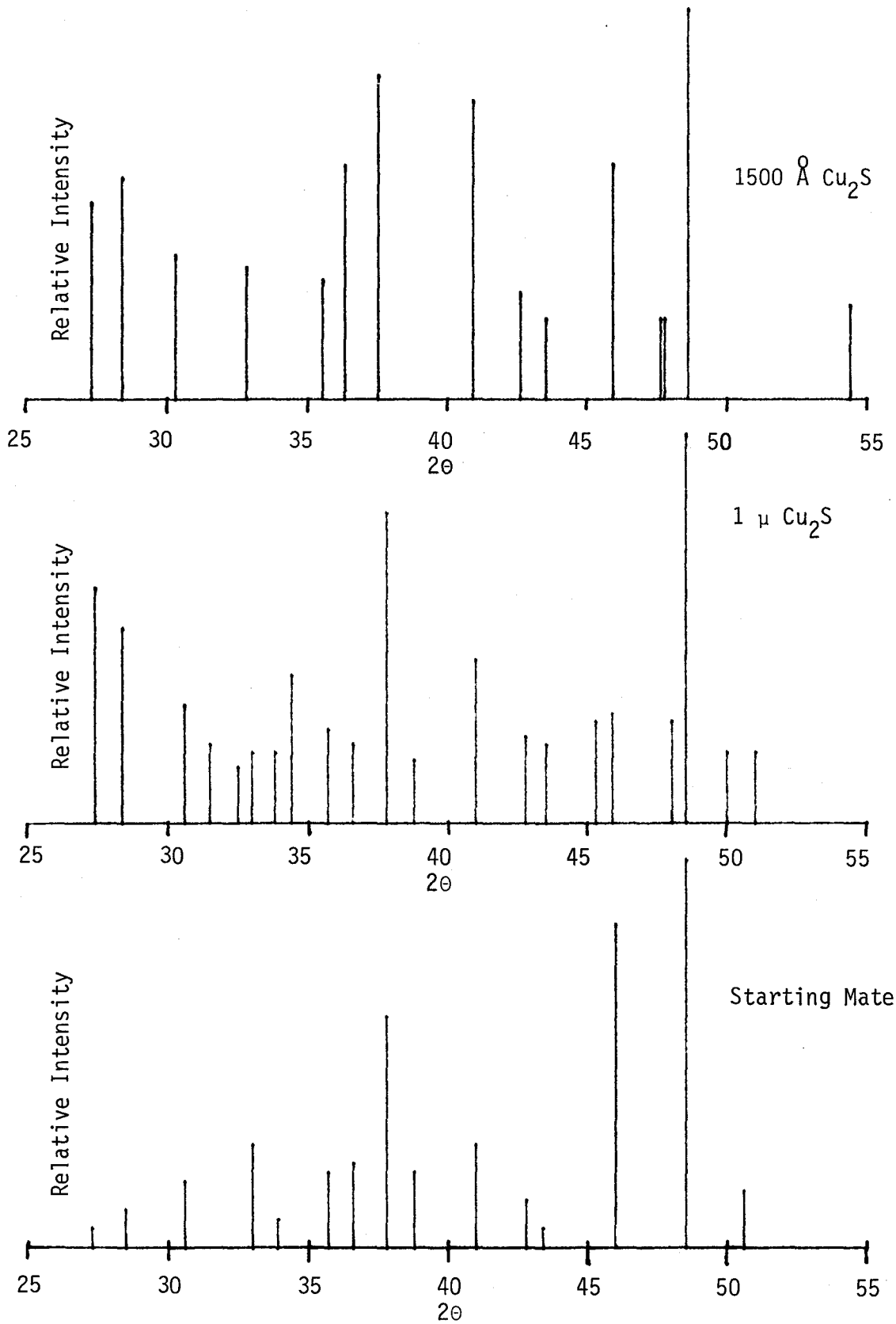
Relative Intensity
1500 Å Cu_2S
25
30
35
40
45
50
55
2θ
Relative Intensity
1 μ Cu_2S
25
30
35
40
45
50
55
2θ
Relative Intensity
Starting Material
25
30
35
40
45
50
55
2θ

FIG. 24

4.2 CATHODOLUMINESCENCE

Cathodoluminescence involves the excitation of recombination radiation by an electron beam.[113] Such recombination radiation is emitted by a semiconductor or insulator when excess holes and electrons injected into the material recombine with each other. The recombination can occur between free electrons in the conduction band and free holes in the valence band, in which case the resulting line has its peak at an energy close to that of the forbidden energy gap E_g. The recombination can also occur between a free electron (hole) and a hole (electron) trapped at a radiative recombination center, in which case the resulting emitted band has its peak at an energy corresponding to the energy difference between the location of the recombination level in the forbidden gap and the appropriate band. The various possible recombination paths compete with other and the spectrum reflects the relative dominance of various paths. Non-radiative paths also exist and they compete with radiative recombination paths; the presence of such paths can reduce the intensity of all the lines in the spectrum. Thus, the cathodoluminescence spectrum can provide information about the energy gap of the semiconductor; about recombination levels associated with chemical or structural defects introduced into the material; and about the effectiveness of non-radiative recombination in the material.

The cathodoluminescence spectrum of a chalcocite mineral sample is shown in Fig.25 . From the centre of the spectrum peak, a band gap of 1.265 eV can be deduced. The FWHM of the spectrum is nearly 80 nm. No luminescent spectra were observed by Brown researchers from djurleite ($Cu_{1.96}S$), digenite ($Cu_{1.8}S$) and covellite (CuS)[104], although it is still not clear whether this is due to experimental or material limitations.

FIGURE 25: Cathodoluminescence spectrum of chalcocite mineral. The experiment was done at Brown University, U.S.A.

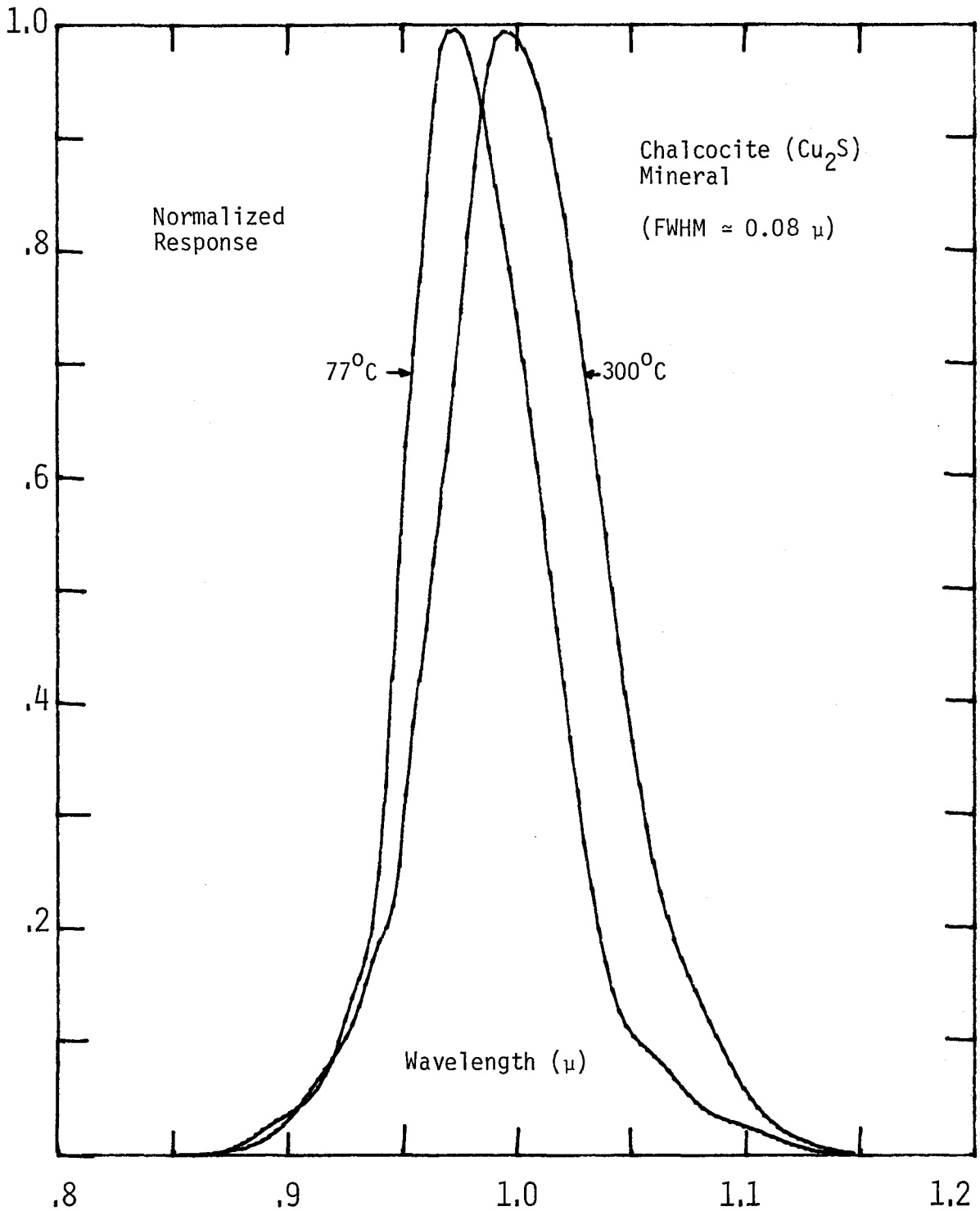
1.0
.8
.6
.4
.2
Normalized
Response
Chalcocite (Cu_2S)
Mineral
(FWHM ≃ 0.08 μ)
77°C
300°C
Wavelength (μ)
.8
.9
1.0
1.1
1.2

FIG. 25

Luminescence spectrum of Cu_2S pressed bar is similar to that of chalcocite and is given in Fig. 26. However, the spectrum of the pressed bar appears to be dependent on the applied pressure. The effect of applied pressure on the bar is shown in Fig27 and its effect on luminescence spectrum is summarized in table V. It is worth noting that the peak intensity increases till 7 ton of pressure and then decreases. FWHM also changes with the pressure. It appears that the pressure to which the Cu_2S powder was subjected in forming the pressed bars may have resulted in unrelieved strains which could produce changes in band gap parameters and these changes are reflected in the luminescence spectra. Pressure dependant changes on the density of the pressed bar and its resistivity, shown in Fig.27 are as expected.

Cathodoluminescence spectrum of a 1μ evaporated film is shown in Fig.28 . This spectrum again resembles to the chalcocite spectrum. It must be noticed that the annealingof the film resulted in a higher peak intensity. This could be interpreted as the reduction in the recombination centers due to annealing. Thinner films of $Cu_{2-x}S$ could not be tested because the electron beam just went through the samples.

From the intensity and FWHM of these spectra, it appears that Cu_2S has a direct band gap of about 1.26 eV[104] . For direct band gap materials, the corresponding onset of recombination emission as a function of photon energy is proportional to $(\hbar\omega - E_g)^{1/2}$. Therefore, theoretically the low energy edge is abruptly cut-off at $\hbar\omega = E_g$ and the high energy edge will have a temperature dependant tail due to recombination of free carriers in the band tail. Typical half width for direct gap material is of the order of 10 meV or less, with this increasing with carrier concentration and non-crystallinity. On the

FIGURE 26: Cathodoluminescence spectrum of a pressed bar of Cu_2S. Experiment done at McMaster by Glen Chapman.

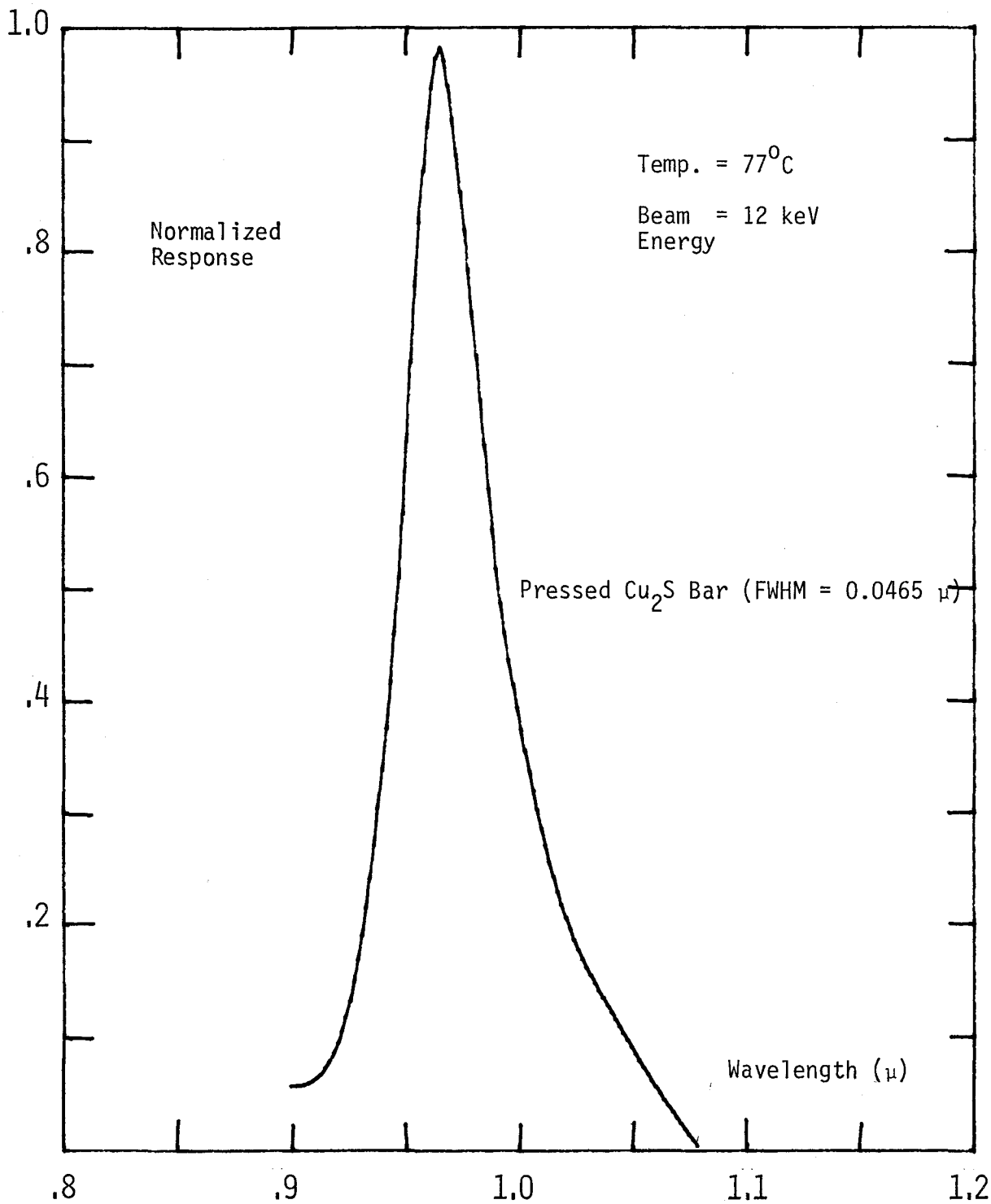
1.0
.8
.6
.4
.2
Normalized
Response
Temp. = 77°C
Beam = 12 keV
Energy
Pressed Cu2S Bar (FWHM = 0.0465 μ)
Wavelength (μ)
.8
.9
1.0
1.1
1.2

FIG. 26

FIGURE 27: Pressure dependance of density and resistivity of a pressed bar of Cu_2S.

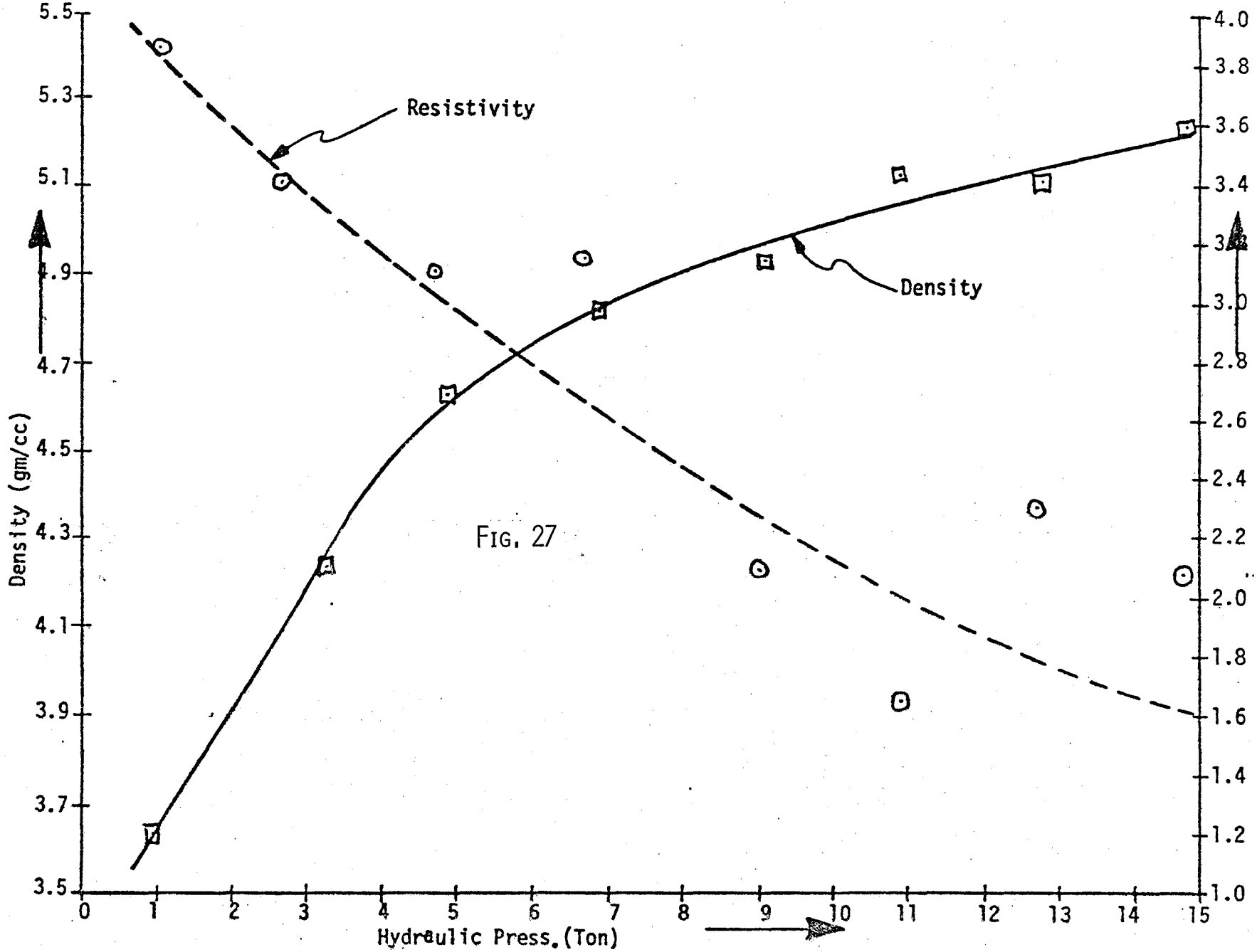
Resistivity
Density
Density (gm/cc)
Resistivity (ohms - cm x 10^{-4})
Hydraulic Press. (Ton)
5.5
5.3
5.1
4.9
4.7
4.5
4.3
4.1
3.9
3.7
3.5
4.0
3.8
3.6
3.4
3.2
3.0
2.8
2.6
2.4
2.2
2.0
1.8
1.6
1.4
1.2
1.0
0 1 2 3 4 5 6 7 8 9 10 11 12 13 14 15

FIG. 27

TABLE V

EFFECT OF PRESSURE ON CATHODOLUMINESCENCE SPECTRUM OF Cu_2S

(Experiments by Glen Chapman)

Hydraulic Pressure (Tons)	Peak (nm)	FWHM (nm)	Intensity (V/A)
3	933 ±1	98	2.1
5	931	90	2.1
7	929	88	14.8
9	924	90	2.8
11	*		
13	942	-	0.3
15	*		

FIGURE 28: Cathodoluminescence spectrum of 1μ thick evaporated film of copper sulfide. Film was annealedfor 24 hours in air ambient at 72^{o}C. Experiments carried out by Glen Chapman.

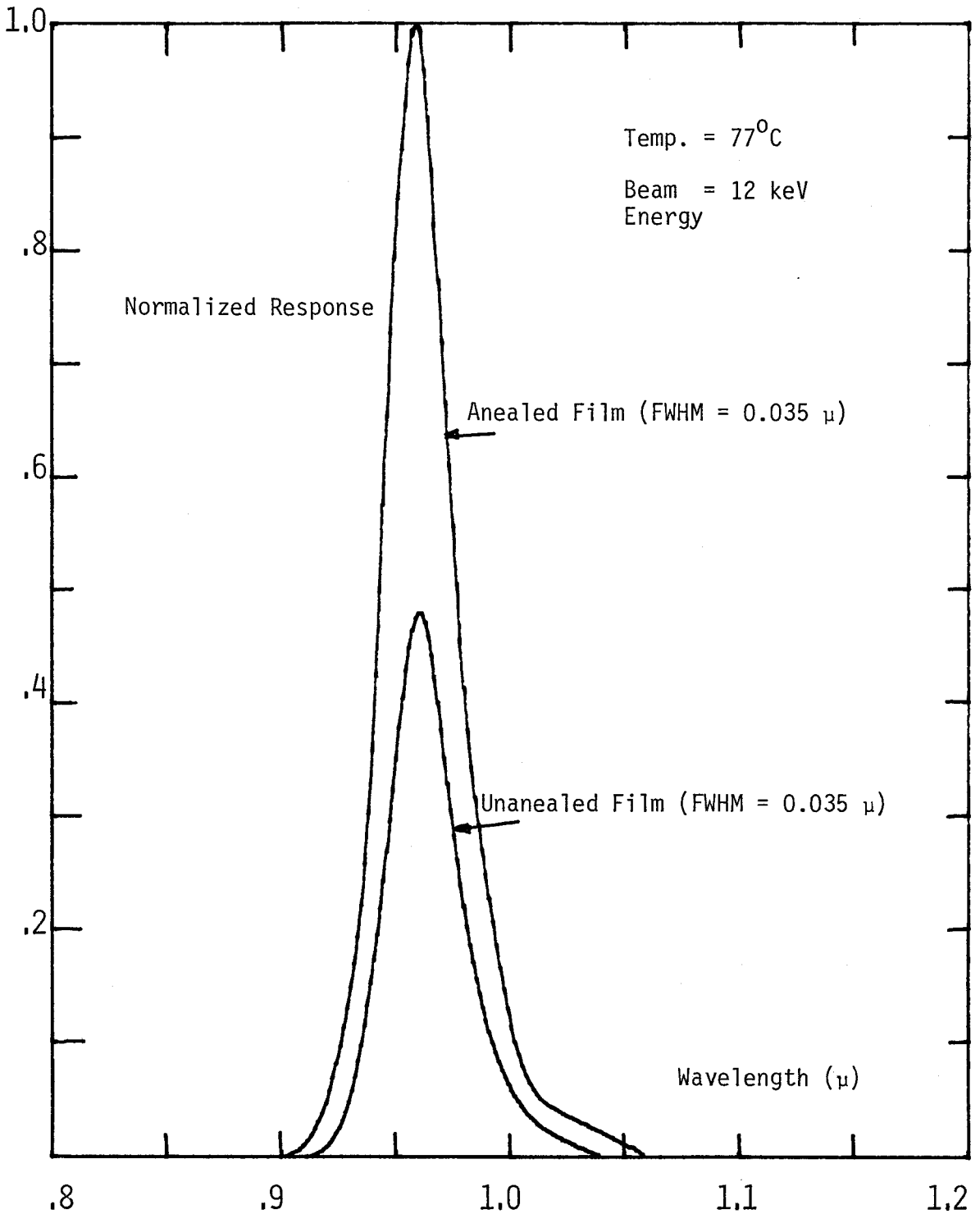
1.0
.8
.6
.4
.2
Normalized Response
Temp. = 77°C
Beam = 12 keV
Energy
Anealed Film (FWHM = 0.035 μ)
Unanealed Film (FWHM = 0.035 μ)
Wavelength (μ)
.8
.9
1.0
1.1
1.2

FIG. 28

other hand, for indirect gap material, the onset of emission is usually proportional to $(\hbar\omega - E_g + E_p)^2$, where E_p is the phonon energy. For these materials the peak intensity would be much lower than for direct gap materials due to lower transition probability. The half width of the emission band for indirect transition is usually much greater than for direct case. Cu_2S luminescence quite intensely (compared to indirect gap Si) which would indicate that the 1.26 eV band gap of Cu_2S is a direct gap. The observed half width appears to be large for a direct gap material, but considering the fact that it has a high carrier concentration and the test samples were either pressed bars or thin films, this observation could be accounted for. There is, however, one thing which makes this semiconductor different than other direct gap materials. The peak intensity is about 50-100 times less than for direct gap materials (like CdS) but is definitely larger than indirect gap materials as mentioned before. This fact coupled with the observation of large FWHM, leads one to conclude that Cu_2S may be a border line semiconductor or the conduction band may be skew-symmetric around the centre of Brillouin zone. These possible band schemes are drawn in Fig.29. These band schemes are capable of explaining the rather strange optical behaviour of Cu_2S. In fact, non-symmetrical bands are quite frequent in semiconductors. In the case of Cu_2S, it appears that the band at the centre of Brillouin zone is highly non-symmetric, to make it quasi direct band gap material.

FIGURE 29: Possible energy band diagram of Cu_2S near the centre of Brillouin zone. Fig. 29(a) depicts an indirect band with required phonon energy approaching to zero. In 29(b), a direct band is closely associated with an indirect band. In 29(c), the band is highly unsymmetric at k=0, so that the elctrons can "slide" across the band. In all three schemes, because the conduction band minima is very close to k=0, the material will behave like a direct gap semiconductor - but would be weaker than true direct gap semiconductors.

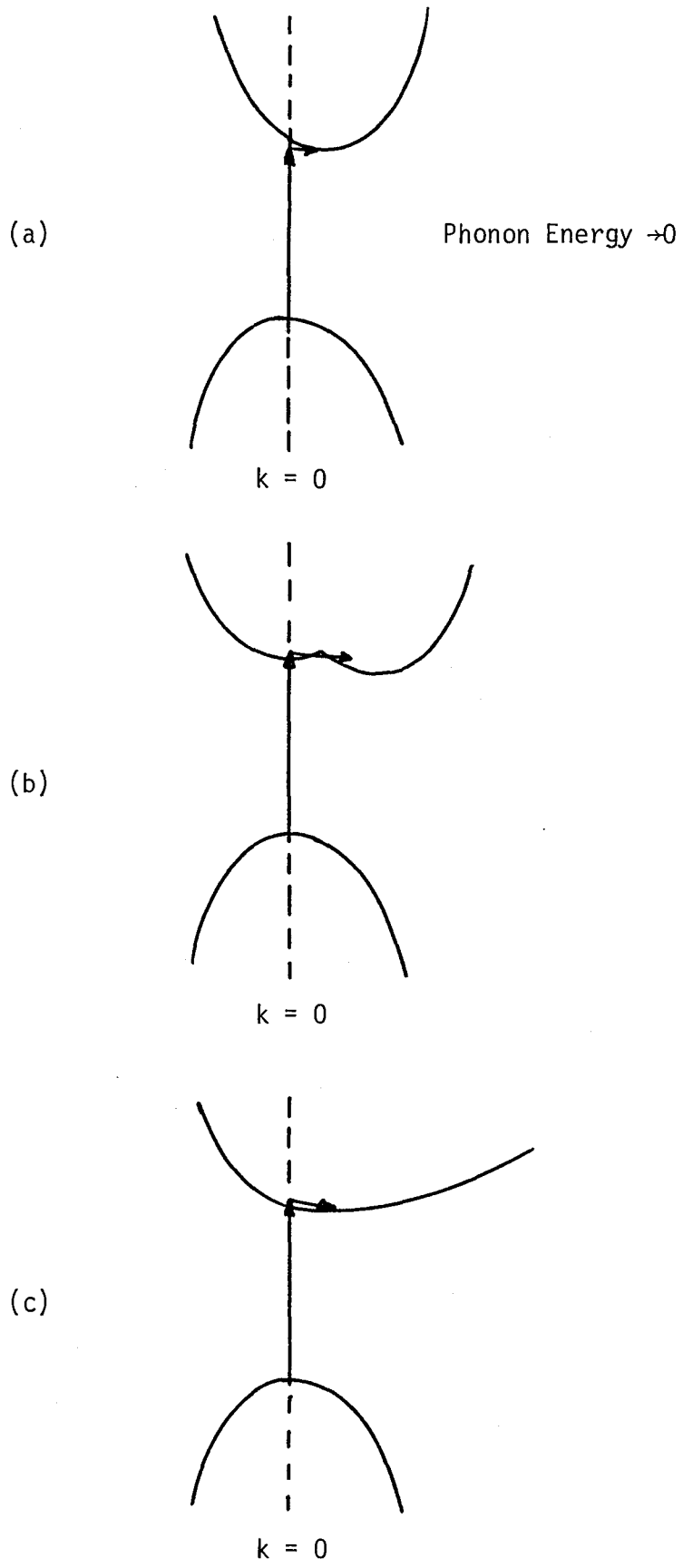

FIG. 29

4.3 HALL EFFECT MEASUREMENTS

The Hall equipment is able to provide information on the electrical properties of our films, such as carrier concentration, mobility etc. The capabilities of the particular system employed are discussed in detail in an article by J. Shewchun et al.[114] . Hall measurements can be made between room temperature and helium temperature automatically with electric and magnetic field switching controlled by a computer.

The experimental sample arrangement is shown in Figure 30 . This configuration yields the Hall coefficient R_H so that:

$$R_H = \frac{E_y}{J_x B_z} = \frac{V_H t}{IB} = \frac{-r}{qn} \qquad (4.1)$$

Where:

E_y is the field in the y direction $(= \frac{V_H}{W})$

J_x is the current density in the x direction $(\frac{I_x}{Wt})$

B_z is the magnetic field in the z direction

V_H is the Hall voltage and V_C the conductivity voltage

t,W are the film thickness and width respectively

r is a scattering parameter $\approx$ 1

q is the charge on an electron

The current is arranged to keep V_c = 1 volt. Thus the film resistivity ρ is given by:

$$\rho = \frac{Wt}{I\ell} \qquad (4.2)$$

FIGURE 30: Schematic of Hall sample arrangement.

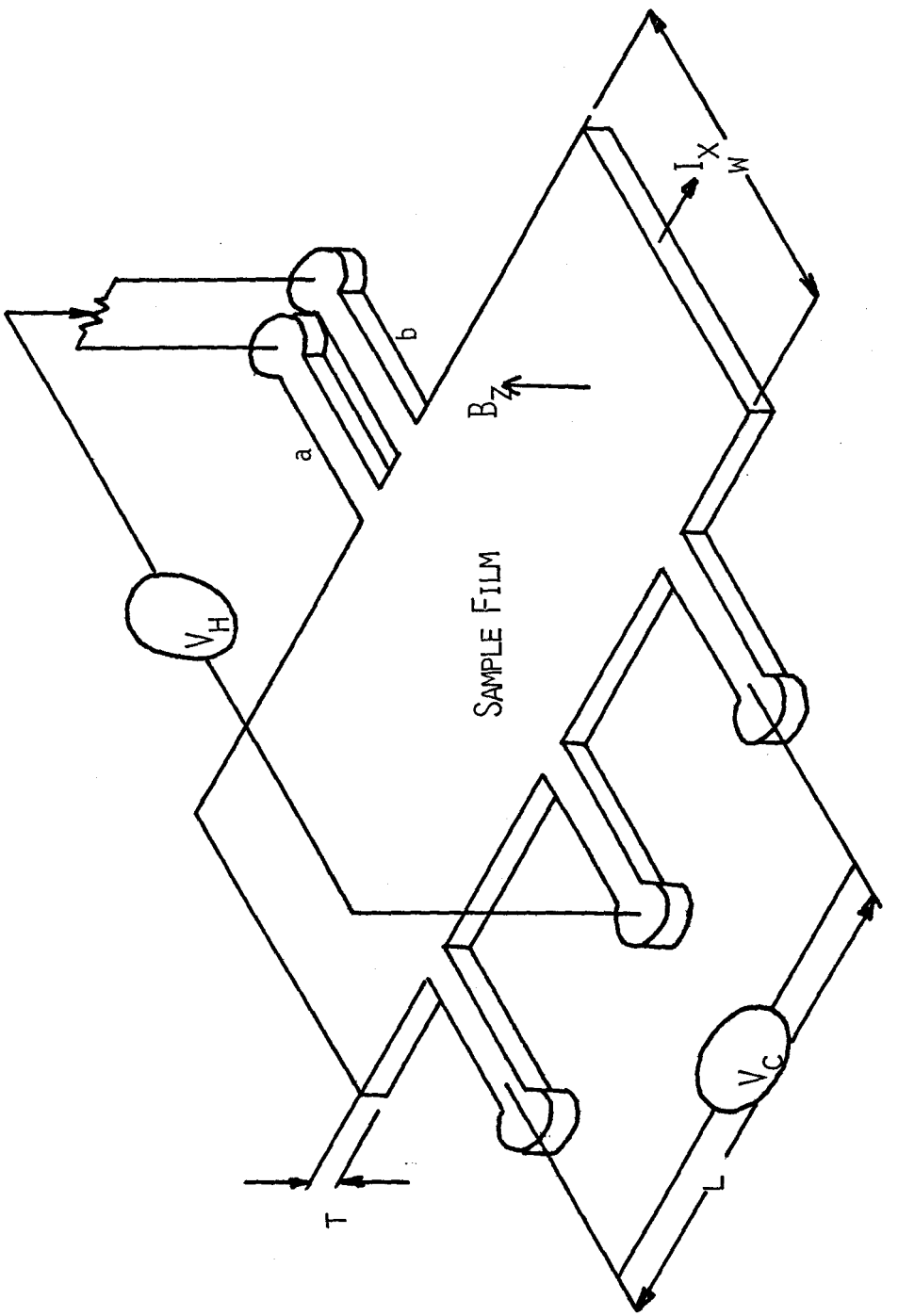

FIG. 30

while the carrier mobility μ_H is given by:

$$\mu_H = \frac{R_H}{\rho} \qquad (4.3)$$

In practice, the Hall contacts usually have a finite offset and the Hall Voltage V_H is masked in a large conductivity component. This conductivity component can usually be zeroed out by adjusting the potentiometer between contact "a" and "b" (See Figure 30) with B = 0.

A summary of Hall Effect data on Cu_2S samples is shown in Table VI. These samples show high "hole" concentrations. The p-type nature was also confirmed with hot point test. For comparison typical values for bulk Cu_2S have been taken from the literature [84]. Resistivities are observed to range from 0.4 to 0.06 Ω-cm while Hall coefficients were $2 < R_H < 10^{-3} cm^3/cb$ and mobilities were $\sim 4\ cm^2/v/sec$. An examination of this table reveals that while pressed bar data and a number of samples reported here compare favorably with the literature values, many other film samples exhibit aging/annealing effects. The deviation in other sample may be because of the differences in scattering parameter, r, which is taken to be unity, because of the lack of this type of information on thin films. The aging (self anneal)/annealing causes higher carrier concentrations and the film properties approach the reported values. The optical and cathodoluminescence experiments have suggested reduced number of recombination/trap centres and increased film continuity. From these results, the increase in carrier concentration is expected, because now fewer carriers would be trapped.

TABLE VI

HALL DATA ON EVAPORATED COPPER SULFIDE FILMS

(Experiments carried out by T. Vanderwel)

Preparation	Treatment	R_H cm^3/cb	ρ $\Omega.cm$	μ $(cm^2/V.s)$	Hole Conc. (cm^{-3})
Pressbar	-	.13	.04	3.1	4.8×10^{19}
877 Å,15.5 Å/s	fresh	.0016	.0006	2.6	3.9×10^{21}
700 Å,14.7 Å/s	fresh	.0016	.0006	2.6	4.0×10^{21}
700 Å,15 Å/s	5 days	.0031	.0011	2.9	2.0×10^{21}
900 Å,15.5 Å/s	9 days	3.5	.55	6.5	1.8×10^{18}
500 Å,15.5 Å/s	9 days	.0062	.0029	2.2	1.0×10^{21}
1000 Å,15.4 Å/s	8 days	-	50.	-	$>5. \times 10^{17}$
800 Å,5.3 Å/s	15 days	.027	.0081	3.4	2.3×10^{20}
800 Å,20.6 Å/s	17 days	.27	.044	6.1	2.3×10^{19}
1500 Å,1.0 Å/s	fresh	.37	.055	6.7	1.7×10^{19}
800 Å,20.6 Å/s	1 day	-	100.	-	$>1. \times 10^{18}$
- do -	15 days+ 24 hr bake in air(72°C)	.087	.016	5.4	7.0×10^{19}
1500 Å, 15 Å/s	3 days	1200.	100.	12.	5.0×10^{15}
- do -	16 days+ 24 hr bake in air(72°C)	.089	.02	4.4	7.0×10^{19}
1500 Å,10.4 Å/s	3 days	5700.	240.	23.	1.1×10^{15}
1500 Å,20 Å/s	3 days	6000.	240.	25.	$1. \times 10^{15}$
1 μ, 15 Å/s	fresh	2000.	150.	13.	$3. \times 10^{15}$
- do -	3 days+ 24 hr bake in air(72°C)	2000.	190.	11.	$3. \times 10^{15}$
1500 Å,50 Å/s	7 days	2200.	180.	12.	$3. \times 10^{15}$
2000 Å,15.5 Å/s	9 days	6000.	260.	23.	$1. \times 10^{15}$
1500 Å, 5.3 Å/s	6 days	10000.	220.	47.	$6. \times 10^{14}$
- do -	7 days+ 2 hr bake in vac(∿10μ),175°C	23	3.2	7.2	$3. \times 10^{17}$

4.4 OPTICAL MEASUREMENTS

A major asset in the optimization of Cu_2S film properties and composition has turned out to be the optical analysis of films on glass substrate with the DK-2 Beckman spectrophotometer.[115] A normalized reflectance or transmittance spectrum is obtained by constant comparison of sample beam with a reference beam at the same wavelength. For this purpose a single beam of radiation is utilized which is chopped into alternate reference and sample beams to provide a double beam system within the sample compartment. Both sample and reference beams have common detection and amplification components. Ratio recording eliminates inaccuracies due to such effects as source fluctuations, changes in amplifier gain, sensitivity or spectral response of the detector and the presence of common absorbing gases in the sample and reference path. Total reflectance measurements are made by mounting both sample and white reference (MgO) at a five degree angle to the radiation beam, so that both specular and diffuse components are integrated in the white integrating sphere before reaching the detector. A schematic of the integrating sphere is shown in Fig.31, indicating sample positions in various modes of operation.

Initially, attempts were made to calculate n and k from experimentally measured reflectivity (R_m) and transmissivity (T_m) data as a function of wavelength, λ. For a single absorbing film of thickness d, on a non-absorbing substrate (refractive index, n_s), R_m and T_m can be obtained from the following set of equations:[116]

FIGURE 31: Schematic of integrating sphere of Beckman DK- 2 spectrophotometer for the measurement of reflectance and transmittance of the sample. Various modes of operations are shown in the actual experimental sequence.

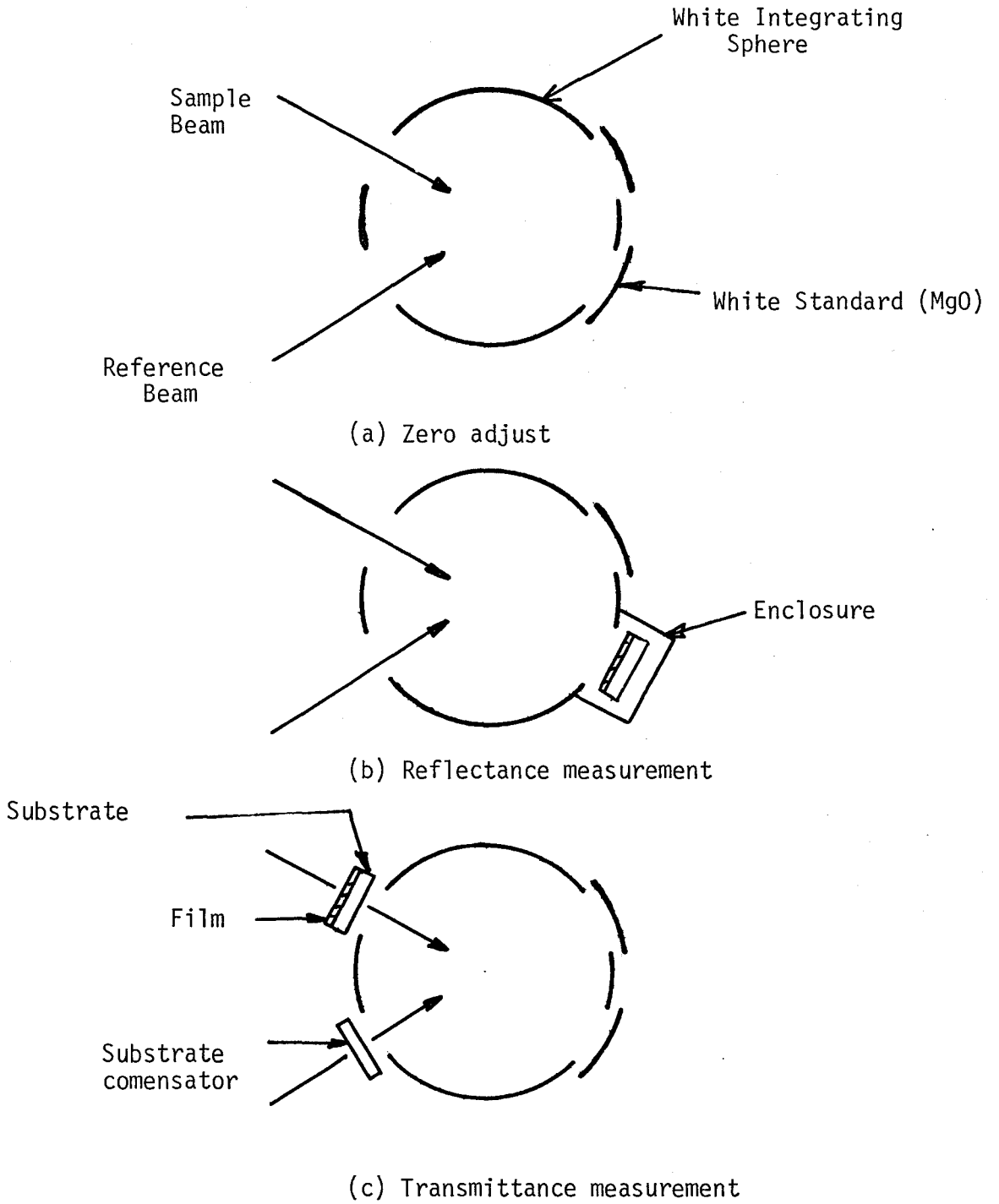
White Integrating Sphere
Sample Beam
White Standard (MgO)
Reference Beam
(a) Zero adjust
Enclosure
(b) Reflectance measurement
Substrate
Film
Substrate comensator
(c) Transmittance measurement

FIG. 31

$$R_m = R + \frac{T^2 R_s}{1 - R' R_s}$$

$$T_m = T\left[1 - R_s \frac{1 - R'}{1 - R' R_s}\right] \qquad (4.4)$$

$$R = \frac{A^2 + B^2 + 2e^{-\alpha}\{(\cos\beta)(AC + BD) + \sin\beta)(BC-AD)\} + e^{-2\alpha}(C^2+D^2)}{E^2 + F^2 + 2e^{-\alpha}\{(\cos\beta)(EG + FH) + (\sin\beta)(FG-EH)\} + e^{-2\alpha}(G^2+H^2)}$$

$$R' = \frac{C^2 + D^2 + 2e^{-\alpha}\{(\cos\beta)(AC + BD) - (\sin\beta)(BC-AD)\} + e^{-2\alpha}(A^2+B^2)}{E^2 + F^2 + 2e^{-\alpha}\{(\cos\beta)(EG + FH) + (\sin\beta)(FG-EH)\} + e^{-2\alpha}(G^2+H^2)}$$

$$T = \frac{16 n_s e^{-\alpha}(n^2 + k^2)}{E^2 + F^2 + 2e^{-\alpha}\{(\cos\beta)(EG + FH) + (\sin\beta)(FG-EH)\} + e^{-2\alpha}(G^2+H^2)}$$

where

$$\alpha = 4\pi k \frac{d}{\lambda}$$

$$\beta = 4\pi n \frac{d}{\lambda}$$

and

$$A = n(n_s + n - 1) - n_s - k^2$$

$$B = k(2n + n_s - 1)$$

$$C = n(n_s - n - 1) + n_s + k^2$$

$$D = k(-2n + n_s - 1)$$

$$E = n(n_s + n + 1) + n_s - k^2$$

$$F = k(2n + n_s + 1)$$

$$G = n(n_s - n + 1) - n_s + k^2$$

$$H = k(-2n + n_s + 1)$$

Such a complex set of equations can be solved only by iterative methods. Unfortunately neither Newton-Raphson nor a Brown algorithm[117] could provide solutions for all λ. The multi-valued solutions at several points and systematic errors in the measurements made convergence impossible or at best misleading and non-physical. The wavelength range (0.5 - 2.5 μ) was not large enough to try Kramers-Kronig type of analysis.[118,119]

An alternative approach has since been taken in which n and k data as a function of and "x" (of Cu_xS) have been obtained from literature[63,64] and the corresponding R_m and T_m curves calculated.[115] These theoretical curves can then be compared with experimental results. As the original data of Mulder[63,64] was for polarized light (perpendicular and parallel to optical axis), averages were calculated. For the averaging purpose, the average dielectric constant ε was calculated and from its real and imaginary parts, average n and k were calculated as follows:

$$\varepsilon_{real} = n^2 - k^2$$

$$\varepsilon_{imag} = 2nk \qquad (4.5)$$

therefore

$$n^2 = 1/2\ [\varepsilon_r + (\varepsilon_r^2 + \varepsilon_e^2)^{1/2}]$$

$$k^2 = 1/2\ [-\varepsilon_r + (\varepsilon_r^2 + \varepsilon_i^2)^{1/2}]$$

Once n and k are obtained (Fig. 32), R_m and T_m can be calculated from equation 4.4. Families of curves for various film thicknesses are shown in Fig.33-36 for x - 1.995, 1.95, 1.86 and 1.77 respectively. These curves can be seen to be extremely sensitive to both d and "x". An

FIGURE 32: Average values of optical constants (n and k) for $Cu_{1.995}S$, $Cu_{1.95}S$, $Cu_{1.86}S$ and $Cu_{1.77}S$.

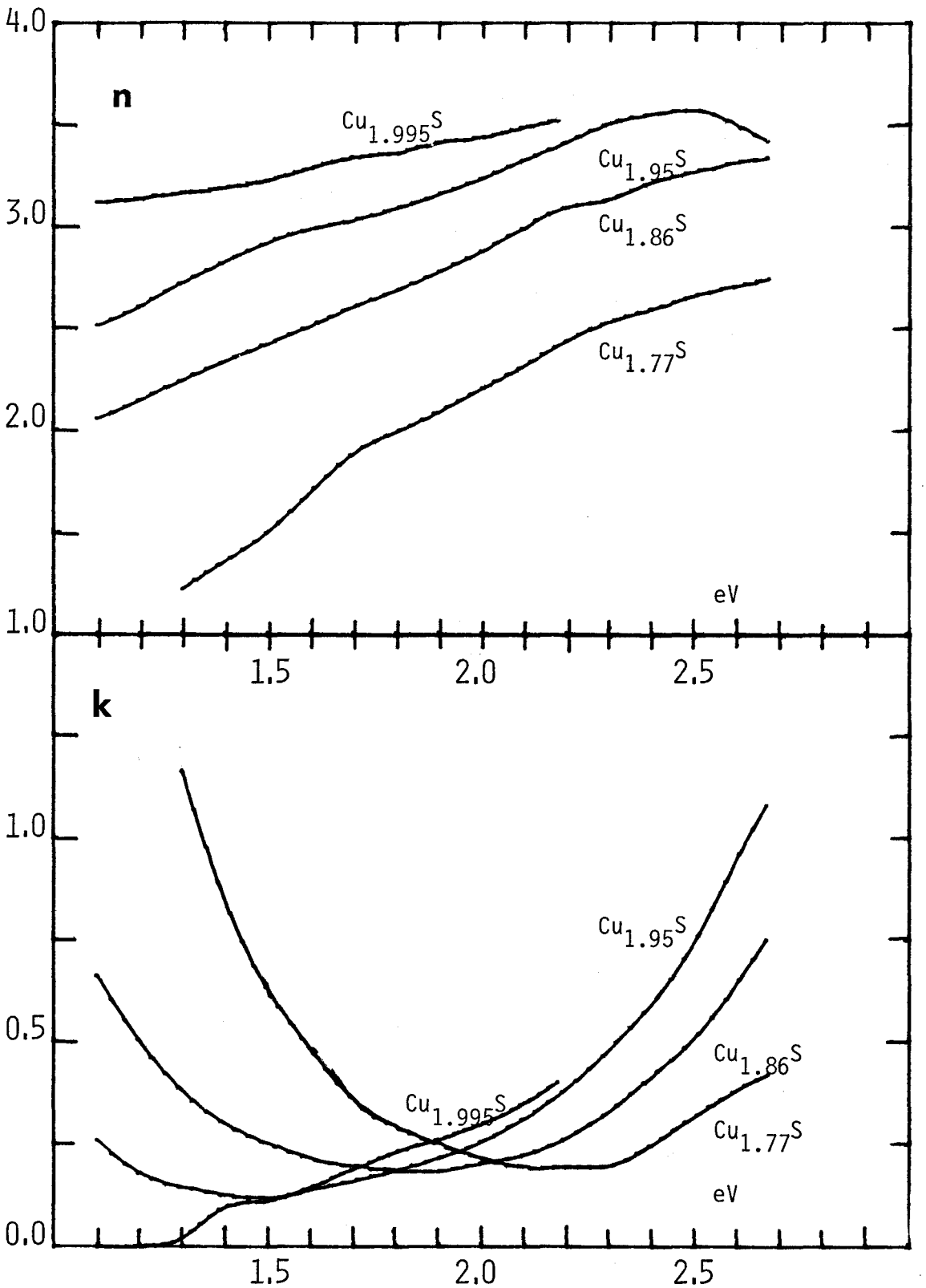
n
$Cu_{1.995}S$
$Cu_{1.95}S$
$Cu_{1.86}S$
$Cu_{1.77}S$
eV
4.0
3.0
2.0
1.0
1.5
2.0
2.5
k
$Cu_{1.95}S$
$Cu_{1.86}S$
$Cu_{1.995}S$
$Cu_{1.77}S$
eV
1.0
0.5
0.0
1.5
2.0
2.5

FIG. 32

FIGURE 33,34,35,36 : Calculated values of reflectance and transmittance for different thicknesses of $Cu_{1.995}S$, $Cu_{1.95}S$, $Cu_{1.86}S$ and $Cu_{1.77}S$, respectively, on a glass substrate.

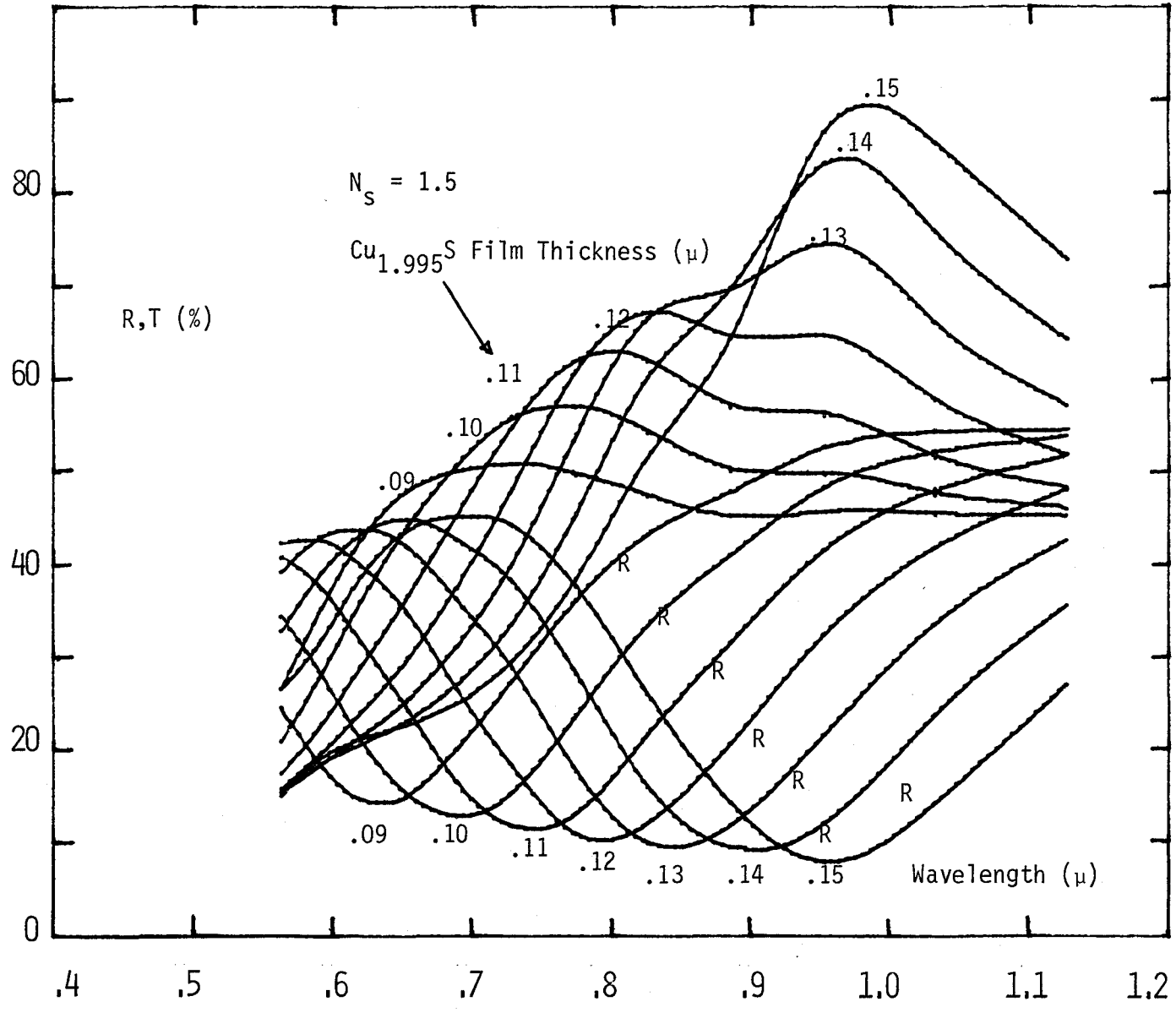
80
60
40
20
0
R,T (%)
N_s = 1.5
$Cu_{1.995}S$ Film Thickness (μ)
.15
.14
.13
.12
.11
.10
.09
R
.4
.5
.6
.7
.8
.9
1.0
1.1
1.2
Wavelength (μ)

FIG. 33

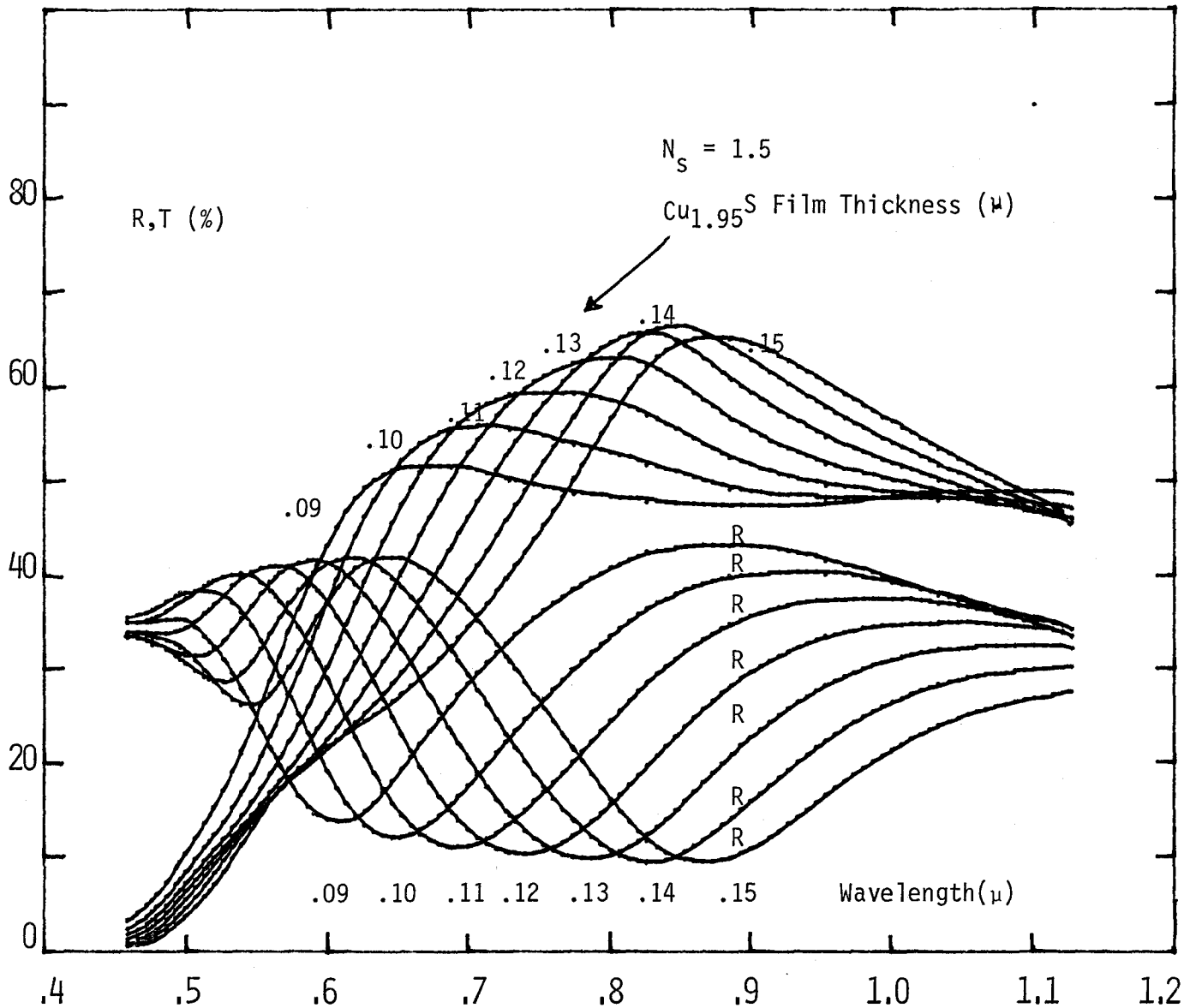
N_s = 1.5
$Cu_{1.95}S$ Film Thickness (μ)
R,T (%)
.09
.10
.11
.12
.13
.14
.15
R
Wavelength(μ)
0
20
40
60
80
.4
.5
.6
.7
.8
.9
1.0
1.1
1.2

FIG. 34

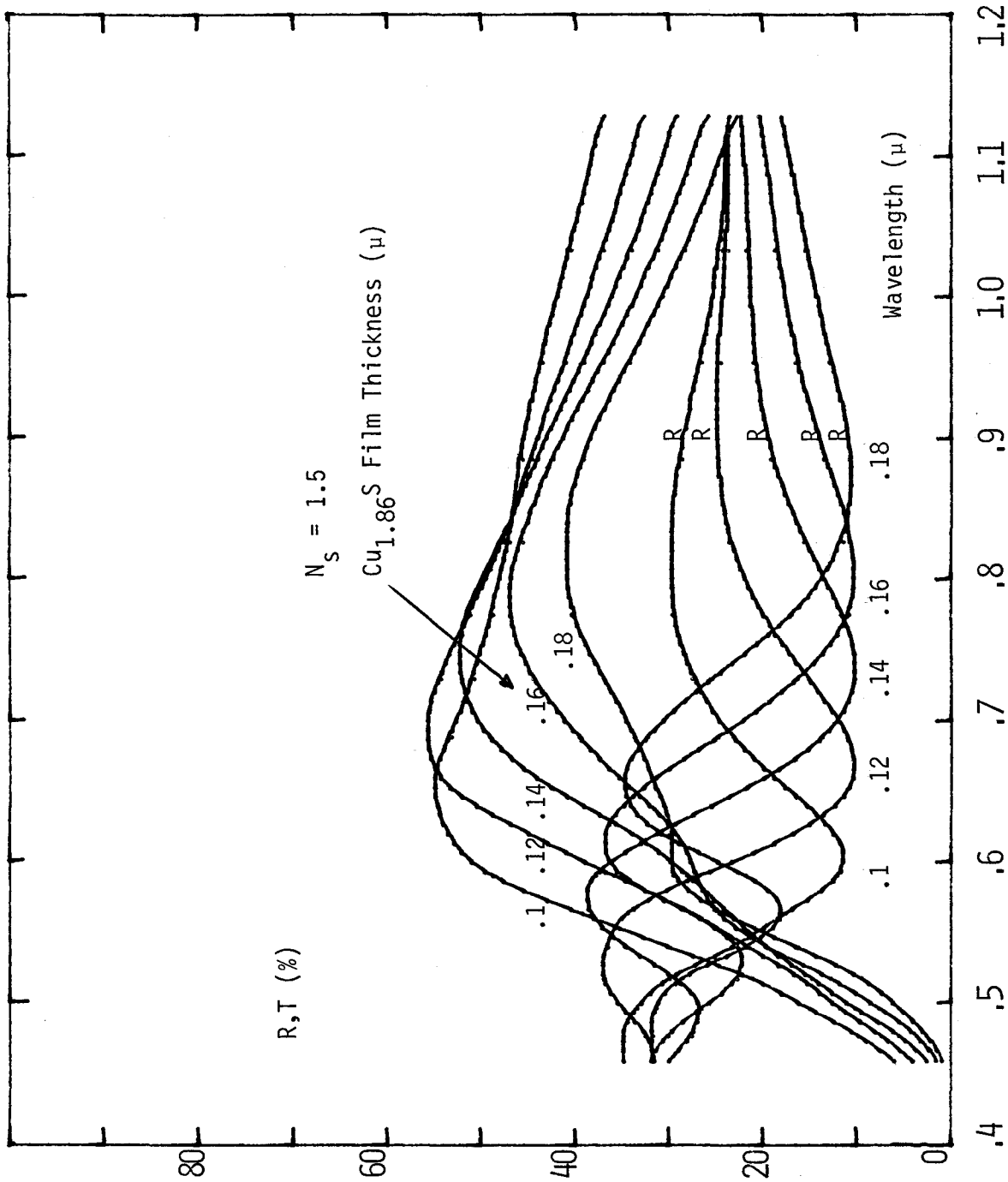
R,T (%)
0
20
40
60
80
.4
.5
.6
.7
.8
.9
1.0
1.1
1.2
Wavelength (μ)
N_s = 1.5
$Cu_{1.86}S$ Film Thickness (μ)
.1
.12
.14
.16
.18
R

FIG. 35

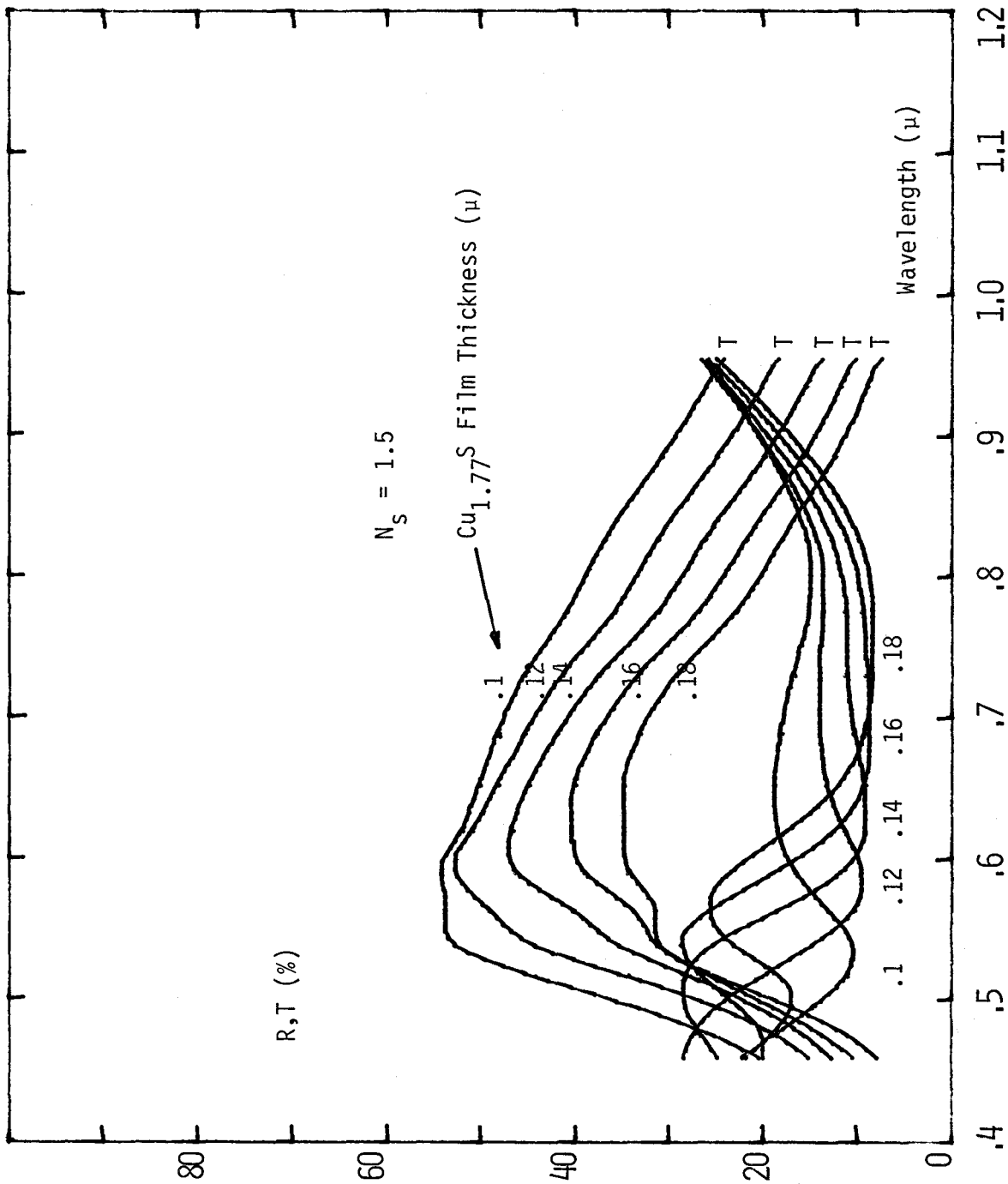
R,T (%)
80
60
40
20
0
.4
.5
.6
.7
.8
.9
1.0
1.1
1.2
Wavelength (μ)
N_s = 1.5
$Cu_{1.77}S$ Film Thickness (μ)
.1
.12
.14
.16
.18
T

FIG. 36

indication of this sensitivity is given in Fig.37,38. The position of equal reflectance-transmittance and position of reflectance minima have been plotted as a function of film thickness for various values of "x". Using these two curves, the composition and the film thickness can be uniquely determined if the reflectance minimum position and equal reflectance - trasmittance position is known.

Several times the composition of the Cu_xS film is not $Cu_{1.995}S$ or $Cu_{1.95}S$ or $Cu_{1.86}S$ or $Cu_{1.77}S$, but lies in between them. Since no single Cu_xS structure exists for in-between values of x, a mixture of phases is to be expected. Depending on the relative amounts of phases and the way they are mixed (i.e. crystal size) one can find average n and k and hence R_m and T_m for these mixtures. For large particle sizes (i.e. $>> \lambda$) a simple weighted average of R's and T's would be appropriate, for very small particle sized ($<< \lambda$) without dipole - dipole interaction, weighted average of dielectric constants has to be taken. In the case where particle sizes are small and dipole-dipole interaction is important, Maxwell Garnett theory should be applied[120,121]. In the range of 0.5 - 1.1 μ, there seems to be little difference in three approaches, as it is evident from Fig.39 to 44. However, we have chosen to use Maxwell Garnett theory, as it is the most appropriate description of segregated thin films, According to this theory, the effective dielectric constant, ε_e is related to the host dielectric constant, ε_h, and the dielectric constant of the foreign molecules, ε_f, as

$$\frac{\varepsilon_e - \varepsilon_h}{\varepsilon_e + 2\varepsilon_h} = q \frac{\varepsilon_f - \varepsilon_h}{\varepsilon_f + 2\varepsilon_h} \qquad (4.6)$$

FIGURE 37: Theoretical position of equal reflectance - transmittance for different phases of copper sulfide as a function of film thickness. Substrate is glass.

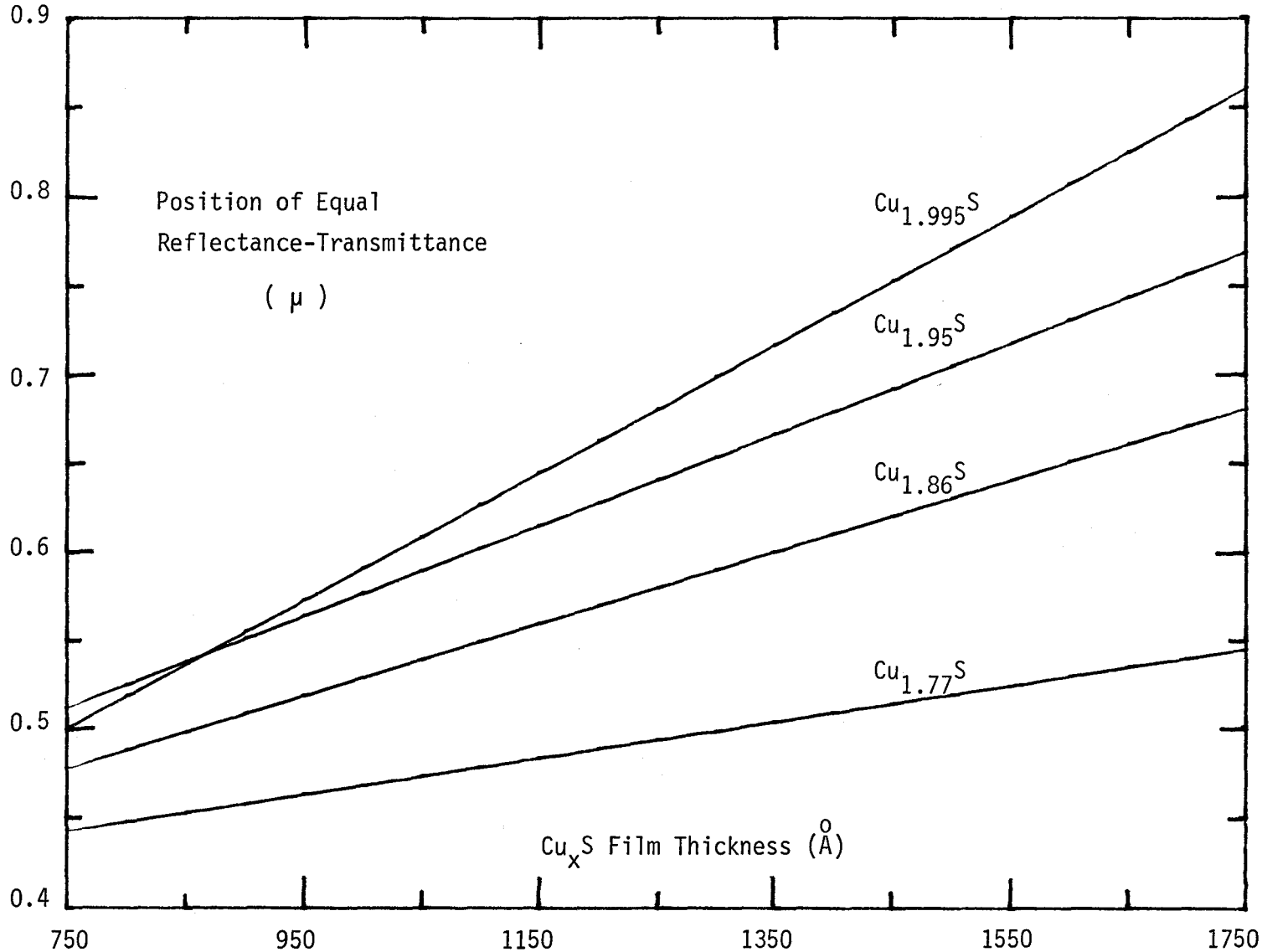
0.9
0.8
0.7
0.6
0.5
0.4
Position of Equal
Reflectance-Transmittance
(μ)
$Cu_{1.995}S$
$Cu_{1.95}S$
$Cu_{1.86}S$
$Cu_{1.77}S$
Cu_xS Film Thickness (Å)
750
950
1150
1350
1550
1750

FIG. 37

FIGURE 38: Theoretical position of reflectance minimum for different phases of copper sulfide, as a function of film thickness. Substrate is glass.

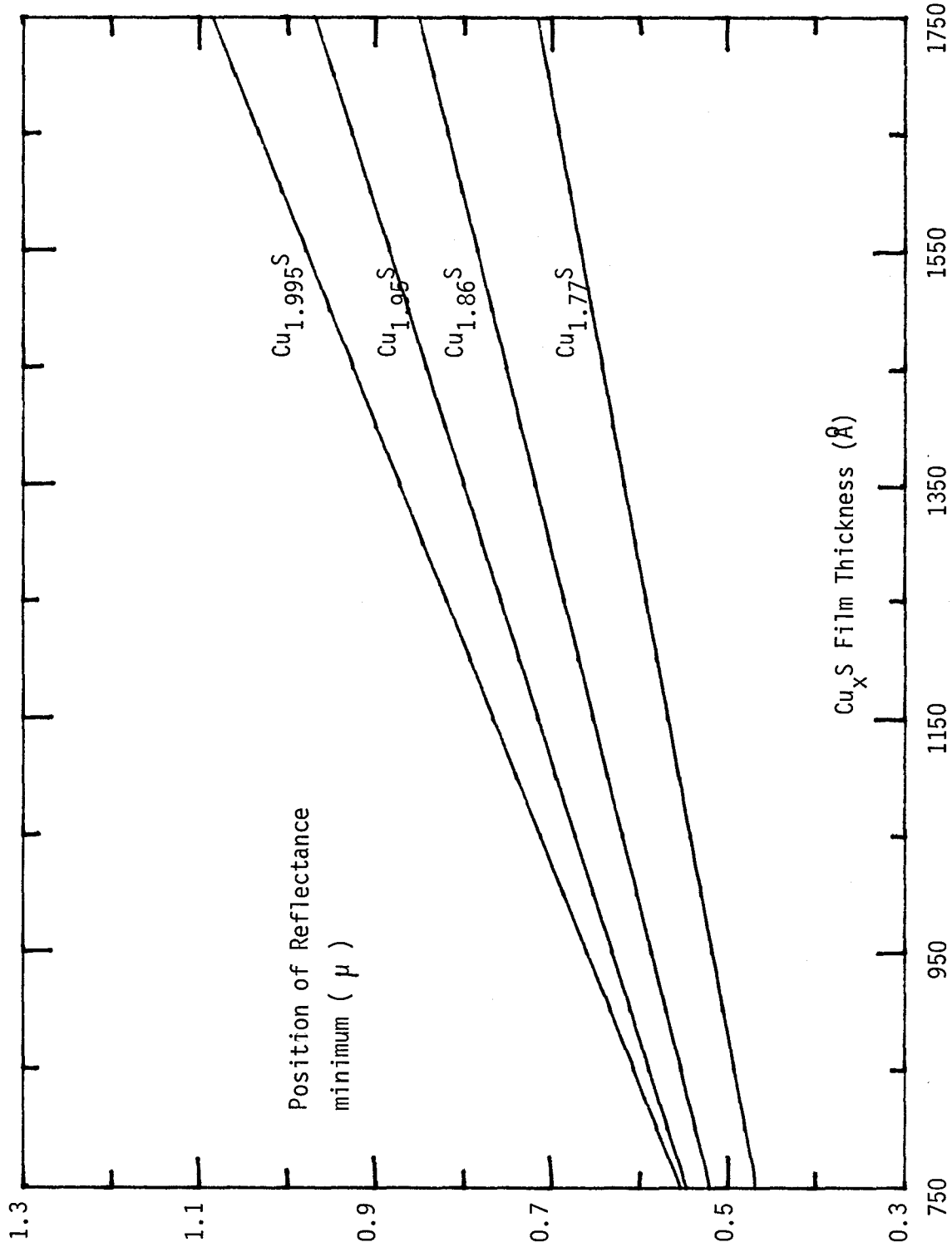
1.3
1.1
0.9
0.7
0.5
0.3
750
950
1150
1350
1550
1750
Position of Reflectance minimum (μ)
$Cu_{1.995}S$
$Cu_{1.95}S$
$Cu_{1.86}S$
$Cu_{1.77}S$
Cu_xS Film Thickness (Å)

FIG. 38

FIGURE 39,40,41,42,43,44: Theoretical R/T curves for different mixtures of $Cu_{1.995}S$ and $Cu_{1.95}S$.

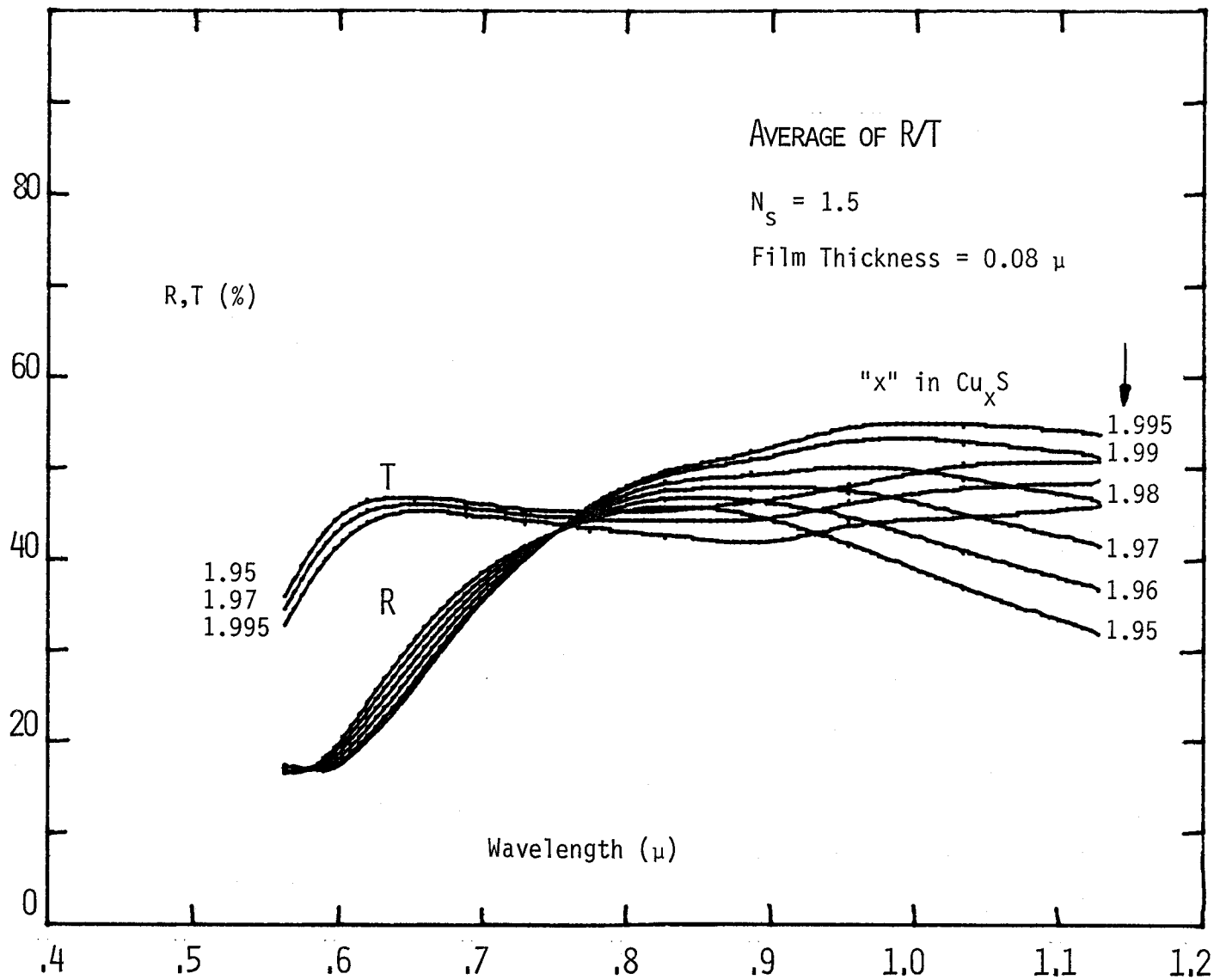
AVERAGE OF R/T
N_s = 1.5
Film Thickness = 0.08 μ
R,T (%)
"x" in Cu_xS
1.995
1.99
1.98
1.97
1.96
1.95
T
R
1.95
1.97
1.995
Wavelength (μ)
0
20
40
60
80
.4
.5
.6
.7
.8
.9
1.0
1.1
1.2

FIG. 39

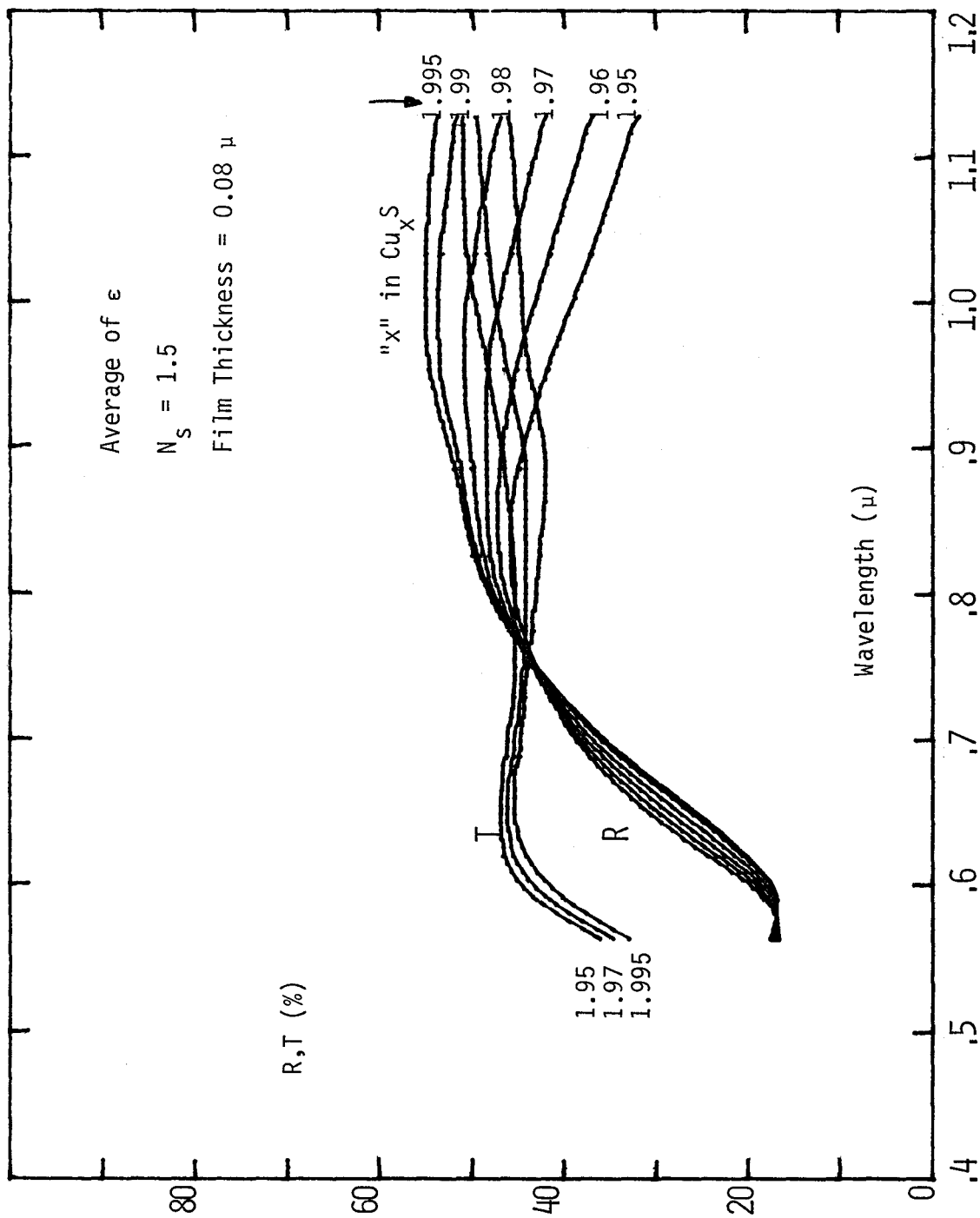
Average of ε
N_s = 1.5
Film Thickness = 0.08 μ
"x" in Cu_xS
1.995
1.99
1.98
1.97
1.96
1.95
I
R
1.95
1.97
1.995
R,T (%)
Wavelength (μ)
0
20
40
60
80
.4
.5
.6
.7
.8
.9
1.0
1.1
1.2

FIG. 40

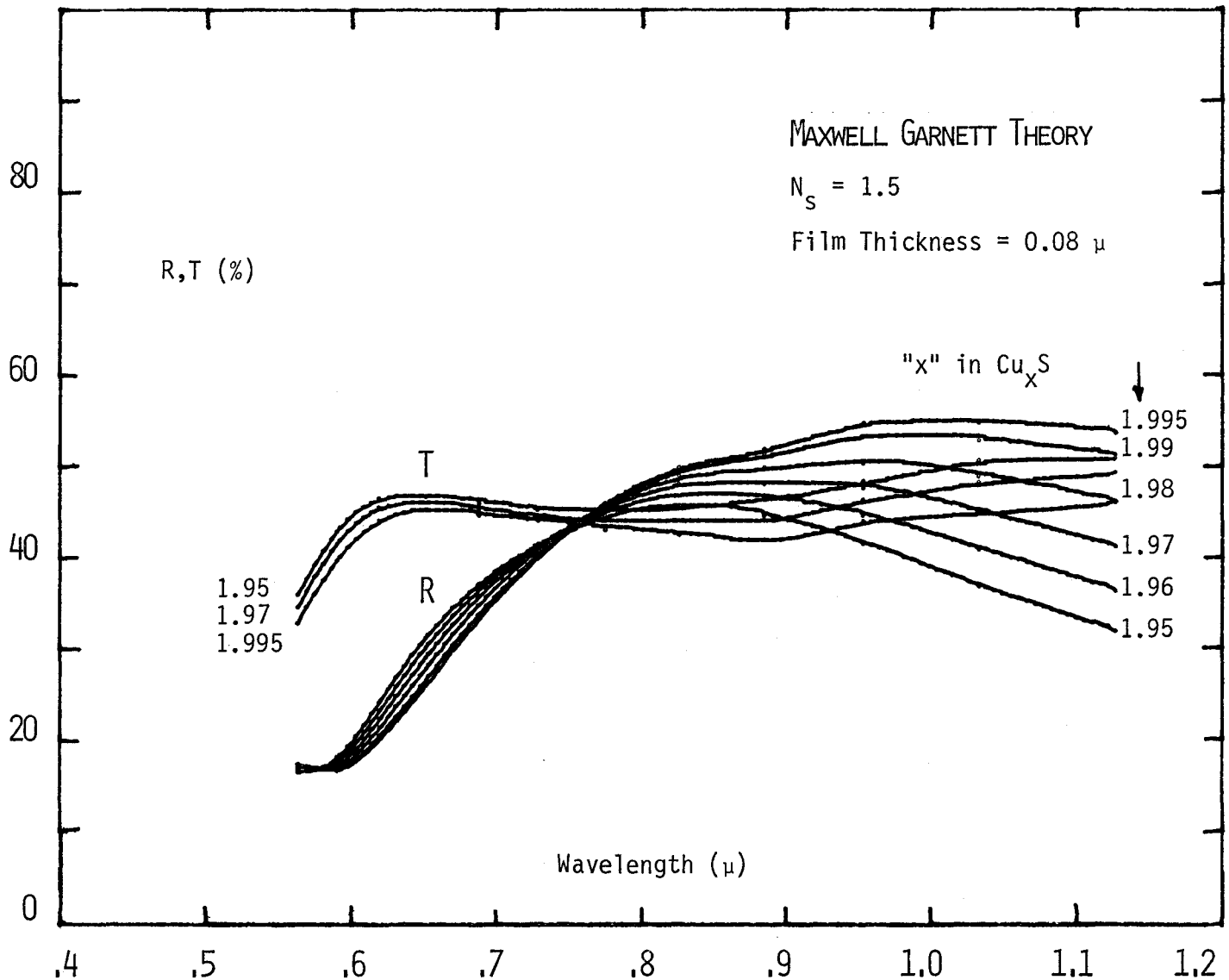
MAXWELL GARNETT THEORY
N_s = 1.5
Film Thickness = 0.08 μ
R,T (%)
"x" in Cu_xS
1.995
1.99
1.98
1.97
1.96
1.95
T
R
1.95
1.97
1.995
Wavelength (μ)
0
20
40
60
80
.4
.5
.6
.7
.8
.9
1.0
1.1
1.2

FIG. 41

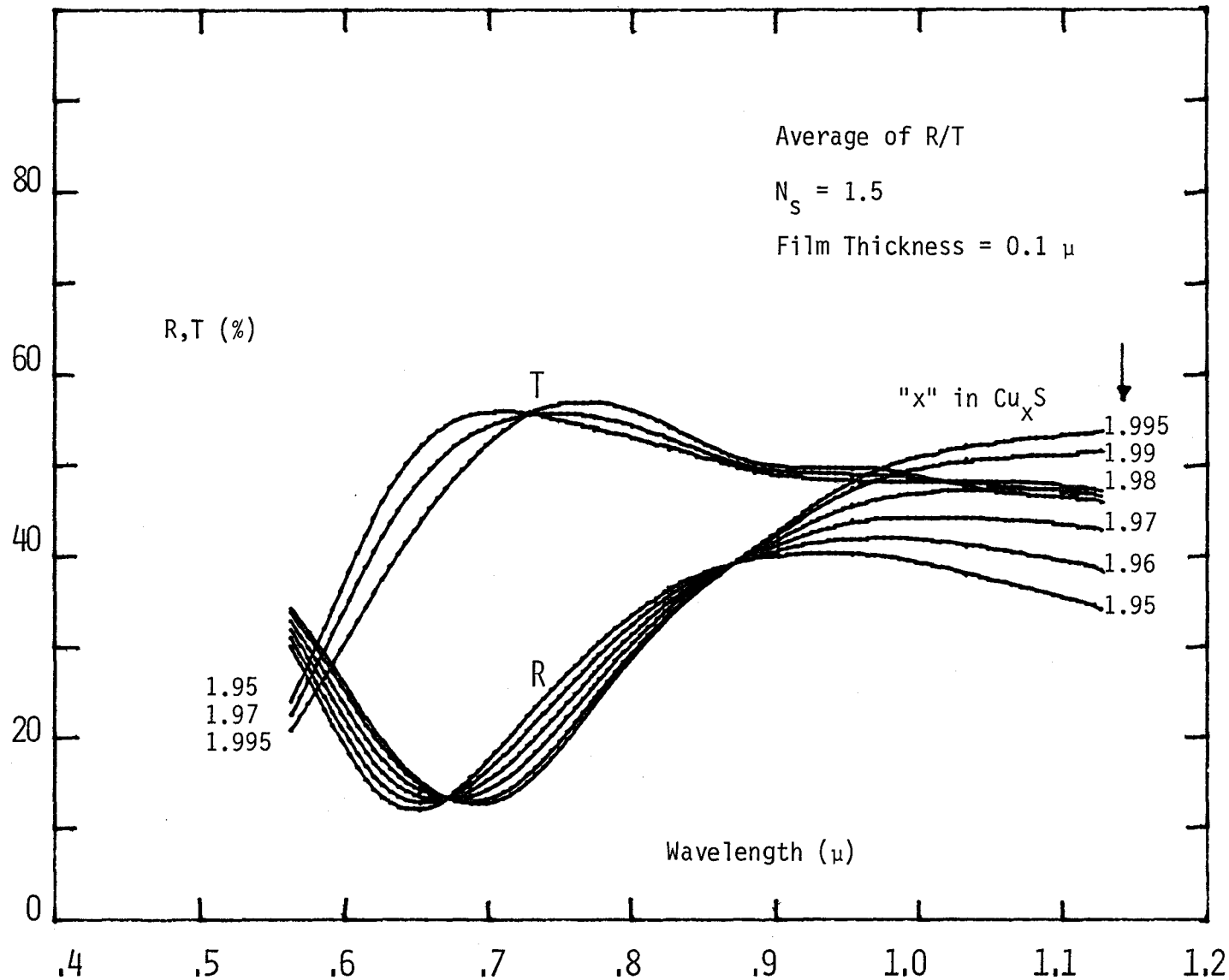
Average of R/T
N_s = 1.5
Film Thickness = 0.1 μ
R,T (%)
T
R
"x" in Cu_xS
1.995
1.99
1.98
1.97
1.96
1.95
1.95
1.97
1.995
Wavelength (μ)
0
20
40
60
80
.4
.5
.6
.7
.8
.9
1.0
1.1
1.2

FIG. 42

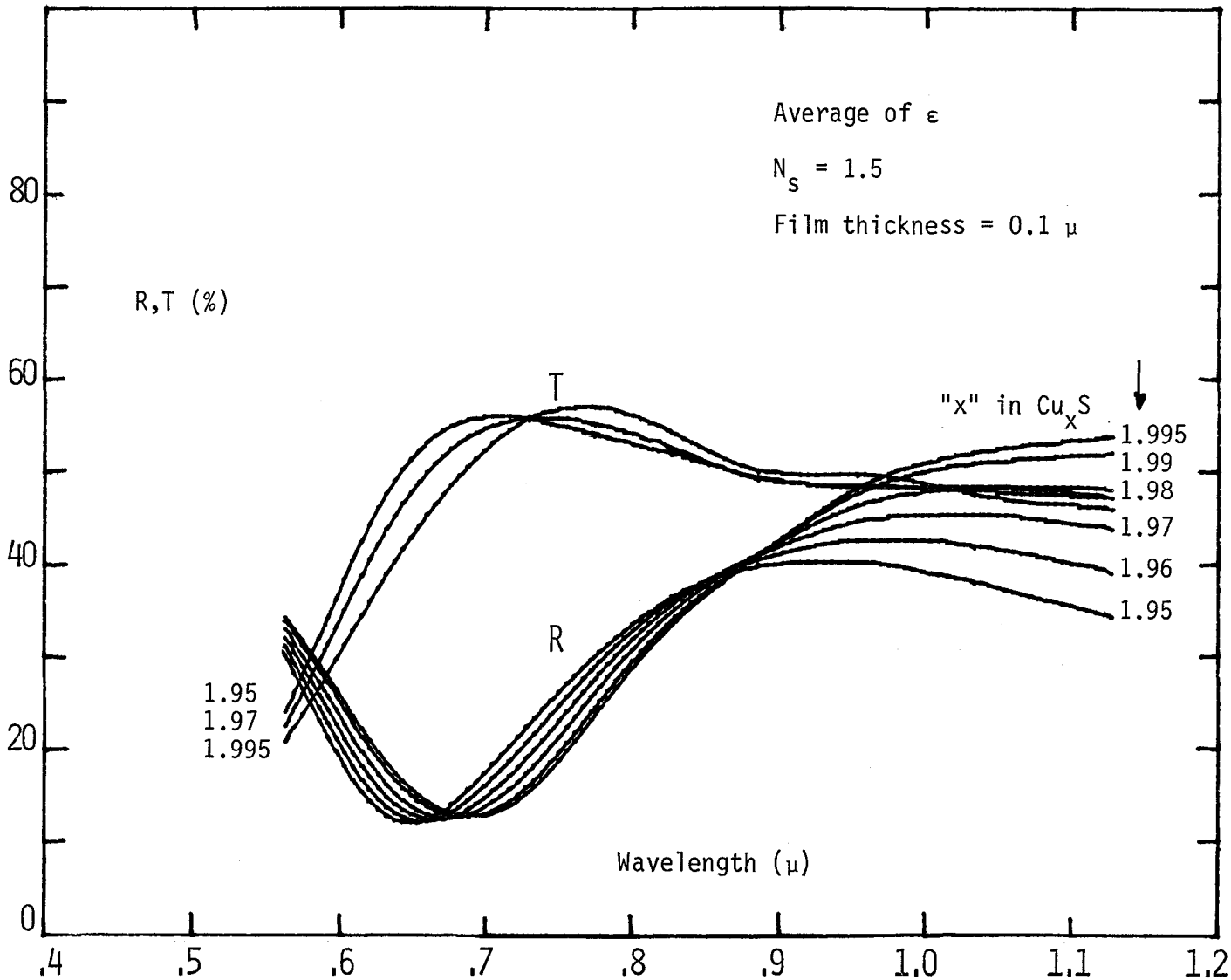
Average of ε
N_s = 1.5
Film thickness = 0.1 μ
R,T (%)
T
R
"x" in Cu_xS
1.995
1.99
1.98
1.97
1.96
1.95
1.95
1.97
1.995
Wavelength (μ)
0
20
40
60
80
.4
.5
.6
.7
.8
.9
1.0
1.1
1.2

FIG. 43

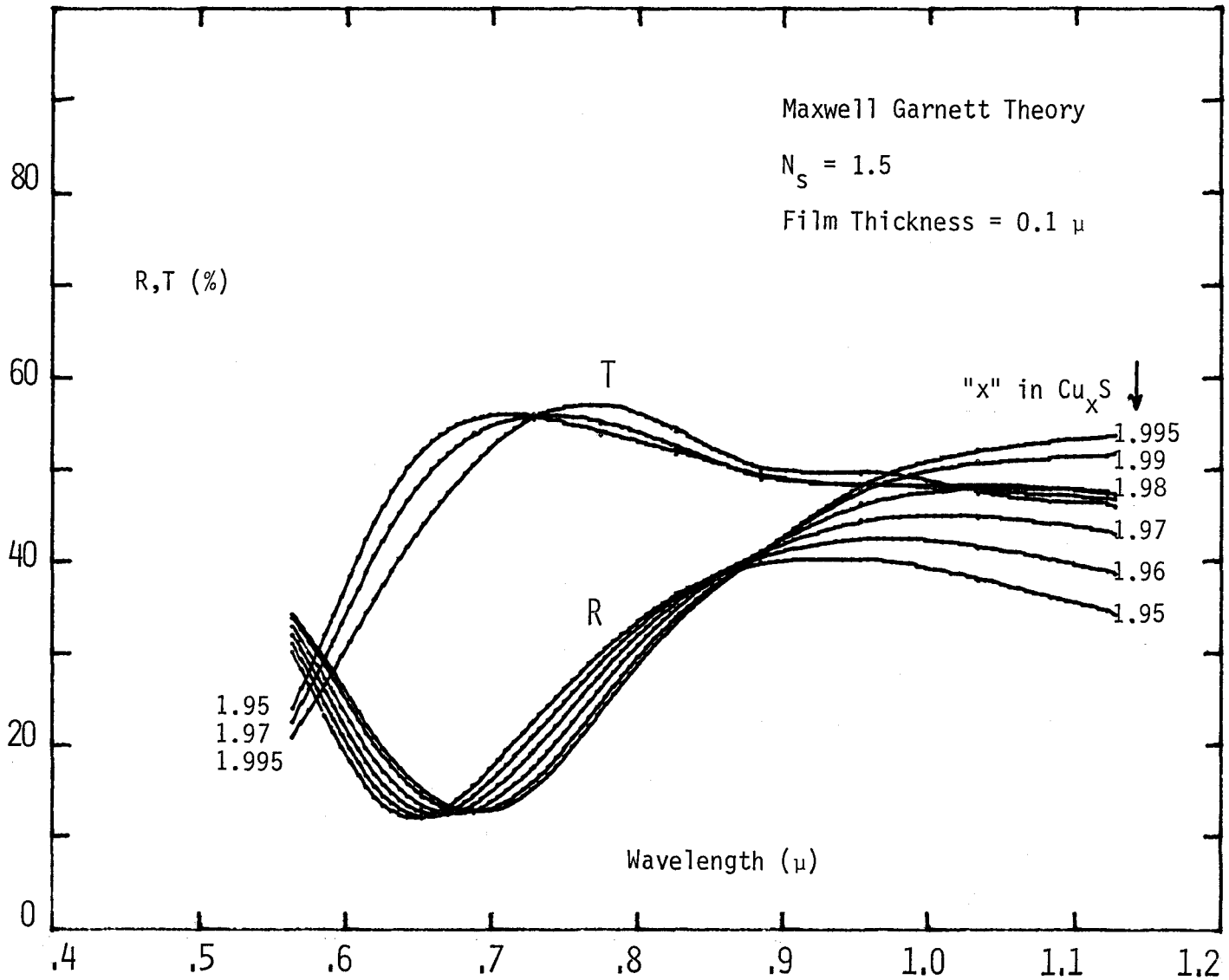
Maxwell Garnett Theory
N_s = 1.5
Film Thickness = 0.1 μ
R,T (%)
T
"x" in Cu_xS
1.995
1.99
1.98
1.97
1.96
1.95
R
1.95
1.97
1.995
Wavelength (μ)
0
20
40
60
80
.4
.5
.6
.7
.8
.9
1.0
1.1
1.2

FIG. 44

where q = no. of foreign particle/total no. of particles.

The real and imaginary parts can be separated, to give

$$\varepsilon_e^r = \frac{AC + BD}{A^2 + B^2}$$

$$\varepsilon_e^i = \frac{AD - BC}{A^2 + B^2} \qquad (4.7)$$

where

$$A = \varepsilon_f^r (1 - q) + \varepsilon_h^r (q + 2)$$

$$B = \varepsilon_f^i (1 - q) + \varepsilon_h^i (q + 2)$$

$$C = \varepsilon_h^r [\varepsilon_f^r (1 + 2q) + 2\varepsilon_h^r (1 - q)] - \varepsilon_h^i [\varepsilon_f^i (1 + 2q) + 2\varepsilon_h^i (1 - q)]$$

$$D = \varepsilon_h^r [\varepsilon_f^i (1 + 2q) + 2\varepsilon_h^i (1 - q)] + \varepsilon_h^i [\varepsilon_f^r (1 + 2q) + 2\varepsilon_h^r (1 - q)]$$

The effective R_m and T_m can now be calculated using equation 4.4. In some cases, even this technique could not explain the observed features of R, T curves, because of the film discontinuities. It is a well recognized fact that the properties of thin films are different than that of the corresponding bulk, mainly because of reduced packing fraction which saturates only after a certain thickness of the film[122]. When the porosity of thin films were taken into account by using $\varepsilon_h = (1 + i.0)$, all the experimental results could be explained in a reasonable manner. Some examples of the theoretical cases are shown in Fig.45,46.

Experimental results for various films are shown in Fig.47 to 56 . The oscillations in both reflection and transmission are due to the interference effects produced by the multiple relections in thin films of Cu_xS. The period of these oscillations is a function of the wavelength

FIGURE 45,46: Theoretical R/T curves of $Cu_{1.995}S$ films with with different porosity

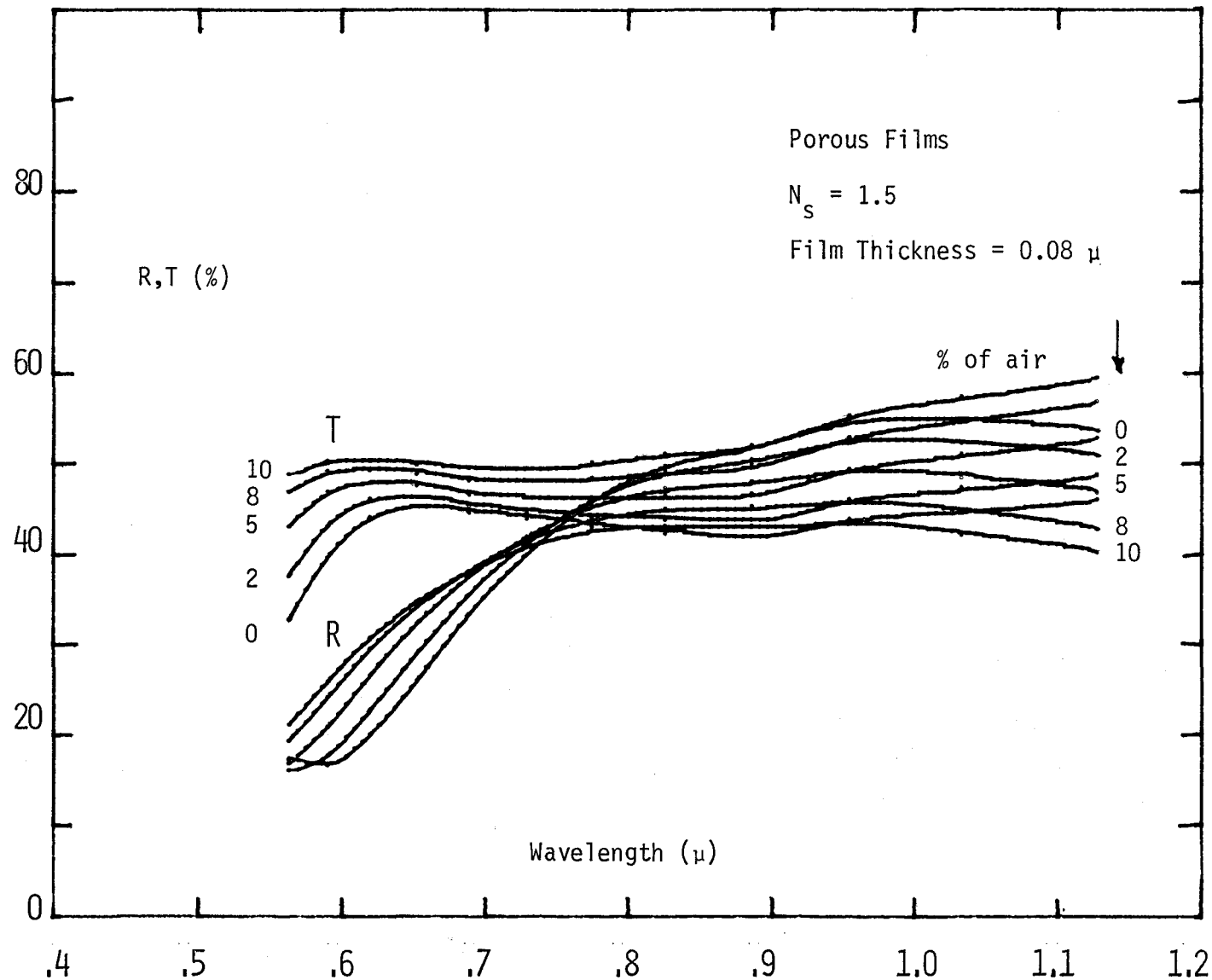
Porous Films
N_s = 1.5
Film Thickness = 0.08 μ
R,T (%)
% of air
T
R
10
8
5
2
0
0
2
5
8
10
80
60
40
20
0
.4
.5
.6
.7
.8
.9
1.0
1.1
1.2
Wavelength (μ)

FIG. 45

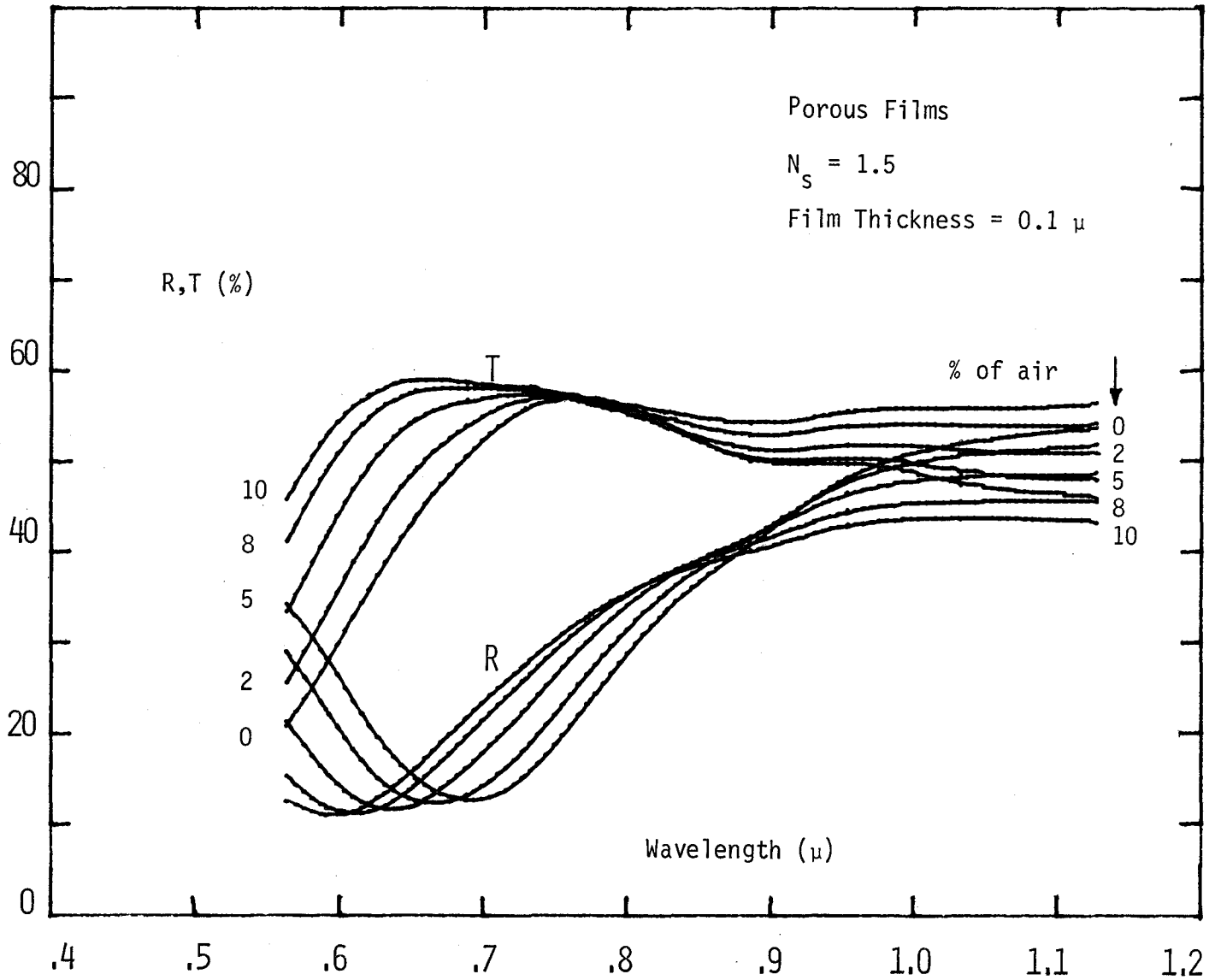
Porous Films
N_s = 1.5
Film Thickness = 0.1 μ
R,T (%)
T
% of air
0
2
5
8
10
10
8
5
2
0
R
Wavelength (μ)
80
60
40
20
0
.4
.5
.6
.7
.8
.9
1.0
1.1
1.2

FIG. 46

FIGURE 47,48,49,50,51,52,53,54,55,56:

Experimental R/T curves for different films of copper sulfide and corresponding theoretical R/T curves. In Fig. 53 and Fig. 55 some extra theoretical curves are also shown to illustrate the goodness of the fit.

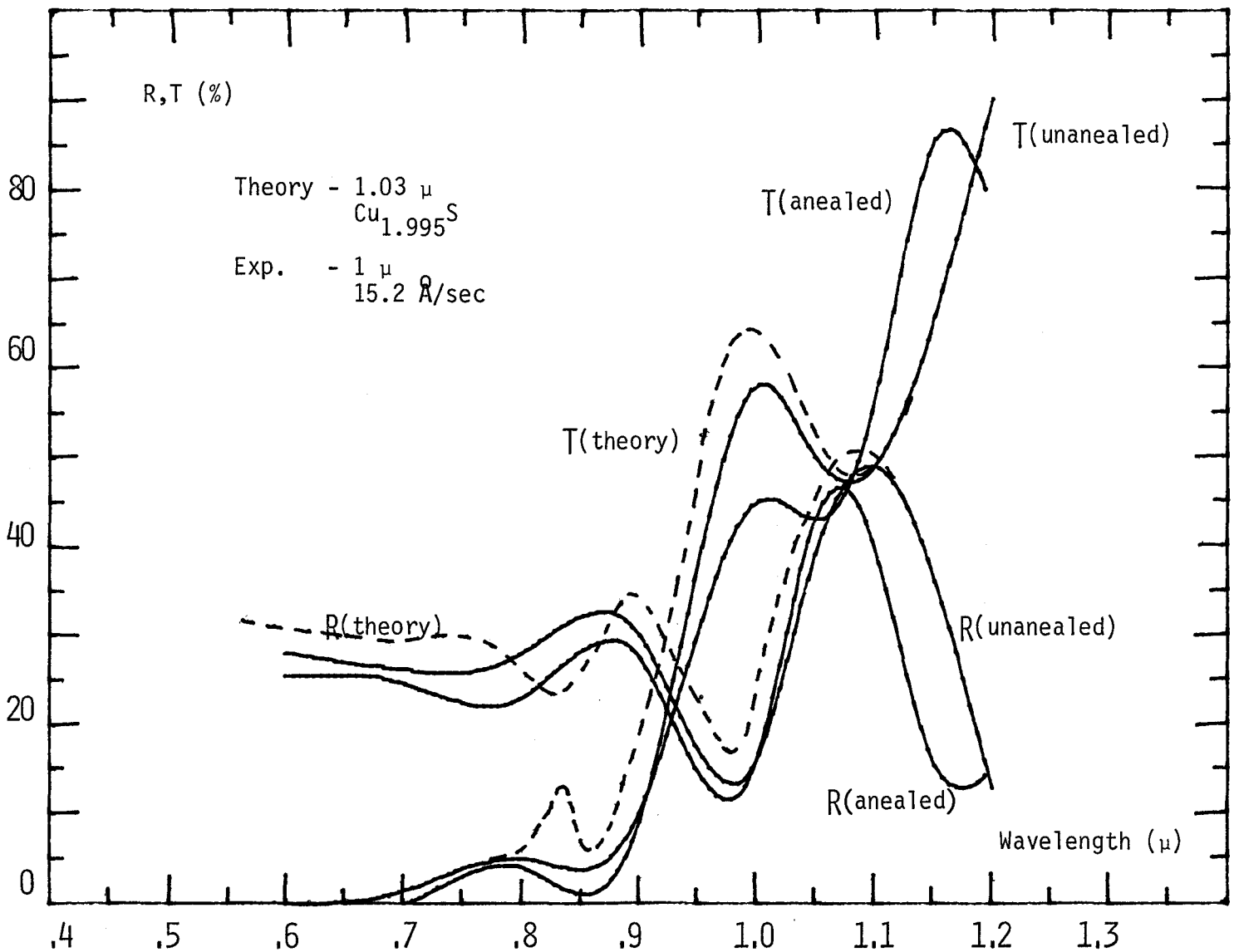
R,T (%)
Theory - 1.03 μ
$Cu_{1.995}S$
Exp. - 1 μ
15.2 Å/sec
T(unanealed)
T(anealed)
T(theory)
R(theory)
R(unanealed)
R(anealed)
Wavelength (μ)
80
60
40
20
0
.4
.5
.6
.7
.8
.9
1.0
1.1
1.2
1.3

FIG. 47

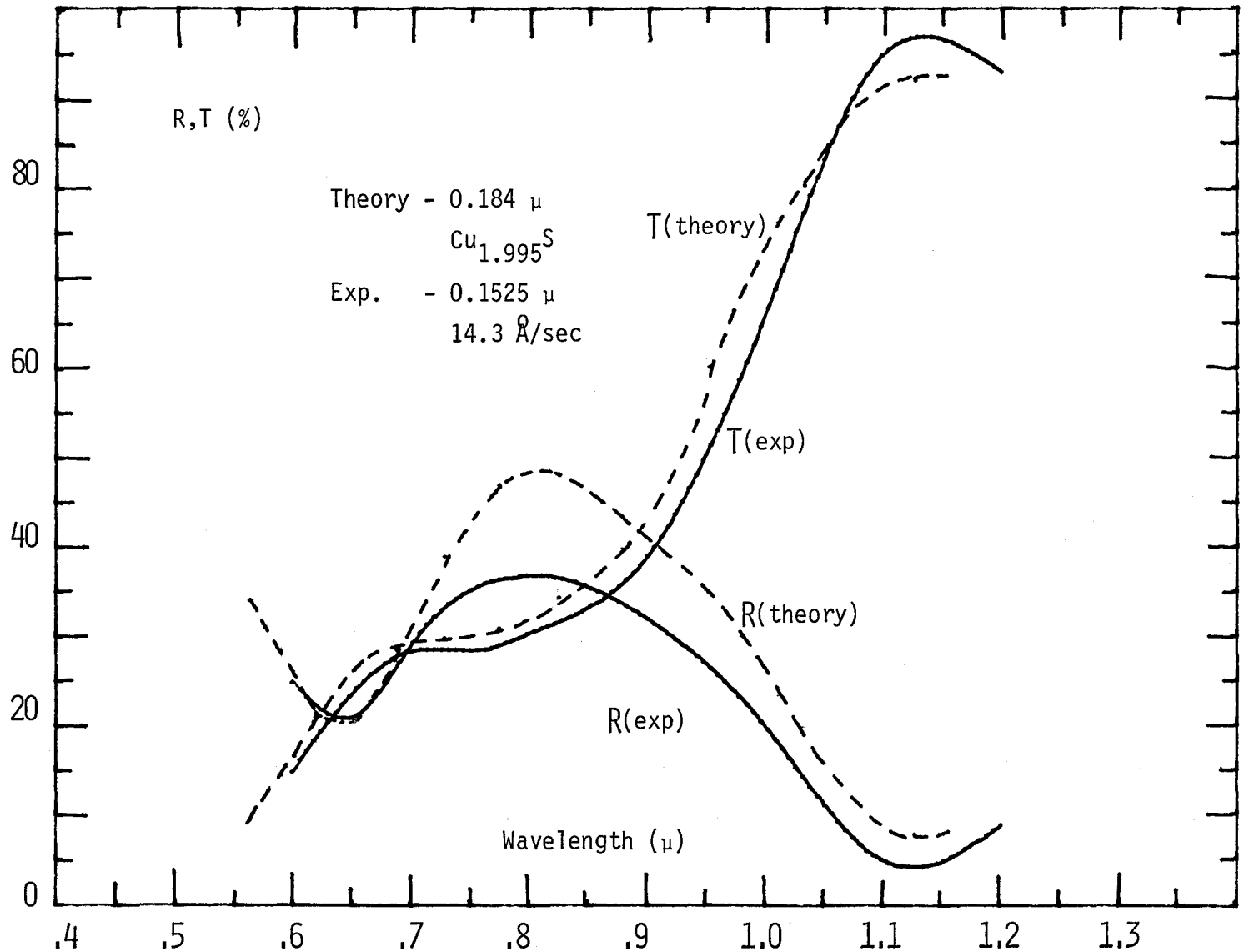
R,T (%)
Theory - 0.184 μ
$Cu_{1.995}S$
Exp. - 0.1525 μ
14.3 Å/sec
T(theory)
T(exp)
R(theory)
R(exp)
Wavelength (μ)
0
20
40
60
80
.4
.5
.6
.7
.8
.9
1.0
1.1
1.2
1.3

FIG. 48

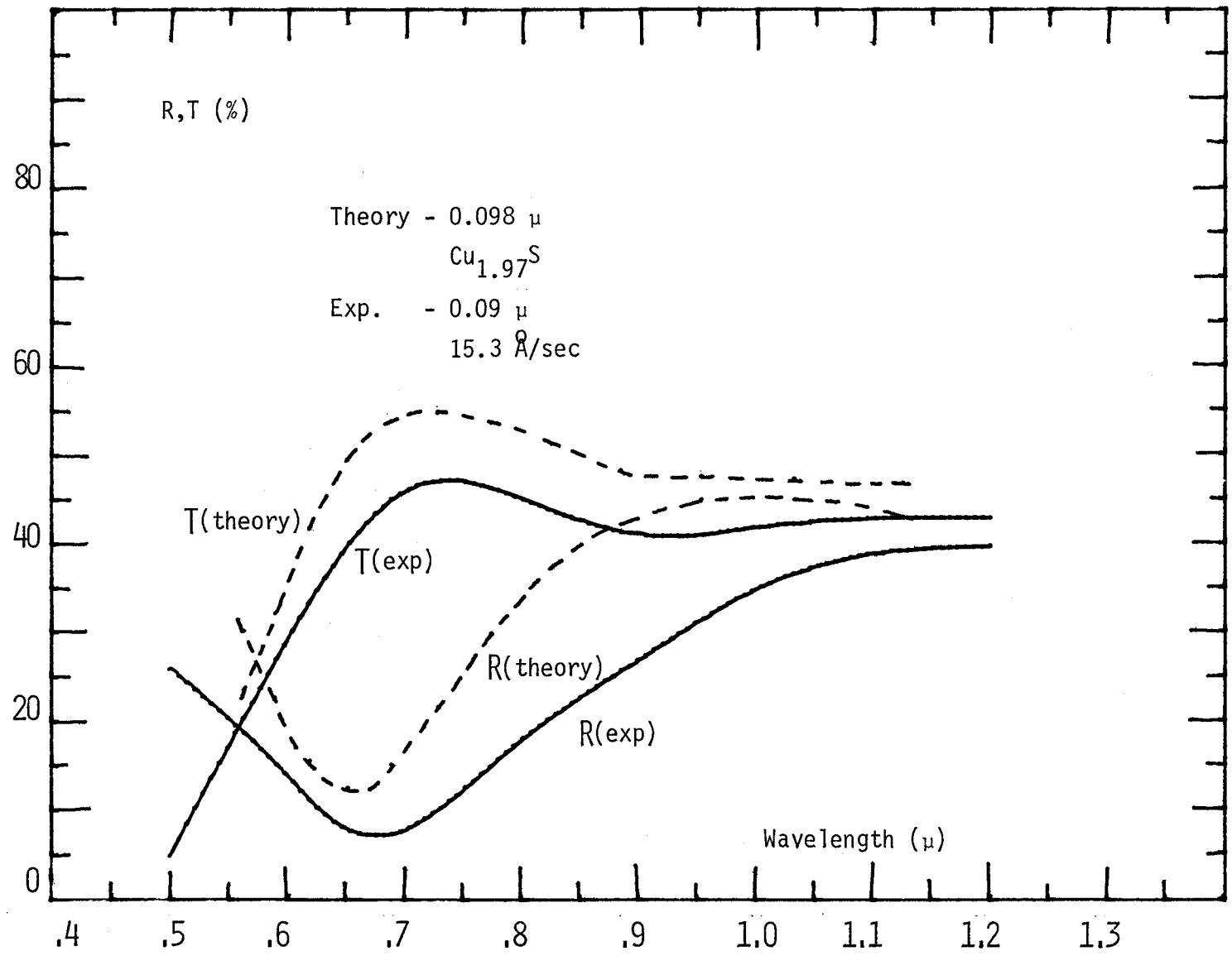
R,T (%)
Theory - 0.098 μ
$Cu_{1.97}S$
Exp. - 0.09 μ
15.3 Å/sec
T(theory)
T(exp)
R(theory)
R(exp)
Wavelength (μ)
80
60
40
20
0
.4
.5
.6
.7
.8
.9
1.0
1.1
1.2
1.3

FIG. 49

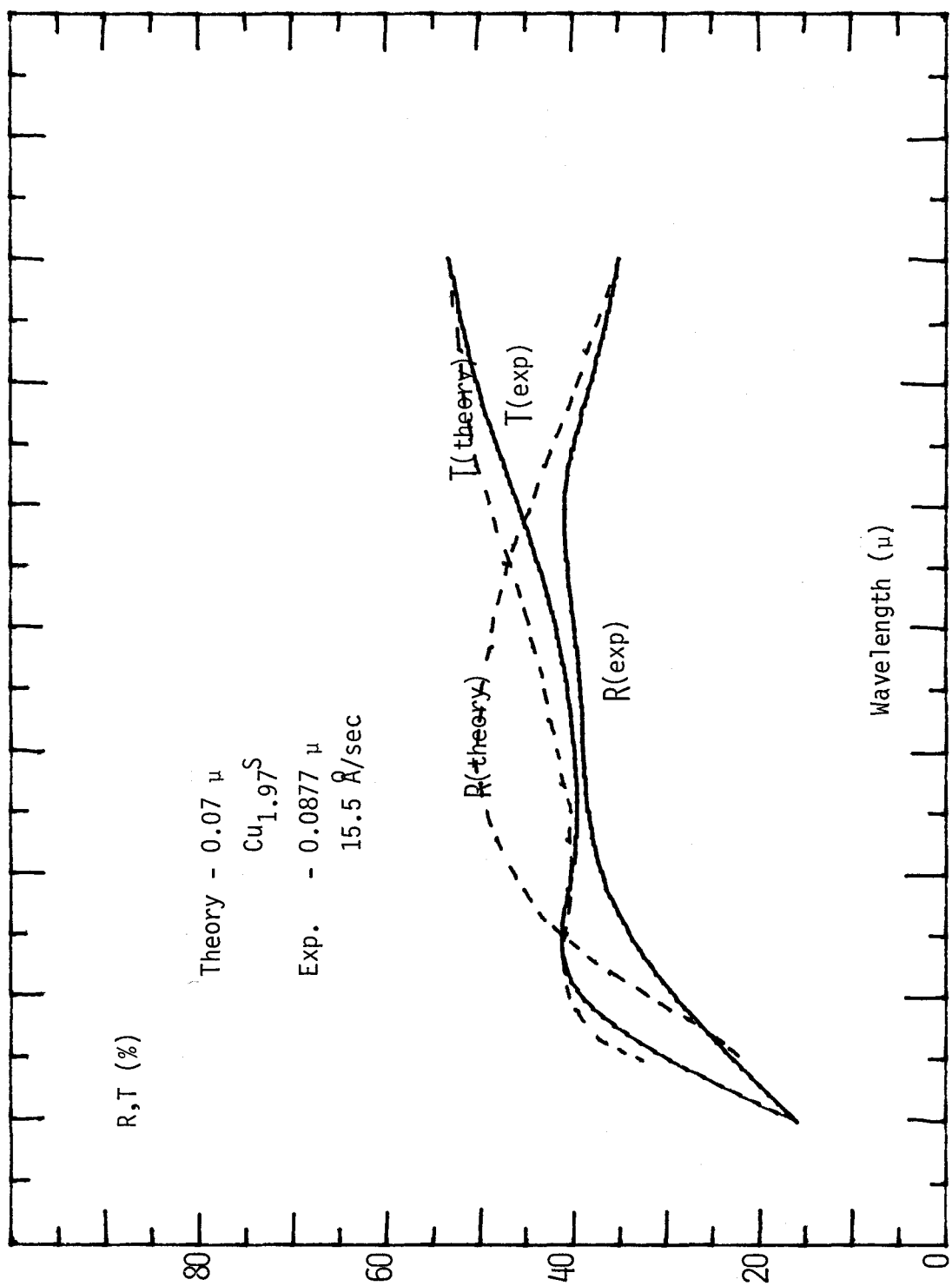
R,T (%)
Theory - 0.07 μ
$Cu_{1.97}S$
Exp. - 0.0877 μ
15.5 Å/sec
T(theory)
R(theory)
T(exp)
R(exp)
Wavelength (μ)
0
20
40
60
80
.4
.5
.6
.7
.8
.9
1.0
1.1
1.2
1.3

FIG. 50

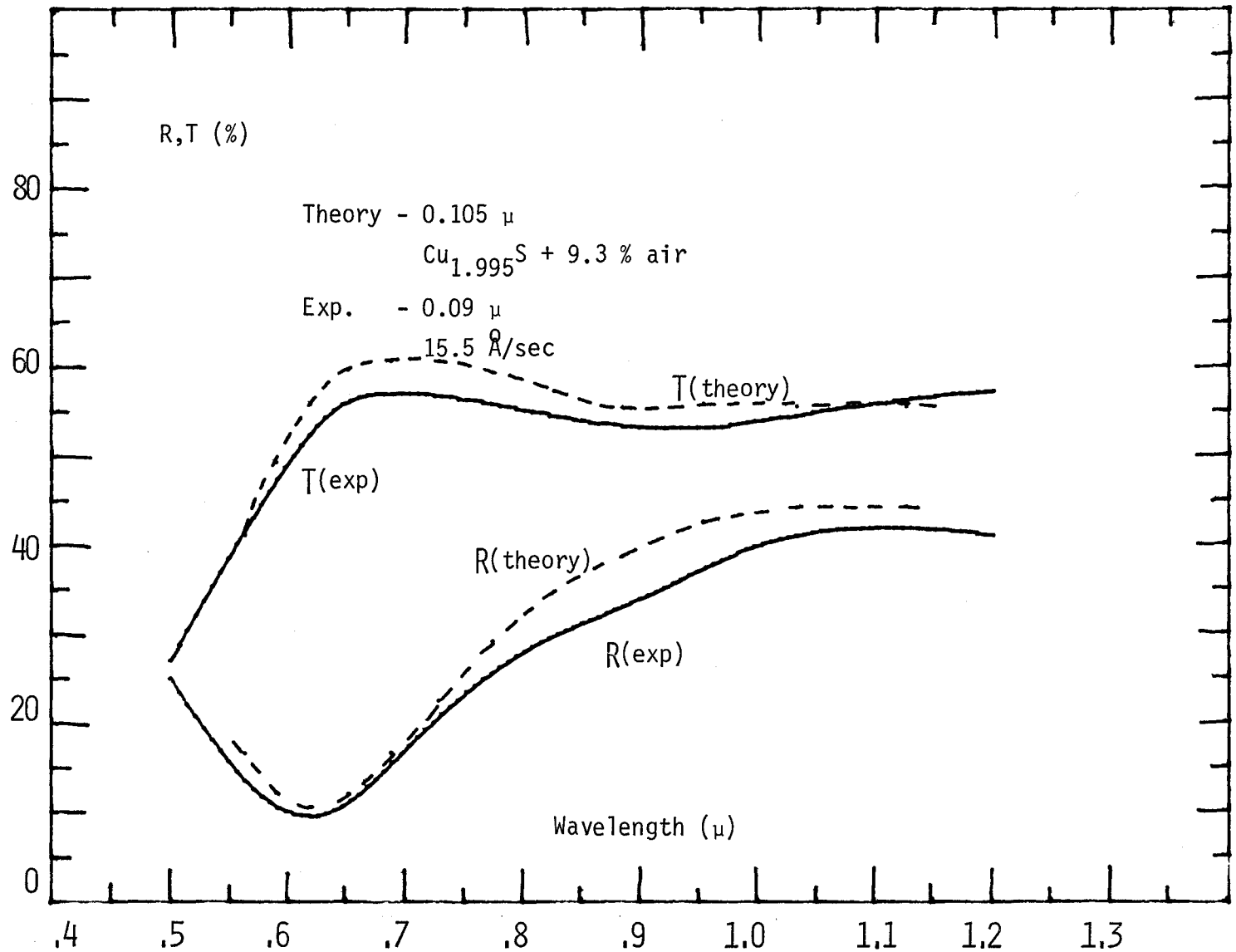
R,T (%)
Theory - 0.105 μ
$Cu_{1.995}S$ + 9.3 % air
Exp. - 0.09 μ
15.5 Å/sec
T(theory)
T(exp)
R(theory)
R(exp)
Wavelength (μ)
80
60
40
20
0
.4
.5
.6
.7
.8
.9
1.0
1.1
1.2
1.3

FIG. 51

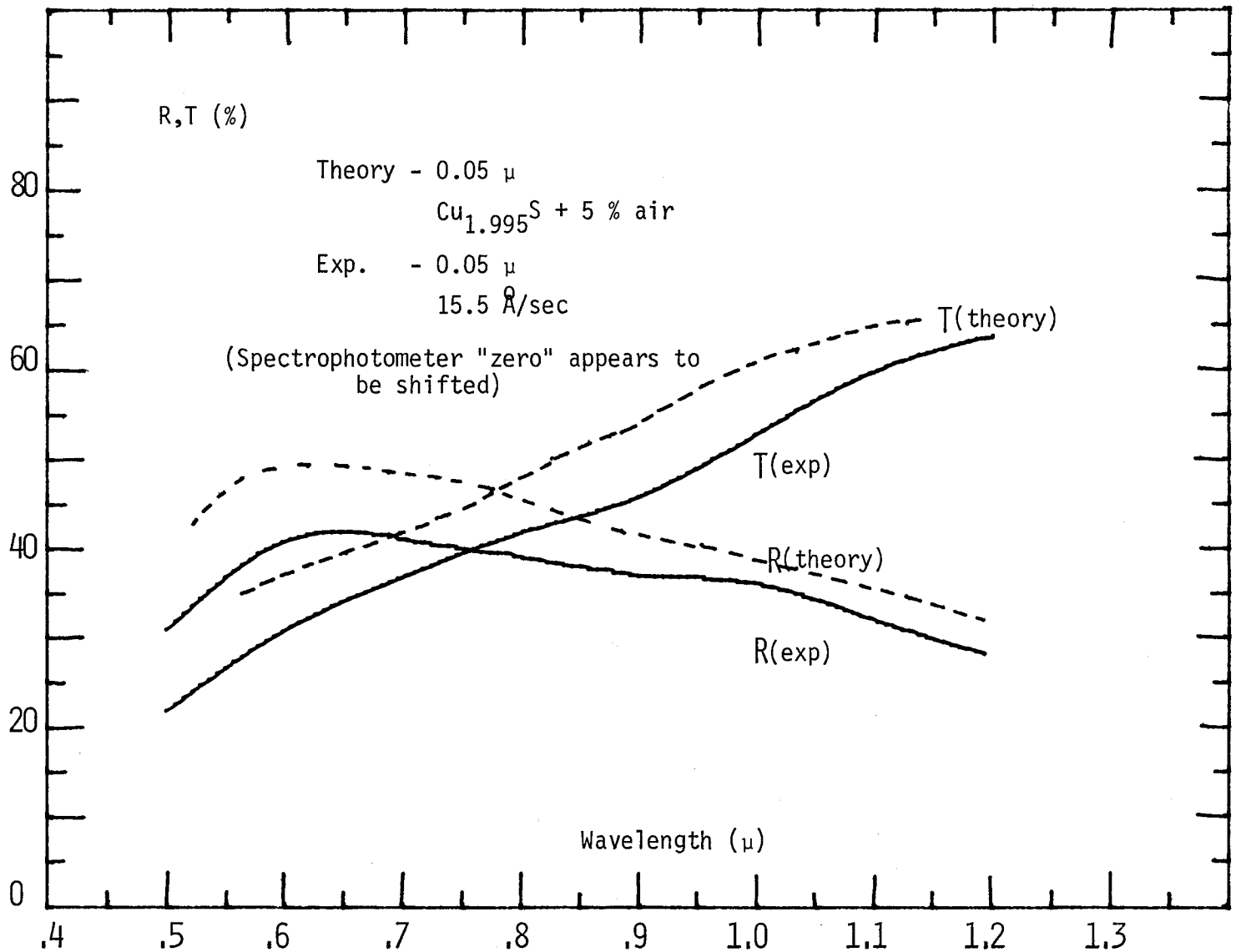
R,T (%)
Theory - 0.05 μ
$Cu_{1.995}S$ + 5 % air
Exp. - 0.05 μ
15.5 Å/sec
(Spectrophotometer "zero" appears to be shifted)
T(theory)
T(exp)
R(theory)
R(exp)
Wavelength (μ)
0
20
40
60
80
.4
.5
.6
.7
.8
.9
1.0
1.1
1.2
1.3

FIG. 52

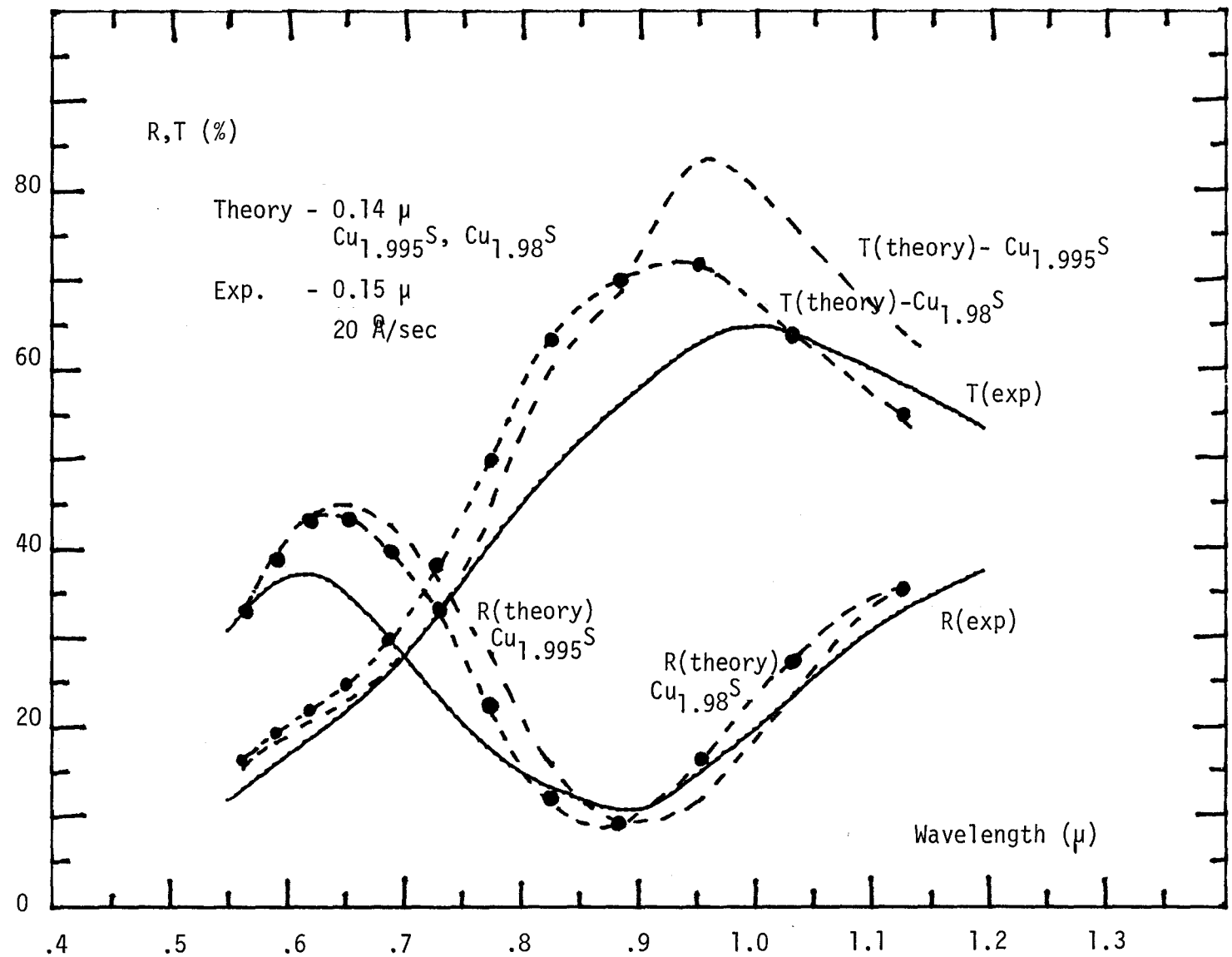
R,T (%)
Theory - 0.14 μ
$Cu_{1.995}S$, $Cu_{1.98}S$
Exp. - 0.15 μ
20 Å/sec
T(theory)- $Cu_{1.995}S$
T(theory)-$Cu_{1.98}S$
T(exp)
R(theory)
$Cu_{1.995}S$
R(theory)
$Cu_{1.98}S$
R(exp)
Wavelength (μ)
0
20
40
60
80
.4
.5
.6
.7
.8
.9
1.0
1.1
1.2
1.3

FIG. 53

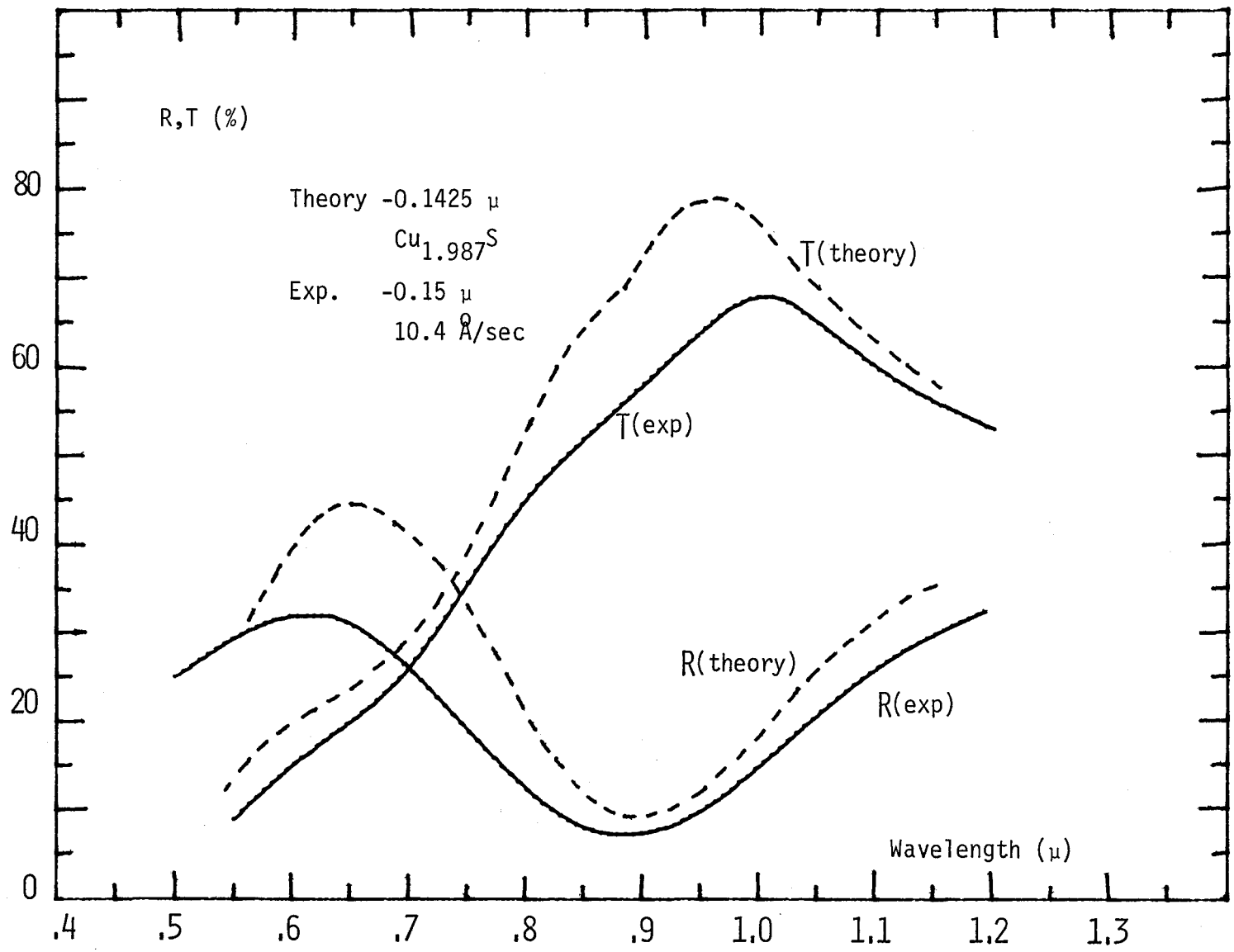
R,T (%)
Theory -0.1425 μ
$Cu_{1.987}S$
Exp. -0.15 μ
10.4 Å/sec
T(theory)
T(exp)
R(theory)
R(exp)
Wavelength (μ)
0
20
40
60
80
.4
.5
.6
.7
.8
.9
1.0
1.1
1.2
1.3

FIG.54

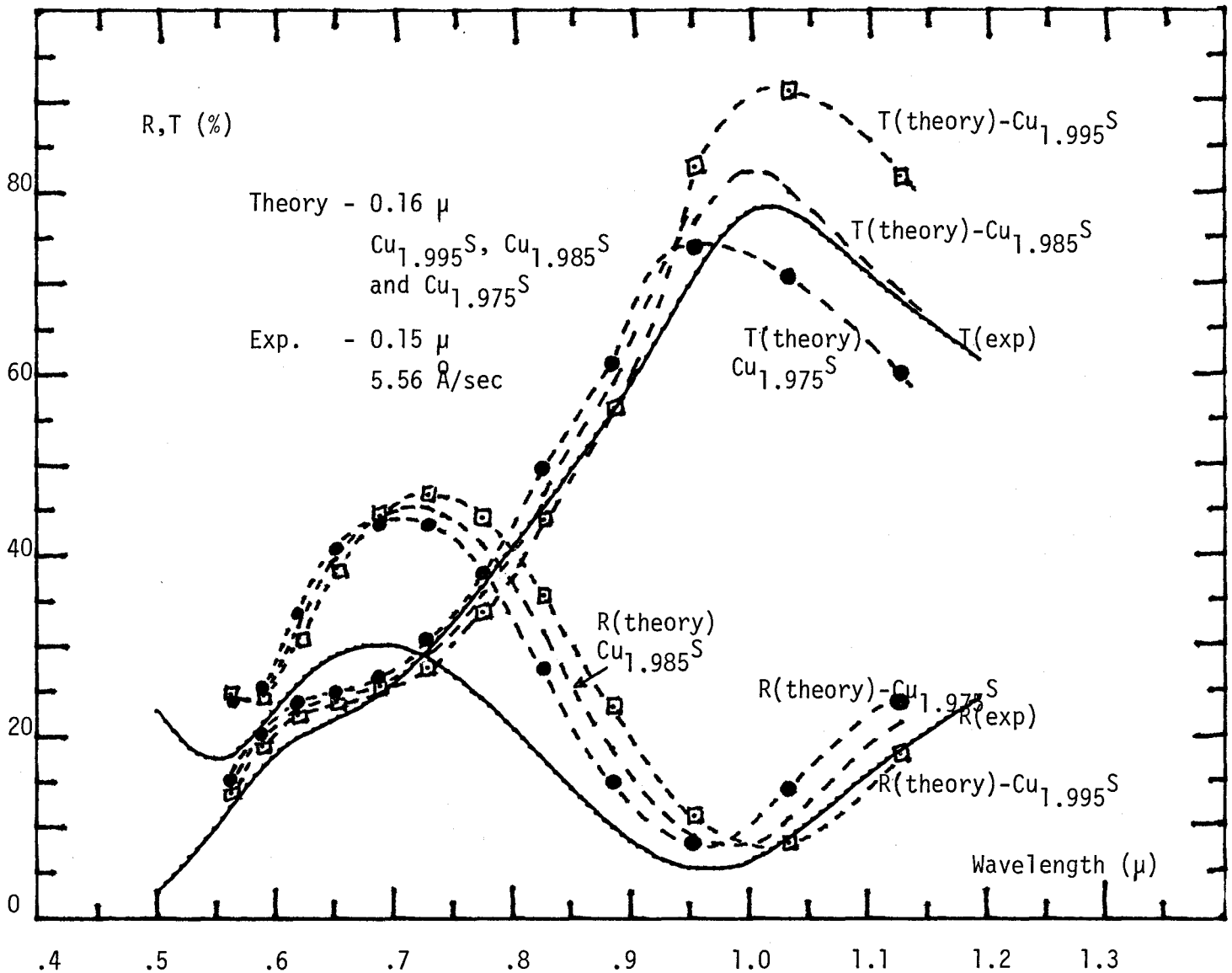
R,T (%)
Theory - 0.16 μ
Cu1.995S, Cu1.985S
and Cu1.975S
Exp. - 0.15 μ
5.56 Å/sec
T(theory)-Cu1.995S
T(theory)-Cu1.985S
T(theory)
Cu1.975S
T(exp)
R(theory)
Cu1.985S
R(theory)-Cu1.975S
R(exp)
R(theory)-Cu1.995S
Wavelength (μ)
0
20
40
60
80
.4
.5
.6
.7
.8
.9
1.0
1.1
1.2
1.3

FIG. 55

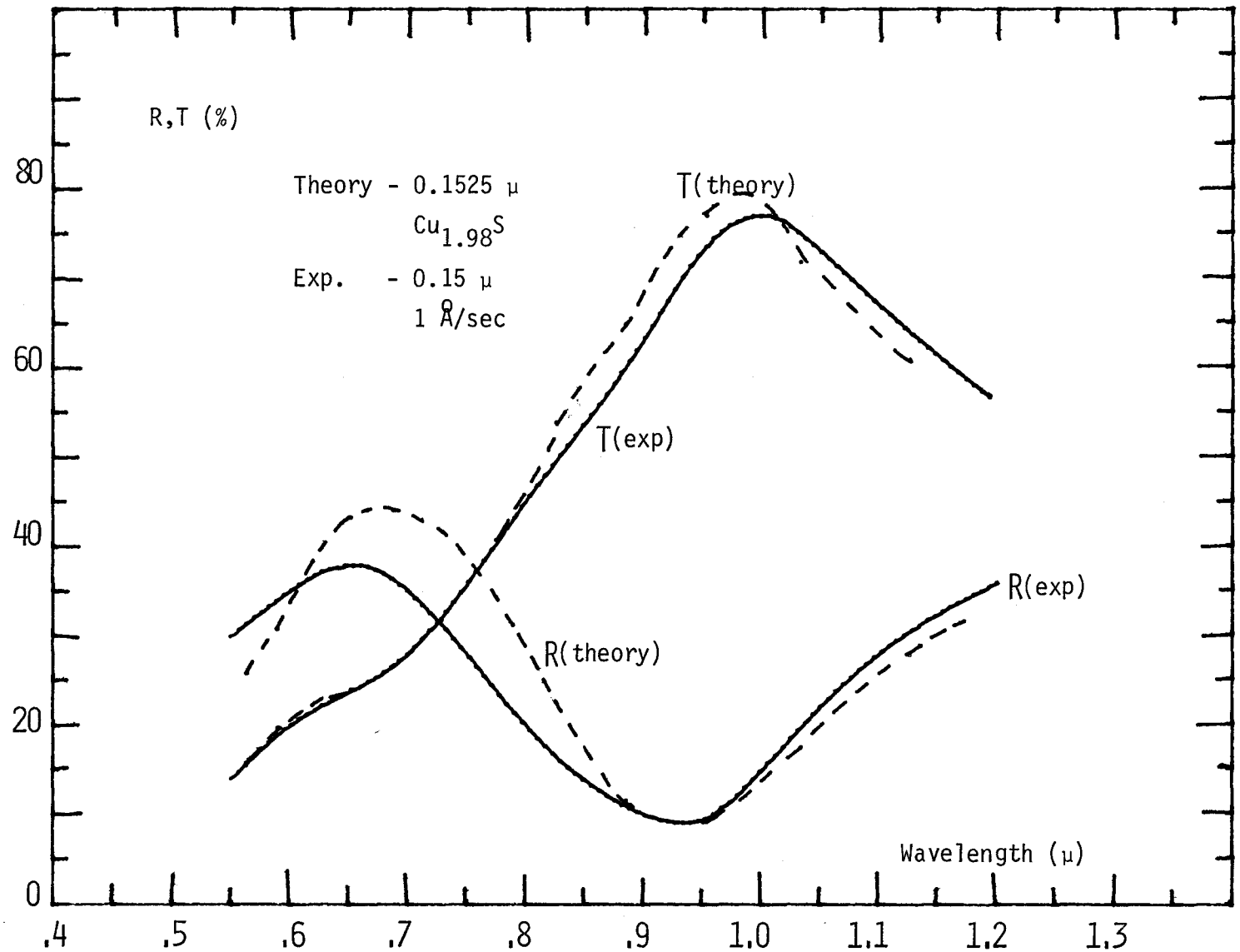
R,T (%)
Theory - 0.1525 μ
$Cu_{1.98}S$
Exp. - 0.15 μ
1 Å/sec
T(theory)
T(exp)
R(exp)
R(theory)
Wavelength (μ)
80
60
40
20
0
.4
.5
.6
.7
.8
.9
1.0
1.1
1.2
1.3

FIG. 56

and can be seen to increase with increasing λ. The position of maxima and minima are a function of the film thickness, d, and its refractive index, n. For normally incident light reflection maxima will occur where

$$2nd = (m + 1/2)\lambda \qquad (4.8)$$

where m is an integer[123] . Theoretical points have also been plotted on these curves for comparison. As seen previously, the theoretical R, T are quite sensitive to film thickness. To determine film thickness experimentally, both a diamond stylus method (Talysurf) and optical interferometer (Sloan angstrometer) were used to corroborate the in-situ quartz crystal monitor thickness determination. Unfortunately,experimental accuracy appears to be no better than ± 100 Å which is clearly insufficient for theoretical purposes. Therefore, the thickness was varied around the experimental thickness and then the composition of the film to obtain the best fit. This type of fitting had to be done manually with the help of HP 9820 A computer, because of couple of percent of error in the measured R and T and also because in some cases it appears that the spectrophotometer's zero relectance position drifted.

Figure[47] to [52] are the results from a series of run in which copper sulfide was evaporated at a constant rate of ~15 Å/sec. For films thinner than 900 Å or so, certain amount of porosity had to be assumed to obtain the best fit. This is examplified in Fig.51,52. In Fig[49,50] even if film composition is assumed to be $Cu_{1.97}S$, the theoretical points appear to be way off. On the other hand if we assume porous films, the experimental data resemble to the theoretical curve

rather well. For thicker films, only the thickness deviation was necessary to assume (Fig.47,48). The 1 μ thick film (Fig. 47) was also annealed in air at 72°C for 24 hours and the two results have been plotted. Although there are some apparent changes in R, T, the basic features are similar. The changes can be explained by assuming further reduced porosity of the film during annealing. This is consistent with the cathodoluminescence experiment where the luminescence intensity doubled after annealing because of reduced recombination centres (density of recombination centres is directly related to the film porosity).

In another set of experiments, the deposition rate was varied while the film thickness, as monitored by the quartz crystal monitor, was held constant at 1500 Å. The optical results are shown in Fig.53 to 56.

From these sets of data, some remarkable conclusions can be drawn which relate to the optimum evaporation technique. From the first set of experiments, it appears that the film composition is rather independant of the film thickness, only the film porosity will effect the overall physical properties of the films. As it turned out from the experiments on Si-$Cu_{2-x}S$ solar cells, the effects of film porosity were reduced by proper annealing of these films. This was also confirmed by the experiments on 1 μ thick Cu_2S film. On the other hand, the evaporation rate seems to change the film composition. The film composition is plotted against the evaporation rate in Fig.57 . From this plot, it is apparent that the films are more sulfur rich for evaporation rates below 15-20 Å/sec. Because the source to substrate distance was fixed

FIGURE 57: Film composition vs evaporation rate.

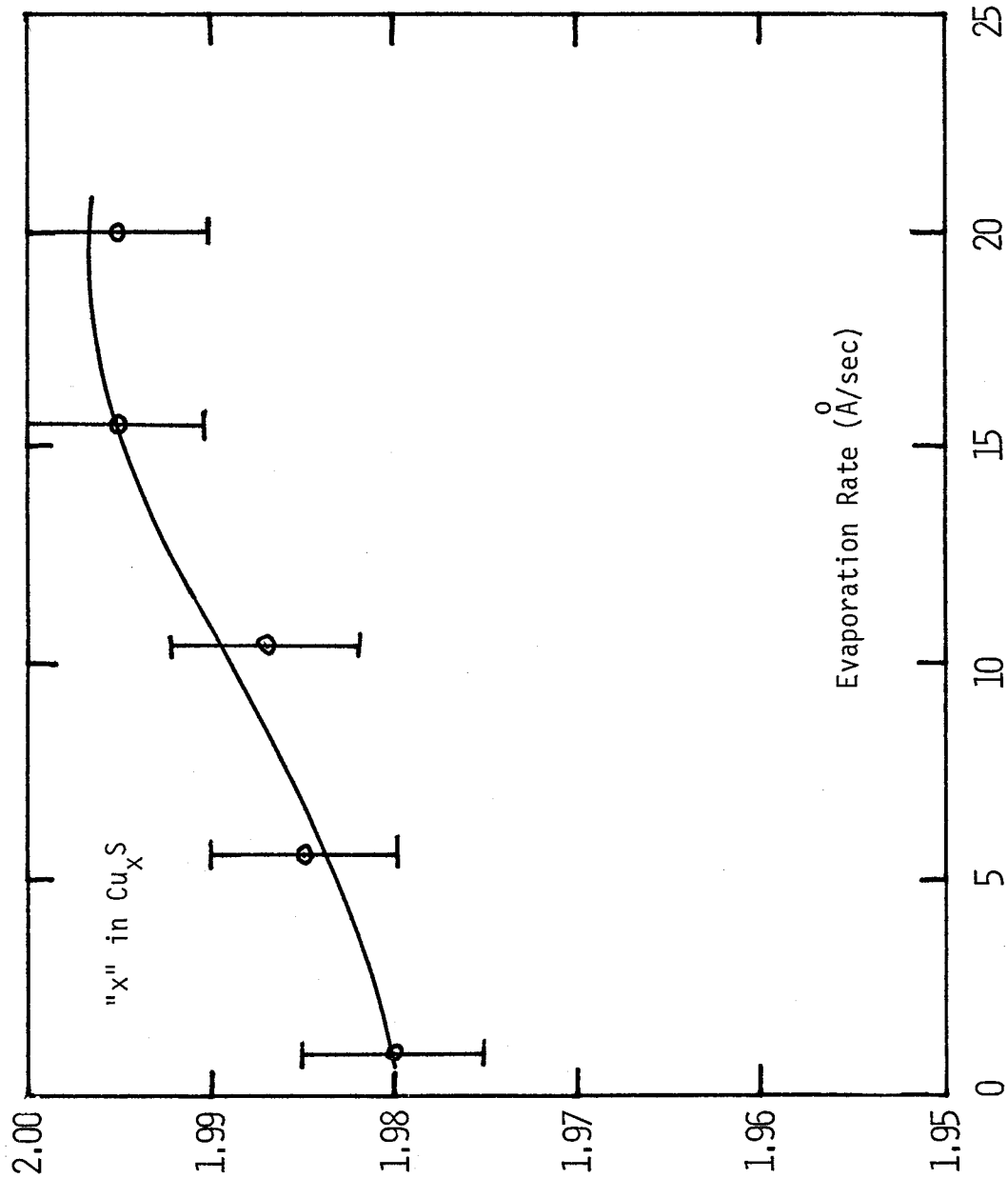
"x" in Cu_xS
2.00
1.99
1.98
1.97
1.96
1.95
0
5
10
15
20
25
Evaporation Rate (Å/sec)

FIG. 57

at 20 cm and other evaporation parameters were also held constant, it then implies that different source temperatures give different film compositions. This is not surprising because in most binary compound evaporations, there is a segregation of different atomic species due to differences in their vapor pressures.[122] The result is usually a film with an excess of lower vapor pressure species (if the substrate is cold). In our case, sulfur has a lower vapor pressure and therefore the films showed excess sulfur. This then also implies that if we do not want rate dependence of film composition, then either the evaporation has to be done at rates higher than 15-20 Å/sec (for source to substrate distance of 20 cm) or the substrate should be at elevated temperature to drive off excess sulfur. For solar cell purposes, higher substrate temperatures may not be desirable because $Cu_{2-x}S$ may diffuse into the substrate semiconductor, shorting the junction. Flash evaporation can provide a unique opportunity of having very high rates of instantaneous evaporation[122] and yet with sufficiently low deposition rates to keep good control over the film thickness. In the thermal evaporation technique, which we have employed, the evaporation rate is the same as deposition rate, therefore we used evaporation rates of about 15 Å/sec to have good control over the desired film thickness and also to obtain film compositions close to Cu_2S.

The optical absorption A=1-R-T, of a 500Å copper film sulphurized for 1.5, 2, 5 and 10 min. respectively are shown in Fig.58 . For the shortest sulphurization time a large infra red absorption is observed, that is characteristic of a metal such as copper. With increasing sulphurization times (to 5 min.) infra red absorption drops to ∿20%

FIGURE 58: Optical absorption, A = 1-R-T, for sulfurized copper film at different times.

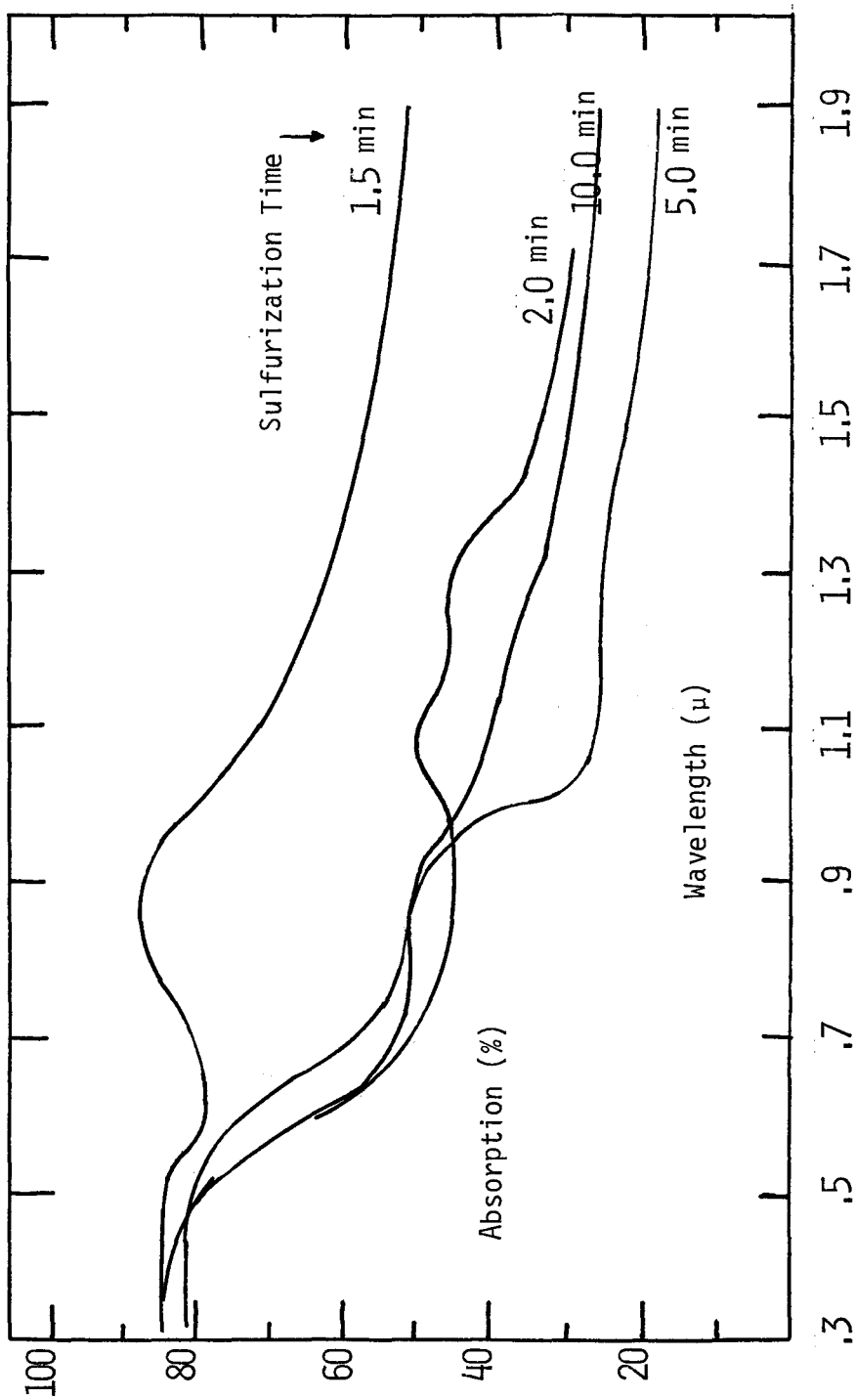
Sulfurization Time
1.5 min
2.0 min
10.0 min
5.0 min
Absorption (%)
Wavelength (μ)
100
80
60
40
20
.3
.5
.7
.9
1.1
1.3
1.5
1.7
1.9

FIG. 58

and then begins to increase again. For Cu_2S, the defect density and, therefore, the carrier density would be smallest, compared to other phases of copper sulfide near Cu_2S. This, then implies that the infrared absorption in Cu_2S would be smallest. From fig. 58, it can be interpreted that the complete sulfurization was achieved between 2 to 5 min. If properly calibrated, this technique can be used to monitor the stoichiometry of copper sulfide films. However, there is one limitation. The infrared absorption not only depends on crystal defects and carrier concentration, it also depends on physical defects of the film, like porosity etc. Therefore, this technique is to be used with proper consideration to the physical defects of the film.

4.5 OTHER TECHNIQUES

Besides the techniques described in the previous sections, we also tried Rutherford backscattering technique, secondary emmision measurements and electrochemical analysis to establish the stochiometry of the evaporated copper sulfide films.

Rutherford backscattering technique has been previously applied[124] to copper sulfide samples. In this technique, MeV He^+ (1 MeV in our case) ions are beamed at the sample and backscattered ions collected. The backscattered ion energy is a function of the atomic masses encountered and film thickness through which the incident beam passes. Low atomic mass substrates of carbon or beryllium coated with copper sulfide films of about 500 Å thickness provide easily resolvable peaks corresponding to Cu and S respectively. Peak area corresponds to the concentration of the constituent atoms.

Backscattering experiments were carried out on 500 Å of Cu_xS evaporated at 15 Å/sec on carbon substrates. The results are shown in Fig. 59. The amount of peak overlap is too large for accurate determination of peak area despite the thinness of the film. This overlap is attributed to the porosity of the carbon substrate. Since spectra are dependant on distance of C and S from the surface as well as on atomic mass, any deep penetration of the constitutents beyond 500 Å will result in a peak smearing and hence poorer resolution. A simple comparison of peak heights however, is encouraging. Correcting for the differences in the cross-section, the ratio of Cu to S peak height is 2 to 1. This approach is accurate to no better than 10%, unfortunately.

FIGURE 59: Result of Rutherford backscattering experiment on a 500 Å thick copper sulfide film. (Experiments by Dr. D.A. Thompson of McMaster).

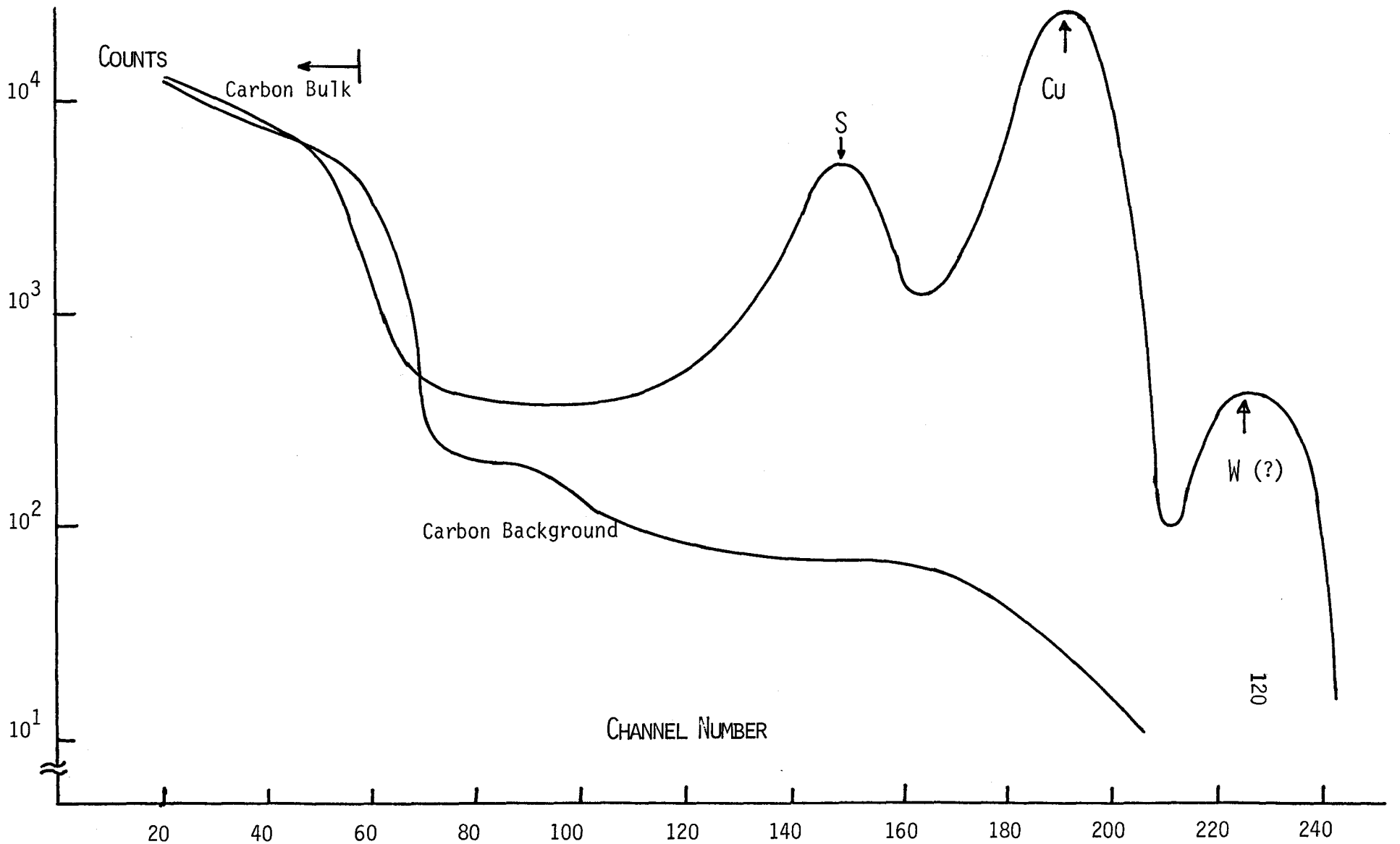
COUNTS
Carbon Bulk
S
Cu
W (?)
Carbon Background
CHANNEL NUMBER
120
10^4
10^3
10^2
10^1
20
40
60
80
100
120
140
160
180
200
220
240

FIG. 59

Secondary x-ray emission due to impingement of 20 keV electron beam on copper sulfide sample was also analysed. Again the emission energy depends on the atmoic mass and the peak area corresponds to the amount of the element. A 2270 Å thick copper sulfide film deposited on a glass substrate at 15 Å/sec was analysed and the result is shown in Fig.60. Again a simple ratio of peak areas corresponding to Cu and S indicate a stochiometry of about Cu_2S.

Electrochmeical analysis of Cu_xS films has been widely used by certain research groups[125,126] to establish the film stochiometry. In this technique films of Cu_xS are electrochemically reduced. The time taken at a fixed current to convert the film to pure copper is a measure of "x" in the initial film. Extremely accurate measurements of stochiometry can, therefore, be made with a single phase materials. The technique is fast and in principle simple. It's main drawbacks are that it is destructive and not quite as easy to perform as it first appears. The main problem which we encountered was electrochemical reaction was too fast to control and the kinks in the terminal voltage vs. time elapsed, which represent the reduction of Cu_xS to Cu were hard to resolve. Therefore, this technique was not pursued vigorously.

FIGURE 60: Secondary x-ray emission spectrum of a 2270 Å thick copper sulfide film on glass slide.

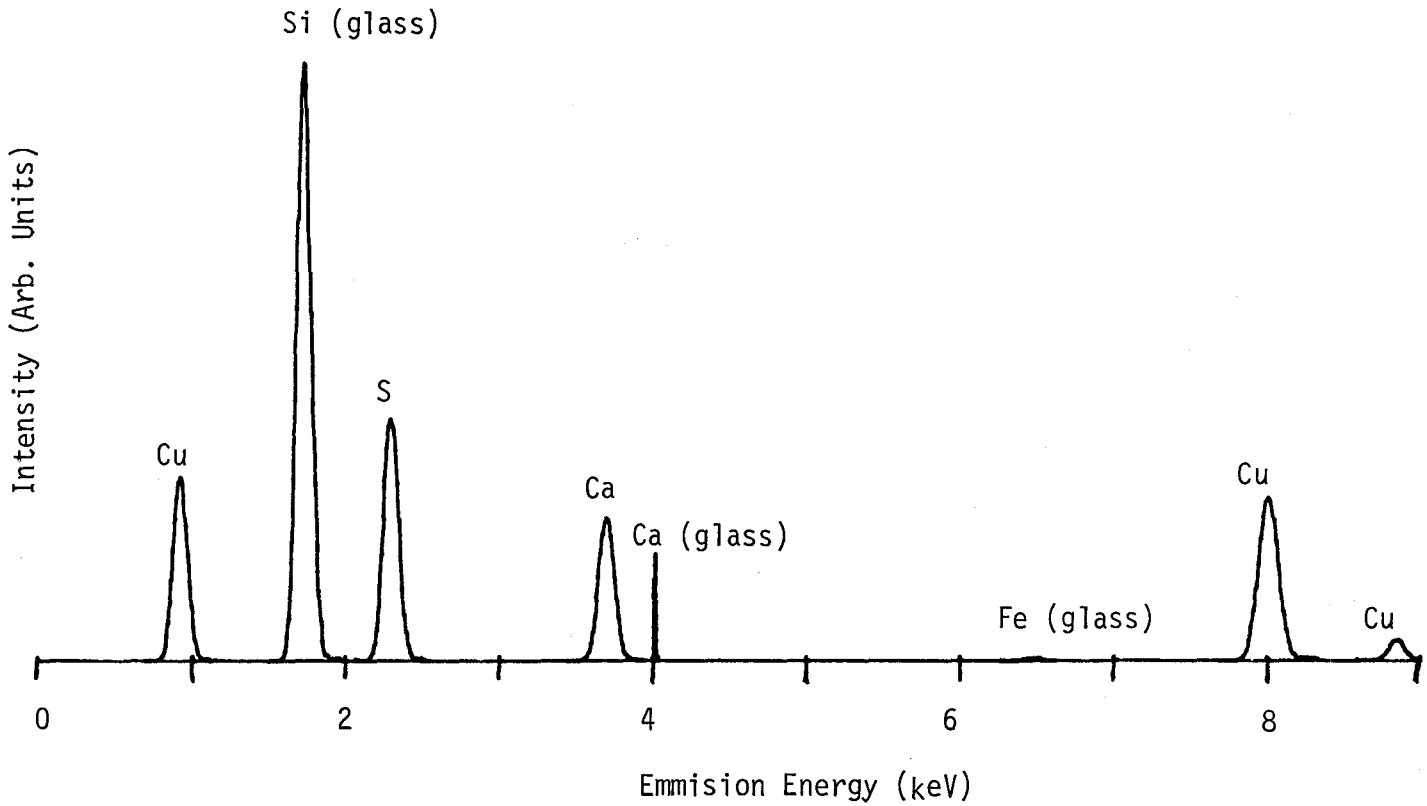
Si (glass)
Intensity (Arb. Units)
S
Cu
Ca
Ca (glass)
Fe (glass)
Cu
Cu
0
2
4
6
8
Emmision Energy (keV)

FIG. 60

CHAPTER 5

APPLICATION OF Cu_2S FOR SOLAR CELLS

5.1 PHOTOVOLTAIC EFFECT

The appearance of the photovoltaic effect in a solid requires the existence of some sort of heterogeneity, which can influence the system of free carriers and thus cause an electric field inside the solid, capable of separating photon generated electrons and holes to give a photovoltage. This heterogeneity may be due to doping gradient, work function or band gap differences, and is usually achieved in some sort of semiconductor junction. The most important systems which have been studied are:

1. p-n homojunction (gradient of doping)
2. p-n heterojunction (gradient of doping, work function and band gap)
3. Schottky junction (gradient of work function)
4. Other systems like MIS, SIS structures.

The photovoltaic effect in these systems has been described by many authors.[127] The only comments that will be made here concerning the electrical characteristics and the photovoltaic conversion process are for a p-n homo - junction, and broadly the same ideas apply to other systems also.

The current flowing in an ideal diode is governed by an equation of the form[129]

$$J = J_S\{\exp (qv/nkT) \ -1\} \qquad (5.1)$$

with ideality factor, n = 1. When space charge recombination dominates at low bias level, n = 2, and when high level current injection occurs, n = 2 again.[129] The dark saturation current, J_S, is due to the diffusion flow of minority carriers and is characteristics of the junction. Illuminating the p-n junction with a flux Φ of a monochromatic photons causes the generation of electron - hole pairs at a depth x, according to

$$g(x) = \Phi\alpha. \exp (-\alpha x) \qquad (5.2)$$

where α is the absorption coefficient at that photon energy. Minority carriers on both sides of junction drift across the junction and junction biases itself in forward direction by an amount sufficient to counter this flow by injection of majority carriers. The junction develops an open circuit voltage, V_{oc}, which cannot exceed the diffusion potential of the junction. In the short circuited condition, the short circuit current, I_{sc}, flows through the circuit and this corresponds to the light generated minority carriers. Usually I_{sc} is slightly smaller than the light generated current, I_L, due to resistive elements in the real device. The current-voltage relationship of a real device, under illumination can be written[137] as

$$I - \frac{V - IR_s}{R_{sh}} = I_o \left[\exp \frac{q(V - IR_s)}{nkT} - 1 \right] - I_L \qquad (5.3)$$

where R_s is the effective series resistance and R_{sh} is the effective shunt resistance of the device. Ideally

$$I_{sc} = I_L$$
$$V_{oc} = \frac{nkT}{q} \ln \left[\frac{I_L}{I_o} + 1\right] \qquad (5.4)$$

Because of the nature of Eq.5.3 , photovoltaic devices are neither constant voltage sources, nor constant current sources, but are a hybrid of the two. There exists a maximum power point somewhere on the I-V curve of the solar cell. The relative position of this point can be estimated by the quantity called "curve factor" of the solar cell and it is defined as

$$CF = \frac{I_{max} \cdot V_{max}}{I_{sc} \cdot V_{oc}} \qquad (5.5)$$

Ideal p-n homojunctions have curve factor of about 0.8[127] and this value varies with the ideality factor, n, series resistance, R_s and temperature T. Obviously, the conversion efficiency of a solar cell will be

$$EFF = I_{sc} \cdot V_{oc} \cdot CF/\text{input power} \qquad (5.6)$$

Theoretical conversion efficiencies of silicon devices are around 20% at AM1 illumination (solar illumination at sea level).

Because of photon energy dependance of α in Eq. 5.2, the generated current depends on the wavelength of the photons. It also depends on the band gap of the semiconductor, temperature, surface and other (in bulk or at the junction) recombination processes. Therefore, the short circuit current exhibits a spectral response, which is characteristics of the device. Conversion efficiency also depends on the spectrum of the incident light because absolute spectral response will be different for different spectra.

Terrestrial sunlight spectrum is characterized in terms of air-mass. Usually AM1 (100 mW/cm^2) and AM2 (75 mW/cm^2) are encountered depending on the location. Because of the spectral differences in these spectra, AM2 conversion efficiency is greater than AM1 conversion efficiency.

Number of electron-hole pairs generated depends on the absorption coefficient of the semiconductor and its band gap; the smaller the band gap, larger number of photons can be absorbed to give a larger short circuit current. However, each photon absorbed in a low band gap material, does only a small amount of work corresponding to the low barrier height, i.e. the open circuit voltage will be small. By optimizing these two competing factors, it can be shown that for most efficient solar energy conversion, semiconductors having a band gap around 1.5 eV are required. Certainly, good lifetime and mobility of the carriers are desirable.

5.2 APPLICATION OF Cu_2S IN SOLAR ENERGY CONVERSION

Usefulness of chalcocite in solar cells was discussed in Chapter 2. In Chapter 4, it was shown that it has a direct gap at about 1.2eV, so that all the photons above this energy are absorbed without needing a large penetration depth. As the band gap of the $Cu_{2-x}S$ phases increases with increasing copper deficiency[63,64], other phases will loose some photons. Similarly in chalcocite phase, since the carrier density is minimum of all other phases, the diffusion length is larger in chalcocite and therefore all the carriers can be collected even if a thin layer of Cu_2S is used as a front layer. A thin front layer results in a shallow junction depth, which provides better spectral response of the solar cell.

It has been shown that the vacuum evaporation of high purity cuprous sulfide will provide the desired control over the stochiometry and other electro-optical properties of copper sulfide films.

5.3 THEORETICAL BACKGROUND FOR p-Cu_2S-n-Si HETEROJUNCTION

Based on the above considerations, we have chosen to explore the photovoltaic properties of the p-Cu_2S-n-Si system. Silicon has been chosen as the substrate because of its well characterized properties. Also, the electron affinity and band gap considerations indicate that Cu_xS-(n-Si) junction whould exhibit the photovoltaic characteristics with a good barrier height[128]. Therefore, the photovoltaic properties of this junction would provide additional tool for the optimization of the evaporation variables.

The diffusion potential, V_D, of a heterojunction is determined by the electron affinities (χ) [129] through the equation

$$V_D = \phi_p - \phi_n$$

$$= E_{gp} + (\chi_p - \chi_n) - (E_{fp} + E_{fn}) \quad , \qquad (5.7)$$

where ϕ's are work functions for n- and p-semiconductors, E_{gp} is band gap of p-semiconductor, $E_{fn} = E_c - E_f$ on the n-side and $E_{fp} = E_f - E_v$ on the p-side; E_c, E_v, and E_f being conduction band, valence band and fermi energy levels, respectively. The energy gap of Cu_2S is generally accepted to be about 1.2 eV, and this study also indicates the similar value. The electron affinity of Cu_2S has never been measured, primarily, it would seem due to a lack of good single crystal material. However, affinity can be estimated from work on the Cu_2S-CdS and p-Si-CdS systems[130,131]. The diffusion potential for the Cu_2S-CdS system is 1.1 eV[130] and for the p-Si-CdS system it is 0.9 eV[131] . Then using the relation for V_D, Cu_2S would have an electron affinity of 3.85 eV. Since Cu_2S and CdS are near degenerate, E_{fp} and E_{fn} for them are assumed to be zero in above estimation of electron affinity for cuprous sulfide. On the basis of this electron affinity of cuprous sulfide, the diffusion potential for the n-Si-p-Cu_2S system using 0.2 - 0.4 Ωcm n-Si, would be about 0.8 eV. Our preliminary experiments seem to bear out these predictions. An energy band diagram based on these considerations is shown in Fig.61.

Current-voltage characteristics of a heterojunction are influenced by various current conduction mechanisms depending on the band discontinuities at the interface and the density of interface states. There is a significant difference in lattice parameters and thermal expansion coefficients of silicon and copper sulfide. Therefore a large interface state

FIGURE 61: Energy band diagram for p-Cu_2S - n-Si junction.

FIG. 61

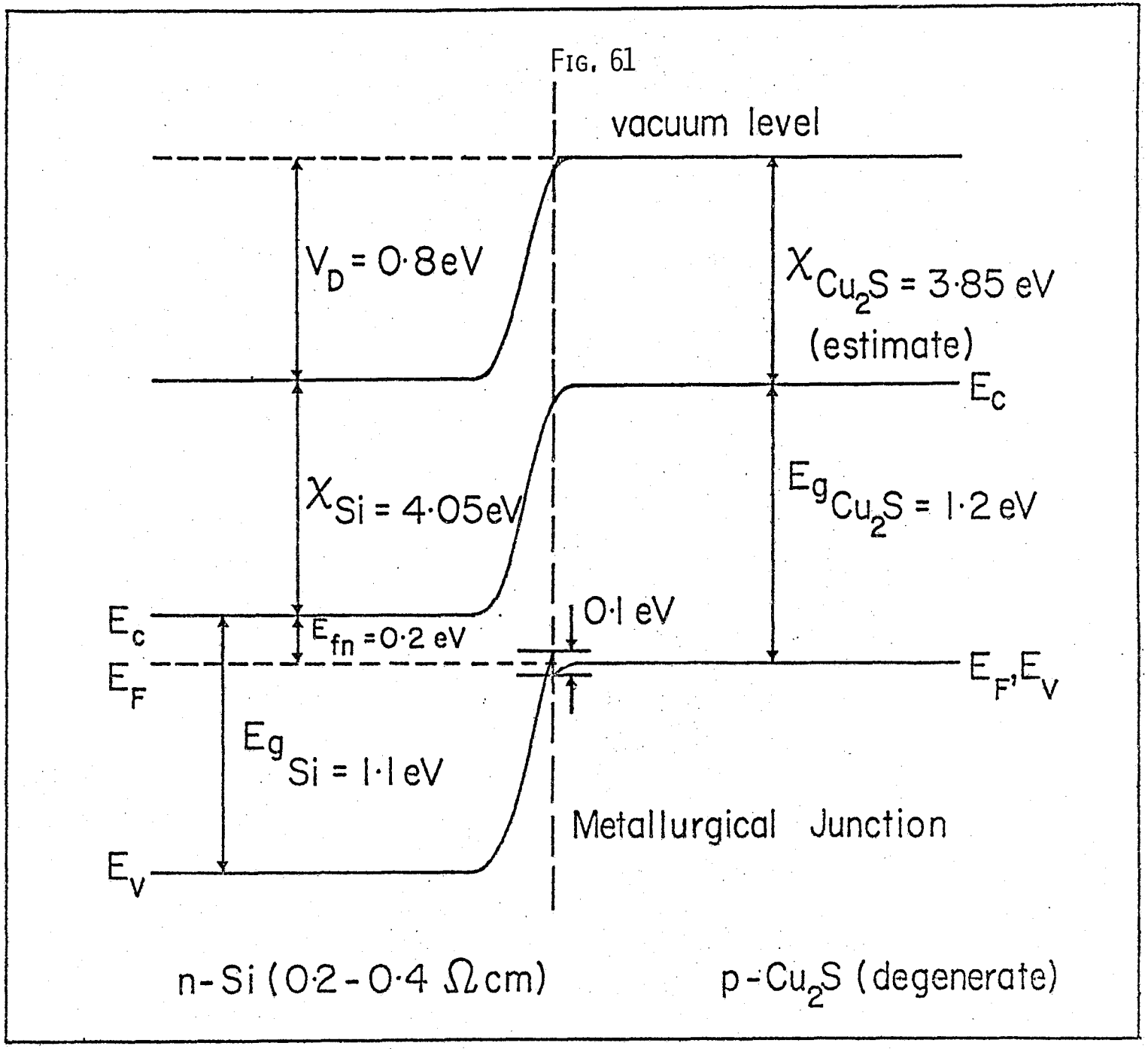
vacuum level
V_D = 0·8eV
χ_{Cu_2S} = 3·85 eV
(estimate)
E_c
χ_{Si} = 4·05eV
Eg_{Cu_2S} = 1·2 eV
E_c
E_{fn} = 0·2 eV
0·1 eV
E_F
E_F, E_V
Eg_{Si} = 1·1 eV
Metallurgical Junction
E_V
n-Si (0·2 - 0·4 Ω cm)
p-Cu_2S (degenerate)

density is expected. Assuming that the interface states are caused by edge dislocations only, we can write the interface state density, N_s as

$$N_s \simeq [(1/a_{Si}^2) - (1/a_{Cu_2S}^2)] \ , \tag{5.8}$$

$$a_{Si} = 5.43 \ \mathring{A} \text{ and } a_{Cu_2S} \simeq (11.88/3) = 3.69 \ \mathring{A} \ .$$

Therefore, $N_s \simeq 3 \times 10^{14}$ cm^{-2} and the lattice mismatch is about 31%. For such a high interface state density, the dominant current conduction mechanism is expected to be via interface states, i.e. electrons from Si conduction band edge or higher energy levels would flow through the interface states combining with holes in the Cu_2S near the interface. Also the electron capture cross-section would be fairly high, with σ_n equal to 10^{-14} cm^2 being a good approximation. Therefore, at room temperature with thermal velocity, V_{th}, of 10^7 cm/s, the surface recombination velocity, S, is approximately

$$S = V_{th}\sigma_n N_s \simeq 3 \times 10^7 \text{ cm/s} \ . \tag{5.9}$$

Now for the current conduction mechanixm we have just described and assuming that the carrier drift velocity approaches surfaces recombination velocity, dark leakage current density, J_o, would be[132]

$$J_o \simeq qSN_c \exp(-q\phi_B/kT) \quad , \qquad (5.10)$$

where N_C is the effective density of states in the conduction band of Si and is equal to 2.8×10^{19} cm^{-3}, ϕ_B is activation energy. In our case $\phi_B = V_D + E_{fn} \simeq 0.8$ eV, which follows from preliminary capacitance-voltage characteristics of the junction. Therefore, $J_o \simeq 1.7 \times 10^{-6}$ A/cm^2 would be expected. Also, the ideality factor, n, of the junction would be around 2 because of the dominant generation-recombination mechanism.

When the p-Cu_2S-n-Si heterojunction is illuminated, a short-circuit current density, J_{sc}, of about 20-30 mA/cm^2 would be expected, as most of the carriers are likely to be generated in the Cu_2S much as in the Cu_2S-CdS solar cell. Therefore, the open circuit voltage, V_{oc}, is expected to be 0.45-0.50 V, using the simple relation given by Eq. 5.4.

Therefore, it seems that the photovoltaic properties of this system are interesting in their own right. It should be pointed out that a very high theoretical conversion efficiency cannot be expected from this structure because of the poor minority carrier injection efficiency due to the large recombination current. The interface states also effect the cell efficiency. Further discussion on short circuit current and the open circuit voltage of these cells is presented in the next sections. At this point it is worth mentioning that the above analysis is rudimentary but such analyses are important to explore the potentiality of a device.

5.4 CELL FABRICATION

Cu_2S-Si cells have been fabricated both by evaporating high purity Cu_2S on n-Si substrates, as well as by sulfurizing pure copper thin films deposited on silicon.

Polished n-type Si wafers of resistivity 0.01-0.2 Ωcm, of orientation <111> were used. These wafers were chemically cleaned using the usual techniques[133,134]. Reagent grade chemicals were used and it has been observed that the use of the di-sodium salt of ethylenediamenetetra acetic acid as chelating agent[135] improves the performance of the cells. Polished surface of Si is etched for 20-30 seconds in a selective etch solution of $5HNO_3$:$3CH_3COOH$:3HF. This etch reduces the reflectivity of the finished cell by roughening the surface; the adherence of evaporated cuprous sulfide films to Si substrate is also increased.

Cuprous sulfide is evaporated from tungsten boat in a vacuum better than 10^{-6} Torr. The Si substrate is kept at about 17°C. For source to substrate distance of about 20 cm, evaporation rate of 15 Å/s and 800-900 Å thick evaporated cuprous sulfide film has given the best results so far. After the evaporation of cuprous sulfide, a 1000 Å thick Au grid (4 lines/cm) is evaporated on cuprous sulfide film to make front ohmic contact. The rate of evaporation of Au grid seems to affect the cell performance - a quick grid deposition on cold cell appears to give better results[136]. Cr - Au contacts have been tried, but it appears that an aluminium back contact on lapped n-Si and vacuum baked at about 200-

300 ^{o}C for a few minutes is also satisfactory. The geometry used to verify the ohmic nature of n-Si - Al contact and the current - voltage characteristics of the contact are shown in fig. 62. The complete flow chart of the fabrication steps is shown in fig. 63. After the fabrication steps are completed, the cell is heat treated and tested for its electrical and optical characteristics.

Another technique for making n-Si - p-Cu_2S solar cells has also been used. Copper films on Si substrates have been sulfurized using the technique described earlier. These cells have also been tested for their photovoltaic response. The yield of this type of solar cells has been, however, very poor, because of the adhesion problems. Copper itself has a poor adhesion to silicon, when it is sulfurized, it seems to peel off the substrate. It appears that the growth of copper sulfide, during the sulfurization process, is by the outward diffusion of copper through the copper sulfide lattice, as had been hypothesized in previous chapter. This mechanism causes the delamination of the copper film, resulting in poor adhesion of sulfurized films.

FIGURE 62: The current - voltage characteristics of n-Si - Al contact and the geometry of the contact.

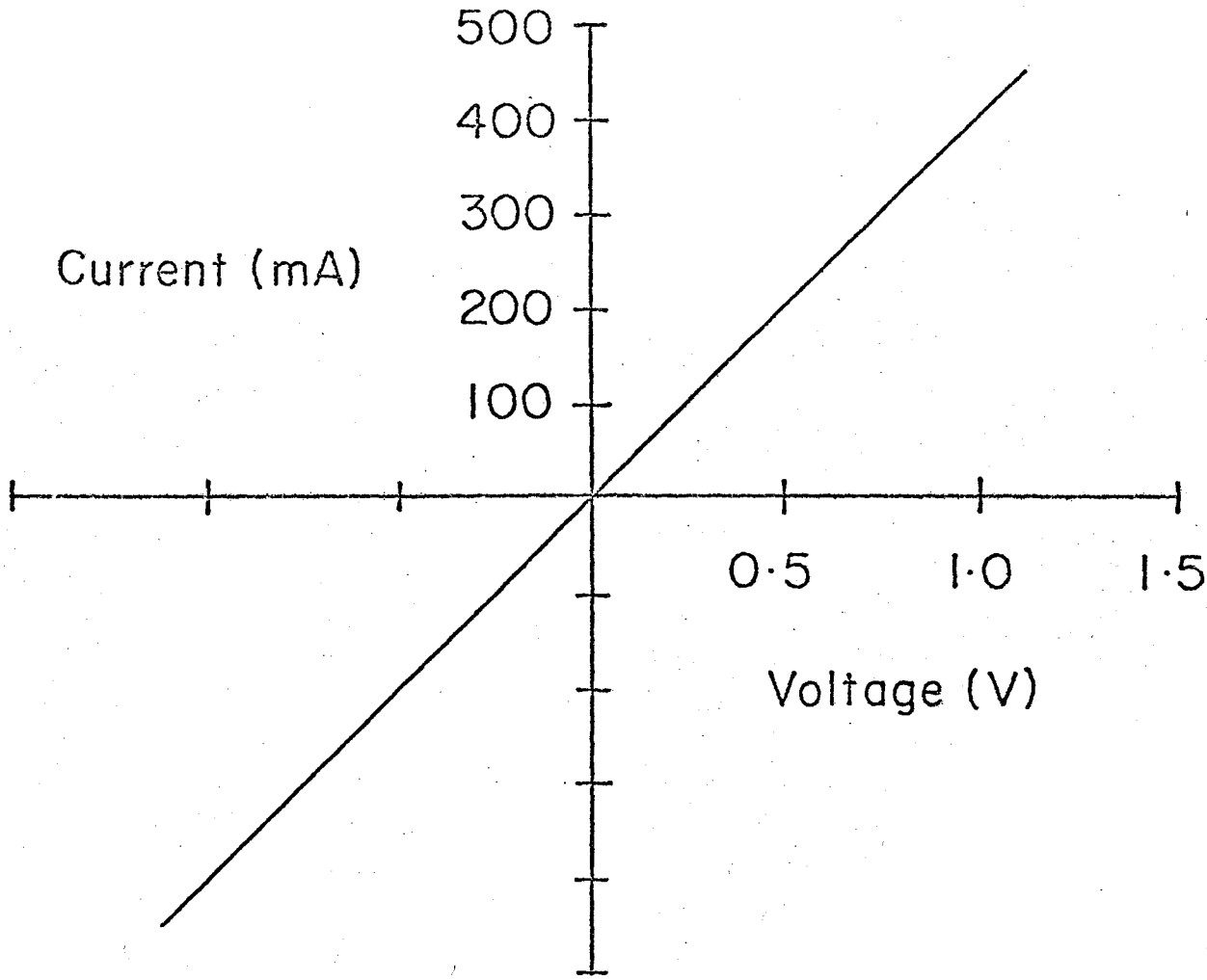
500
400
300
200
100
Current (mA)
0·5
1·0
1·5
Voltage (V)

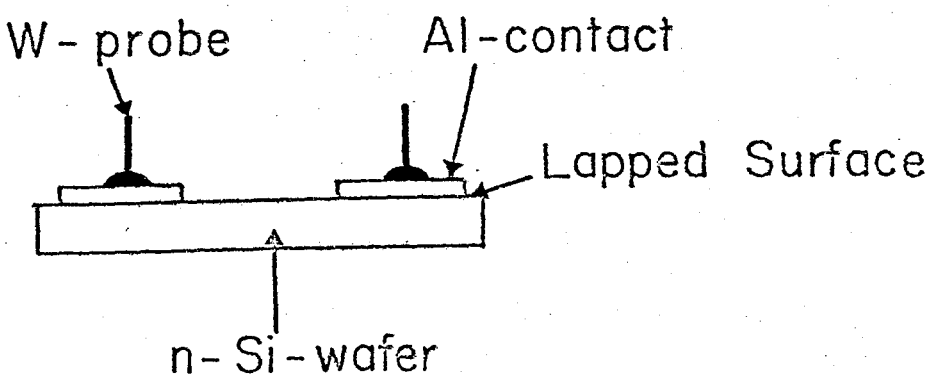
W-probe
Al-contact
Lapped Surface
n-Si-wafer

FIG. 62

FIGURE 63: Flow chart for the fabrication of Cu_2S - Si solar cells.

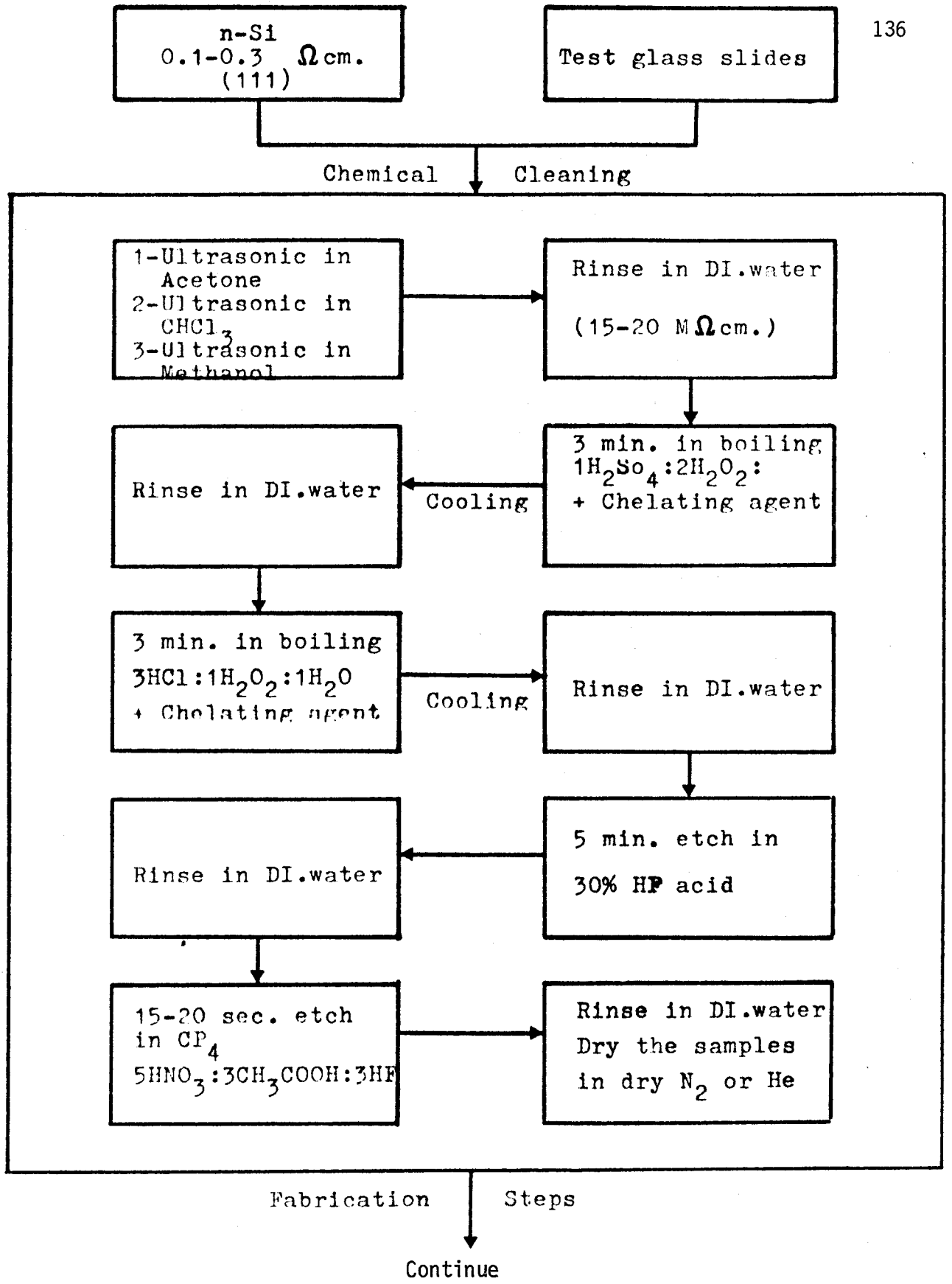
n-Si
0.1-0.3 Ωcm.
(111)
Test glass slides
Chemical Cleaning
1-Ultrasonic in Acetone
2-Ultrasonic in $CHCl_3$
3-Ultrasonic in Methanol
Rinse in DI.water
(15-20 MΩcm.)
3 min. in boiling
$1H_2So_4:2H_2O_2$:
+ Chelating agent
Cooling
Rinse in DI.water
3 min. in boiling
$3HCl:1H_2O_2:1H_2O$
+ Chelating agent
Cooling
Rinse in DI.water
5 min. etch in
30% HF acid
Rinse in DI.water
15-20 sec. etch
in CP_4
$5HNO_3:3CH_3COOH:3HF$
Rinse in DI.water
Dry the samples
in dry N_2 or He
Fabrication Steps
Continue

FIG 63

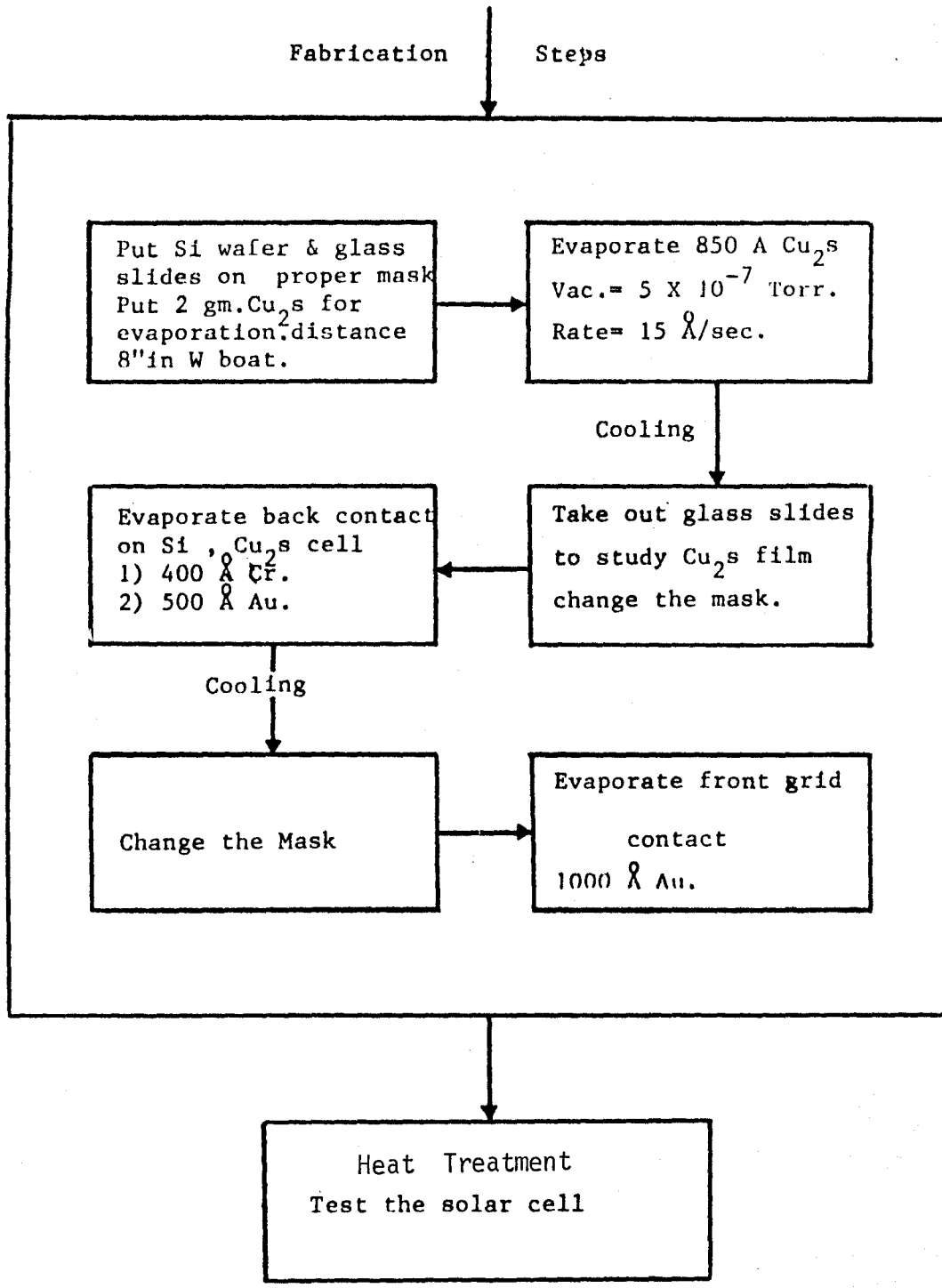

CONT. OF FIG. 63

5.5 ELECTRICAL CHARACTERISTICS OF THE CELL

Immediately following the fabrication of the cell, its current-voltage characteristics are measured. Usually solar cells of 1 cm^2 area are fabricated and tested under AM1 illumination. The solar simulator consists of a set of air-cooled halogen tungsten lamps with incorporated dichroic filters, and is calibrated to AM1 equivalent illumination by adjusting the short-circuit current of a diffused silicon solar cell supplied by NASA-Lewis Research Centre. The schematic of I-V plotter and the measurement flow chart are shown in Fig. 64,65.

About 50% of the evaporated cells show 1-4% conversion efficiency. Typical current-voltage characteristics of different solar cells, without anti-reflection coatings, are shown in Fig.66. Cell 1a is typical of evaporated 4% solar cells. Cell 1b is the same cell measured after 50 days of storage in air atmosphere. The usual characteristics of 4% cells are - open circuit voltage, V_{oc} - 0.33 - 0.42 V, short circuit current density, J_{sc} = 18 - 20 mA/cm^2, and curve factor, CF of 0.6. Actual photovoltaic parameters of different cells are listed in Table VII.The dark current-voltage characteristics of few cells are shown in Fig. 67. From this the ideality factor, n, was deduced to be 1.8 and dark leakage current density was 4.7 x 10^{-6} A/cm^2. The variation of these two parameters is inbetween 1.6-1.9 and 10^{-5}- 10^{-6} A/cm^2, respectively. The series resistance of these cells is about 2-3 Ω, as obtained by the technique described in ref. 137 . The shunt resistance is quite low, usually of the order of 1000-2000 Ω.

Examination of the forward current-voltage characteristics indicates that the forward current is largely due to generation-recombination or

FIGURE 64: Scematic of I-V plotter and its operation.

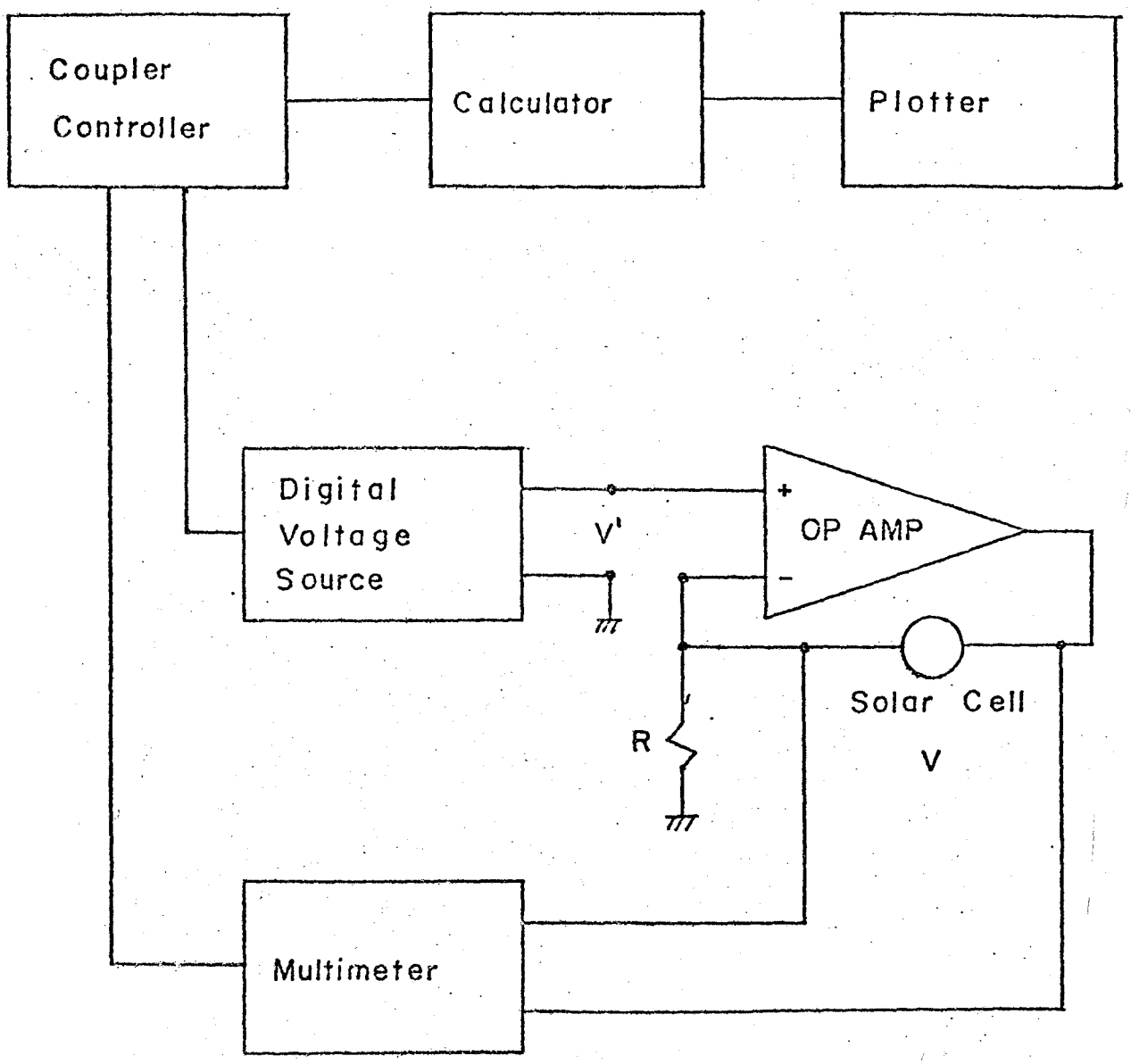
Coupler
Controller
Calculator
Plotter
Digital
Voltage
Source
V'
+
-
OP AMP
R
Solar Cell
V
Multimeter

FIG. 64

FIGURE 65: Flow chart for I-V measurements.

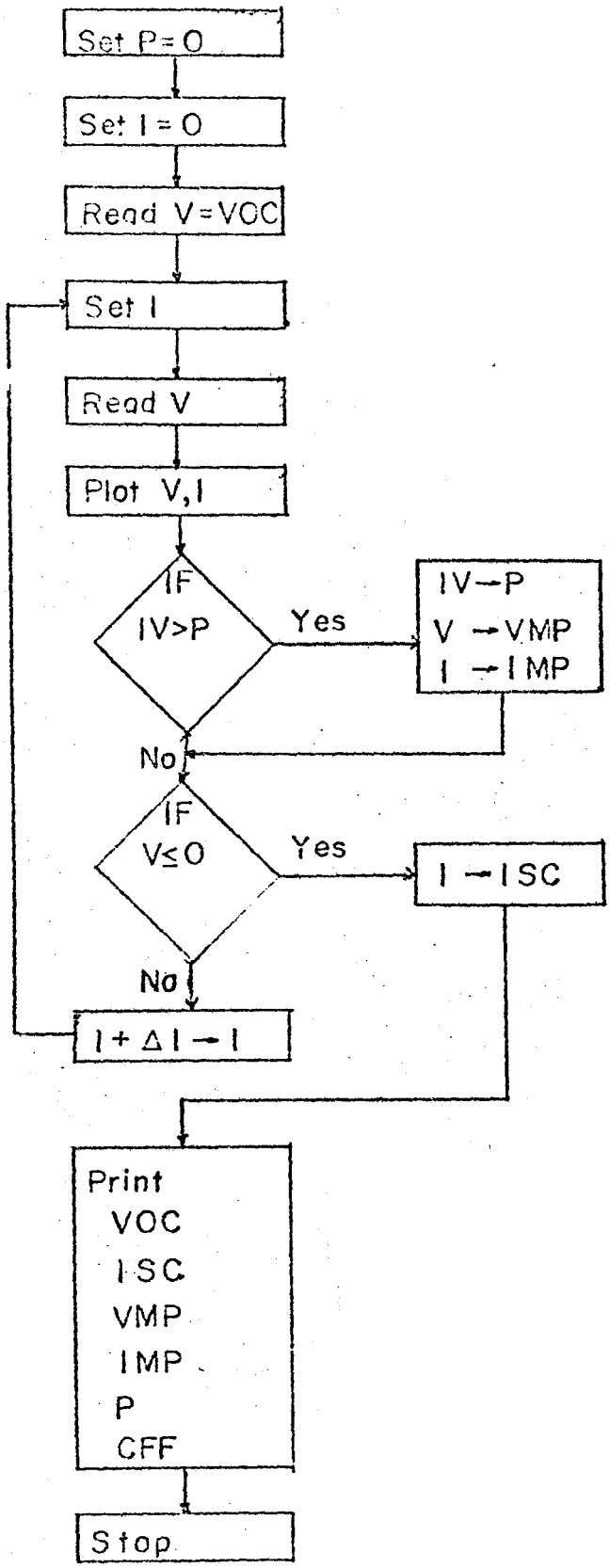
Set P=0
Set I=0
Read V=VOC
Set I
Read V
Plot V,I
IF IV>P
Yes
IV→P
V →VMP
I →IMP
No
IF V≤0
Yes
I →ISC
No
I+ΔI→I
Print
VOC
ISC
VMP
IMP
P
CFF
Stop

FIG. 65

FIGURE 66: Solar I-V plots of different Cu_2S - Si solar cells. Actual parameters are listed in Table VII.

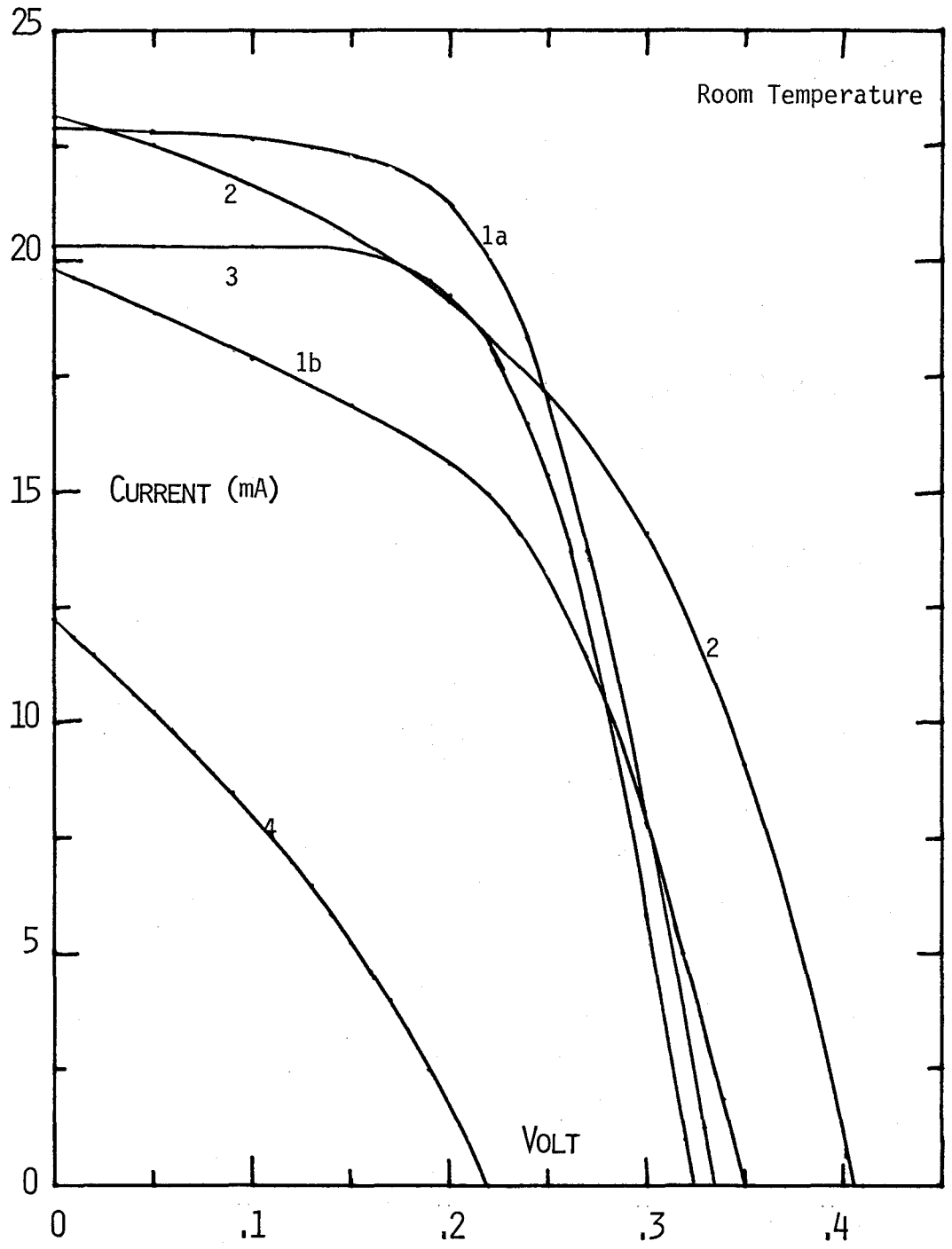
25
20
15
10
5
0
0
.1
.2
.3
.4
Room Temperature
2
1a
3
1b
CURRENT (mA)
2
4
VOLT

FIG. 66

TABLE VII

PHOTOVOLTAIC PARAMETERS OF CELLS SHOWN IN FIG. 66

Cell No.	Open Circuit voltage(V)	Short Circuit Current(mA/cm^2)	Curve Factor	Efficiency (%)
1a	.34	18.3	.61	3.8
1b	.35	15.8	.49	2.7
2	.41	18.5	.45	3.4
3	.33	16.3	.61	3.2
4	.22	19.3	.35	1.5

FIGURE 67: Dark I-V characteristics of some Cu_2S-Si solar cells.

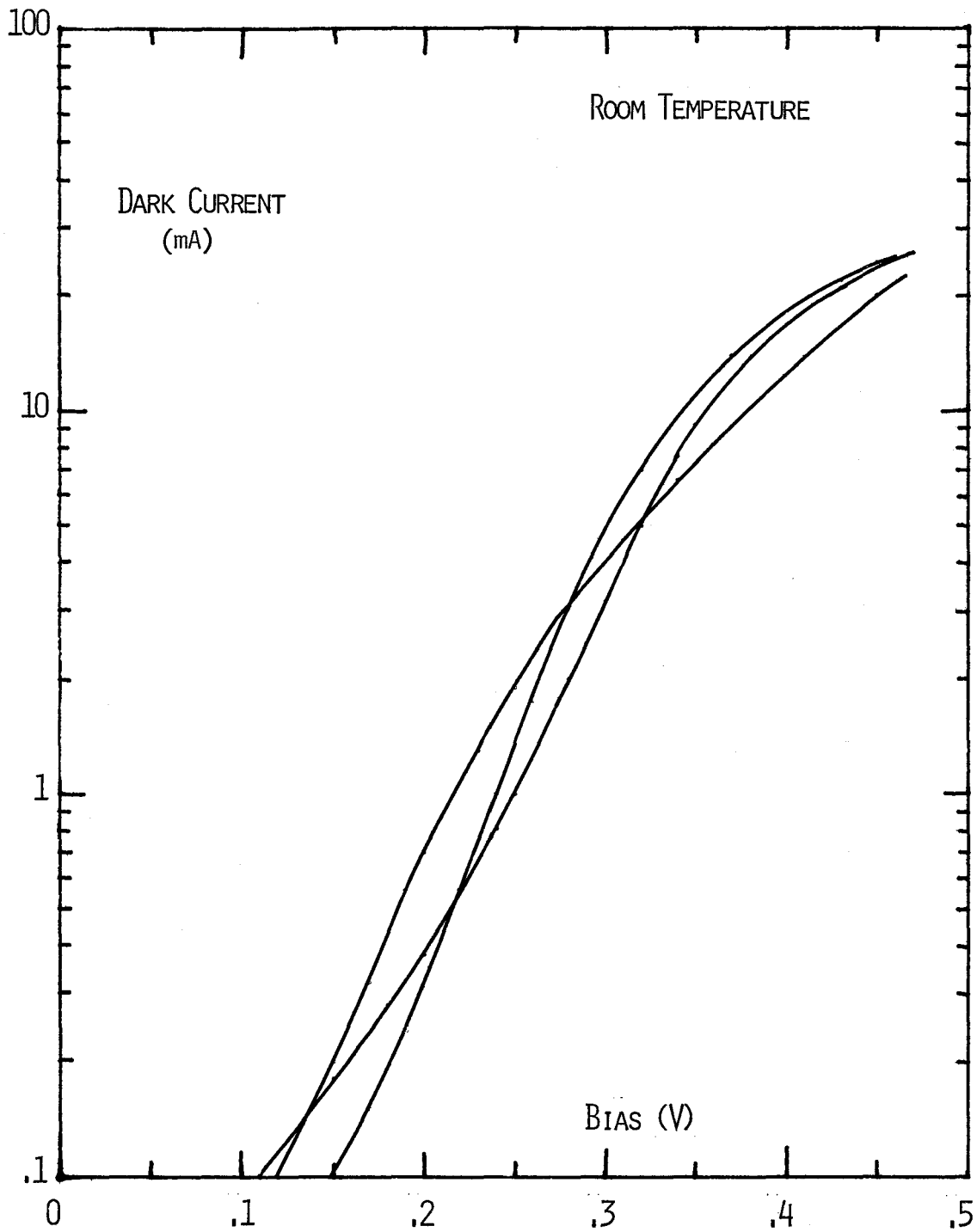

FIG. 67

tunneling through the interface states, producing a leakage current that limits the open circuit voltage and solar efficiency according to our hypothesis. Low shunt resistance value further reduces the open circuit voltage. The value of shunt resistance appears to be related to the deposition of gold grid contacts. Fast deposition rates of gold seem to give higher open circuit voltages. The linear coefficient of thermal expansion for Si is $2.6 \times 10^{-6} {}^{\circ}C^{-1}$ [138] and for copper sulfide it is 2.42×10^{-6}-$6.1 \times 10^{-6} {}^{\circ}C^{-1}$ [139]. The deposition of gold probably heats up the cell, therefore, when the cell is cooled down after the gold deposition, a large number of leakage paths are probably created to give a low shunt resistance. Also, the low temperature phase transitions of Cu_2S might be affecting the results. The low fill factor of 0.6 may be due to non-ohmic nature of grid contact as well as because of high series resistance.

In Fig. 66 the solar I-V curve of a cell fabricated by using sulfurization technique (cell 4) is also shown. The cell area was 0.5 cm^2 and therefore the short circuit current density has the same order of magnitude as for the evaporated cells. The open circuit voltage is particularly small, apparently because of relatively high temperature fabrication. The fill factor of this cell was 0.32 and efficiency was 1.5%. The yield of these cells is also quite poor.

5.6 OPTICAL PROPERTIES OF THE CELL

Spectral response of the cells was determined from the measurement of the short circuit current. Solar cells were illuminated with monochromatic light (bandwidth of about 10 nm) obtained from a Bausch and Lomb high intensity grating monochromator. Light intensity was measured with a Hewlett-Packard (model 8330A) radiant flux meter. The schematic of measurement technique and flow chart are shown in Fig.68,69.

Fig.70 shows the spectral response of two solar cells with different thicknesses of cuprous sulfide films. The maximum response is that at about 1.2 eV. These positions of the spectral peaks and their shift with the thickness of cuprous sulfide have been observed in 6% Cu_2S-CdS solar cells also[140,141] and correspond to Cu_2S phase of cuprous sulfide[140]. In our case the spectral response might have also been enhanced at these peak positions because the spectral response of Si solar cells also peaks around these wavelengths. Crossover of two spectral response curves is probably because of light induced ionization of some impurities in cell b. Collection efficiency at the peak position was calculated to be less than 50%, mainly because of losses in interface reflections, surface and interface recombination and bulk recombination in cuprous sulfide.

All the cells have been fabricated without antireflection coatings. Spectral reflectance studies show that about 30% light is being lost due to reflection. This figure of 30% is estimated by integrating the reflectivity vs wavelength curve over AM1 spectrum. Near normal reflectance curve for a cell is shown in Fig.71 for different cell areas.

FIGURE 68: Schematic for the measurement of spectral response of solar cells.

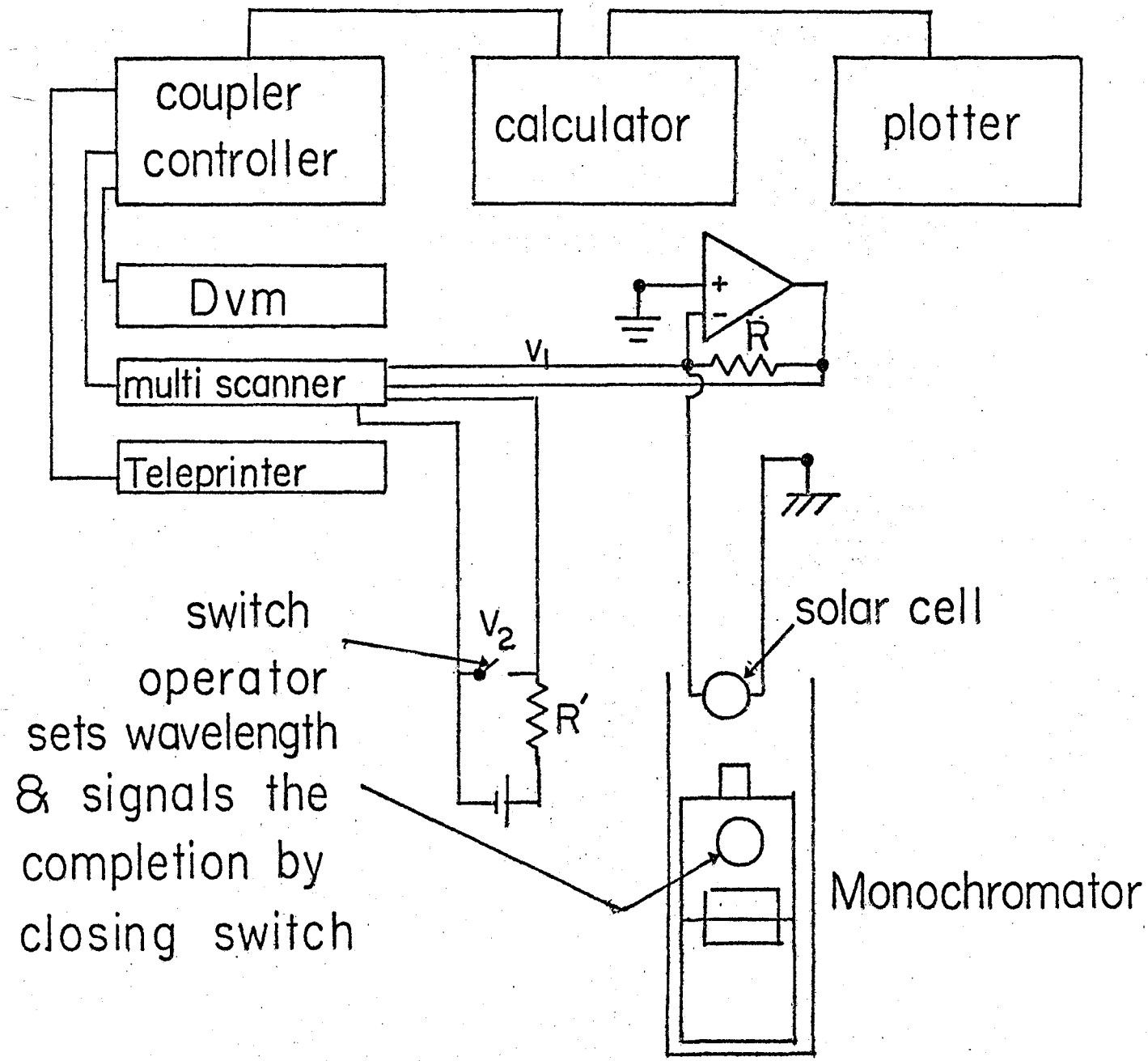
coupler
controller
calculator
plotter
Dvm
multi scanner
Teleprinter
V_1
R
switch
operator
sets wavelength
& signals the
completion by
closing switch
V_2
R'
solar cell
Monochromator

FIG. 68

FIGURE 69: Flow chart for the measurement of spectral response of solar cells.

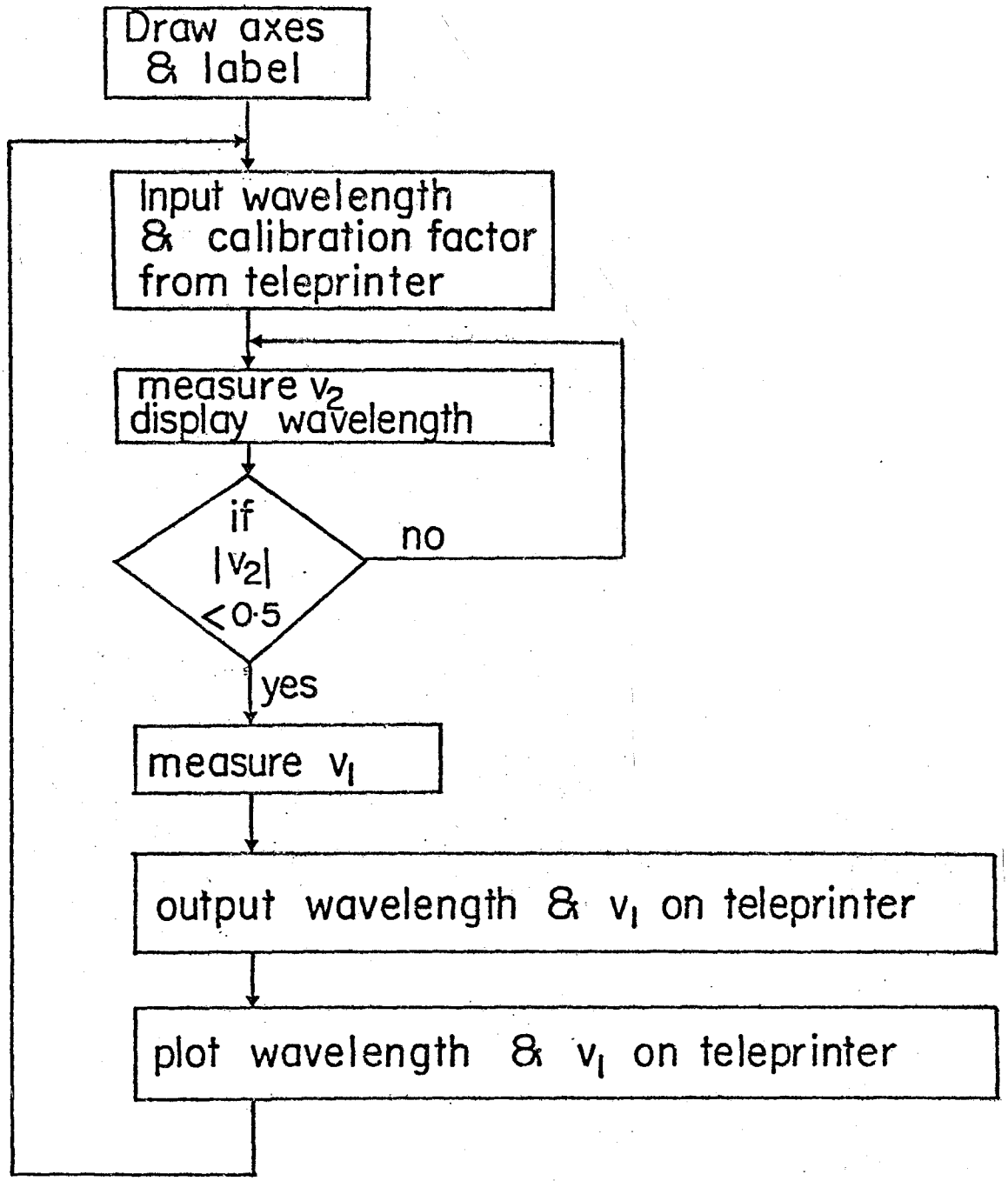
Draw axes & label
Input wavelength & calibration factor from teleprinter
measure v_2 display wavelength
if $|v_2| < 0.5$
no
yes
measure v_1
output wavelength & v_1 on teleprinter
plot wavelength & v_1 on teleprinter

FIG. 69

FIGURE 70: Spectral response of Cu_2S - n-Si solar cells.

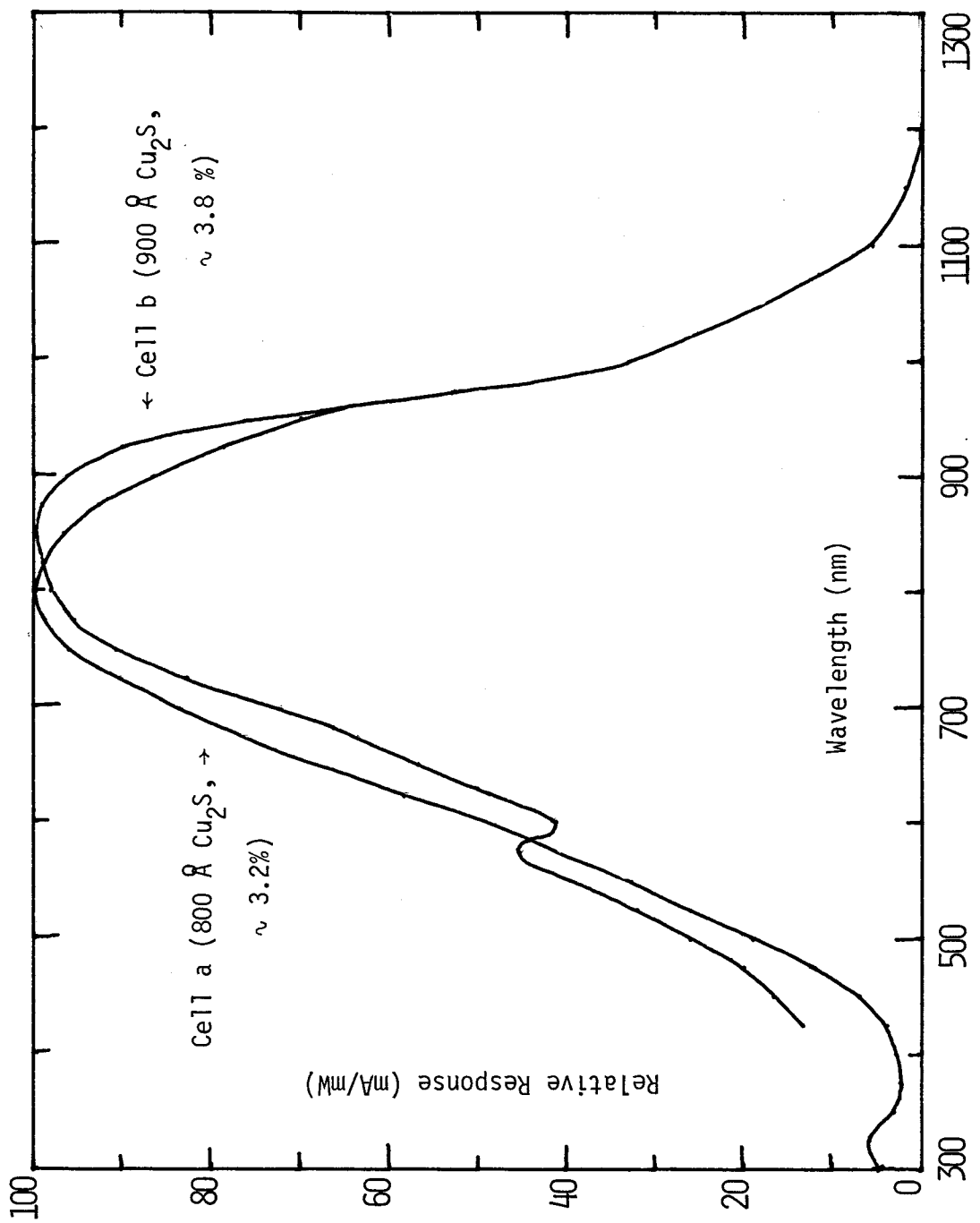
Relative Response (mA/mW)
Wavelength (nm)
Cell a (800 Å Cu_2S, → ~ 3.2%)
← Cell b (900 Å Cu_2S, ~ 3.8 %)
0
20
40
60
80
100
300
500
700
900
1100
1300

FIG. 70

FIGURE 71: Near normal reflectance curve for a Cu_2S - Si solar cell, at different cell area. Cu_2S thickness is about 1500 Å.

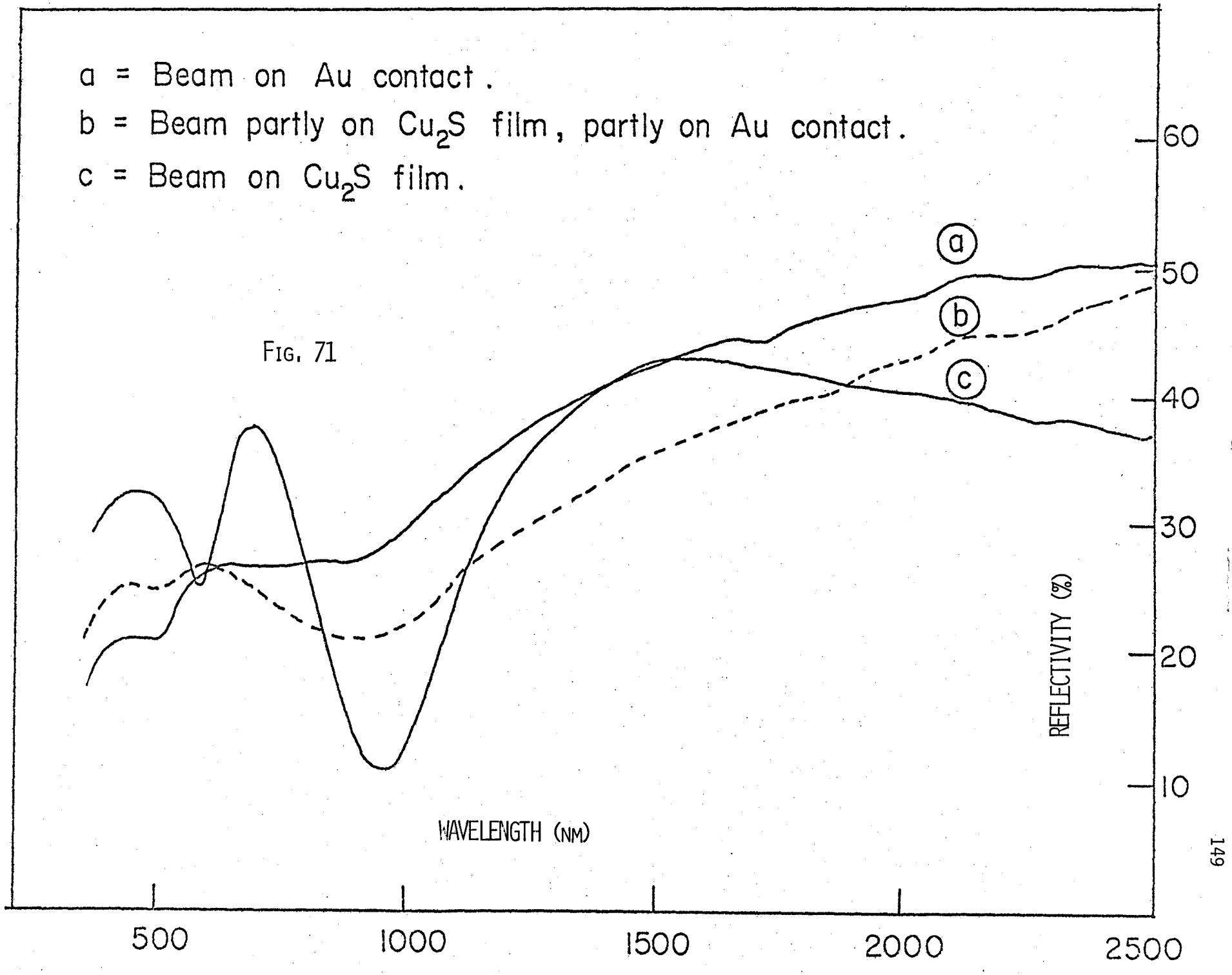
a = Beam on Au contact.
b = Beam partly on Cu_2S film, partly on Au contact.
c = Beam on Cu_2S film.
a
b
c
60
50
40
30
20
10
REFLECTIVITY (%)
WAVELENGTH (NM)
500
1000
1500
2000
2500

FIG. 71

5.7 EFFECT OF EVAPORATION VARIABLES

It was shown in the previous sections that the evaporation variables affect the copper sulfide stochiometry. These effects are, therefore, expected to show up in the photovoltaic characteristics of the solar cells. Vacuum, substrate temperature, source temperature (i.e. evaporation rate) and the film thickness are major variables in our technique. Vacuum and substrate temperature were kept constant for certain reasons. Vacuum was kept below 10^{-6} Torr because higher pressure could affect the surface condition and the film composition in an unpredictable manner due to residual gases. Monitoring of actual substrate temperature is usually cumbersome in high vacuum, therefore, it was also kept constant at about 15-17 °C using running water. The instantaneous radiant heating due to evaporation filament is ruled out due to sufficiently large source to substrate distance of 20 cm and also because the substrate is exposed to the evaporant flux for only about one minute.The $Cu_{2-x}S$ film thickness and its evaporation rate were then varied. It has been previously established that the film composition is independant of thickness but varies with the evaporation rate. We expect to see these effects on cell characteristics also.

The effects of film thickness variation are illustrated in Fig.72-74. It will be seen that short circuit current density remains relatively constant up to about 600 Å of Cu_xS and then drops rather linearly. Open circuit voltage and conversion efficiency show a peak at about 850 Å of film thickness. The generation of carriers due to incident photons can be by two mechanisms. In one, the top copper sulfide layer may act just like a window, without absorbing many photons and most of the carrier

FIGURE 72: Dependance of short circuit current density of Cu_2S - Si solar cells on the Cu_2S film thickness.

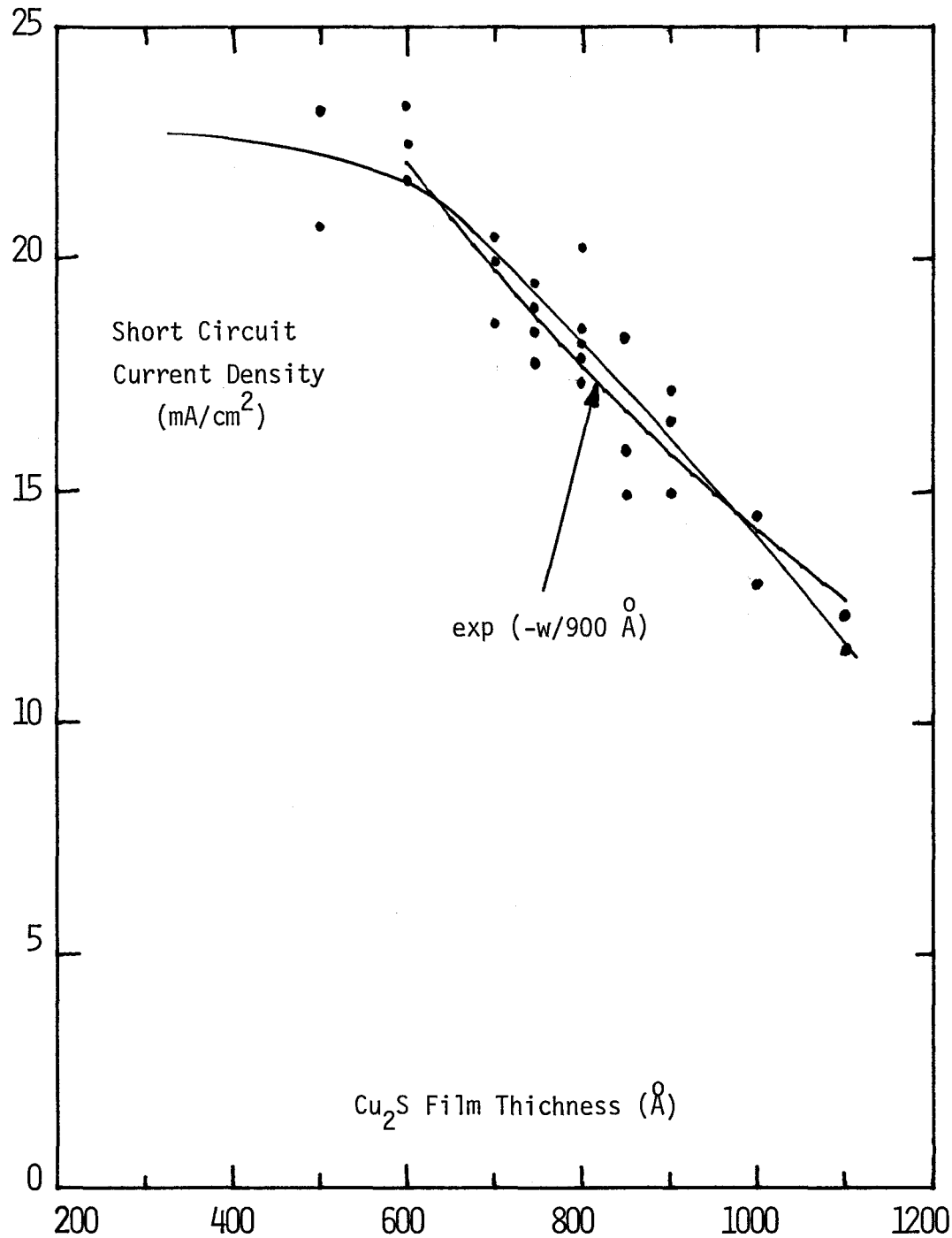
25
20
15
10
5
0
200
400
600
800
1000
1200
Short Circuit
Current Density
(mA/cm^2)
exp (-w/900 Å)
Cu_2S Film Thichness (Å)

FIG. 72

FIGURE 73: Dependance of open circuit voltage of Cu_2S - Si solar cells on the Cu_2S film thickness.

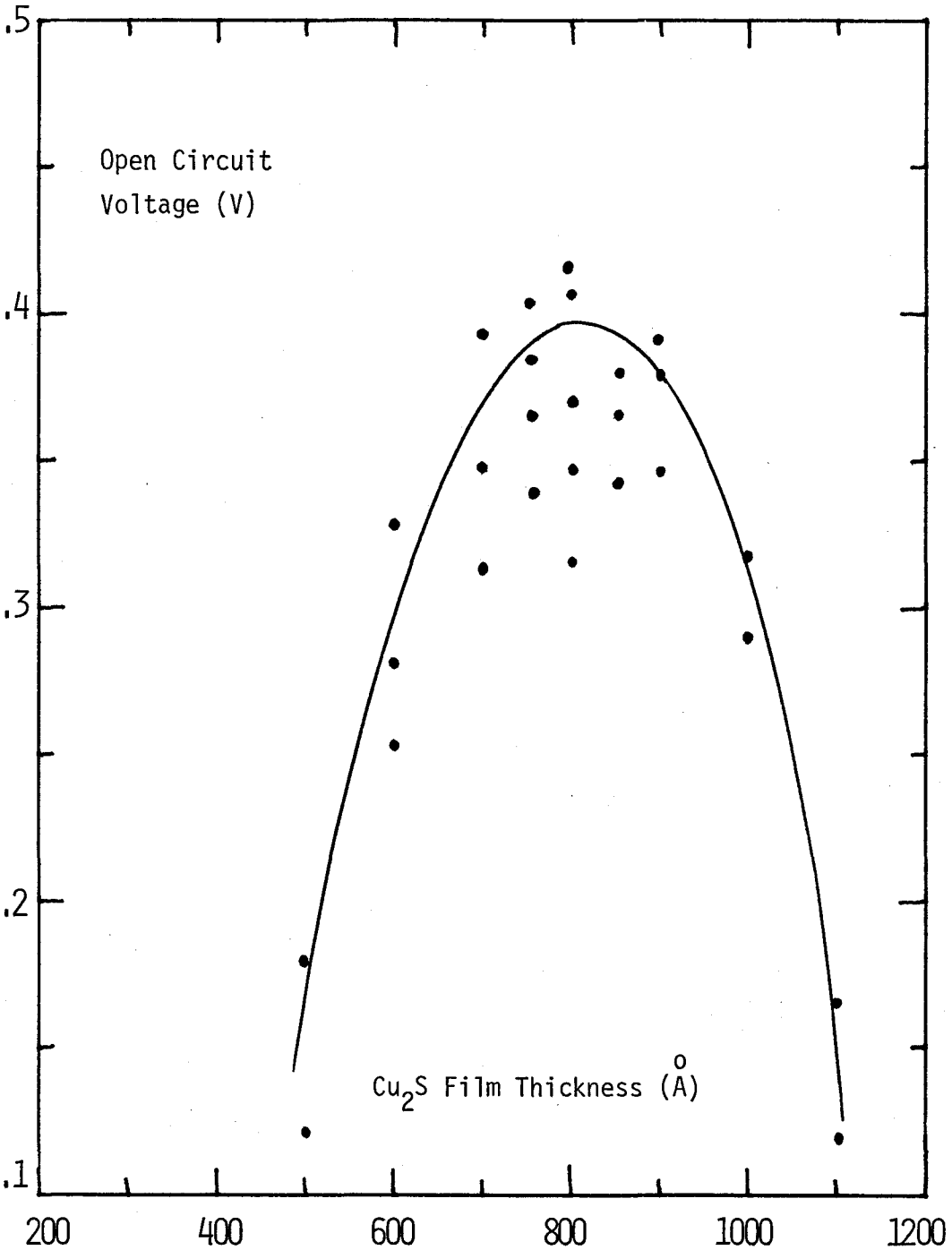
.5
.4
.3
.2
.1
Open Circuit
Voltage (V)
200
400
600
800
1000
1200
Cu2S Film Thickness (Å)

FIG. 73

FIGURE 74: Dependance of conversion efficieny of Cu_2S - Si solar cell on the Cu_2S film thickness.

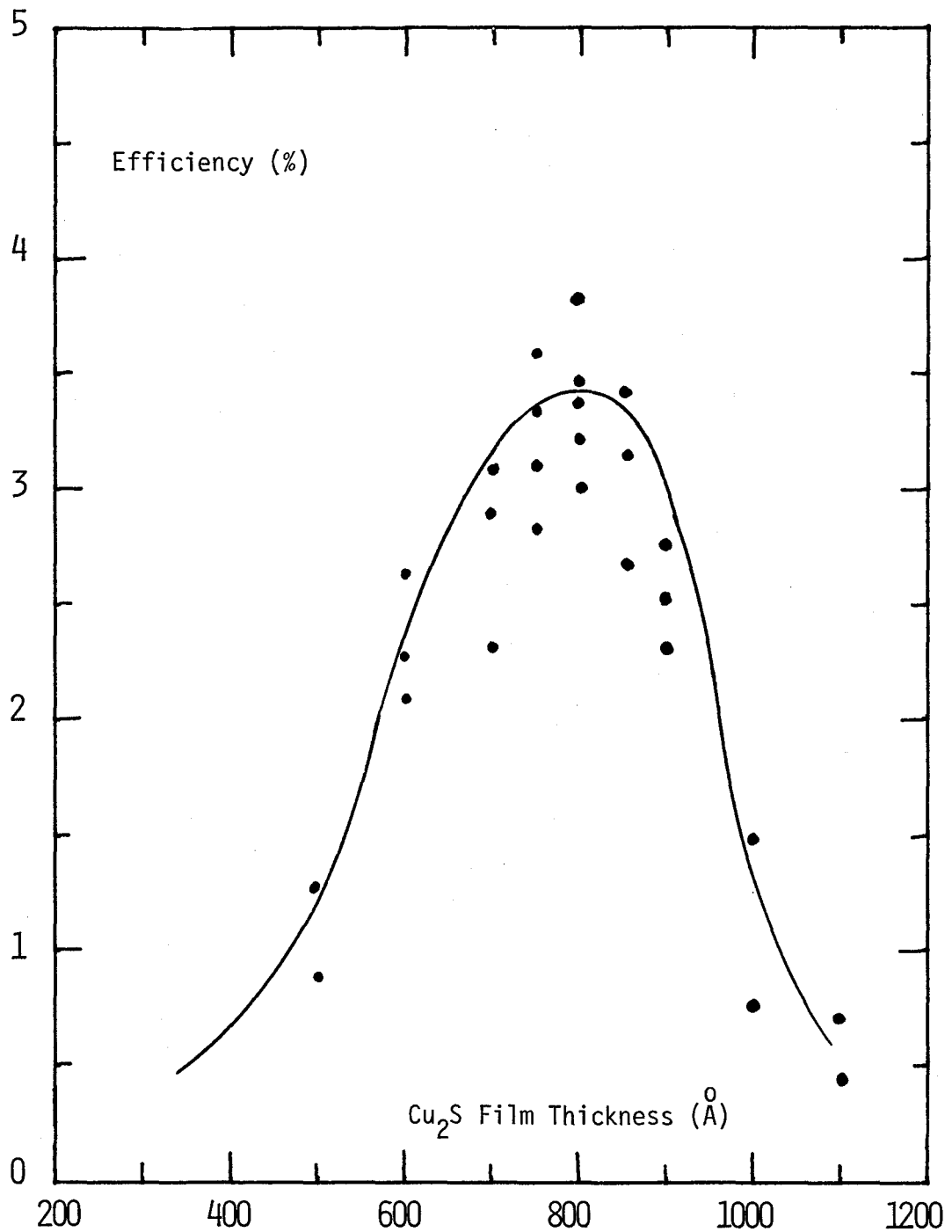
5
4
3
2
1
0
Efficiency (%)
200
400
600
800
1000
1200
Cu2S Film Thickness (Å)

FIG. 74

generation taking place in the silicon substrate. The generation rate at any photon energy will then be

$$g(x,\lambda) = \phi(\lambda)\ T(\lambda)\ \alpha_{Si}(\lambda)\ \exp(-\alpha_{Si}(\lambda).x) \qquad (5.11)$$

where $T(\lambda)$ is the transmittance of copper sulfide layer into the Si substrate. This type of mechanism is most likely for the case where the top copper sulfide layer is very thin. Because the short circuit current is proportional to the carrier generation rate and $T(\lambda)$ for thin ($\sim$500 Å) Cu_2S layers may be as high as 90-95%, the short circuit current will be proportional to $\exp(-\alpha_{Si}\ L_{Si})$ with L_{Si} being effective carrier collection length (may be couple of diffusion langths) in Si. Hence the short circuit current should be relatively constant with the Cu_2S film thickness. The short circuit current density for Si solar cells is usually 30 mA/cm^2 and allowing a factor of 80% for the transmission due to Cu_2S window, short circuit density of about 24 mA/cm^2 should be expected for Cu_xS - Si solar cells. For thin Cu_2S layers, the experimental values are of the same order and remain constant till about 600 Å.

Another mechanism of carrier generation may be due to absorption of photons in the Cu_2S layer. For materials with a high absorption coefficient, it has been known[142] that the short circuit current is proportional to exp(-w/L), where w is the thickness and L is the carrier diffusion length in the semiconductor material. A comparison of such expected behaviour with the experimental results indicate a diffusion length of about 900 Å in copper sulfide. This value is comparable to

the value obtained by Shiozowa and Bube[77,78], but is 6-8 times smaller than the value obtained by Mulder[79] on single crystals of Cu_2S. This difference may be accounted by the polycrystalline nature of the evaporated films. In general both mechanisms must be active and in view of this the experimental behaviour is explainable.

Notwithstanding, how the carriers are generated, the open circuit voltage also depends on the film thickness of Cu_2S and the experimental behaviour is shown in Fig.73 . A peak around 850 Å is observed. The lowering of open circuit voltage above 850 Å is understandable because of lowering of short circuit current as shown in Fig.72 . We propose that the lowering of open circuit voltage for thinner films is associated with the pinning of the minority carrier quasi fermi level to the surface states at the interface.

In an ideal situation where no surface states/traps exist at the interface, the minority carrier quasi fermi level on one side of the junction is pinned to the majority carrier quasi fermi level as shown in Fig.75. This is because of the charge conservation condition across the junction. However, if there exists a source or sink of minority carriers at the interface, the minority carrier quasi fermi level will be pinned to the fermi level of this source/sink. In photovoltaic devices, the carrier source will lead to higher open circuit voltage and the sink will do the opposite. The surface states and traps at the interface are minority carrier sinks. Therefore under illumination the minority carrier quasi fermi level does not rise as much as it would have if there were no surface states/traps. This results in the lowering of the open circuit voltage and the situation

FIGURE 75: Energy band diagrams of Cu_2S - n-Si junction with and without interface states/traps. Various mode of solar cell operation are shown. Quasi fermi levels are shown by dotted lines.

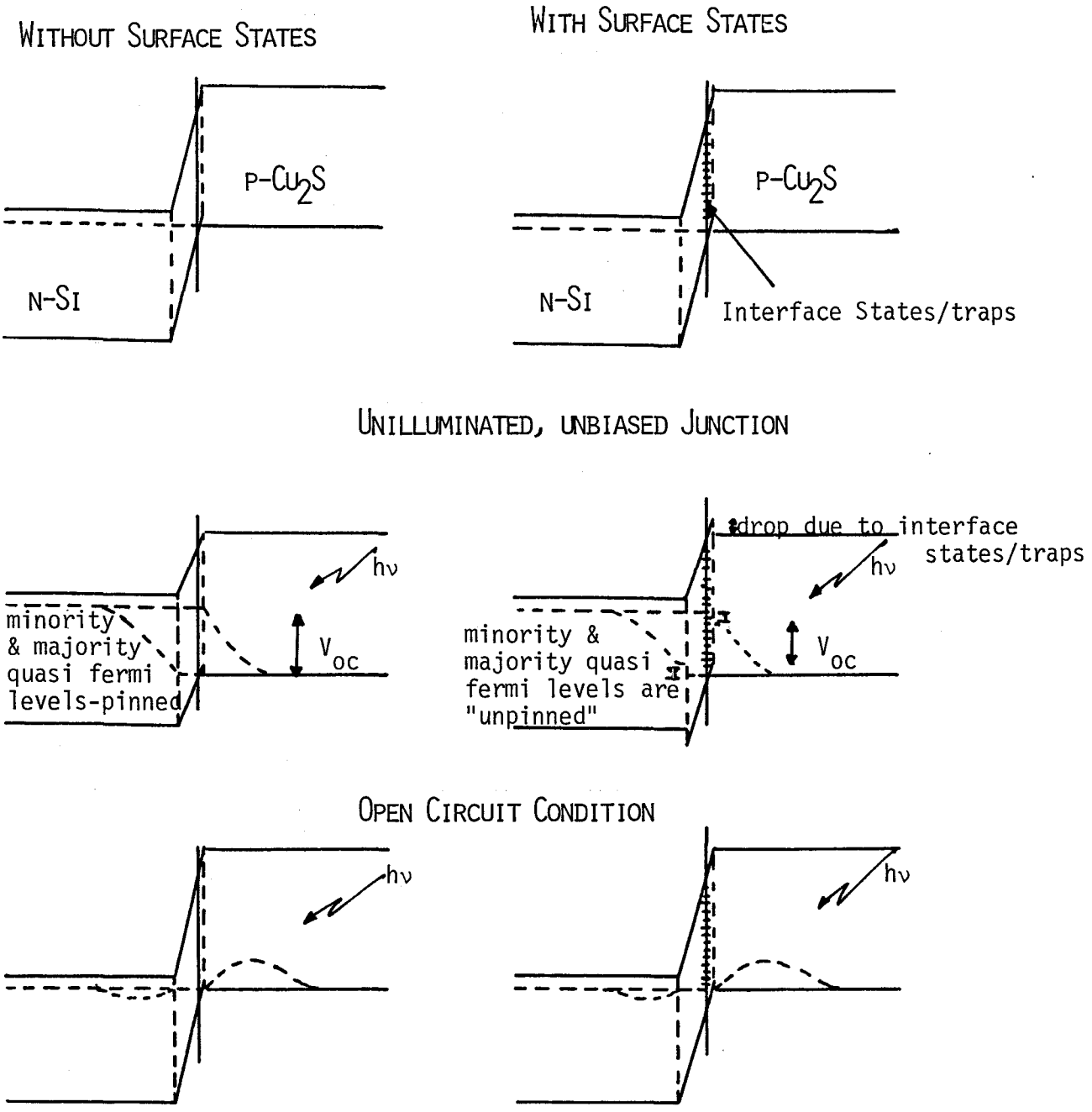
WITHOUT SURFACE STATES
WITH SURFACE STATES
P-Cu2S
N-SI
P-Cu2S
N-SI
Interface States/traps
UNILLUMINATED, UNBIASED JUNCTION
hν
minority
& majority
quasi fermi
levels-pinned
Voc
drop due to interface
states/traps
hν
minority &
majority quasi
fermi levels are
"unpinned"
Voc
OPEN CIRCUIT CONDITION
hν
hν
SHORT CIRCUIT CONDITION

FIG. 75

is illustrated in Fig. 75. The pinning effect is more severe for thinner Cu_2S because of increased number of surface states and traps. This increase in the surface states/trap density is due to larger number of unsaturated bonds and also because of increased film porosity.

Combining the effect of thickness on short circuit current and open circuit voltage, the observed behaviour of cell efficiency (Fig.74) is readily explained. Curve factor of different cells has varied, but no systematic behaviour could be assigned. The curve factor depends on the series resistance of the cell and it is usually difficult to get the same series resistance in different samples. The extraction of the thickness dependance of curve factor was, therefore, quite difficult.

The effect of evaporation rate on the cell parameters was also studied. Some of the results were tabulated in Table VIII. A systematic behaviour is hard to deduce from these data - it appears that other parameters like thickness, temperature etc. were not as constant as they should have been. In principle, because at higher evaporation rate, film stochiometry is closer to Cu_2S, the cell parameters should be better than those at lower evaporation rate.

5.8 EFFECT OF HEATING

It has been long recognized that the anealing of Cu_xS-CdS solar cell improve their efficiency.[143-145] Various research groups have devised their own anealing procedures, but the general consensus is that the improvement

TABLE VIII

EFFECT OF EVAPORATION RATE OF Cu_2S ON Cu_2S-Si CELL PARAMETERS

Cu_2S Thickness ~850 Å

Rate (Å/sec)	V_{oc} (V)	I_{sc} (mA)	Eff. (%)	Area (cm^2)
5.3	.295	21.5	2.107	1.
5.3	.234	5.7	2.345	.25
10.5	.143	10.5	.506	1.
10.5	.158	3.95	.799	.25
20.6	.283	17.25	1.69	1.
20.6	.312	3.75	2.008	.25
10.3	.312	13.625	1.732	1.
15.	.408	18.5	3.385	1.
15.	.316	4.35	3.475	.25

due to anealing is largely because of changes in Cu_xS layer. Possible explanations include improved stochiometry,[144] surface oxidation[145] and interdiffusion.[143]

Anealing of finished Cu_xS -Si solar cells has been tried and here also improvement in the cell efficiency was observed. We have employed a rather unique anealing procedure. The Cu_xS side was illuminated with about 6.5 sun intensity ($\sim$650 mW/cm^2) in the air ambient, for varying periods. The surface temperature reached as high as about 125°C in about 30 - 45 seconds. A quartz-halogen ELH bulb was used for this purpose. In this manner, the film was heated very uniformly. The solar cell characteristics were measured for different anealing periods. A typical result is shown in Fig. 76. It can be noticed that the cell characteristics improve till about 30 sec. of anealing and then start degrading. During the improvement period, both short circuit current and open circuit voltage increased, but during the degradation period, voltage degraded before the degradation of short circuit current. The increment in short circuit current can be related to the reduced number of recombination centres/traps and improvement in the diffusion length and lifetime in the Cu_xS layer. This in turn can be related to decreased film porosity during anealing. The increment in the open circuit voltage can be due to increment in short circuit current as well as due to reduced surface states/trap density at the interface. It appears that after prolonged heating, the junction starts shortening, resulting in the lower open circuit voltage and lower short circuit current. Ultimately, junction is completely shortened and no photovoltaic effect is observed. This junction shortening may be due to contact diffusion, as well as by the diffusion of Cu_xS into Si.

FIGURE 76: Effect of heat treatment in air, on the solar response of Cu_2S - Si cells.

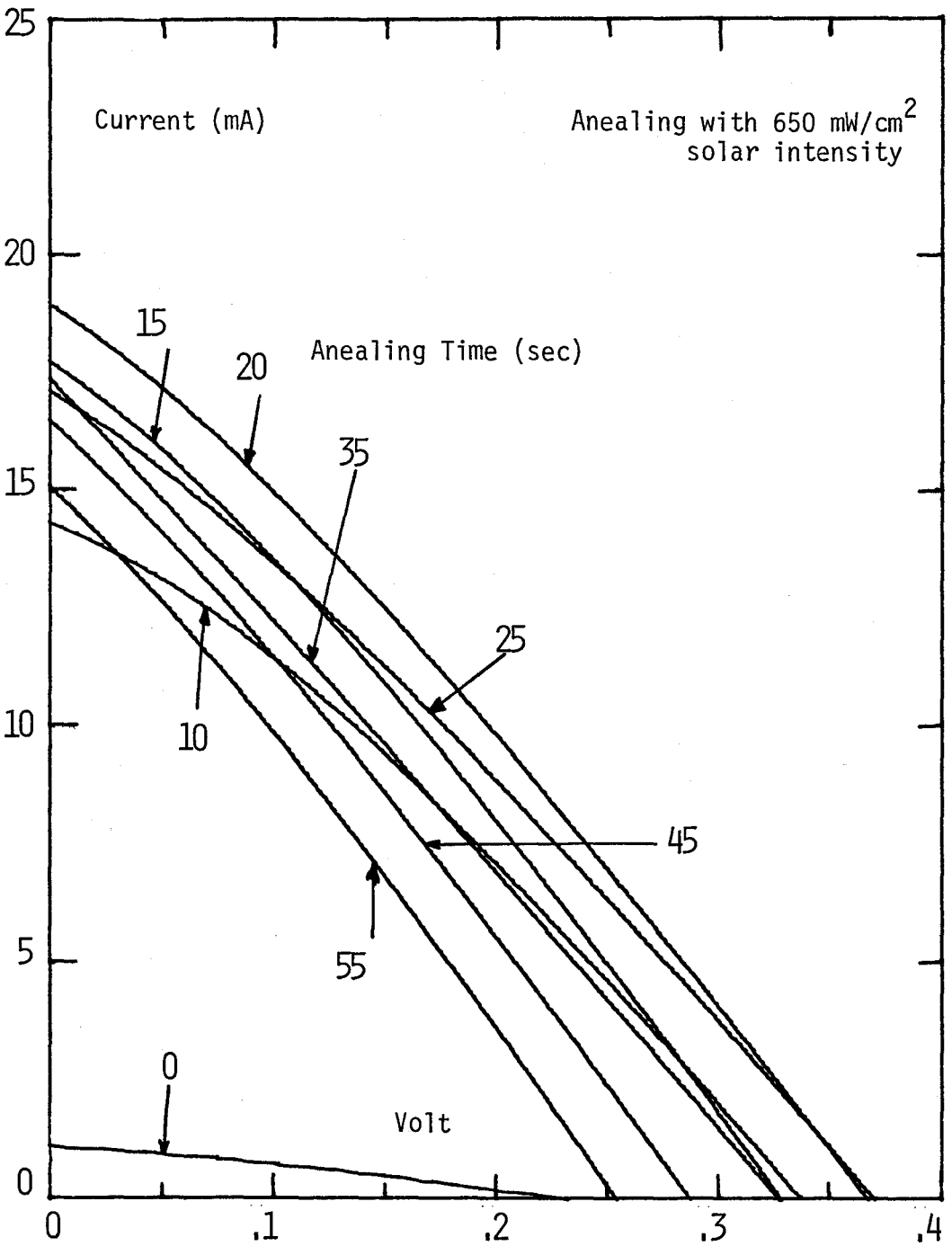
25
20
15
10
5
0
Current (mA)
Anealing with 650 mW/cm2
solar intensity
Anealing Time (sec)
15
20
35
25
10
45
55
0
Volt
0
.1
.2
.3
.4

FIG. 76

The above behaviour of the Cu_xS - Si junction leads to another important result. If the carriers were generated in Si, then the observed increment of short circuit current cannot be explained. Silicon is a well behaved substrate and the photon generated carrier density will not depend on anealing. Contrary to the observations, the short circuit current would have remained constant and only the curve factor and open circuit voltage would have changed with anealing due to changes in polycrystalline Cu_xS film. The anealing behaviour, coupled with the previous results, leads to the conclusion that about 900 Å thick Cu_2S film is enough for photovoltaic conversion, and most of the carrier generation takes place within this thickness. This result may be of some importance for thin film Cu_xS-CdS solar cells also, where,about 2000 Å thick Cu_xS layer is being used.

Once the anealing is done, the effect of ambient temperature variation was also studied. The change in the ambient temperature causes change in dark saturation current and thus changes the open circuit voltage. The short circuit current also changes because of the changes in the optical absorption process, carrier lifetime, mobility etc.[146] The change in the short circuit current is, however, quite small and for temperature variations of even 100°C, it is usually buried in the measurement errors. The experimental dependance of open circuit voltage of Cu_xS - Si solar cells on the ambient temperature is shown in Fig. 77. The open circuit voltage decreases at the rate of about 1 mV/°C. This change is roughly similar to the V_{oc} change in silicon p-n junctions.[147] The reason lies in the origin of dark saturation current. Because the energy band diagram of Cu_xS - Si junction is similar to that of a silicon p-n junction, the saturation current is expected to behave similarly, except for some changes due to the interface states in Cu_xS - Si junction.

FIGURE 77: Effect of ambient temperature variation on the open circuit voltage of Cu_2S - Si solar cell.

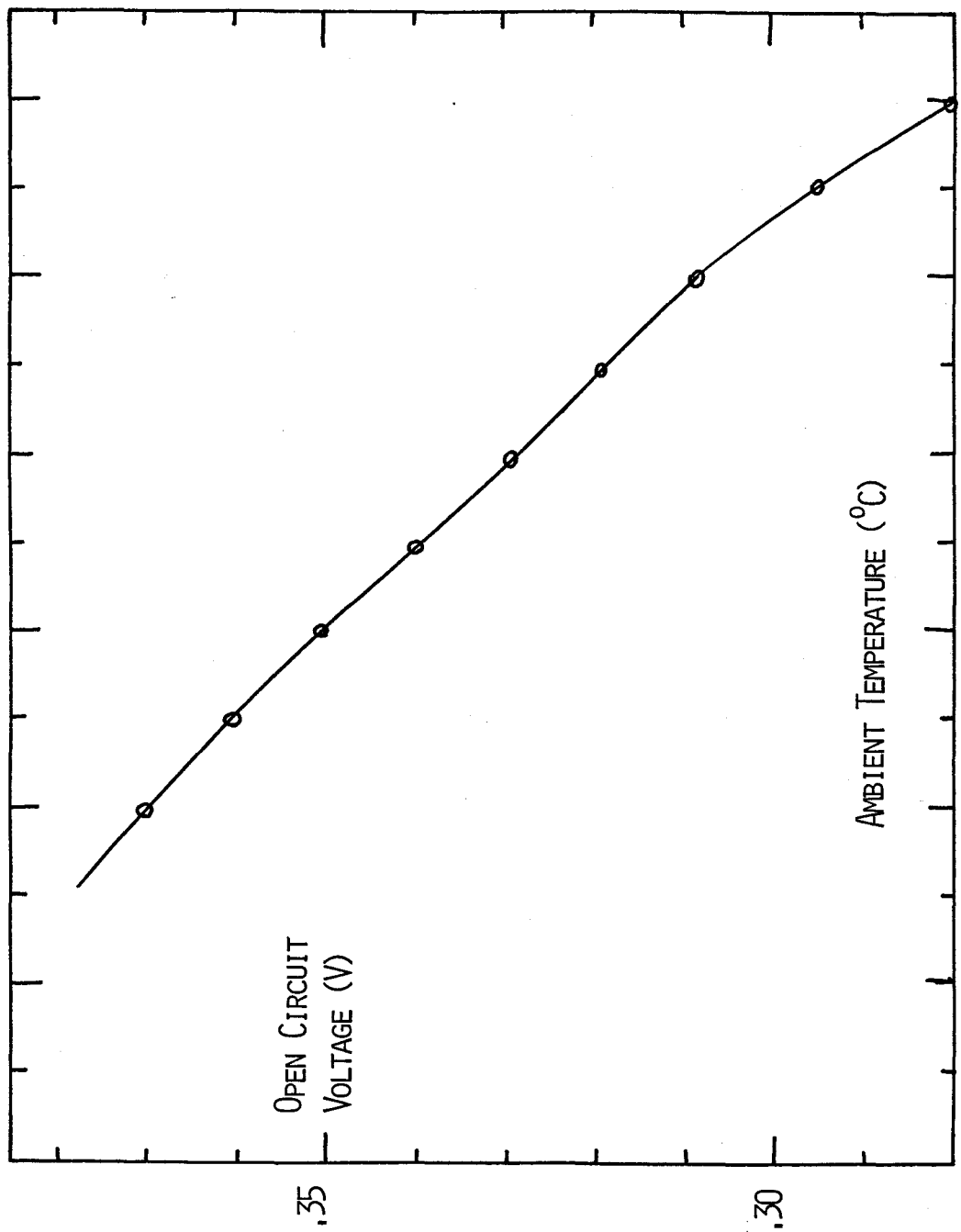
Open Circuit
Voltage (V)
,35
,30
-40
-20
0
+20
+40
+60
+80
Ambient Temperature (°C)

Fig. 77

CHAPTER 6 - CONCLUSIONS

Two methods of preparing copper sulfide thin films have been investigated. Conventional methods of preparing Cu_2S film on CdS substrates provide little control over the formation of Cu_2S. The feasibility of sulfurization and using vacuum evaporated copper sulfide in photovoltaic devices has been demonstrated. In principle, by sulfurization of thin copper films, the desired phase of copper sulfide could be obtained. However, this technique has its own limitations. The adhesion of sulfurized copper films on the substrates is usually not good because the copper sulfide layer grows by the outward diffusion of copper. This method will, therefore, will not be suitable for frontwall solar cells where Cu_2S layer is the top layer. However, backwall solar cells may be feasible with this technique. A possible technique may be the deposition of 2000-3000 Å of copper on some suitable substrate, then the sulfurization of top 1000 Å of copper, after which CdS and contacts on the CdS layer will be deposited. The remaining unsulfurized copper will act as the ohmic contact to the copper sulfide layer.

The other method involving the evaporation of copper sulfide pellets is more adaptable for an all evaporated Cu_2S - CdS solar cell. The prerequisite for this method is the high purity Cu_2S powder which is pressed into pellets for evaporation. The method for making high purity Cu_2S powder has been described. X-ray pattern is enough for checking the powder purity. In this technique the film stochiometry depends on the source and substrate temperatures. The different techniques used for establishing the film stochiometry have indicated that for our experimental set up, evaporation rates of about 15 Å/sec are required to obtain the

desired chalcocite phase of copper sulfide. The optical method of film characterization is in particular quite sensitive to different phases and film structure. Simplicity of this method allows one to use it on a routine basis. Position of reflection minima and the position of equal reflectance and transmittance can be used to monitor the film quality. Cathodoluminescence and x-ray analysis can also be used for film characterization, but these methods require thicker films. Hall measurements depend on the defect structure, as well as on the impurity concentration and it is hard to distinguish between the two. Therefore, Hall measurements may not always give the correct picture.

We have also shown the feasibility of using Cu_2S-Si heterojunctions to monitor the properties of copper sulfide relevant for its application in the photovoltaic energy conversion. This structure can be used to determine the physical properties of copper sulfide like electron affinity, work function etc. The electrical properties of this junction correspond to the theoretical expectations if the effects of interface states are accounted for. The behaviour of this junction indicates that 900 Å thick copper sulfide is sufficient for photovoltaic conversion. This is consistent with the high absorption coefficient of copper sulfide. This result may be of some importance in Cu_2S - CdS solar cells in further reducing their thickness. The sulfurization technique was also used to fabricate Cu_2S-Si heterojunctions and it indicated that this technique can also be used to fabricate thin film Cu_2S-CdS solar cells. However, as commented earlier, this technique will prove more useful in the fabrication of backwall Cu_2S-CdS solar cells.

REFERENCES

1. D.C. Reynold, G. Leies, L.I. Antes and R.E. Marburger, Phys. Rev., 96, 533 (1954).

2. D.C. Reynold and G.M. Leies, Elec. Eng., 73, 734 (1954).

3. D.A. Hammond and F.A. Shirland, Proc. Electron. Components Conf., p. 98 (1959).

4. A.E. Middleton, D.A. Gorski and F.A. Shirland, Progr. Astronaut. Rocketry, 3, 275 (1961).

5. F.A. Shirland, ARL Tech. Rep. 60-293, Harshaw Chem. Co., (1960).

6. R. Williams and R.H. Bube, J. Appl. Phys., 31, 968 (1960).

7. R.R. Bockemuehl, J.E. Kauppila and D.S. Eddy, J. Appl. Phys., 32, 1324 (1961).

8. R.H. Bube, W. Gill and P. Lindquist, Progr. Rep. #1, Grant NGR-05-020-214, Stanford Univ., (1967).

9. W.D. Gill and R.H. Bube, J. Appl. Phys., 41, 3731 (1970).

10. P.F. Lindquist and R.H. Bube, J. Electrochem. Soc., 119, 936 (1972).

11. N. Miya, Jap. J. Appl. Phys., 9, 768 (1970).

12. K.W. Boer, Final Rep., Contract 952666, JPL, Univ. of Delaware, (1970).

13. K.W. Boer, NASA-CR-129675, Grant NGR-08-001-028, Univ. of Delaware, (1971).

14. A. Carlson, WADC Tech. Rep., 56-52, Clevite Corp., (1956).

15. A.E. Carlson, L.R. Shiozawa and J.D. Finegan, U.S. Patent 2,820,841 (1958).

16. D.A. Gorski, U.S. Patent 3,186,874 (1965).

17. F.A. Shirland, G.A. Wolff and J.D. Nixon, ASD-TDR-62-69, Contract AF33(616)-7528, Harshaw Chem. Co. (1962).

18. T.A. Griffin, R.W. Olmstead and J.C. Schaefer, Final Rep., contract NAS3-2493, NASA-CR-54108, Harshaw Chem. Co., 1962-1964.

19. J.C. Schaefer, Tech. Rep. AFAPL-TR-65-1, Harshaw Chem. Co. (1965).

20. J.C. Schaefer, J. Evans and T.A. Griffin, Final Rep., Contract NAS3-8515, Harshaw Chem. Co. (1967).

21. W.J. Deshotels, F. Augustine and A. Carlson, 2nd Quart. Rep., Contract NAS7-203, Clevite Corp. (1963).

22. F.A. Shirland, J.R. Hietanen, F. Augustine and W.K. Bower, Final Rep., Contract NAS3-6461, Clevite Corp., (1965).

23. F.A. Shirland, Adv. Energy Conv., 6, 201 (1966).

24. F.A. Shirland, J.R. Hietanen and W.K. Bower, Final Rep., Contract NAS3-8502, Clevite Corp. (1966).

25. F. Cabannes, C.R. Acad. Sci., 246, 257 (1958).

26. L.E. Ravich, Proc. UN Conf. New Sources Energy, Solar Energy, Wind Power, Geothermal Energy, Vol. 4, p. 258 (1964).

27. C. Pastel, J. Phys., 26, 127 (1965).

28. M. Balkanski and B. Chone, Rev. Phys. Appl., 1, 179 (1966).

29. A.V. Anshon and I.A. Karpovich, Sov. Phys. Semiconductors, 3, 503 (1969).

30. W. Palz, G. Cohen Solal, J. Vedal, J. Fremy, T.N. Duy and J. Valerio, 7th Photovoltaic Specialist Conf., IEEE, p. 54 (1968).

31. W. Palz, J. Besson, J. Fremy, T.N. Duy and J. Vedel, 8th Photovoltaic Specialist Conf., IEEE, p. 16 (1970).

32. G. Coste, J. Fremy and D.T. Nguyen, Proc. Int. Colloq. Solar Cells, (Gordon and Breach), p. 187 (1971).

33. W. Palz, J. Besson, T.N. Duy and J. Vedel, 9th Photovoltaic Specialist Confl, IEEE, p. 91 (1973).

34. W. Palz, J. Besson, T.N. Duy and J. Vedel, 10th Photovoltaic Specialist Conf., IEEE, p. 69 (1974).

35. L. Clark, R. Gale, K. Moore, J.R. Mytton and R.S. Pinder, Proc. Int. Colloq. Solar Cells (Gordon and Breach), p. 241 (1971).

36. K. Bogus, H. Fisher, S. Mattes and N. Peters, Proc. Int. Colloq. Solar Cells (Gordon and Breach), p. 121 (1971).

37. K. Bogus and S. Mattes, 9th Photovoltaic Specialist Conf., IEEE, p. 106 (1973).

38. Univ. of Delware, Final Rep. NSF/RANN/AER 72-03478 A04 (1977).

39. R.A. Mickelsen and D.D. Abbot, Final Rep. Contract NAS3-13232, NASA-CR-120812, Boeing Co. (1971).

40. Univ. of Delaware, Tech. Rep. NSF/RANN/SE/GI-34872/PR73/L, (1973).

41. T.S. TeVelde and J. Dielman, Philips Res. Rep., 28, 573 (1973).

42. W.R. Cook Jr., L. Shiozawa and F. Augustine, J. Appl. Phys, 41, 3058 (1970).

43. W.R. Cook Jr., "The Copper Sulfur Phase Diagram", Ph.D. Thesis, Case Western Reserve Univ. (1971).

44. S. Djurle, Acta Chem. Scand., 12, 1415 (1958).

45. E.H. Roseboom, Econ. Geology, 61, 641 (1966).

46. N. Morimoto, K. Koto and Y. Shimazaki, Amer. Mineral., 54, 1252 (1969).

47. N. Morimoto and K. Koto, Amer. Mineral., 55, 106 (1970).

48. E. Posnjak, E.T. Allen and H.E. Merwin, Econ. Geol., 10, 491 (1975).

49. W. Jost and P. Kubaschewski, Nachr. Acad. Wiss. Goettingen, Math-Phys. Kl, 2, 201 (1967).

50. P. Rahlfs, Z. Phys. Chem., 31, 157 (1936).

51. M.J. Buerger and N.W. Buerger, Amer. Mineral, 29, 55 (1944).

52. J. Singer and P.A. Faeth, Appl. Phys. Lett., 11, 130 (1967).

53. H. Rau, J. Phys. Chem. Solids, 28, 903 (1967).

54. H. Rau, Solid State Comm., 16, 1041 (1975).

55. L.R. Shiozawa, G.A. Sullivan, F. Augustine and J.M. Jost, Tech. Rep., Contract AF 33(615)-5224, Clevite Corp., (1967).

56. R.H. Bube, E.L. Lind and A.B. Dreeben, Phys. Rev., 128, 532 (1962).

57. L. Eisenmann, Ann. Phys. (Leipzig), 10, 129 (1952).

58. D.A. Cusano, Solid-State Electron., 6, 217 (1963).

59. R. Marshall and S.S. Mitra, J. Appl. Phys., 36, 3882 (1965).

60. G.P. Sorokin, Yu.M. Papshev and P.T. Oush, Sov. Phys., Solid State, 7, 1810 (1966).

61. M. Ramoin, J.P. Sorbier, J.F. Bretzner and S. Martinuzzi, C.R. Acad. Sci., 268, 1097 (1969).

62. N. Nakayama, J. Phys. Soc. Jap., 25, 290 (1968).

63. B.J. Mulder, Phys. Stat. Sol., a15, 409 (1973).

64. B.J. Mulder, Phys. Stat. Sol., a18, 633 (1973).

65. S.G. Ellis, J. Appl. Phys., 38, 2906 (1967).

66. V.P. Kryzhanovskii, Opt. Spectrosc. (USSR), 24, 135 (1968).

67. B. Selle and J. Maege, Phys. Stat. Sol., 30, K153 (1968).

68. I.V. Egorava, Sov. Phys. - Semicond., 2, 266 (1968).

69. G. Gustavino, H. Luquet and J. Bougnot, C.R. Acad. Sci, 269, 831 (1969).

70. S. Couve, L. Gouskov, N. Szepessy, J. Vedel and E. Castel, Thin Sol. Film, 15, 223 (1973).

71. E. Hirahara, J. Phys. Soc. Jap., 2, 211 (1947).

72. E. Hirahara Proc. Phys. Soc. Jap., 4, 10 and 12 (1949).

73. E. Hirahara, J. Phys. Soc. Jap., 6, 422 (1951).

74. E. Hirahara, J. Phys. Soc. Jap., 6, 428 (1951).

75. C. Tubandt, S. Eggert and G. Schiebbe, Z. Anorg. Allg. Chem., 117, 1 (1921).

76. G.B. Abdullaev, Z.A. Aliyarova, E.H. Zamanova and G.A. Asodov, Phys. Stat. Sol., 26, 65 (1968).

77. L.R. Shiozawa, G.A. Sullivan, F. Augustine and J.M. Jost, 8th Quart. Rep., Contract AF 33(615)-5224, Clevite Corp. (1968).

78. W.D. Gill and R.H. Bube, J. Appl. Phys., 41, 1694 (1970).

79. B.J. Mulder, Proc. Int. Colloq. Solar Cells, (Gordon and Breach), p. 131 (1971).

80. E.R. Hill, B.G. Keramidas and D.J. Krus, 6th Photovoltaic Specialist Conf. IEEE, Vol. I, p. 35 (1967).

81. A.E. Potter and R.L. Schalla, 6th Photovoltaic Specialist Conf., IEEE, Vol. I, p. 24 (1967).

82. A.E. Potter and R.L. Schalla, NASA Tech. Note, NASA-TN-D-3849 (1967).

83. S. Martinuzzi, Phys. Stat. Sol., a2, K9 (1970).

84. J. Bougnot, F. Gustavino, H. Luquet and D. Sodini, Phys. Stat. Sol., a8, K93, (1971).

85. A.E. Spakowski, A.E. Potter and R.L. Schalla, NASA Tech. Memo, NASA-TMX-52144 (1965).

86. A.E. van Aerschott, J.J. Capart, K.H. David, M. Fabricotti, K.H. Heffels, J.J. Loferski and K.K. Reinhartz., IEEE Trans. Elect. Devices, ED-18, 471 (1971).

87. R. Singh and K. Rajkanan, Young Authors Symposium on Electrochemistry of Thin Films, ECS Ont.-Que. Sect. Meeting, Ottawa, May, 1976.

88. K. Rajkanan, Youngh Authors Symposium on Electrochemical Properties of Materials, ECS Ont.-Que. Sect. Meeting, Hamilton, Jan. 1978.

89. A.S. Grove, Physics and Tech. of Semicond. Devices (John Wiley), Ch.1 (1967).

90. P. Van Der Putte, L.J. Gilling and J. Bloem, J. Crystal Grwoth, 31, 299 (1975).

91. R.E. Treybal, Mass Transfer Operations (McGraw Hill), 1968.

92. B.W. Wojciechowski, Chemical Kinetics for Chemical Engineers, (Stirling Swift Pub Co.), p. 113 (1975).

93. M. Charbonnier and M. Murat, Mat. Res. Bull., 8, 1035 (1973).

94. M.M. Factor and I. Garrett, Growth of Crystals from the Vapour (Chapman and Hall), p. 65 (1974).

95. J. Furer, M. Lambertin and J.C. Colson, Mat. Res. Bull., 10, 1047 (1975).

96. G. Pawlowski, C. Mathiron, D. Delafosse, J.C. Colson, Bull. Soc. Chim. Fr., 2, 555, 1972.

97. J.E. Dutrizac, R.J.C. MacDonald, Mat. Res. Bull., 8, 961 (1973).

98. B. Chattopadhyay and Sadigh-Esfaniary, Corr. Sci., 13, 747 (1973).

99. H. Nakai and T. Saegusa, Nippon Kinzoku Gakkaishi, 38, 819 (1974).

100. M.M. Kazinets, Izv. Akad. Nauk. SSSR Neorg. Mater, 8, 1011 (1974).

101. M. Lambertin, J.C. Colson and D. Delafosse, C.R. Acad. Sc. Ser.C, 272, 267 (1971).

102. J.P. Crousier and M. Laffitte, C.R. Acad. Sc., Ser. C, 267, 951 (1968).

103. M. Takeda, K. Fueki and T. Mukaibo, J. Electrochem. Soc., Jap. (overseas ed.), 36, 95, (1968).

104. J. Shewchun, J.J. Loferski, A. Wold, R. Arnott, E.A. DeMeo, R. Bealieu, C.C. Wu and H.L. Hwang, 11th Photovoltaic Specialist Conf., IEEE, p. 482, (1975).

105. R. Clarke, J. Shewchun, J. Marton, D. Thompson, A. Myskowski, D. Burk, G. Chapman, K. Rajkanan, T. Vanderwel and A. Kazandian, GML Rep.-77E1134, Contract - 11SQ31042-6-8142, 1SQ76-00164, Garrett Manufact. Ltd. (1977).

106. J.P. David, S. Martinuzzi, F. Cabane-Brouty, J.P. Sorbier, J.M. Mathieu, J.M. Roman and J.F. Bretzner, Proc. Int. Colloq. Solar Cells, (Gordon and Breach), p. 81 (1971).

107. E.J. Hsieh, Proc. First ERDA Semiannual Solar Photovoltaic Conv. Prog. Conf., Univ. Calif., Los Angeles, p. 462 (1975).

108. R. Clarke, J. Shewchun, J. Marton, D. Thompson, A. Myskowski, D. Burk, G. Chapman, K. Rajkanan, T. Vanderwel and A. Kazandian, GML Rep.-77E1145, Contract - 11SQ31042-6-8142, 1SQ76-00164, Garrett Manufact. Ltd., (1977).

109. W.N. Tuller (ed.), The Sulphur Data Book, McGraw Hill (1954).

110. J.J. Loferski (ed.), First Semi-annual Prog. Rep. NSF/RANN/SE/GI-38102x/73/4, Brown Univ., (1974).

111. Powder Diffraction File, Joint Comm. on Powder Diffraction Standards, Swarthmore, Pa (1974).

112. J.J. Loferski (d.), Quarterly Prog. Rep., NSF/RANN/SE/GI-38102x/PR/75/1, Brown Univ., (1975).

113. R.H. Bube, Photoconductivity of Solids, John Wiley (1960).

114. J. Shewchun, K.M. Ghanekar, R. Yager, H.D. Barber and D. Thompson, The Rev. Sci. Instruments, 42, 1797 (1971).

115. R. Clarke, J. Shewchun, J. Marton, D. Thompson, H. Rosen, D. Burk, G. Chapman, K. Rajkanan, T. Vanderwel and A. Kazandian, GML Rep. 77E1150, Contract 11SQ31042-6-8142, 1 SQ 76-00164, Garret Manufact. Ltd. (1977).

116. J.P. Marton, Electrical and Optical Properties of Electroless Nickel Films, Ph.D. Thesis, Univ. of Western Ont., p. 138 (1968).

117. K.M. Brown, SIAM J. Numer. Analy., 6, 560 (1969).

118. D.M. Roessler, Brit, J. Appl. Phys., 16, 1119 (1965).

119. S. Maeda, G. Thyagrajan, P.N. Schatz, J. Chem. Phys., 39, 3474 (1963).

120. J.C. Maxwell Garnett, Phil. Trans. Royal Soc. Lond., A203, 385 (1904).

121. J.C. Maxwell Garnett, Phil. Trans. Royal Soc. Lond., A205, 237 (1906).

122. K.L. Chopra, Thin Film Phenomena, McGraw Hill (1969).

123. F.A. Jenkins and H.E. White, Fundamentals of Optics, McGraw Hill, p. 266 (1957).

124. J.A. Borders, J. Electrochem Soc., 123, 37 (1976).

125. J. Vedel and E. Castel, Proc. Int. Cong. The Sun in the Service of Mankind Paris, p. 199 (1973).

126. H.J. Mathieu and H. Rickert, Z. Phys. Chem., 79, 315 (1972).

127. H.J. Hovel, Solar Cells, (Semiconductors and Semimetals, Vol. 11), Academic Press, (1975).

128. K. Rajkanan, J. Shewchun and J.J. Loferski, World Electrotech. Cong., Moscow, June 21-25, 1977.

129. A.G. Milnes and D.L. Feucht, Heterojunctions and Metal-Semiconductor Junctions, Academic Press, Ch. 2 (1972).

130. W.D. Gill and R.H. Bube, J. Appl. Phys., 41, 3731 (1970).

131. H. Okimura and R. Kondo, Jap. J. Appl. Phys., 9, 274 (1970).

132. A. Rothwarf, Proc. Int. Workshop on Cadmium Sulfide Solar Cells and Other Abrupt Heterojunctions, Univ. of Delaware, p. 9 (1975).

133. W. Kern and D.A. Puotinen, RCA Rev., 31, 187 (1970).

134. J.A. Amick, Solid State Tech., 19, 47 (1976).

135. Handbook of Chemistry and Physics, The Chemical Rubber Pub. Co., 44th ed., p. 1476 (1962).

136. W.J. Biter, Proc. Int. Symp. on Solar Energy, Wash. D.C., p. 337 (1976).

137. K. Rajkanan and J. Shewchun, "A Better Approach to the Evaluation of the Series Resistance of Solar Cells and Area Dependance of Performance Characteristics", accepted for publication in Solid State Electronics.

138. S.M. Sze, Physics of Semiconductor Devices, John Wiley, p. 58 (1969).

139. E. Hirahara, J. Phys. Soc. Japan, 6, 422 (1951).

140. N. Nakayama, A. Gyobu and N. Morimoto, Jap. J. Appl. Phys., 10, 1415 (1971).

141. J. Besson, J. Fremy, T.N. Duy, G. Pichard and W. Palz, Proc. Int. Cong. The Sun in the Service of Mankind, Paris, p. 117, (1973).

142. J.J. Loferski and J.J. Wysocki, RCA Tech. Rev., 22, 38 (1961).

143. L.R. Shiozawa, F. Augustine, G.A. Sullivan, J.M. Smith and W.R. Cook Jr., Clevite final Rep., ARL 69-0155, Clevite Corp. (1969).

144. A.L. Fahrenbruch and R.H. Bube, J. Appl. Phys., 45, 1264 (1974).

145. L.C. Burton and V. Ricca, Tech. Rep. NSF/RANN/AER 72-03478 A04/TR75/7, Univ. of Delaware, (1975).

146. J.J. Wysocki and P. Rappaport, J. Appl. Phys., 31, 571 (1960).

147. K.L. Kennerud, IEEE Trans. Aerospace and Elect. Syst., AES-3, 586 (1967).